STRUCTURAL BIFURCATION TESTS FOR VOLTAGE COLLAPSE AND LOW FREQUENCY OSCILLATION IN MULTIMACHINE POWER SYSTEMS

By

TZONG-YIH GUO

A DISSERTATION

Submitted to
Michigan State University
in partial fulfillment of the requirements
for the degree of

DOCTOR OF PHILOSOPHY

Department of Electrical Engineering

1992

ABSTRACT

STRUCTURAL BIFURCATION TESTS FOR VOLTAGE COLLAPSE AND LOW FREQUENCY OSCILLATION IN MULTIMACHINE POWER SYSTEMS

By

TZONG-YIH GUO

A differential-algebraic power system model is developed that is more complete than previous models utilized to study bifurcations of power system dynamics. The added modeling complexity and accuracy is essential for studying both voltage collapse and low frequency oscillation in a power system.

This dissertation systematically classifies the bifurcation and stability problems, establishes necessary conditions for each bifurcation and stability problem, and identifies the generic types of bifurcation associated with steady state angle stability, voltage instability, and low frequency oscillation. The three generic types of bifurcation in the differential-algebraic power system model are shown to be: (1) Static/Algebraic Bifurcation due to the singularity of the equivalent static/algebraic Jacobian matrix; (2) Static Bifurcation and (3) Dynamic Bifurcation due to the equivalent system Jacobian matrix having eigenvalues with zero real parts. Voltage-angle bifurcation in the load flow model is shown to be an excellent approximation to the static/algebraic bifurcation. The prerequisite for the static/algebraic bifurcation test is the single machine stability; the one for the static and dynamic bifurcation tests is the causality condition. These two special stability problems are argued to be improbable in a practical sense, even though they are not argued to be non-generic.

The static/algebraic and static bifurcations are shown to be equivalent under the assumption that single machine stability and causality condition hold. Three types of static bifurcation are identified to occur and necessary conditions for each are derived; one in mechanical dynamics, one in flux decay dynamics, and the third one in both mechanical and flux decay dynamics. The load flow bifurcation is shown to be nearly identical to the static bifurcation in mechanical dynamics; but not the other two types. This dissertation suggests utilizing the static/algebraic Jacobian matrix rather than the test matrix for static bifurcation as the test for identifying static bifurcation. The static/algebraic bifurcation test avoids inverting causality matrix, and can be performed by slightly modifying the load flow program. Both analytical and simulation results for the load flow bifurcation test and the static bifurcation test illustrate the important role of maintaining the reactive generation reserves at generators in preventing voltage collapse and steady state stability. These results also point out that both loss of causality and loss of single machine stability are not likely to occur.

Three types of dynamic bifurcation are identified and necessary conditions for each are established; in mechanical dynamics, in flux decay dynamics, and in both mechanical and flux decay dynamics. Experimental results indicate that tests for various types of dynamic bifurcation actually classify the type of bifurcation in terms of the dynamics (mechanical, flux decay, or both) in which it occurs. Such classification is shown to be more precise than eigenvalue analysis. It is expected that the structurally represented test conditions for various types of static/dynamic bifurcation will be useful in establishing the factors of these bifurcations.

The proposed approach provides a basis for static/dynamic point of collapse/oscillation method, that is similar to a $V-P$ or $Q-V$ point of collapse method in the load flow model, but detects the first mode to become unstable as stress is added to the network. This unstable mode can be associated with any of the stability problems classified and identified in this dissertation.

To my parents

ACKNOWLEDGEMENTS

I am indebted to my parents, wife, brother, and sisters for their support and encouragement over the years. Special remembrance goes to my mother, who passed away during the pursuit of my degree. I would like to express the sincerest thanks to my wife for her understanding, support, patience, encouragement, and love.

I would like to thank my dissertation advisor, Dr. Robert A. Schlueter, for his valuable and constructive guidance. I am also grateful to my committee members, Dr. Gerald Park, Dr. Hassan Khalil, and Dr. Wei-Eihn Kuan, for their professional opinions and advice.

The financial support of Taiwan Power Company (Taiwan, ROC) is gratefully acknowledged for making the completion of my Ph.D. dissertation possible. The research support of Electric Power Research Institute (EPRI), and Detroit Edison Company (DECO) is also appreciated.

TABLE OF CONTENTS

LIST OF TABLES

LIST OF FIGURES

Chapter 1
Introduction

Low frequency oscillations have been one of the most common and frequent stability problems in utilities around the world. Voltage collapse is a stability problem that is less common and frequent than low frequency oscillations, but has captured widespread attention because its causes and cures were less understood. The bifurcations of a power system mid-term transient stability model, that are observed and labeled as low frequency oscillations and voltage collapse, are the subjects of this dissertation. The determination of different types of bifurcation and stability problems that could happen in multimachine power system load flow and dynamic models, and the development of necessary condition tests for existence of the identified types of bifurcation are the main purposes of this dissertation. An improved power system mid-term transient stability model is developed and structurally organized in this dissertation, which has the modeling accuracy needed to perform the classification and identification of bifurcations leading to low frequency oscillations and voltage collapse. Therefore, each developed bifurcation test structurally shows the effects of power system components.

The power system dynamic model is characterized by a set of differential-algebraic equations (or differential-algebraic model). The set of algebraic equations describes the active and reactive power balance equations of the transmission network, i.e., the power balance equations at the internal and terminal buses of machines, at the transformer high-side buses of machines (simply called as high-side buses), and at the load buses. The set of differential equations can include (1) synchronous machine mechanical and flux decay model, and (2) control systems of machines: excitation systems with load compensators, power system stabilizers, and speed-governing-turbine systems. The coupling between the differential equations and the algebraic equations is through the terminal bus of each machine. The load flow model describes the power system steady state operation condition of the transmission network, and is a set of algebraic equations composed of the active and reactive power balance equations of the transmission network excluding the reactive power balance equations at generator terminal PV-buses, since the excitation systems of these generators are assumed to have infinite gain. Note that the load demand model adopted in this dissertation can be voltage dependent.

Based on the representation of the power systems, this dissertation will study the bifurcations that lead to low frequency oscillations and voltage collapse by systematically developing simple tests for each class of bifurcation identified. These tests not only avoid the intensive computation of eigenvalue analysis, but also analytically and structurally show the effects of transmission network as well as each control system. Based on the load flow model, the load flow bifurcation is defined, and the generic form of the load flow bifurcation test matrix is derived and is proven to be consistent with the generic voltage-angle bifurcation in the load flow model. In power system dynamic model, static and dynamic bifurcations will lead to voltage and angle instability, and will occur due to the coupling of the network, generator, and control systems. The singularity induced static bifurcation and dynamic bifurcation will be systematically analyzed in this dissertation. The static/algebraic bifurcation will be defined and shown to be identical to the generic singularity induced static bifurcation. The static and dynamic bifurcations will be defined and shown principally associated with the generator mechanical and flux decay dynamics, and test conditions for these bifurcations will be established. The proposed approach to assessing the studies of voltage and angle dynamic stability in multimachine power systems provides a static/dynamic point of collapse/oscillation method. The proposed approach clearly identifies the modes mainly associated with mechanical and flux decay dynamics and structurally shows the effects of the control systems and transmission network, yet avoids the computationally intensive eigenvalue analysis.

1.1 Literature Review about Dynamic Stability

Time-domain simulation has being popularly used to assess the dynamic stability problems of a power system differential-algebraic model (e.g., [1,2]). However, recently most of the literature dealing with the problem of dynamic stability is filled with eigenvalue analysis orientation [3-22]. For eigenvalue analysis, the linearized power system dynamic model is used, and the elimination of network variables in the algebraic equations has to be feasible such that the equivalent power system dynamic model can be obtained and is well defined. Major part of these eigenvalue analysis studies concentrated on the solution of eigenvalues of the whole equivalent power system dynamic model; others on the computation of some particular modes of oscillation, especially the electro-mechanical modes which in general are of the low frequency oscillatory modes [3,4,21,22], since the electro-mechanical modes of low frequency oscillation is more common if oscillations would occur in power systems. Some special eigenvalue analysis programs have been developed for the above purposes, such as the AESOPS (Analysis of Essentially Spontaneous Oscillations in Power Systems) [3] and the PEALS (Program for Eigenvalue Analysis of Large Systems) in the Small Signal Stability Package (SSSP) [4] for particular modes of eigenvalue analysis, and the MASS (Multi-Area Small Signal Stability Program) in SSSP [4] for the eigenvalue analysis of the whole equivalent power system dynamic model.

However, eigenvalue analysis of a linearized power system dynamic model has some drawbacks, such as:

(1) The dimension of the system matrix for a large power system model becomes extremely large since each synchronous generator has at least

eleven states (see Section 2.4 of Chapter 2: Power System Dynamic Model).

(2) The computation required to compute all the eigenvalues of such a large system matrix is beyond the capability of most computers. Numerical error can make the results invalid when the dimension of the system matrix is so large.

(3) Eigenvalue analysis provides little information about the factors causing the existence of zero or positive real part of any eigenvalue. Computation of left and right eigenvectors and participation factor matrix for each eigenvalue for iterative variation of parameters can provide some information but at extremely high computational cost.

As mentioned above, this dissertation will develop bifurcation tests for the power system dynamic model, especially on the mechanical and flux decay dynamics, that avoid the eigenvalue analysis and provide insight into the effects of power system components on each identified bifurcation.

Another group of the literature about dynamic stability emphasized the computation on the damping and synchronizing power coefficients of a power system [23-30]. The concept of damping and synchronizing power coefficients is very important to the study on dynamic stability. This concept has been utilized extensively since deMello and Concordia extended it to study the stability of a synchronous machine affected by excitation control [23]. However, most of the studies applying this concept were limited to a single machine case with or without excitation system dynamics [23-25]. In order to compute the damping and synchronizing power coefficients of multimachine power systems, some studies even needed to use some time domain signals or to compute the equivalent loading condition of each machine [27-29]. Eliasson and Hill computed damping power coefficient matrix for a power system where each generator was represented by the classical model [30]. The application of Lyapunov or energy function method is another approach to study the stability problems of a power system. Lyapunov methods have been applied for the most part when the electrical dynamics and the control systems dynamics were ignored [31-35]. In this dissertation, damping and synchronizing power coefficient matrices associated with the mechanical dynamics for multimachine power systems will be derived by taking the effects of network and control systems into account. Lyapunov stability theory will be applied to obtain conditions on these test matrices for prevention of bifurcations of the mechanical dynamics.

The theory of bifurcation [36-38] has been applied to the study of steady-state stability and low frequency oscillation based on the differential-algebraic power system model [39-45]. Similar to the eigenvalue analysis, the studies of static and dynamic bifurcations need the equivalent linearized power system dynamic model, provided that the elimination of network variables in the algebraic equations is feasible. This requirement is called as the causality condition of the differential-algebraic model [39,40]. The equilibrium point is a bifurcation point when the system satisfies one of the following conditions:

(a) The complete system Jacobian matrix of the differential-algebraic model is singular;

(b) The equivalent static/algebraic equation Jacobian matrix is singular, which is obtained by aggregating the differential equations into algebraic equations provided that this reduction is feasible;

(c) The equivalent system Jacobian matrix has eigenvalues with zero real parts, provided that the causality condition holds.

Note that in terms of the static bifurcation due to the singularity of the equivalent system Jacobian matrix, these three conditions are equivalent to each other. The static bifurcation could be saddle node bifurcation if the equivalent system Jacobian matrix has a simple zero eigenvalue, and the transversality condition of this matrix at the bifurcation point holds. The dynamic bifurcation could be Hopf bifurcation if the equivalent system Jacobian matrix has a pair of pure imaginary eigenvalues, and the nondegeneracy condition of this matrix at the bifurcation point holds [36-38].

The static bifurcation on the study of steady-state stability of the power system was proposed to analyze the singularity of the Jacobian matrix associated with the differential-algebraic model or with the equivalent power system dynamic model [40,41,45]. The static bifurcation leading to loss of steady-state stability (and/or voltage stability) was shown to occur in a power system model where only mechanical dynamics was involved [40,41]. Hopf bifurcation theory has also been applied to study the dynamic stability of a power system by taking the effects of nonlinearity into account, assuming that the system is at the operating condition with a pair of pure imaginary eigenvalues associated with the equivalent system Jacobian matrix [41-44]. The focus was on determining the condition for stability of Hopf bifurcation of a simple power system model for changes in the bifurcation parameter. These Hopf bifurcations were shown to be pertaining to the mechanical and/or flux decay dynamics due to the effects of control systems. This dissertation will focus on detecting occurrence of instabilities due to low frequency oscillations, particularly associated with the mechanical and flux decay dynamics, rather than on determining the behavior of the power system when Hopf bifurcation occurs.

The role of load demand modeling on power system stability studies has been discussed [46,47]. However, even though it is obvious that load demand modeling plays an important role on the stability studies, a proper load demand model for each time frame of stability study has not yet come to a fairly clear point. The load demand model adopted in this dissertation will be voltage-dependent.

1.2 Literature Review about Voltage Collapse

Basically, voltage collapse problem has been considered as either a static phenomenon by analyzing the load flow model or a dynamic voltage behavior by taking the differential equations of synchronous machines and/or of load into account as well.

Voltage collapse is a phenomenon where the voltage at some bus(es) of a power system is slowly declining over a one to several minute interval and then is observed to drop rapidly. Voltage collapse has been claimed to be a power supply-demand problem, and has been associated with the power transfer over long and/or weak transmission systems because of the trend of siting generators far from load centers (mostly due to the location of power resources and environmental concerns) and because of insufficient enhancement in the load center or weak transmission lines [48-52].

Most of the studies on voltage collapse were based on point of collapse methods, such as the $V-P$, $V-Q$, and $Q-V$ curve approaches, sensitivity analysis approaches, and optimization approaches, that attempt to establish a load flow bifurcation point by increasing load or transfer [48-61]. These load flow voltage collapse methods are assumed to be associated with a lack of convergence to a load flow solution. These methods determine the additional load or transfer at some bus(es) or on some branch(es) before voltage collapse occurs. The additional load or power transfer that can be added or shifted before voltage collapse occurs is the voltage stability margin.

Testing a sign change of the determinant of the load flow Jacobian matrix was also proposed to indicate voltage instability of a power system [62]. The existence of a pair of closely related multiple load flow solutions was shown to be an indication of the singularity of load flow Jacobian matrix and be a proximity to voltage instability [58]. Modal analysis is another approach by applying the SSSP algorithms [4] to compute the eigenvalues, eigenvectors, and participation factors of an equivalent $Q-V$

Jacobian matrix. The magnitude of the small eigenvalues approaching zero is used as a proximity measure to voltage instability for a large power system [63].

Dynamic voltage instability methods take into account the dynamics of synchronous machines and their control systems, and the dynamics of load modeling. However, most of the research on dynamic voltage stability did not include the complete control systems dynamics. Some only included the mechanical dynamics of the generator in the dynamic model [39-41,64-68]; while others neglected the mechanical dynamics, and only kept the flux decay dynamics and/or excitation system dynamics [69-72]. Still others included both flux decay dynamics and excitation system dynamics [41,48,52,53,73]. The effects of load (line drop) compensator and saturation on the problem of voltage stability was investigated in [52,53]. The effects of load demand model on voltage stability was included in [46,64,65,71,74-79].

Time domain simulation was used to show that the proximity to voltage collapse in a single machine case could occur because of the dynamics of induction machine load or tap changer [76,77]. Eigenvalue analysis was proposed to capture the proximity to voltage collapse by tracking the eigenvalue of a simple dynamic system [71-75]. Singular perturbation theory was also applied to investigate voltage stability problem in [78], where different types of voltage instability patterns were shown to be related to the singularity of load flow Jacobian matrix, to eigenvalue analysis, or to direct nonlinear analysis. The relationship between the singularity of the power system dynamic Jacobian matrix and that of the load flow model Jacobian matrix was presented in [45,48,52,53,73].

The theory of bifurcation [36-38] has also been applied based on power system differential-algebraic model, to investigate dynamic stability and voltage collapse problems. Most of the research analyzed the existence (and/or uniqueness) of the equilibrium point of the system by testing the singularity of the system Jacobian matrix directly or indirectly. The research was generally confined to a simple power system where excitation systems were simplified or neglected, and speed-governing-turbine systems and power system stabilizers were omitted [39-41,52,53,64-70].

One of the necessary conditions for the static bifurcation in a power system leading to voltage collapse and/or loss of steady-state stability is the singularity of the equivalent system Jacobian matrix [52,53,39-41,45,64-67,73,78,79]. Schlueter developed test matrices for static voltage collapse that included the flux decay dynamics and excitation systems dynamics of generators, and the effects of network [51-53]. One of the necessary conditions for the dynamic bifurcation in a power system leading to dynamic voltage-angle instability is that the equivalent system Jacobian matrix has eigenvalues with pure imaginary parts. Schlueter also mentioned that Hopf bifurcation can likely occur in the mechanical dynamics [53]. Hopf bifurcation was shown to exhibit dynamic voltage instability in a small system [41,42,67-72,79]. The bifurcation theory was also intensively applied to the study of what occurs just prior to or just after bifurcation of a dynamic model [41].

In this dissertation, the tests for load flow bifurcation and static/algebraic bifurcation will provide a simply generic approach to assessing voltage collapse and steady state stability in multimachine power systems. The tests for dynamic bifurcations will precisely identify that the modes of oscillation are mainly associated with mechanical and flux decay dynamics. Moreover, the effects of the control systems and the transmission network will be structurally shown in the test matrices.

1.3 Organization and Main Contributions of This Dissertation

(A) Power System Dynamic Model

In Chapter 2, the representation of the components of power systems is discussed. First, the general form of the active and reactive power flow between any two buses connected by any kind of branch is shown. The general branch can be any combination of the following network apparatus: (a) a regular transmission line with or without series capacitor, (b) a tap changing transformer, and (c) a phase shifter. The models utilized in previous studies of voltage collapse and low frequency oscillation omitted the series capacitor, tap changing transformer, or phase shifter. Since these components can affect voltage stability and low frequency oscillation, their models should be included. The equivalent π-circuit of a general branch is derived, and then the active and reactive power balance equations at any bus can be formulated. The voltage-dependent load demand model at any bus is adopted in this dissertation, which could be any combination of (1) constant power load, (2) constant impedance load, (3) constant current load, and (4) any other voltage dependent load.

The differential equations of the power system will include synchronous machines, and the control systems of machines. These control systems are adopted from general IEEE models, and will be (a) excitation systems with load compensators, (b) power system stabilizers, and (c) speed-governing-turbine systems. The model of synchronous generators takes the armature and salient-pole effects into account. The active and reactive power balance equations at the synchronous machine terminal buses, and the representation of the load compensator which describes the feedback from the terminal bus to the excitation system will also be derived in order to model the coupling between the differential equations and the algebraic equations. These models of power system dynamics are much more detailed than those generally utilized to study voltage stability and low frequency oscillation [23-35,39-45,48-79]. Again, such modeling detail is necessary to study these stability problems.

The equilibrium point representing the steady state operation condition is discussed by organizing the algebraic power balance equations of the transmission network and the algebraic equations obtained by setting all the derivatives of the differential equations to be zero. This chapter is ended with the linearized power system model to set up the foundation of Jacobian matrices that are necessary for the discussion of bifurcations in the power system model.

(B) Voltage/Angle Bifurcation in Load Flow Model

The simplified model of the power system is the load flow model, where the differential equations are omitted and generators are only modeled by their terminal buses. The load flow model and its linearized representation in matrix form is discussed in the first section of Chapter 3. The linearized load flow model is structurally described based on the three bus types: terminal bus of generator, generator-transformer high-side bus (simply as high-side bus), and load bus.

The load flow bifurcation point is defined as the operating condition where the load flow Jacobian matrix is singular. The voltage, angle, and voltage/angle bifurcations will be shown to be the three types of bifurcations that could occur in a power system load flow model. The voltage bifurcation and angle bifurcation, which occur when the rows of the load flow Jacobian matrix associated with reactive power balance equations and active power balance equations are respectively dependent, are shown to be non-generic bifurcations which can only occur when a decoupled load flow model is used. Moreover, the load flow bifurcations due to the row dependence of some particular rows of the load flow Jacobian matrix associated with single buses are shown to never occur. Hence, analogies between bifurcations in a two-bus model have limited usefulness in understanding how voltage instability develops in the large power system load flow model. Thus, the generic form of load flow bifurcation test matrix is proven theoretically and experimentally to be the voltage-angle bifurcation which is due to row dependence of all the rows associated with both active and reactive power balance equations. This result indicates the important effects of the coupling between active power and voltage, and the coupling between reactive power and angle on the voltage-angle bifurcation.

Finally, the simulation for the load flow bifurcation will be performed on a 9-bus 3-machine power system. The simulation results for the load flow bifurcation illustrate the important role of maintaining reactive power generation reserves at PV-buses in preventing voltage collapse.

(C) Stability Problems in a Differential-Algebraic Model

Chapter 4 is devoted to the classification of stability problems in a power system differential-algebraic model, and to the discussion of the conditions of these identified stability problems. The linearized differential-algebraic power system dynamic model is first developed and the properties of its Jacobian matrix are discussed in Section 4.1.

Next, based on the complete power system Jacobian matrix, basic bifurcation theory is reviewed and six possible types of bifurcation in the power system differential-algebraic model are identified, and two related non-bifurcation stability problems are also identified. Necessary condition tests for each of the bifurcation and stability problems are given. However, only three of these bifurcations are then identified to be generic:

(a) The static/algebraic bifurcation is defined when the equivalent static/algebraic Jacobian matrix is singular, which is obtained by aggregating the linearized equilibrium equations associated with the differential equations into the algebraic equations provided that this reduction is feasible.

(b) The static bifurcation occurs when the equivalent system Jacobian matrix is singular, which is produced by the elimination of the network variables in the linearized algebraic equations provided that this reduction is feasible.

(c) The dynamic bifurcation occurs when the equivalent system Jacobian matrix has pure imaginary eigenvalues.

Note that the reduction in (a) of the linearized equilibrium equations associated with the differential equations requires the stability of the single machine dynamics; the reduction in (b) and (c) is the so-called causality condition [39] of the differential-algebraic model. These two special stability problems, loss of single machine stability and loss of causality, will be argued to be improbable in a practical power system model.

Both the static/algebraic bifurcation and the static bifurcation are the type of singularity induced static bifurcation, and will be shown to be equivalent to each other. In this chapter, testing singularity of the static/algebraic Jacobian matrix for the singularity induced static bifurcation is suggested rather than testing the singularity of the equivalent system Jacobian matrix. This static/algebraic bifurcation test avoids the inverse of the transmission network Jacobian submatrix (causality matrix) which is non-sparse and has high dimension, and yet preserves the structure of the causality matrix which is very similar to the load flow Jacobian matrix. The static/algebraic Jacobian matrix corresponds to a set of algebraic equations that are similar to those of a load flow model, and yet is the Jacobian matrix for computing the (dynamic) equilibrium point of the differential-algebraic model. Moreover, this approach shows that each synchronous machine can be represented by the single-axis model, and that only the D.C. gain of the excitation system of each machine is required to model the control systems.

The similarity and the difference between the static/algebraic Jacobian matrix, the causality matrix, and the load flow Jacobian matrix will be comprehensively discussed. It is concluded that if the D.C. gains of the excitation systems are very large which is generally true, the singularity induced static bifurcation test will have similar results as the load flow bifurcation test. Furthermore, if the reactive power generation limits are included in the model, the static/algebraic Jacobian matrix will more likely be singular than the causality matrix. The analysis is conducted for the case where generator flux decay and exciter dynamics is replaced by an algebraic equation that specifies the reactive power generation and models the reactive power balance equation at the generator terminal bus when the reactive power generation limit is reached. An alternative is to model the field current limiter that adjusts the voltage reference on the excitation system to hold the field current constant. When this alternative is used, static bifurcation may occur in flux decay dynamics and in both flux decay and mechanical dynamics for the generators which reach field current limits. This possibility is eliminated if the generator flux decay and exciter dynamics is replaced by the algebraic reactive power balance equation. The static bifurcation is solely associated with the mechanical dynamics of the generators that reach field current limits when their flux decay and exciter dynamics are replaced by the algebraic reactive power balance equations. No discussion of the comparison of the static/algebraic Jacobian matrix and the load flow Jacobian matrix is conducted in this dissertation when the field current limiter is used to adjust voltage reference on the excitation system to control the field current to be constant.

The simulation results utilizing the static/algebraic bifurcation test on the same power system as used for the load flow bifurcation test show that static bifurcation and load flow bifurcation occur at approximately the same operating point and for the same reason. The results for the load flow model and the differential-algebraic model both indicate that exhaustion of reactive power generation reserves causes the bifurcation to occur if the generator electrical dynamics are replaced by the PQ-bus bus load flow model when the reactive power generation limits are reached.

(D) Static/Dynamic Bifurcation

The static bifurcation and dynamic bifurcation are generic types of bifurcation in the power system differential-algebraic model. The static or dynamic bifurcation can occur when the equivalent system Jacobian matrix has eigenvalues with zero real parts, provided that the causality condition holds. Based on (a) the proof that the control system themselves should have asymptotically stable eigenvalues, and (b) the experimental results of the eigenvalue analysis [4] that most oscillations occur in the mechanical and/or flux decay dynamics, Chapter 5 mainly focuses on the derivation of simple necessary condition tests for static and dynamic bifurcations in multimachine power systems associated with mechanical dynamics and with flux decay dynamics.

First, the portion of the equivalent system Jacobian matrix associated with the control systems themselves is shown to have asymptotically stable eigenvalues. A reduced Laplace transformed ($S = j\Omega$) model of the equivalent system Jacobian matrix pertaining to solely mechanical and flux decay dynamics is produced by the elimination of the control system dynamics since they are proven to be nonsingular for any $\Omega \geq 0$. This resultant matrix provides the test of static bifurcation if it is singular at $\Omega = 0$, and the test of dynamic bifurcation if it is singular at some $\Omega > 0$. Note that this test matrix also structurally shows the effects of network and control systems.

Damping and synchronizing power coefficient matrices associated with the mechanical dynamics will be further derived by further elimination of flux decay dynamics. Test conditions on these matrices for identification and prevention of static ($\Omega = 0$) and dynamic ($\Omega > 0$) bifurcations of the mechanical dynamics will be established. Test matrices for identification and prevention of flux decay bifurcation will be similarly generated from the reduced model.

A static/dynamic point of collapse/oscillation method is proposed that would test for the closest bifurcation as the system is continually stressed, as is the case when a $Q-V$ or $P-V$ curve is produced in a load flow model. The method would increase a transfer or loading level for some active power loading pattern or reactive power load at some bus(es), determine when the first bifurcation occurs and its type. This methodology would assess proximity to both steady state voltage-angle stability and low frequency oscillation.

T

dynar

appro

decay

show

wher

elect

(E)

tion

tage

on

(2)

mo

tion

The simulation results on a power system [4] in the proximity to experiencing dynamic bifurcation leading to low frequency oscillation illustrate that the proposed approach clearly identifies the modes associated with mechanical dynamics and flux decay dynamics without performing eigenvalue analysis. The proposed approach is shown to identify whether the bifurcation is in the mechanical or flux decay dynamics when eigenvalue analysis can only shows that the mode affects both mechanical and electrical dynamics.

(E) Conclusion and Discussion

This last chapter ends this dissertation with the brief summary of the contributions of the proposed approaches to assessing the generic bifurcations leading to voltage collapse and low frequency oscillation in the multimachine power system based on two different models: (1) the voltage/angle bifurcation in the load flow model, and (2) the static and dynamic bifurcations in the differential-algebraic power system model. A flow chart for the identification and prevention the generic types of bifurcation is provided. Some potential future research about this topic is also proposed.

Chapter 2
Power System Dynamic Model

Figure 2-1 represents a general model of any element of the network that can connect any two buses i and j. The general model for a network element or branch can represent a transmission line, transformer, phase shifter or any combination. A specific example is a step-up transformer between a generator terminal bus and its high-side bus, which allows a general discussion of the modeling of both power injection (the mismatch between power generation and load demand) at a bus and power flow on a general branch.

This general branch can be represented by an equivalent π-circuit, which will be discussed in Section 2.2. The power injection at each bus i, $P_i + j\ Q_i$, is the algebraic sum of power supply, $P_{Gi} + j\ Q_{Gi}$, and power demand, $P_{Di} + j\ Q_{Di}$. The power demand model, in general, can be any combination of constant power model, constant current model, constant impedance model, and other types of voltage dependent model, which will be discussed in Section 2.3. Section 2.4 shows the generator model. The load flow model or the power balance equations that integrate the expression of a power system is now discussed in the next section.

2.1 Load Flow Model

Figure 2-2 shows the power flow diagram of any two buses, i and j. The connection between them is represented by an equivalent general π-circuit. Note that the equivalent charging admittance at bus i, $\overline{Y}_{Cij}$, could be different from that at bus j, $\overline{Y}_{Cji}$, and that the equivalent transfer admittances, $\overline{Y}_{ij}$ and $\overline{Y}_{ji}$, might not be the same. These effects are due to the branch types of transformer and phase shifter (see Section

Ge

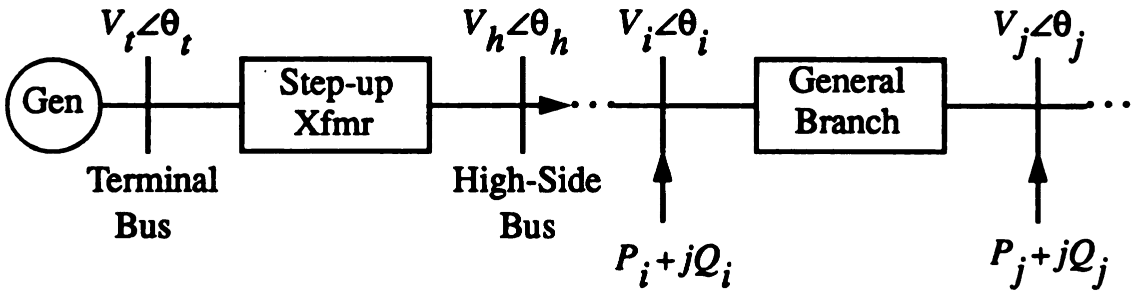

$$P_i = P_{Gi} - P_{Di} \qquad Q_i = Q_{Gi} - Q_{Di}$$

Fig. 2-1 A General Branch Between Two Buses

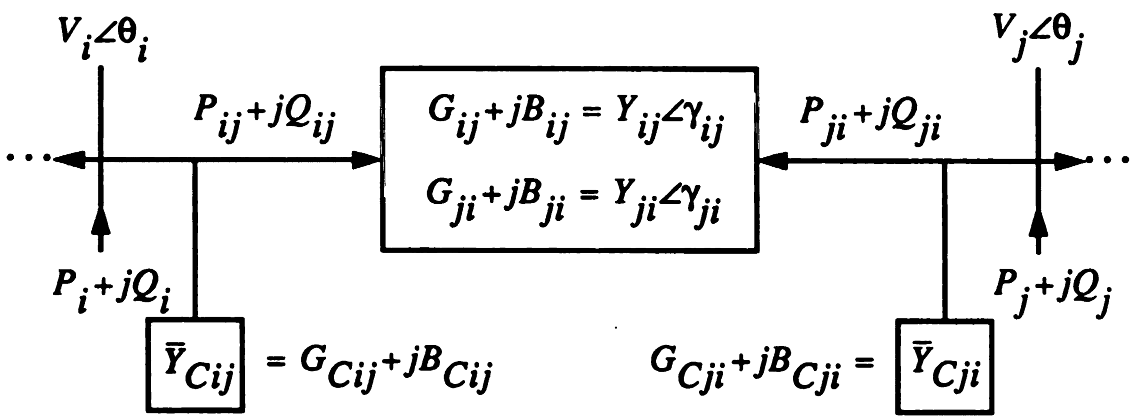

$$P_{ij} = V_i^2 G_{ij} - V_i V_j T_{ij}$$

$$Q_{ij} = -V_i^2 B_{ij} - V_i V_j U_{ij}$$

Fig. 2-2 Power Flow Diagram

2.2). The generality of this branch model is introduced to permit modeling of transformer and phase shifter [80].

Assume that there are n buses in a power system. Then the power flow between bus i and bus j, and the power balance equation at each bus i can be expressed as follows [81]:

$$\begin{aligned} P_{ij} &= V_i^2\, G_{ij} - V_i\, V_j\, [\, G_{ij} \cos(\theta_i - \theta_j) + B_{ij} \sin(\theta_i - \theta_j)\,] \\ &= V_i^2\, G_{ij} - V_i\, V_j\, Y_{ij} \cos(\theta_i - \theta_j - \gamma_{ij}) \\ &= V_i^2\, G_{ij} - V_i\, V_j\, T_{ij} \end{aligned} \tag{2-1a}$$

$$\begin{aligned} Q_{ij} &= -\, V_i^2\, B_{ij} - V_i\, V_j\, [\, G_{ij} \sin(\theta_i - \theta_j) - B_{ij} \cos(\theta_i - \theta_j)\,] \\ &= -\, V_i^2\, B_{ij} - V_i\, V_j\, Y_{ij} \sin(\theta_i - \theta_j - \gamma_{ij}) \\ &= -\, V_i^2\, B_{ij} - V_i\, V_j\, U_{ij} \end{aligned} \tag{2-1b}$$

$$\begin{aligned} P_i &= P_{Gi} - P_{Di} = \sum_{j=1}^{n} (V_i^2\, G_{Cij} + P_{ij}) \\ &= V_i^2 \sum_{j=1}^{n} (G_{Cij} + G_{ij}) - \sum_{j=1}^{n} V_i\, V_j\, T_{ij} \quad ; \; j \neq i \end{aligned} \tag{2-2a}$$

$$\begin{aligned} Q_i &= Q_{Gi} - Q_{Di} = \sum_{j=1}^{n} (-\, V_i^2\, B_{Cij} + Q_{ij}) \\ &= -\, V_i^2 \sum_{j=1}^{n} (B_{Cij} + B_{ij}) - \sum_{j=1}^{n} V_i\, V_j\, U_{ij} \quad ; \; j \neq i \end{aligned} \tag{2-2b}$$

where

$$Y_{ij} = \sqrt{G_{ij}^2 + B_{ij}^2} \; ; \; \gamma_{ij} = \tan^{-1} (B_{ij}/G_{ij}) \tag{2-3}$$

$$\begin{aligned} T_{ij} &= G_{ij} \cos(\theta_i - \theta_j) + B_{ij} \sin(\theta_i - \theta_j) \\ &= Y_{ij} \cos(\theta_i - \theta_j - \gamma_{ij}) \end{aligned} \tag{2-4a}$$

$$U_{ij} = G_{ij} \sin(\theta_i - \theta_j) - B_{ij} \cos(\theta_i - \theta_j) \tag{2-4b}$$

$$= Y_{ij} \sin(\theta_i - \theta_j - \gamma_{ij})$$

Note that the above branch power flow is expressed without taking the equivalent charging admittance into account, since in the "dumped" model of a general branch the equivalent charging admittances is considered to be connected at the buses.

During solving the power flow equations, the following variables are specified:

(1) V_i ($i = 1, 2, \cdots, m$), i.e., voltages at the swing bus (bus number 1 with $\theta_1 = 0$) and the $m-1$ PV-buses.

(2) P_i ($i = 2, \cdots, m$) which are the model of net active power injection at the PV-buses.

(3) P_i and Q_i ($i = m+1, m+2, \cdots, n$) which are the model of net active and reactive power injection respectively at the load buses (PQ-buses).

Note that

$$P_i = P_{Gi} - P_{Di} \ , \ i = 1, 2, \cdots, n \ ; \tag{2-5}$$

$$P_{Gi} = 0 \ , \ i = m+1, m+2, \cdots, n \ ;$$

$$Q_i = Q_{Gi} - Q_{Di} \ , \ i = 1, 2, \cdots, n \ ;$$

$$Q_{Gi} = 0 \ , \ i = m+1, m+2, \cdots, n \ ;$$

and that P_{Di} and Q_{Di} are the load demand which may be functions of V_i. Then the $2n - m - 1$ unknowns (V_i, $i = m+1, \cdots, n$, and θ_i, $i = 2, \cdots, n$) can be solved from $2n - m - 1$ equations ($n - 1$ active power equations (2-2a) and $n - m$ reactive power equations (2-2b)), if they are independent. After that, the voltage and angle (with respect to swing bus) at each bus are known, and the proper reactive power generation at each PV-bus and active and reactive power generation at swing bus can be obtained from (2-2). Note that when the reactive power generation of any PV-bus hits its limits, it becomes a PQ-bus with fixed reactive power generation equal to the limit and with varying voltage. Thus, the voltage and reactive power generation at this bus become an additional dependent and independent variable, respectively; and the load flow equations have an additional reactive power balance equation at this bus. Then, the load flow is re-solved until every variable converges within its limits; otherwise the load flow diverges.

2.2 Transformer and Phase Shifter Model

Figure 2-3 shows the physical one-line diagram of a general branch between bus i and bus j, where bus i is called tap-side bus, bus j is called impedance-side bus, and the bus between them is a dummy bus, bus k [80,82]. Between the tap-side bus and the dummy bus, an ideal transformer with phase shifter is represented by the complex value $\bar{a}_{ij} = a_{ij} \exp (j\ \alpha_{ij})$, where a_{ij} is the tap ratio and α_{ij} is the phase shift. The π-circuit between the dummy bus and the impedance-side bus represents the leakage impedance and magnetizing admittance of a transformer, or the line impedance and line charging admittance of a transmission line, and hence

$$\bar{Y}_{kj} = \bar{Y}_{jk} = \bar{Y} = Y \exp (j\ \gamma) = G + j\ B \tag{2-6a}$$

$$\bar{Y}_{Ckj} = \bar{Y}_{C1} = G_{C1} + j\ B_{C1} \tag{2-6b}$$

$$\bar{Y}_{Ckj} = \bar{Y}_{C2} = G_{C2} + j\ B_{C2} \tag{2-6c}$$

Note that usually

(1) $\bar{Y}$ represents the leakage impedance of a transformer, or the line impedance of a regular transmission line;

(2) for a transformer, $\bar{Y}_{C1} = 0$ and $\bar{Y}_{C2}$ represents the magnetizing admittance;

(3) for a transmission line, $\bar{Y}_{C1} = \bar{Y}_{C2} = \bar{Y}_C/2$, where $\bar{Y}_C$ is the total line charging admittance.

Thus, Fig. 2-3 can represent a general branch between any two buses.

Fi

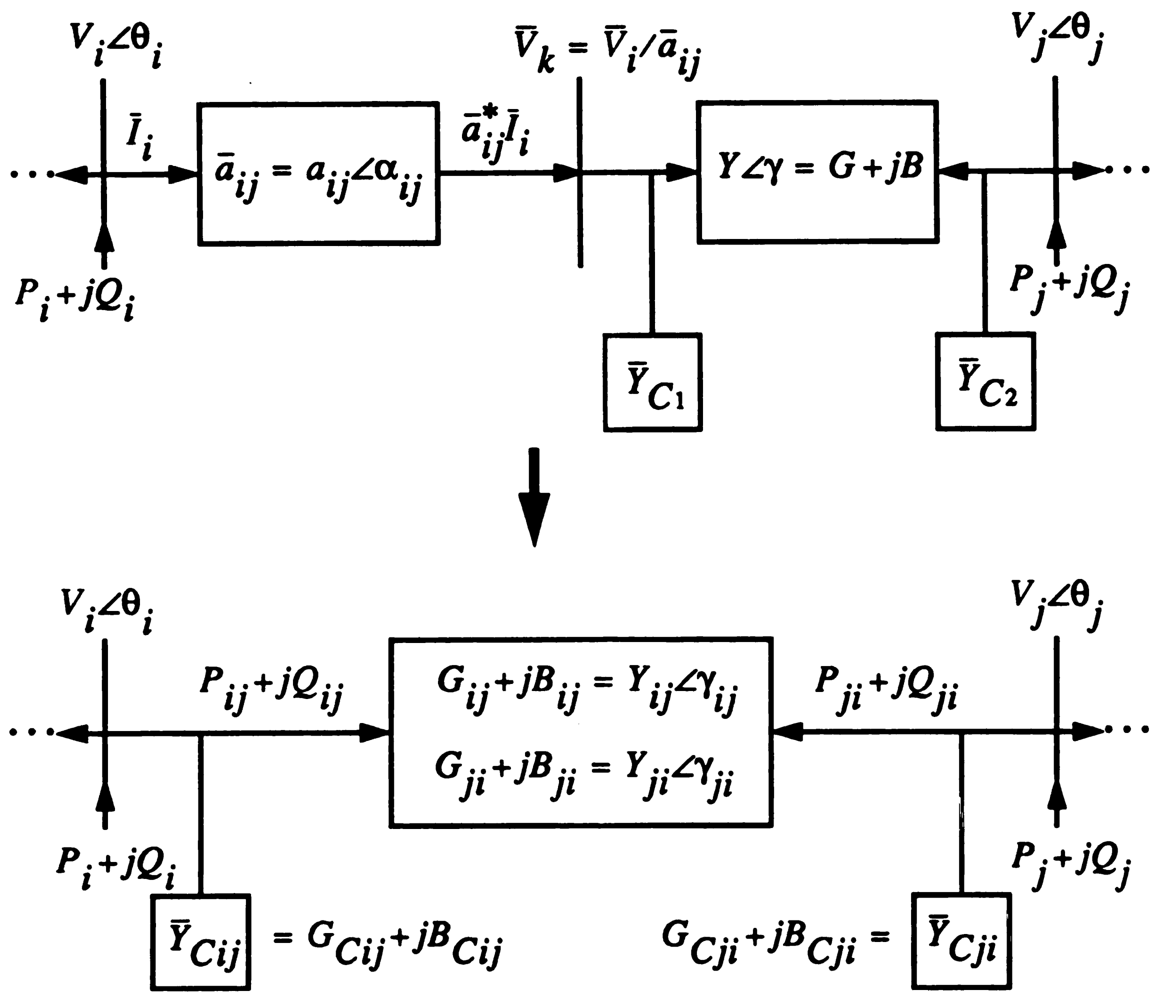

$$\bar{Y}_{ij} = \frac{\bar{Y}}{\bar{a}^*_{ij}} = \frac{Y}{a_{ij}}\angle(\gamma+\alpha_{ij}) = G_{ij}+jB_{ij} \qquad \bar{Y}_{Cij} = \frac{1}{a^2_{ij}}(\bar{Y}_{C1} + (1-\bar{a}_{ij})\bar{Y})$$

$$\bar{Y}_{ji} = \frac{\bar{Y}}{\bar{a}_{ij}} = \frac{Y}{a_{ij}}\angle(\gamma-\alpha_{ij}) = G_{ji}+jB_{ji} \qquad \bar{Y}_{Cji} = \bar{Y}_{C2} + \left(1-\frac{1}{\bar{a}_{ij}}\right)\bar{Y}$$

Fig. 2-3 Equivalent π-circuit of a General Branch Between Two Buses

The current-voltage relationship between bus i and bus j can be derived by considering the relationship between bus k and bus j first:

$$\begin{bmatrix} \bar{a}_{ij}^{*} \bar{I}_i \\ \bar{I}_j \end{bmatrix} = \begin{bmatrix} \bar{Y}_{C1} + \bar{Y} & -\bar{Y} \\ -\bar{Y} & \bar{Y}_{C2} + \bar{Y} \end{bmatrix} \begin{bmatrix} \bar{V}_i / \bar{a}_{ij} \\ \bar{V}_j \end{bmatrix} \tag{2-7a}$$

$$\begin{bmatrix} \bar{I}_i \\ \bar{I}_j \end{bmatrix} = \begin{bmatrix} (\bar{Y}_{C1} + \bar{Y})/a_{ij}^2 & -\bar{Y}/\bar{a}_{ij}^{*} \\ -\bar{Y}/\bar{a}_{ij} & \bar{Y}_{C2} + \bar{Y} \end{bmatrix} \begin{bmatrix} \bar{V}_i \\ \bar{V}_j \end{bmatrix} \tag{2-7b}$$

From (2-7b), we can represent a general branch as an equivalent π-circuit, Fig. 2-2, with the following parameters:

$$\bar{Y}_{ij} = \frac{\bar{Y}}{\bar{a}_{ij}^{*}} = \frac{Y}{a_{ij}} \exp\,[\,j\,(\gamma + \alpha_{ij})\,]$$

$$= Y_{ij} \exp\,(j\ \gamma_{ij}) = G_{ij} + B_{ij} \tag{2-8a}$$

$$\bar{Y}_{ji} = \frac{\bar{Y}}{\bar{a}_{ij}} = \frac{Y}{a_{ij}} \exp\,[\,j\,(\gamma - \alpha_{ij})\,]$$

$$= Y_{ji} \exp\,(j\ \gamma_{ji}) = G_{ji} + B_{ji} \tag{2-8b}$$

$$\bar{Y}_i = \bar{Y}_{Cij} + \bar{Y}_{ij} = \frac{\bar{Y}_{C1} + \bar{Y}}{a_{ij}^2}$$

$$\bar{Y}_{Cij} = \frac{\bar{Y}_{C1} + (1 - \bar{a}_{ij})\,\bar{Y}}{a_{ij}^2} \tag{2-8c}$$

$$\bar{Y}_j = \bar{Y}_{Cji} + \bar{Y}_{ji} = \bar{Y}_{C2} + \bar{Y}$$

$$\bar{Y}_{Cji} = \bar{Y}_{C2} + (1 - \frac{1}{\bar{a}_{ij}})\,\bar{Y} \tag{2-8d}$$

From the above, the following important phenomena is observed:

(1) for a phase shifter, the equivalent π-circuit is completely asymmetric because the transfer admittances, $\bar{Y}_{ij}$ and $\bar{Y}_{ji}$, are different, and the equivalent shunt admittances, $\bar{Y}_{Cij}$ and $\bar{Y}_{Cji}$, are also different.

(2) for a transformer ($\alpha_{ij} = 0$), the equivalent π-circuit is partially asymmetric in that the transfer admittances, $\bar{Y}_{ij}$ and $\bar{Y}_{ji}$, are identical, but the equivalent shunt admittances, $\bar{Y}_{Cij}$ and $\bar{Y}_{Cji}$, are different.

(3) in IEEE Common Format [82], the bus at which its voltage is controlled at specific value by adjusting the tap ratio if the tap ratio is still within its limits, is called controlled bus. If the controlled bus is the tap-side bus, to raise its voltage, the tap ratio is set to be greater than 1.0; to lower its voltage, the tap ratio is set to be less than 1.0. If the controlled bus is the impedance-bus, the setting of tap ratio is reversed.

(4) for a transformer ($\alpha_{ij} = 0$), the magnetizing admittance $\bar{Y}_{C2}$ is approximately zero, so $(-B) \gg B_{C2}$. Thus, from (2-8), it is observed that a transformer has opposite effects on the equivalent shunt admittances, $\bar{Y}_{Cij}$ and $\bar{Y}_{Cji}$. Regardless whether the tap-side bus and the impedance-side bus are step-up and step-down, respectively; or reverse, the step-up side always has capacitive equivalent shunt, and the step-down side always has inductive equivalent shunt. These transformer effects are interesting and important in the problems of voltage collapse and low frequency oscillation [52,53,77].

(5) if $a_{ij} = 1$ and $\alpha_{ij} = 0$, then the dummy bus is no more needed and the original π-circuit (Fig. 2-3) becomes the same representation as the equivalent π-circuit (Fig. 2-2).

(6) after computing all the parameters of the equivalent π-circuit of any general branch, i.e., $\bar{Y}_{ij}$, $\bar{Y}_{ji}$, $\bar{Y}_{Cij}$, and $\bar{Y}_{Cji}$, we can formulate the load flow equations by substituting them into (2-1) - (2-2).

2.3 Load Demand Model

Since the models derived in this dissertation are to be used in the studies of voltage collapse and inter-area oscillation, it can be assumed that frequency deviation is small, and thus the effects of frequency deviation on the load model can be ignored. Then a fairly general load demand model at each bus can be put into a voltage dependent form as follows:

$$P_D = P_L + I_P\ V + G_S\ V^2 + k_P\ V^{n_P} \tag{2-9a}$$

$$Q_D = Q_L + I_Q\ V - B_S\ V^2 + k_Q\ V^{n_Q} \tag{2-9b}$$

where

$P_L + j\ Q_L$	represents constant power load model;
$(I_P + j\ I_Q)\ V$	represents constant current load model;
$(G_S - j\ B_S)\ V^2$	represents constant impedance load model ($B_S < 0$, if inductive; $B_S > 0$, if capacitive);
$k_P\ V^{n_P} + j\ k_Q\ V^{n_Q}$	represents other load model different from the above.

Substituting (2-9) into (2-2), we have the following load flow model.

For each bus i,

$$P_{Gi} - (P_{Li} + I_{Pi}\ V_i + k_{Pi}\ V^{n_{Pi}}) = V_i^2\ [\ G_{Si} + \sum_{j=1}^{n} (G_{Cij} + G_{ij})\ ] - \sum_{j=1}^{n} V_i\ V_j\ T_{ij}$$

$$= V_i^2\ G_{ii} - \sum_{j=1}^{n} V_i\ V_j\ T_{ij}\ \ ;\ j \neq i \tag{2-10a}$$

$$Q_{Gi} - (Q_{Li} + I_{Qi}\ V_i + k_{Qi}\ V^{n_{Qi}}) = -\ V_i^2\ [\ B_{Si} + \sum_{j=1}^{n} (B_{Cij} + B_{ij})\ ] - \sum_{j=1}^{n} V_i\ V_j\ U_{ij}$$

$$= -\ V_i^2\ B_{ii} - \sum_{j=1}^{n} V_i\ V_j\ U_{ij}\ \ ;\ j \neq i \tag{2-10b}$$

where

$$\bar{Y}_{ii} = G_{ii} + j\, B_{ii}$$

with

$$G_{ii} = G_{Si} + \sum_{i=1}^{n} (G_{Cij} + G_{ij}) \;\; ; \;\; j \neq i$$

$$B_{ii} = B_{Si} + \sum_{i=1}^{n} (B_{Cij} + B_{ij}) \;\; ; \;\; j \neq i$$

is the so called self admittance or the diagonal element of Y_{bus} matrix under the assumption that only the combination of constant-current-and-constant-impedance load model is used in the network. Then $-(G_{ij} + j\, B_{ij})$ is the off-diagonal element of Y_{bus} matrix. For a constant impedance load, G_S is nonnegative; but B_S is negative if it is inductive, and positive if capacitive.

Note, from (2-10), that load demand model plays an important role in solving the load flow equations, since it is voltage dependent [46,47].

2.4 Synchronous Machine Model

The synchronous machine model adopted in this dissertation is the single-axis model which is very common for the representation of synchronous machines [26,83,84]. Figure 2-4(a) and Figure 2-4(b) represent its one-line diagram and phasor diagram respectively. The notation is as follows:

$\bar{V}_t$: terminal bus voltage

$\bar{I}_t = I_d + j\, I_q$: current output of the machine at terminal bus

I_d : direct-axis (d-axis) current

I_q : quadrature-axis (q-axis) current

$\delta - \theta_t$: angle difference between internal bus (rotor) and terminal bus

$P_t + j\, Q_t$: power output from the machine at terminal bus

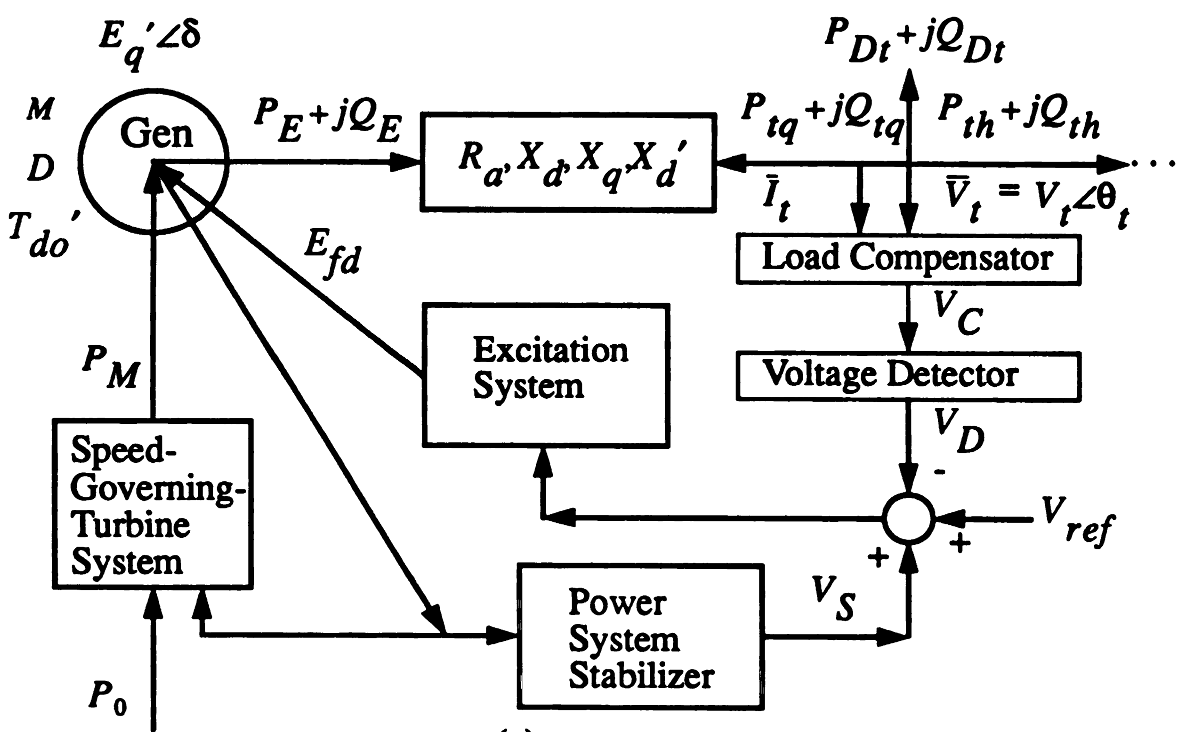

(a)

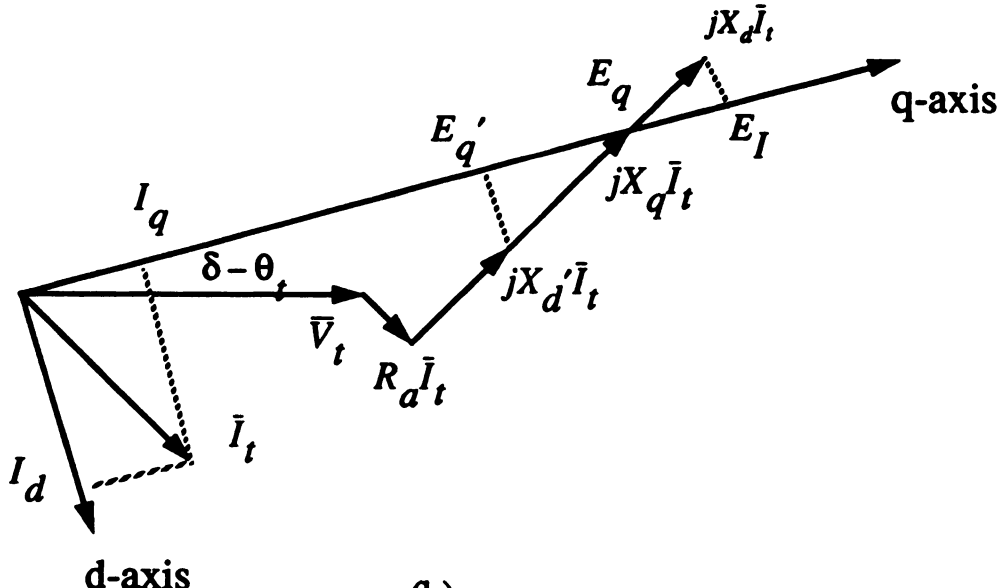

(b)

Fig. 2-4 Synchronous Machine Model

$P_{Dt} + j\ Q_{Dt}$: load demand at terminal bus

$P_{th} + j\ Q_{th}$: power flow from terminal bus to its transformer high-side bus

$P_E + j\ Q_E$: power output from the machine at internal bus

R_a : armature resistance

X_d : d-axis synchronous reactance

X_q : q-axis synchronous reactance

X_d' : d-axis transient reactance

E_q' : internal bus voltage proportional to d-axis flux linkage of field circuit

T_{do}' : d-axis open-circuit transient time constant (sec)

E_{fd} : field voltage of the machine

P_M : mechanical power input to the machine

ω : angular speed of the machine (rad/sec)

H : moment of inertia constant ($MW-sec/MVA$)

$M = 2H/\omega_0$: moment of inertia (sec/(rad/sec))

ω_0 : nominal angular speed (at ω_0)

D : damping constant due to damper winding effects (pu/(rad/sec)).

Note that all the above parameters of each synchronous machine are in per unit (pu) based on machine base, except those with specified units.

The dynamics of the induced stator voltage (at internal bus), E_q', is characterized by the flux decay equation through the open-circuit time constant, T_{do}', and is controlled by the excitation system whose output is the field voltage of the machine, E_{fd}. The angular speed of the unit, ω, is governed by its speed-governor-and-turbine (or simply governor-turbine) system whose output is the mechanical power, P_M. The detailed dynamic models of the synchronous machine and its control systems will be discusse

nous ma

termina

parame

2.4.1

T

from

2.4.7)

powe

wher

discussed later in this section to complete the whole dynamic model of the synchronous machine. Before them, the power balance equations at the internal bus and at the terminal bus are expressed in terms of bus variables (voltage and angle), and branch parameters in the following subsections.

2.4.1 Power Equation at Internal Bus

The power balance equation at internal bus describes the electrical power output from the stator, and its active power output will be used in the swing equation (Section 2.4.7) which expresses the rotor dynamics due to the unbalance between mechanical power input and electrical active power output.

From the phasor diagram shown in Fig. 2-4(b), we can obtain:

$$E_q' - V_t \cos(\delta - \theta_t) = R_a I_q + X_d' I_d$$

$$V_t \sin(\delta - \theta_t) + R_a I_d = X_q I_q$$

$$I_d = \frac{X_q [E_q' - V_t \cos(\delta - \theta_t)] - R_a V_t \sin(\delta - \theta_t)}{R_a^2 + X_d' X_q}$$

$$= - E_q' B_q - V_t U_{qt} \tag{2-11a}$$

$$I_q = \frac{R_a [E_q' - V_t \cos(\delta - \theta_t)] + X_d' V_t \sin(\delta - \theta_t)}{R_a^2 + X_d' X_q}$$

$$= E_q' G_a - V_t T_{dt} \tag{2-11b}$$

where

$$T_{dt} = G_a \cos(\delta - \theta_t) + B_d' \sin(\delta - \theta_t) \tag{2-12a}$$

$$U_{qt} = G_a \sin(\delta - \theta_t) - B_q \cos(\delta - \theta_t) \tag{2-12b}$$

$$G_a = \frac{R_a}{R_a^2 + X_d' X_q} \;\; ; \;\; B_d' = \frac{-X_d'}{R_a^2 + X_d' X_q} \;\; ; \;\; B_q = \frac{-X_q}{R_a^2 + X_d' X_q} \tag{2-13}$$

The electrical power output at internal bus (for the swing equation (see Section 2.4.7)) is

$$P_E + j\,Q_E = \bar{E}_q\,\vec{I}_t^{\,*} = j\,E_q\,(I_d + j\,I_q)^* = E_q\,I_q + j\,E_q\,I_d \tag{2-14}$$

$$E_q = E_q' + (\,X_q - X_d'\,)\,I_d$$

$$P_E = E_q\,I_q = E_q'\,I_q + (X_q - X_d')\,I_d\,I_q \tag{2-14a}$$

$$Q_E = E_q\,I_d = E_q'\,I_d + (\,X_q - X_d'\,)\,I_d^2 \tag{2-14b}$$

Substituting (2-11) into (2-14), we have

$$P_E = E_q'^2\,G_{EE} - E_q'\,V_t\,T_{PE} + V_t^2\,G_{Et} \tag{2-15a}$$

$$Q_E = -\,E_q'^2\,B_{EE} - E_q'\,V_t\,U_{QE} - V_t^2\,B_{Et} \tag{2-15b}$$

where

$$G_{EE} = k_1\,G_a \;\;;\;\; k_1 = 1 - (X_q - X_d')\,B_q > 1$$

$$T_{PE} = k_1\,T_{dt} + G_a\,(X_q - X_d')\,U_{qt}$$

$$= G_{PE}\,\cos(\delta - \theta_t) + B_{PE}\,\sin(\delta - \theta_t)$$

$$G_{PE} = k_2\,G_a \;\;;\;\; k_2 = 1 - 2\,(X_q - X_d')\,B_q > 1$$

$$B_{PE} = k_1\,B_d' + G_a^2\,(X_q - X_d')$$

$$G_{Et} = (X_q - X_d')\,T_{dt}\,U_{qt}$$

$$B_{EE} = k_1\,B_q$$

$$U_{QE} = k_2\,U_{qt} = G_{QE}\,\sin(\delta - \theta_t) - B_{QE}\,\cos(\delta - \theta_t)$$

$$G_{QE} = k_2\,G_a = G_{PE}$$

$$B_{QE} = k_2\,B_q$$

$$B_{Et} = -\,(X_q - X_d')\,U_{qt}^2$$

2.4.2 Power Equation at Terminal Bus

It is observed, from Fig. 2-4(a), that the power balance equation at the terminal bus have three components: (1) net power injection which is the negative sign of the local load demand, $P_{Dt} + j\,Q_{Dt}$; (2) power flow from the terminal bus to its high-side bus through a step-up transformer, $P_{th} + j\,Q_{th}$, whose model has been shown in Section 2.2; (3) power flow from the terminal bus to the internal bus, $P_{tq} + j\,Q_{tq}$, which is the negative sign of the power sent from the internal bus and received at the terminal bus, $-(P_{Gt} + j\,Q_{Gt})$.

Thus, from Fig. 2-4 and (2-11) - (2-13), we have

$$P_{Gt} + j\,Q_{Gt} = \bar{V}_t\,\bar{I}_t^{\,*}$$

$$P_{Gt} = V_t\,\sin(\delta - \theta_t)\,I_d + V_t\,\cos(\delta - \theta_t)\,I_q$$

$$P_{tq} = -\,P_{Gt} = V_t^2\,G_{tq} - V_t\,E_q'\,T_{tq} \tag{2-16a}$$

$$Q_{Gt} = V_t\,\cos(\delta - \theta_t)\,I_d - V_t\,\sin(\delta - \theta_t)\,I_q$$

$$Q_{tq} = -\,Q_{Gt} = -\,V_t^2\,B_{tq} - V_t\,E_q'\,U_{tq} \tag{2-16b}$$

where

$$\begin{aligned} T_{tq} &= G_a\,\cos(\delta - \theta_t) - B_q\,\sin(\delta - \theta_t) \\ &= G_a\,\cos(\theta_t - \delta) + B_q\,\sin(\theta_t - \delta) \end{aligned} \tag{2-17a}$$

$$\begin{aligned} U_{tq} &= -\,G_a\,\sin(\delta - \theta_t) - B_q\,\cos(\delta - \theta_t) \\ &= G_a\,\sin(\theta_t - \delta) - B_q\,\cos(\theta_t - \delta) \end{aligned} \tag{2-17b}$$

$$\begin{aligned} G_{tq} &= U_{qt}\,\sin(\delta - \theta_t) + T_{dt}\,\cos(\delta - \theta_t) \\ &= G_a - (B_d' - B_q)\,\sin(\theta_t - \delta)\,\cos(\theta_t - \delta) \end{aligned} \tag{2-18a}$$

$$\begin{aligned} B_{tq} &= T_{dt}\,\sin(\delta - \theta_t) - U_{qt}\,\cos(\delta - \theta_t) \\ &= B_d'\,\sin^2(\theta_t - \delta) + B_q\,\cos^2(\theta_t - \delta) \end{aligned} \tag{2-18b}$$

Note that since $B_d^{'}$ ($X_d^{'}$) and B_q (X_q) are different, both G_{tq} and B_{tq} are functions of the angle difference between the terminal bus and the internal bus, $\theta_t - \delta$.

2.4.3 Flux Decay Equation

The internal bus voltage, $E_q^{'}$, is the induced stator voltage through the flux linkage from the field winding with field voltage E_{fd} at the rotor of a synchronous machine. For the single-axis machine model, the dynamics of $E_q^{'}$ is governed by the following flux decay equation through the d-axis open-circuit transient time constant, $T_{do}^{'}$.

$$T_{do}^{'} \dot{E}_q^{'} = E_{fd} - E_I = E_{fd} - [\, E_q^{'} + (X_d - X_d^{'}) I_d \,] \tag{2-19a}$$

Substituting (2-11) into (2-19a), we can express the flux decay equation in terms of bus variables (voltage and angle):

$$T_{do}^{'} \dot{E}_q^{'} = E_{fd} - K_{E3} E_q^{'} + (X_d - X_d^{'}) U_{qt} V_t \tag{2-19b}$$

where

$$K_{E3} = 1 - (X_d - X_d^{'}) B_q > 1$$

We can also describe the flux decay dynamics as a function of reactive power generation at the internal bus, Q_E, by substituting (2-14b):

$$I_d = \frac{- E_q^{'} + \sqrt{E_q^{'2} + 4 (X_q - X_d^{'}) Q_E}}{2 (X_q - X_d^{'})}$$

$$T_{do}^{'} \dot{E}_q^{'} = E_{fd} - [\, 1 - \frac{X_d - X_d^{'}}{2 (X_q - X_d^{'})} \,] E_q^{'}$$

$$- \frac{X_d - X_d^{'}}{2 (X_q - X_d^{'})} \sqrt{E_q^{'2} + 4 (X_q - X_d^{'}) Q_E} \tag{2-19c}$$

This expression has been used in [52,53] to see the role of Q_E in the problem of voltag

that X

2.4

tag

tag

IEI

use

der

2

7

voltage collapse due to the instability of the flux decay dynamics under the assumption that $X_q = X_d'$:

$$I_d = \frac{Q_E}{E_q'}$$

$$T_{do}' \dot{E}_q' = E_{fd} - E_q' - (X_d - X_d') \frac{Q_E}{E_q'}$$

2.4.4 Excitation System Model

For adjusting the generator field voltage, E_{fd}, in order to control the terminal voltage properly, there are many control schemes to do so. Basically, the terminal voltage and/or current feedback has been applied. A typical excitation control model is IEEE Type DC1 Excitation System Model [85], as shown in Fig. 2-5(a) that will be used in this dissertation. Most of other types of excitation control model can be derived from this IEEE-DC1 excitation system model.

The notation is as follows:

V_C: output of load (or line-drop) compensator (see Section 2.4.5)

V_S: output of power system stabilizer (PSS) (see Section 2.4.6)

V_{ref}: reference (set point) voltage

V_D: output of voltage detector

K_D: DC (Direct Current) gain of voltage detector

T_D: time constant of voltage detector

TGR: transient gain reduction

T_B: lagging time constant of TGR

T_C: leading time constant of TGR

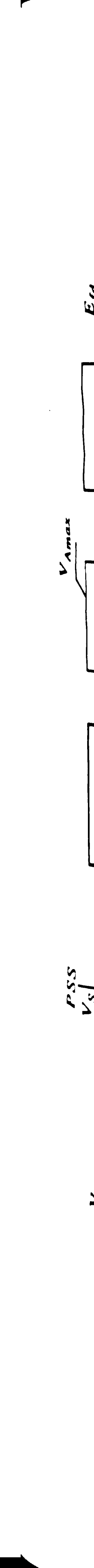

PSS
V_s
V_{Amax}

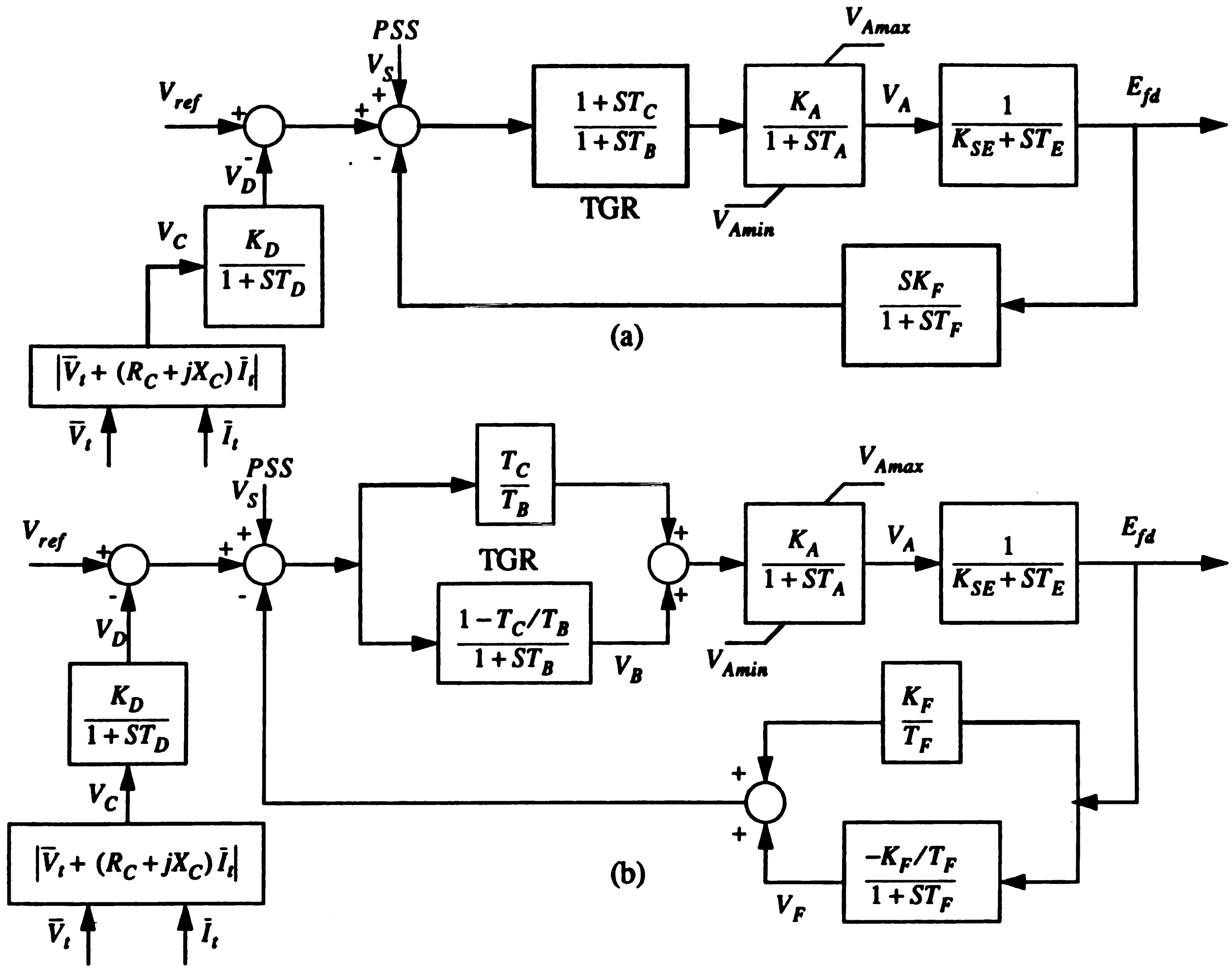

Fig. 2-5 IEEE - DC1 Excitation System Model

V_A

K_A

T_A

E

can

lel

IEI

$$\begin{bmatrix} T \\ T \\ T \\ T \\ T \end{bmatrix}$$

V_A: output of automatic voltage regulator (AVR)

K_A: DC gain of AVR

T_A: time constant of AVR

E_{fd}: output of exciter or excitation system (field voltage of synchronous machine)

$1/K_{SE}$: DC gain of exciter (Note: K_{SE} is function of the saturation effect of exciter)

T_E/K_{SE}: time constant of exciter

K_F: washout gain of stabilizing feedback of excitation system

T_F: washout time constant of stabilizing feedback of excitation system

In order to transfer the above excitation system model into state space form, we can express both lead-lag and wash-out transfer function blocks as a gain block parallel to a lagging block, as shown in Fig. 2-5(b). Then the state space form of the IEEE-DC1 excitation system model is as follows:

$$\begin{bmatrix} T_D\,\dot{V}_D \\ T_F\,\dot{V}_F \\ T_A\,\dot{V}_A \\ T_B\,\dot{V}_B \\ T_E\,\dot{E}_{fd} \end{bmatrix} = \begin{bmatrix} -1 & 0 & 0 & 0 & 0 \\ 0 & -1 & 0 & 0 & -K_F/T_F \\ -K_A\,T_C/T_B & -K_A\,T_C/T_B & -1 & K_A & -K_A\,(T_C/T_B)\,(K_F/T_F) \\ -(1-T_C/T_B) & -(1-T_C/T_B) & 0 & -1 & -(1-T_C/T_B)\,K_F/T_F \\ 0 & 0 & 1 & 0 & -K_{SE} \end{bmatrix}$$

$$\cdot \begin{bmatrix} V_D \\ V_F \\ V_A \\ V_B \\ E_{fd} \end{bmatrix} + \begin{bmatrix} K_D\,V_C \\ 0 \\ K_A\,(T_C/T_B)\,(V_{ref}+V_S) \\ (1-T_C/T_B)\,(V_{ref}+V_S) \\ 0 \end{bmatrix} \tag{2-20}$$

2.4.5 Load Compensator Model

This section and next one will respectively describe the models of the common accessory functions of excitation systems, load compensator and power system stabilizer [85]. Load compensator usually uses the terminal voltage (and current) as feedback measurement of the excitation system model. The block diagram of a load compensator is shown in Fig. 2-6(a). Fig. 2-6(b) shows its phasor diagram.

From the phasor diagram, we have

$$\bar{V}_C = \bar{V}_t + (R_C + j\,X_C)\,\bar{I}_t = V_{Cd} + j\,V_{Cq}$$

$$= V_t\,\sin(\delta - \theta_t) + j\,V_t\,\cos(\delta - \theta_t)$$

$$+ (R_C + j\,X_C)\,(I_d + j\,I_q)$$

Substituting (2-11) for I_d and I_q, we obtain

$$V_{Cd} = V_t\,\sin(\delta - \theta_t) + R_C\,(-E_q'\,B_q - V_t\,U_{qt}) - X_C\,(E_q'\,G_a - V_t\,T_{dt})$$

$$= K_{d2}\,E_q' + K_{d7}\,V_t \qquad (2\text{-}21a)$$

$$V_{Cq} = V_t\,\cos(\delta - \theta_t) + R_C\,(E_q'\,G_a - V_t\,T_{dt}) + X_C\,(-E_q'\,B_q - V_t\,U_{qt})$$

$$= K_{q2}\,E_q' + K_{q7}\,V_t \qquad (2\text{-}21b)$$

$$V_C = \sqrt{V_{Cd}^2 + V_{Cq}^2} \qquad (2\text{-}21c)$$

where,

$$K_{d2} = -(X_C\,G_a + R_C\,B_q)$$

$$K_{q2} = R_C\,G_a - X_C\,B_q$$

$$K_{d7} = (1 + X_C\,B_d' - R_C\,G_a)\,\sin(\delta - \theta_t) - K_{d2}\cos(\delta - \theta_t)$$

$$K_{q7} = (1 - K_{q2})\cos(\delta - \theta_t) - (X_C\,G_a + R_C\,B_d')\,\sin(\delta - \theta_t)$$

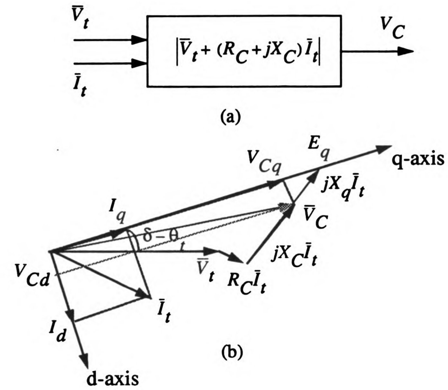

$$\bar{V}_C = \bar{V}_t + (R_C + jX_C)\bar{I}_t = V_{Cd} + jV_{Cq}$$

$$V_{Cd} = K_{d2}E_q' + K_{d7}V_t$$

$$V_C = \sqrt{V_{Cd}^2 + V_{Cq}^2}$$

$$V_{Cq} = K_{q2}E_q' + K_{q7}V_t$$

$$K_{d2} = -(X_C G_a + R_C B_q) \qquad K_{q2} = R_C G_a - X_C B_q$$

$$K_{d7} = (1 + X_C B_d' - R_C G_a)\sin(\delta - \theta_t) + (X_C G_a + R_C B_q)\cos(\delta - \theta_t)$$

$$K_{q7} = (1 + X_C B_q - R_C G_a)\cos(\delta - \theta_t) - (X_C G_a + R_C B_d')\sin(\delta - \theta_t)$$

Fig. 2-6 Load Compensator Model

V_C

tra

wh

2-5

R_C

ho

[85

in

is

dif

2.

bil

na

ch

me

ac

as

Note that when load compensator is not employed ($R_C = 0$, $X_C = 0$), then $V_C = V_t$. In other words, the magnitude of terminal voltage is sensed and is transferred to be a DC (direct current) quantity, then is fed into the voltage detector whose filtering can usually be modeled as a very small time constant ($T_D \approx 0$ in Fig. 2-5(a)).

On the other hand, when load compensator is desired, the appropriate values of R_C and X_C are entered. Both R_C and X_C can be positive or negative, depending on how the synchronous machine is connected to other units and to the power system [85], and how the synchronous machine is set to control the voltage of a certain point in the system. In most case, the R_C component is negligible and only a value for X_C is required. For these cases, the coefficients, K_{d7} and K_{q7}, are functions of the angle difference, $\delta - \theta_t$, so is the load compensator voltage, V_C.

2.4.6 Power System Stabilizer Model

The function of power system stabilizer (PSS) is mainly to improve dynamic stability of a synchronous machine and/or power system, using other regulator input signals in addition to terminal voltage through its excitation system. These signals are chosen to provide positive damping to oscillations. Figure 2-7(a) shows the general model of such a power system stabilizer. Some common stabilizer input signals are: accelerating power, speed, frequency, and terminal voltage [85].

Transferring the lead-lag blocks and washout block into first order lagging blocks, as shown in Fig. 2-7(b), we have the state space form for PSS model.

$$\begin{bmatrix} T_S \dot{V}_{S0} \\ T_{S2} \dot{V}_{S2} \\ T_{S4} \dot{V}_{S4} \end{bmatrix} = \begin{bmatrix} -1 & 0 & 0 \\ 1 - T_{S1}/T_{S2} & -1 & 0 \\ (1 - T_{S3}/T_{S4})(T_{S1}/T_{S2}) & 1 - T_{S3}/T_{S4} & -1 \end{bmatrix} \begin{bmatrix} V_{S0} \\ V_{S2} \\ V_{S4} \end{bmatrix}$$

v_{SI}
$K_S T_S S$
$1 + T_{S1} S$
$1 + T_{S3} S$
v_S

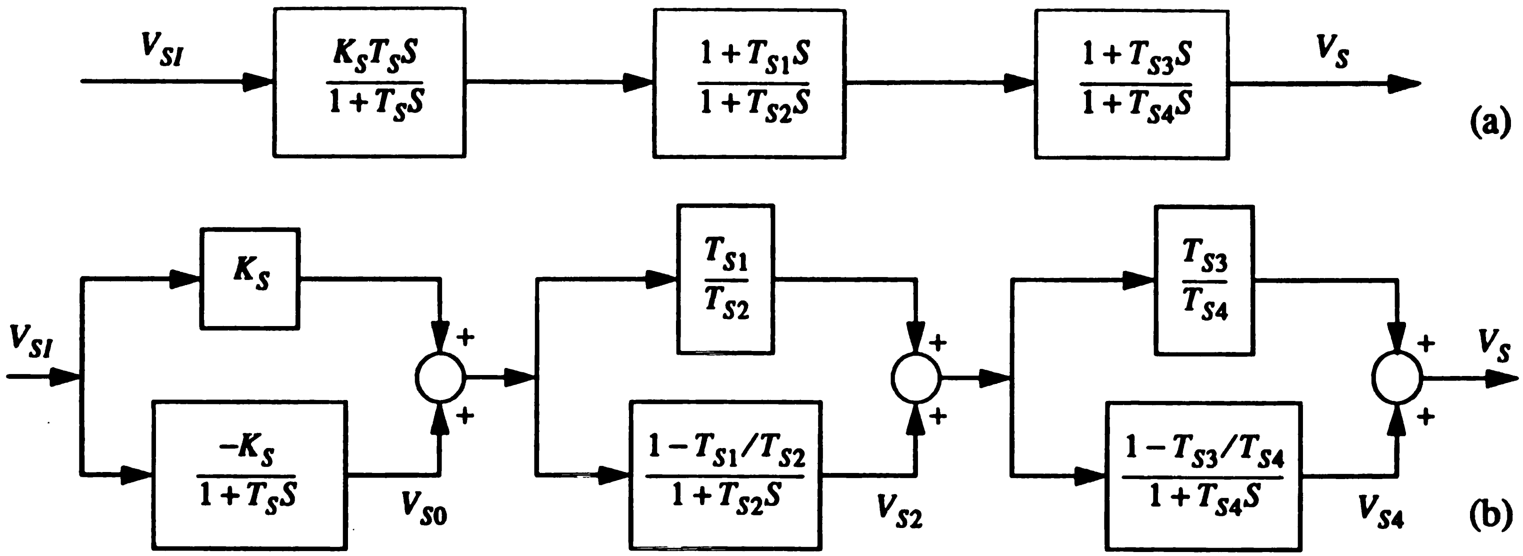

$$\begin{pmatrix} T_S\dot{V}_{S0} \\ T_{S2}\dot{V}_{S2} \\ T_{S4}\dot{V}_{S4} \end{pmatrix} = \begin{pmatrix} -1 & 0 & 0 \\ \left(1-\frac{T_{S1}}{T_{S2}}\right) & -1 & 0 \\ \left(1-\frac{T_{S3}}{T_{S4}}\right)\frac{T_{S1}}{T_{S2}} & \left(1-\frac{T_{S3}}{T_{S4}}\right) & -1 \end{pmatrix} \begin{pmatrix} V_{S0} \\ V_{S2} \\ V_{S4} \end{pmatrix} + \begin{pmatrix} -K_S \\ \left(1-\frac{T_{S1}}{T_{S2}}\right)K_S \\ \left(1-\frac{T_{S3}}{T_{S4}}\right)\frac{T_{S1}}{T_{S2}}K_S \end{pmatrix} V_{SI}$$

$$V_S = \frac{T_{S3}}{T_{S4}}\frac{T_{S1}}{T_{S2}}K_S V_{SI} + \frac{T_{S3}}{T_{S4}}\frac{T_{S1}}{T_{S2}}V_{S0} + \frac{T_{S3}}{T_{S4}}V_{S2} + V_{S4}$$

Fig. 2-7 Power System Stabilizer Model

$$+ \begin{bmatrix} -K_S \\ (1 - T_{S1}/T_{S2})\, K_S \\ (1 - T_{S3}/T_{S4})\, (T_{S1}/T_{S2})\, K_S \end{bmatrix} V_{SI}$$

$$V_S = \frac{T_{S3}}{T_{S4}} \frac{T_{S1}}{T_{S2}} K_S\, V_{SI} + \frac{T_{S3}}{T_{S4}} \frac{T_{S1}}{T_{S2}} V_{S0} + \frac{T_{S3}}{T_{S4}} V_{S2} + V_{S4} \quad (2\text{-}22)$$

2.4.7 Swing Equation

The mechanical dynamics of a synchronous generator is at the rotor of this unit. The motion of the rotor is due to the acceleration torque/power, mainly which is the difference between the mechanical power input to the rotor and the electrical power induced in the stator. The acceleration power will be used:

(1) to change the kinetic energy, or angular speed, of the unit;

(2) to overcome the damping power that develops mainly in the damper windings and in the form of mechanical frictions.

Equation (2-23) is the so called swing equation which describes the above phenomena:

$$\frac{d\, W_K}{d\, t} + T_d = T_M - T_E \quad (2\text{-}23a)$$

$$\frac{2\, H}{\omega_0} \frac{d^2\, \delta}{d\, t^2} + D\, \frac{d\, \delta}{d\, t} = P_M - P_E \quad (2\text{-}23b)$$

$$\frac{d\, \delta}{d\, t} = \omega - \omega_0 \quad (2\text{-}23c)$$

where,

$T =$ $\omega_0 P$: T represents torque, and P represents power;

ω_0: nominal angular speed (*rad*/sec);

P_M: mechanical power input to the rotor (*pu*);

P_E: equivalent electrical power output from the rotor (pu), which includes the power loss due to armature effect and the power received at the terminal bus ($P_{Gt} + j\ Q_{Gt}$, see Section 2.4.2);

P_d: damping power (pu);

$W_K = (W_{K0}/S_{3b})\ (\omega^2/\omega_0^2)$: total kinetic energy of the generator and turbine (pu−sec);

W_{K0}: nominal W_K (at ω_0);

S_{3b}: 3-phase MVA base;

$H = W_{k0}/S_{3b}$: per unit inertia constant (sec);

ω: angular speed (rad/sec);

δ: the angular rotor position, measured in electrical radians of the rotor relative to a synchronously rotating reference (rad);

t: time (sec);

D: approximate damping coefficient (pu/(rad/sec)).

$M = 2\ H/\omega_0$: moment of inertia (sec/(rad/sec))

2.4.8 Speed-Governing-Turbine System Model

The mechanical power P_M is controlled by the speed-governing system through turbine system, using rotor speed as an input signal. Even though there are mechanical-hydraulic control (MHC) and electro-hydraulic control (EHC) types of speed-governing system, basically, their models are very similar. Figure 2-8(a) and Figure 2-8(b) are the general models of speed-governing system for steam-turbine and hydro-turbine, respectively [86].

P_{GV} is the power at gate or valve and is the input of turbine system. The general models of steam-turbine and hydro-turbine systems are shown in Fig. 2-8(c) and Fig.

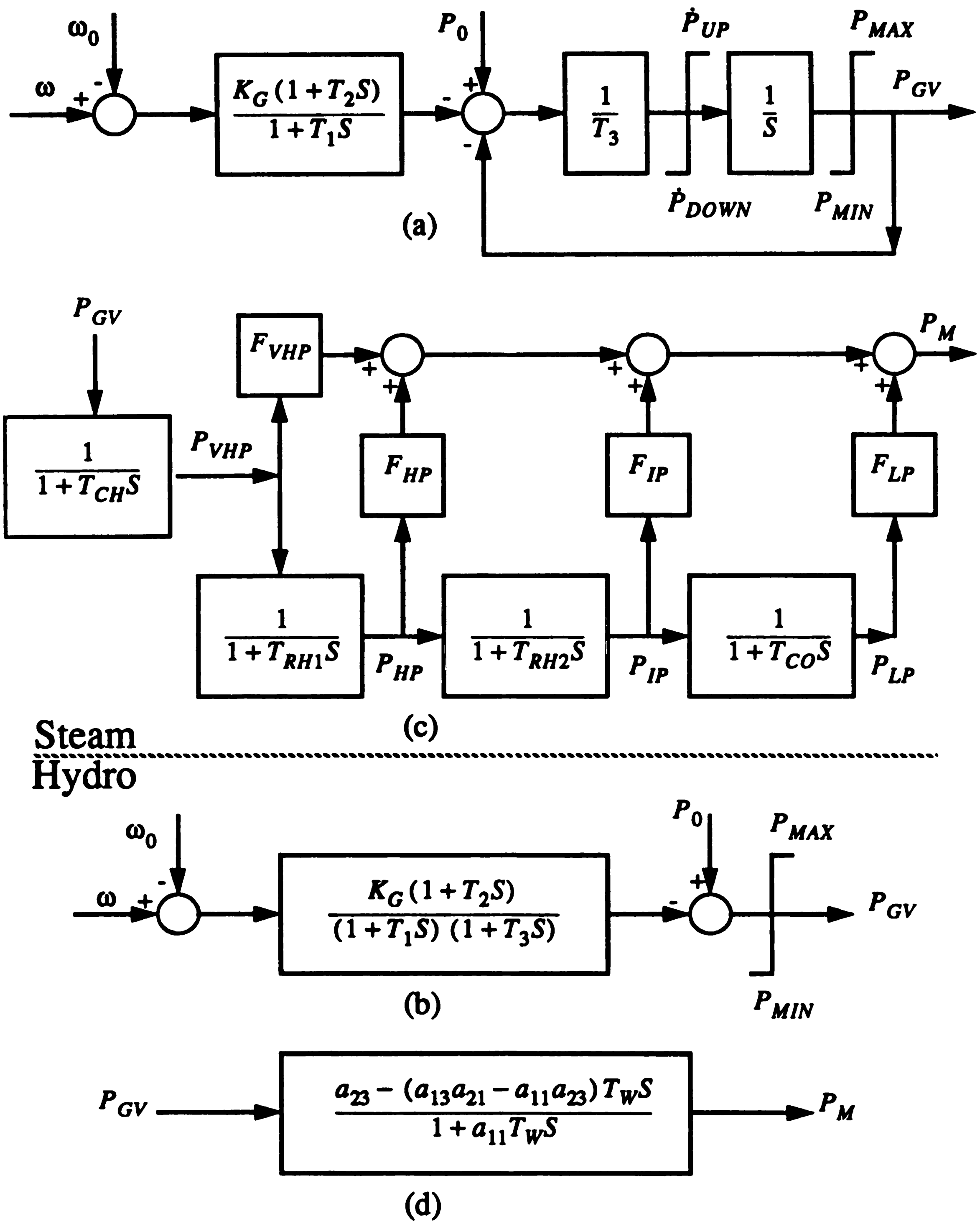

Fig 2-8 Speed-Governing-Turbine System Model

2-8

gov

ten

(a)

(

2-8(d), respectively [86].

After transferring the lead-lag blocks into first-order lagging blocks in the speed-governing and turbine systems, the state space model of speed-governing-turbine system can be obtained by combining their models together.

(a) Steam Governor-Turbine

$$\begin{bmatrix} T_1 \dot{P}_1 \\ T_3 \dot{P}_{GV} \\ T_{CH} \dot{P}_{VHP} \\ T_{RH1} \dot{P}_{HP} \\ T_{RH2} \dot{P}_{IP} \\ T_{CO} \dot{P}_{LP} \end{bmatrix} = \begin{bmatrix} -1 & 0 & 0 & 0 & 0 & 0 \\ -1 & -1 & 0 & 0 & 0 & 0 \\ 0 & 1 & -1 & 0 & 0 & 0 \\ 0 & 0 & 1 & -1 & 0 & 0 \\ 0 & 0 & 0 & 1 & -1 & 0 \\ 0 & 0 & 0 & 0 & 1 & -1 \end{bmatrix} \begin{bmatrix} P_1 \\ P_{GV} \\ P_{VHP} \\ P_{HP} \\ P_{IP} \\ P_{LP} \end{bmatrix}$$

$$+ \begin{bmatrix} K_G \, (1 - T_2/T_1) \, (\omega - \omega_0) \\ -K_G \, (T_2/T_1) \, (\omega - \omega_0) + P_0 \\ 0 \\ 0 \\ 0 \\ 0 \end{bmatrix}$$

$$P_M = F_{VHP} \, P_{VHP} + F_{HP} \, P_{HP} + F_{IP} \, P_{IP} + F_{LP} \, P_{LP} \qquad \text{(2-24a)}$$

(b) Hydraulic Governor-Turbine

$$\begin{bmatrix} T_1 \dot{P}_1 \\ T_3 \dot{P}_{GV} \\ T_W \dot{P}_W \end{bmatrix} = \begin{bmatrix} -1 & 0 & 0 \\ -1 & -1 & 0 \\ 0 & a_{WG} & -a_{WW} \end{bmatrix} \begin{bmatrix} P_1 \\ P_{GV} \\ P_W \end{bmatrix}$$

$$+ \begin{bmatrix} K_G \, (1 - T_2/T_1) \, (\omega - \omega_0) \\ -K_G \, (T_2/T_1) \, (\omega - \omega_0) + P_0 \\ 0 \end{bmatrix}$$

$$P_M = F_{GV} \, P_{GV} + P_W \qquad \text{(2-24b)}$$

$$a_{WG} = a_{13} \, a_{21} / a_{11}^2 \;\; ; \;\; a_{WW} = 1/a_{11} \;\; ; \;\; F_{GV} = a_{23} - \frac{a_{13} \, a_{21}}{a_{11}}$$

2.5 Equilibrium point of Power System Dynamic Model

This section will organize the models derived in the previous sections to clearly describe the dynamic model of a power system, and to discuss obtaining its equilibrium point(s).

Without loss of generality, it is assumed that the connection between the terminal bus of a synchronous machine and its high-side bus is equivalently one-to-one, as shown in Fig. 2-1, and that the power system has n buses, including m machines with m high-side buses, and $n-m$ other (load) buses. From previous derivation, the dynamics of the power system can be described by the differential equations associated with rotor dynamics and control system dynamics, and the algebraic equations associated with active power and reactive power balance (load flow) equations, as follows.

(a) Swing Equation:

For each synchronous machine, from (2-23),

$$\dot{\delta} = \omega - \omega_0 \tag{2-25a}$$

$$M\ \dot{\omega} = -D\ (\omega - \omega_0) - P_E + P_M \tag{2-25b}$$

where P_M is the mechanical power output from the speed-governing-turbine system of the unit (see (2-24)).

(b) Flux Decay Equation:

For each synchronous machine, from (2-19),

$$T_{do}^{'}\ \dot{E}_q^{'} = E_{fd} - K_{E3}\ E_q^{'} + (\ X_d - X_d^{'}\ )\ U_{qt}\ V_t \tag{2-26}$$

$$K_{E3} = 1 - (\ X_d - X_d^{'}\ )\ B_q > 1$$

$$U_{qt} = G_a\ \sin(\delta - \theta_t) - B_q\ \cos(\delta - \theta_t)$$

where, E_{fd} is the output of the excitation system of the unit (see (2-20) - (2-22)).

(c) Algebraic Load Flow Equation:

[1] At internal bus, for each synchronous machine, from (2-15),

$$P_E = E_q'^2 \, G_{EE} - E_q' \, V_t \, T_{PE} + V_t^2 \, G_{Et} \tag{2-27a}$$

$$Q_E = - E_q'^2 \, B_{EE} - E_q' \, V_t \, U_{QE} - V_t^2 \, B_{Et} \tag{2-27b}$$

The expressions of parameters are listed in (2-15).

[2] At terminal bus, $t = n + 1, \cdots, n + m; \; h = 1, \cdots, m$, from (2-16),

$$\begin{aligned} - P_{Dt} &= P_{tq} + P_{ht} \\ &= V_t^2 \, G_{tq} - V_t \, E_q' \, T_{tq} + V_t^2 \, (G_{Cth} + G_{th}) - V_t \, V_h \, T_{th} \end{aligned} \tag{2-28a}$$

$$\begin{aligned} - Q_{Dt} &= Q_{tq} + Q_{ht} \\ &= - V_t^2 \, B_{tq} - V_t \, E_q' \, U_{tq} - V_t^2 \, (B_{Cth} + B_{th}) - V_t \, V_h \, U_{th} \end{aligned} \tag{2-28b}$$

The expressions of T_{tq}, U_{tq}, G_{tq}, and B_{tq} can be found in (2-17) and (2-18). The expressions of T_{th} and U_{th} are similar to those of T_{tq} and U_{tq}, as follows:

$$T_{th} = G_{th} \cos(\theta_t - \theta_h) + B_{th} \sin(\theta_t - \theta_h) \tag{2-29a}$$

$$U_{th} = G_{th} \sin(\theta_t - \theta_h) - B_{th} \cos(\theta_t - \theta_h) \tag{2-29b}$$

[3] At high-side bus, $h = 1, \cdots, m; \; t = n + h$, from (2-1) and (2-16),

$$\begin{aligned} - P_{Dh} &= V_h^2 \, (G_{Cht} + G_{ht}) - V_h \, V_t \, T_{ht} \\ &\quad + V_h^2 \sum_{j=1}^{n} (G_{Chj} + G_{hj}) - \sum_{j=1}^{n} V_h \, V_j \, T_{hj} \quad , \; j \neq h \end{aligned} \tag{2-30a}$$

$$\begin{aligned} - Q_{Dh} &= - V_h^2 \, (B_{Cht} + B_{ht}) - V_h \, V_t \, U_{ht} \\ &\quad - V_h^2 \sum_{j=1}^{n} (B_{Chj} + B_{hj}) - \sum_{j=1}^{n} V_h \, V_j \, U_{hj} \quad , \; j \neq h \end{aligned} \tag{2-30b}$$

[4] At load bus, $i = m + 1, \cdots, n$, from (2-1),

$$- P_{Di} = V_i^2 \sum_{j=1}^{n} (G_{Cij} + G_{ij}) - \sum_{j=1}^{n} V_i \, V_j \, T_{ij} \quad , \; j \neq i \tag{2-31a}$$

ma

era

dy

igr

wh

tim

the

sta

an

po

ma

of

the

ou

ha

to

po

Fo

$$- Q_{Di} = - V_i^2 \sum_{j=1}^{n} (B_{Cij} + B_{ij}) - \sum_{j=1}^{n} V_i \, V_j \, U_{ij} \quad , \; j \neq i \tag{2-31b}$$

Note that in the load flow equations, the load demand at each bus $P_D + j\,Q_D$ may be function of its bus voltage, see (2-9), and that we have used the following general formulas.

$$T_{ij} = G_{ij} \cos(\theta_i - \theta_j) + B_{ij} \sin(\theta_i - \theta_j) \quad , \; j \neq i \tag{2-32a}$$

$$U_{ij} = G_{ij} \sin(\theta_i - \theta_j) - B_{ij} \cos(\theta_i - \theta_j) \quad , \; j \neq i \tag{2-32b}$$

The above power system dynamic model is nonlinear, except the control system dynamics of governor-turbine systems and excitation systems, if their limits are ignored. The equilibrium point(s) can be solved by the set of algebraic equations which include the load flow algebraic equations and those obtained by setting all the time derivative terms in dynamic equations to be zero. This is equivalent to solve for the steady state operating condition of the power system dynamic model. At steady state, each synchronous machine can be equivalently represented by single-axis model, and its control systems are represented by their D.C. gains. Note that the reactive power output equation at internal bus is only a "side-output" output the synchronous machine, and has to be replaced by the algebraic equation governored by the D.C. gain of excitation control K_A / K_{SE} and voltage set point V_{ref}. Since at steady state $\omega = \omega_0$, the electrical active power output P_E at the internal bus is the same as the mechanical output P_M or the set point P_0 of the speed-governing-turbine system which does not have any effects on the equilibrium point, neither does the power system stabilizer due to its washout characteristics. Thus, the set of algebraic equation for the equilibrium point(s) can be described as follows.

For m machines:

$$\omega = \omega_0 \tag{2-33a}$$

$$P_0 = P_M = P_E$$

$$= E_q'^2\, G_{aP} - E_q'\, V_t\, T_P + V_t^2\, G_{tP} \tag{2-33b}$$

$$E_{fd} = \frac{K_A}{K_{SE}}\,(V_{ref} - K_D\, V_C + V_S)$$

$$= K_{E3}\, E_q' - (X_d - X_d')\, U_{qt}\, V_t \tag{2-34a}$$

$$V_S = 0 \tag{2-34b}$$

$$V_C = \sqrt{(K_{d2}\, E_q' + K_{d7}\, V_t)^2 + (K_{q2}\, E_q' + K_{q7}\, V_t)^2} \tag{2-34c}$$

$$-P_{Dt} = V_t^2\, G_{tq} - V_t\, E_q'\, T_{tq} + V_t^2\,(G_{Cth} + G_{th}) - V_t\, V_h\, T_{th} \tag{2-35a}$$

$$-Q_{Dt} = -V_t^2\, B_{tq} - V_t\, E_q'\, U_{tq} - V_t^2\,(B_{Cth} + B_{th}) - V_t\, V_h\, U_{th} \tag{2-35b}$$

For n high-side and load buses: $i = 1, \cdots, n$,

$$-P_{Di} = V_i^2 \sum_{j=1}^{m+n} (G_{Cij} + G_{ij}) - \sum_{j=1}^{m+n} V_i\, V_j\, T_{ij} \;\;,\; j \neq i \tag{2-36a}$$

$$-Q_{Di} = -V_i^2 \sum_{j=1}^{m+n} (B_{Cij} + B_{ij}) - \sum_{j=1}^{m+n} V_i\, V_j\, U_{ij} \;\;,\; j \neq i \tag{2-36b}$$

For n+m loads:

$$P_D = P_L + I_P\, V + G_S\, V^2 + k_P\, V^{n_P} \tag{2-37a}$$

$$Q_D = Q_L + I_Q\, V - B_S\, V^2 + k_Q\, V^{n_Q} \tag{2-37b}$$

Let the swing bus be the terminal bus at machine 1, i.e., bus $n + 1$, with specified terminal voltage V_{n+1} ($\theta_{n+1} = 0$). Then there are $4\,(m - 1) + 2\,n$ equations to be solved for $\bar{E}_q' = E_q' \exp(j\,\delta)$ and $\bar{V}_t = V_t \exp(j\,\theta_t)$ at bus $n + 2, \cdots, n + m$, and for $\bar{V}_i = V_i \exp(j\,\theta_i)$, $i = 1, \cdots, n$, in which $i = 1, \cdots, m$ are the m high-side buses associated with m terminal buses under the assumption that the connection between each terminal bus and its high-side bus is equivalently one-to-one.

However, the above algebraic equations are also nonlinear. The Newton method is a general approach by applying the Jacobian matrix of the system, generated by tak

lin

ap

eq

mo

Th

co

ca

2.

lin

Of

Ta

ho

te

m

st

co

(a

ec

in

its

br

(a

taking partial derivative for each equation with respect to each variable. Doing so, the linearized model of the system is obtained, and the linear system theories can be applied to analyze the characteristics of the system in a neighborhood of the isolated equilibrium point of interest. In next section, we will develop the linearized dynamic model of a power system based on the apparatus dynamic models derived before. Then, the following studies on the static and dynamic bifurcation leading to voltage collapse and oscillation, especially associated with flux decay dynamics and mechanical dynamics, will be investigated on the base of the linearized dynamic model.

2.6 Linearized Power System Model

In analyzing equivalent solutions of a nonlinear system, we generally start by linearizing the system in a neighborhood of the isolated equilibrium point of interest. Of course, every function describing the above power system dynamic model has a Taylor series expansion of the first degree plus higher order rest terms in the neighborhood of of the equilibrium point; linearizing means that we leave out the higher order terms.

Due to the linear representation of the control apparatus of every synchronous machine, linearization work for speed-governing-turbine system model, power system stabilizer model, and excitation system model is not needed, but it is needed for load compensator model. The linearization work will be done in the following sequence: (a) load demand model; (b) power balance equation; (c) swing equation; (d) flux decay equation; (e) load compensator. Note that to simplify the notation, a variable with Δ in front means the deviation of this variable from the equilibrium point of interest, and its coefficient (in front of Δ) consists of variables that are evaluated at their equilibrium values.

(a) Linearized Load Demand Model:

For each load, from (2-9),

$$\Delta P_D = \Delta P_C + F_{PV}\ \Delta V \tag{2-38a}$$

$$\Delta Q_D = \Delta Q_C + F_{QV}\ \Delta V \tag{2-38b}$$

where

$$F_{PV} = I_P + 2\,G_S\ V + n_P\ k_P\ V^{n_P - 1}$$

: coefficient of active power load functional of bus voltage;

$$F_{QV} = I_Q - 2\,B_S\ V + n_Q\ k_Q\ V^{n_Q - 1}$$

: coefficient of reactive power load functional of bus voltage;

$$\Delta P_C = \Delta P_L + V\ \Delta I_P + V^2\,\Delta G_S + V^{n_P}\ \Delta k_P + k_P\ V^{n_P}\ (\ln V)\ \Delta n_P$$

: coefficient of active power load not functional of bus voltage;

$$\Delta Q_C = \Delta Q_L + V\ \Delta I_Q - V^2\,\Delta B_S + V^{n_Q}\ \Delta k_Q + k_Q\ V^{n_Q}\ (\ln V)\ \Delta n_Q$$

: coefficient of reactive power load not functional of bus voltage.

(b) Linearized Power Balance Equation:

[1] At internal bus, for each synchronous machine, substituting the following property

$$\frac{\partial T_{ij}}{\partial \theta_i} = -\frac{\partial T_{ij}}{\partial \theta_j} = -U_{ij}\ \ ;\ i \neq j \tag{2-39a}$$

$$\frac{\partial U_{ij}}{\partial \theta_i} = -\frac{\partial U_{ij}}{\partial \theta_j} = T_{ij}\ \ ;\ i \neq j \tag{2-39b}$$

into (2-11) and (2-15), we can derive

$$\Delta I_d = -B_q\ \Delta E_q' - U_{qt}\ \Delta V_t - T_{qt}\ V_t\ (\Delta\delta - \Delta\theta_t) \tag{2-40a}$$

$$\Delta I_q = G_a\ \Delta E_q' - T_{dt}\ \Delta V_t + U_{dt}\ V_t\ (\Delta\delta - \Delta\theta_t) \tag{2-40b}$$

$$T_{qt} = G_a\ \cos(\delta - \theta_t) + B_q\ \sin(\delta - \theta_t) \tag{2-40c}$$

$$U_{dt} = G_a\ \sin(\delta - \theta_t) - B_d'\ \cos(\delta - \theta_t) \tag{2-40d}$$

$$\Delta P_E = K_{P1}^{gt}\ (\Delta\delta - \Delta\theta_t) + K_{P2}^{gt}\ \Delta E_q^{'} + K_{P7}^{gt}\ \Delta V_t \qquad \text{(2-41a)}$$

$$\Delta Q_E = K_{Q1}^{gt}\ (\Delta\delta - \Delta\theta_t) + K_{Q2}^{gt}\ \Delta E_q^{'} + K_{Q7}^{gt}\ \Delta V_t \qquad \text{(2-41b)}$$

where,

$$K_{P1}^{gt} = E_q^{'}\ V_t\ U_{PE} + V_t^2\ (X_q - X_d^{'})\ (T_{dt}\ T_{qt} - U_{dt}\ U_{qt})$$

$$K_{P2}^{gt} = 2\ E_q^{'}\ G_{EE} - V_t\ T_{PE}$$

$$K_{P7}^{gt} = 2\ V_t\ G_{Et} - E_q^{'}\ T_{PE}$$

$$U_{PE} = k_1\ U_{dt} - G_a\ (X_q - X_d^{'})\ T_{qt}$$

$$T_{PE} = k_1\ T_{dt} + G_a\ (X_q - X_d^{'})\ U_{qt}$$

$$K_{Q1}^{gt} = -\ E_q^{'}\ V_t\ T_{QE} + 2\ V_t^2\ (X_q - X_d^{'})\ U_{qt}\ T_{qt}$$

$$K_{Q2}^{gt} = -\ 2\ E_q^{'}\ B_{EE} - V_t\ U_{QE}$$

$$K_{Q7}^{gt} = -\ 2\ V_t\ B_{Et} - E_q^{'}\ U_{QE}$$

$$T_{QE} = k_2\ T_{qt}$$

$$U_{QE} = k_2\ U_{qt}$$

[2] **At terminal bus,** for each synchronous machine, from (2-28) and (2-29),

$$\Delta P_{tq} + \Delta P_{Dt} + \Delta P_{th} = 0$$

$$\Delta Q_{tq} + \Delta Q_{Dt} + \Delta Q_{th} = 0$$

$$-\ \Delta P_{Gt} = \Delta P_{tq} = K_{P1}^{tq}\ (\Delta\theta_t - \Delta\delta) + K_{P2}^{tq}\ \Delta E_q^{'} + K_{P7}^{tq}\ \Delta V_t \qquad \text{(2-42a)}$$

$$-\ \Delta Q_{Gt} = \Delta Q_{tq} = K_{Q1}^{tq}\ (\Delta\theta_t - \Delta\delta) + K_{Q2}^{tq}\ \Delta E_q^{'} + K_{Q7}^{tq}\ \Delta V_t \qquad \text{(2-42b)}$$

$$-\ \Delta P_{Ct} = -\ K_{P1}^{tq}\ \Delta\delta + K_{P2}^{tq}\ \Delta E_q^{'} + (K_{P1}^{tq} + A_{1tt})\ \Delta\theta_t + B_{1th}\ \Delta\theta_h$$

$$+\ (K_{P7}^{tq} + C_{1tt})\ \Delta V_t + D_{1th}\ \Delta V_h \qquad \text{(2-43a)}$$

$$-\ \Delta Q_{Ct} = -\ K_{Q1}^{tq}\ \Delta\delta + K_{Q2}^{tq}\ \Delta E_q^{'} + (K_{Q1}^{tq} + A_{3tt})\ \Delta\theta_t + B_{3th}\ \Delta\theta_h$$

$$+ (K_{Q7}^{tq} + C_{3tt})\, \Delta V_t + D_{3th}\, \Delta V_h \tag{2-43b}$$

where, the same properties of (2-39) and (2-40) are used such that

$$K_{P1}^{tq} = V_t\, E_q'\, U_{tq} - V_t^2\, (B_d' - B_q)\cos[2(\theta_t - \delta)]$$

$$K_{P2}^{tq} = -\,V_t\, T_{tq}$$

$$K_{P7}^{tq} = 2\, V_t\, G_{tq} - E_q'\, T_{tq}$$

$$A_{1tt} = V_t\, V_h\, U_{th}$$

$$B_{1th} = -\,V_t\, V_h\, U_{th} = -\,A_{1tt}$$

$$C_{1tt} = F_{PV_t} + 2\, V_t\, (G_{Cth} + G_{th}) - V_h\, T_{th}$$

$$D_{1th} = -\,V_t\, T_{th}$$

$$K_{Q1}^{tq} = -\,V_t\, E_q'\, T_{tq} - V_t^2\, (B_d' - B_q)\sin[2(\theta_t - \delta)]$$

$$K_{Q2}^{tq} = -\,V_t\, U_{tq}$$

$$K_{Q7}^{tq} = -\,2\, V_t\, B_{tq} - E_q'\, U_{tq}$$

$$A_{3tt} = -\,V_t\, V_h\, T_{th}$$

$$B_{3th} = V_t\, V_h\, T_{th} = -\,A_{3tt}$$

$$C_{3tt} = F_{QV_t} - 2\, V_t\, (B_{Cth} + B_{th}) - V_h\, U_{th}$$

$$D_{3th} = -\,V_t\, U_{th}$$

[3] At high-side bus, $h = 1\,, \;\cdots\;, m\,, j \neq h$, from (2-30),

$$-\,\Delta P_{Ch} = A_{2ht}\, \Delta\theta_t + B_{2hh}\, \Delta\theta_h + \sum_{j=1}^{n} B_{2hj}\, \Delta\theta_j$$

$$+ C_{2ht}\, \Delta V_t + D_{2hh}\, \Delta V_h + \sum_{j=1}^{n} D_{2hj}\, \Delta V_j \tag{2-44a}$$

$$-\,\Delta Q_{Ch} = A_{4ht}\, \Delta\theta_t + B_{4hh}\, \Delta\theta_h + \sum_{j=1}^{n} B_{4hj}\, \Delta\theta_j$$

$$+ C_{4ht}\ \Delta V_t + D_{4hh}\ \Delta V_h + \sum_{j=1}^{n} D_{4hj}\ \Delta V_j \tag{2-44b}$$

where, we use the same property of (2-39) and have

$$A_{2ht} = -V_h\ V_t\ U_{ht}$$

$$B_{2hh} = V_h\ V_t\ U_{ht} + \sum_{j=1}^{n} V_h\ V_j\ U_{hj}$$

$$B_{2hj} = -V_h\ V_j\ U_{hj}$$

$$C_{2ht} = -V_h\ T_{ht}$$

$$D_{2hh} = F_{PV_h} + 2\ V_h\ [\ G_{Cht} + G_{ht} + \sum_{j=1}^{n} (G_{Chj} + G_{hj})\ ] - V_t\ T_{ht} - \sum_{j=1}^{n} V_j\ T_{hj}$$

$$D_{2hj} = -V_h\ T_{hj}$$

$$A_{4ht} = V_h\ V_t\ T_{ht}$$

$$B_{4hh} = -V_h\ V_t\ T_{ht} - \sum_{j=1}^{n} V_h\ V_j\ T_{hj}$$

$$B_{4hj} = V_h\ V_j\ T_{hj}$$

$$C_{4ht} = -V_h\ U_{ht}$$

$$D_{4hh} = F_{QV_h} - 2\ V_h\ [\ B_{Cht} + B_{ht} + \sum_{j=1}^{n} (B_{Chj} + B_{hj})\ ] - V_t\ U_{ht} - \sum_{j=1}^{n} V_j\ U_{hj}$$

$$D_{4hj} = -V_h\ U_{hj}$$

[4] At load bus, $i = m + 1\ ,\ \cdots\ , n\ , j \neq i$, from (2-31),

$$-\Delta P_{Ci} = B_{2ii}\ \Delta\theta_i + \sum_{j=1}^{n} B_{2ij}\ \Delta\theta_j + D_{2ii}\ \Delta V_i + \sum_{j=1}^{n} D_{2ij}\ \Delta V_j \tag{2-45a}$$

$$-\Delta Q_{Ci} = B_{4ii}\ \Delta\theta_i + \sum_{j=1}^{n} B_{4ij}\ \Delta\theta_j + D_{4ii}\ \Delta V_i + \sum_{j=1}^{n} D_{4ij}\ \Delta V_j \tag{2-45b}$$

where, we use the same property of (2-39) and have

$$B_{2ii} = \sum_{j=1}^{n} V_i \; V_j \; U_{ij}$$

$$B_{2ij} = -\, V_i \; V_j \; U_{ij}$$

$$D_{2ii} = F_{PV_i} + 2\, V_i \sum_{j=1}^{n} (G_{Cij} + G_{ij}) - \sum_{j=1}^{n} V_j \; T_{ij}$$

$$D_{2ij} = -\, V_i \; T_{ij}$$

$$B_{4ii} = -\sum_{j=1}^{n} V_i \; V_j \; T_{ij}$$

$$B_{4ij} = V_i \; V_j \; T_{ij}$$

$$D_{4ii} = F_{QV_i} - 2\, V_i \sum_{j=1}^{n} (B_{Cij} + B_{ij}) - \sum_{j=1}^{n} V_j \; U_{ij}$$

$$D_{4ij} = -\, V_i \; U_{ij}$$

(c) Linearized Swing Equation:

For each synchronous machine, from (2-25),

$$\Delta\dot{\delta} = \Delta\omega \qquad (2\text{-}46a)$$

$$M \; \Delta\dot{\omega} = -\, D \; \Delta\omega - \Delta P_E + \Delta P_M \qquad (2\text{-}46b)$$

where, ΔP_M can be obtained from (2-24); ΔP_E can be substituted by (2-41a).

(d) Linearized Flux Decay Equation:

For each synchronous machine, from (2-19) and the properties of (2-39) and (2-40),

$$T_{do}' \; \Delta\dot{E}_q' = \Delta E_{fd} - K_{E3} \, \Delta E_q' - K_{E4} \, (\Delta\delta - \Delta\theta_t) + K_{E7} \, \Delta V_t \qquad (2\text{-}47)$$

where,

$$K_{E3} = 1 - (X_d - X_d') \, B_q$$

$$K_{E4} = -\, (X_d - X_d') \, T_{qt} \; V_t$$

$$K_{E7} = (X_d - X_d') \, U_{qt}$$

Note that each K_{E3} is a constant coefficient only functional of the machine parameters. ΔE_{fd} can be obtained from (2-20) - (2-22), and from the linearized load compensator model (see (e)).

(e) Linearized Load Compensator Model:

For each excitation system, from (2-21),

$$2\, V_C \, \Delta V_C = 2\, V_{Cd} \, \Delta V_{Cd} + 2\, V_{Cq} \, \Delta V_{Cq}$$

$$\Delta V_C = K_{C1} \, (\Delta\delta - \Delta\theta_t) + K_{C2} \, \Delta E_q' + K_{C7} \, \Delta V_t \qquad (2\text{-}48)$$

where,

$$K_{C1} = (K_{d1} \, V_{Cd} + K_{q1} \, V_{Cq})/V_C$$

$$K_{C2} = (K_{d2} \, V_{Cd} + K_{q2} \, V_{Cq})/V_C$$

$$K_{C7} = (K_{d7} \, V_{Cd} + K_{q7} \, V_{Cq})/V_C$$

$$K_{d1} = [\, (1 + X_C \, B_d' - R_C \, G_a) \cos(\delta - \theta_t) + K_{d2} \sin(\delta - \theta_t) \,] \, V_t$$

$$K_{q1} = - [\, (1 - K_{q2}) \sin(\delta - \theta_t) + (X_C \, G_a + R_C \, B_d') \cos(\delta - \theta_t) \,] \, V_t$$

Having the complete linearized power system dynamic model, the following chapters are going to study the characteristics of the power system based on three different approaches:

(1) voltage-angle bifurcation in the load flow model,

(2) static/algebraic bifurcation in the dynamic model, and

(3) static/dynamic bifurcation in the dynamic model.

Matrix forms of linearized load flow model and linearized power system dynamic model will also be formulated. Different kinds of test matrix for the above bifurcation tests will then be established.

Chapter 3
Bifurcation in a Load Flow Model

The bifurcation in a load flow model (simply called as Load Flow Bifurcation) will occur when the Jacobian matrix of the load flow model is singular. The load flow Jacobian matrix describes the linearized load flow model, and is a square matrix, which will be structurally discussed in the next section. In this chapter, a necessary and sufficient condition test matrix for the load flow bifurcation is derived, that includes effects of PV-bus to PQ-bus changes. It will be shown that the load flow bifurcation can not occur due to the row dependence of the load flow Jacobian matrix associated with the rows of the active and reactive power balance equations at a single bus or at a subset of buses; solely associated with all the rows of active power balance equations; or solely associated with all the rows of reactive power balance equations. The result that load flow bifurcation of a large power system model can not occur at single buses shows that the two-bus analogies used to understand large power system voltage stability problems have very severe limitations. Thus, the load flow Jacobian matrix is the generic test matrix for the load flow bifurcation. The generic load flow bifurcation is also the so called voltage/angle bifurcation, since it occurs only when the load flow Jacobian matrix is singular due to the row dependence associated with active and reactive power balance equations at all the buses. Special cases of the load flow bifurcation, voltage bifurcation and angle bifurcation, will also be discussed to provide better understanding of the causes of the load flow bifurcation in term of active and reactive power transfer and limitations. Finally, the simulation results of a 9-bus 3-machine power system demonstrate the voltage collapse due to the load flow bifurcation, and show the important role of the reactive power generation reserves.

3.1 Linearized Load Flow Model

The load flow model is a simplified model of power system dynamic model under the following assumptions: (1) the coupling between internal bus and terminal bus (or between rotor and stator) of each generator is neglected, (2) the excitation gain of each generator is infinite, and (3) all time constants in the differential equations are zero. Hence, for a generator, its terminal bus is the only bus required to represent it.

All the buses in the load flow model can be classified as the following types of bus.

(0) swing bus: It is one of the generator terminal bus with infinite active and reactive power capacity (reserve), so that its voltage can be specified and its angle is always set to be zero as the angle reference of the system. Its active and reactive power generations are dependent variables, that match the power mismatch in the rest of the system.

(1) PV-bus: This type of bus has its active power generation or injection (generation − load demand) and voltage specified as independent variables, and its reactive power generation and angle to be dependent. This bus type is specified when the bus has adjustable reactive power generation reserves, which implies that its reactive power generation limits have not yet been reached. Generator buses and buses with switchable shunt capacitors are PV-buses.

(2) PQ-bus: This type of bus has its active and reactive power injection specified as independent variables, and its voltage and angle are dependent variables. High-side buses, load buses and PV-buses at their reactive power generation limits are all PQ-buses. Note that the active and reactive power generations at high-side and load buses are zero.

Thus, the load flow model consists of active power balance equations at both PV-buses and PQ-buses, and reactive power balance equation at PQ-buses. The reactive power generation at each PV-bus, and the active and reactive power generations at swing bus are the output equations of the load flow model. The load flow model can be described as follows.

$$0 = g_1\,(\, y_1\,;\, y_2\,,\, y_3\,,\, \mu_1\,) \tag{3-1a}$$

$$Q_{PV} = g_2\,(\, y_1\,;\, y_2\,,\, y_3\,,\, \mu_2\,) \;\rightarrow\; \textit{PV–Bus Output Equation} \tag{3-1b}$$

$$P_S = g_{3P}\,(\, y_1\,,\, y_3\,) \;\rightarrow\; \textit{Swing Bus Output Equation} \tag{3-1c}$$

$$Q_S = g_{3Q}\,(\, y_1\,,\, y_3\,) \;\rightarrow\; \textit{Swing Bus Output Equation} \tag{3-1d}$$

where,

g_1: active power balance equations at PV-buses and PQ-buses, and reactive power balance equations at PQ-buses;

g_2: reactive power balance equations at PV-buses;

g_{3P}: active power balance equation at the swing bus;

g_{3Q}: reactive power balance equation at the swing bus;

y_1: angles at PV-buses and PQ-buses, and voltages at PQ-buses;

y_2: specified voltage at PV-buses;

y_3: voltage at the swing bus;

μ_1: active power demand at PV-buses and PQ-buses, and reactive power demand at PQ-buses;

μ_2: reactive power load demands at PV-buses;

Q_{PV}: reactive power generations at PV-buses;

P_S: active power injection at swing bus;

Q_S: reactive power injection at swing bus.

Note that since the swing bus is assumed to have infinite active and reactive power generation capacity, the characteristics of the swing bus will not be further discussed in the load flow model, and the voltage at swing bus is assumed to be always constant, i.e., y_3 is a specified constant.

Consider an n bus power system with one of the generator terminal buses selected as the swing bus (bus# 1), $m-1$ generator terminal PV-buses and $n-m$ PQ-buses. It is assumed that no generator PV-bus has become a PQ-bus, referring to the power balance equations derived in Chapter 2, the linearized load flow model and the load flow Jacobian matrix J_{LF} can be structurally represented as follows:

$$-\Delta\mu_1 = \frac{\partial g_1}{\partial y_1}\Delta y_1 + \frac{\partial g_1}{\partial y_2}\Delta y_2 \tag{3-2a}$$

$$\Delta Q_{PV} - \Delta\mu_2 = \frac{\partial g_2}{\partial y_1}\Delta y_1 + \frac{\partial g_2}{\partial y_2}\Delta y_2 \rightarrow \textit{Output Equation} \tag{3-2b}$$

$$\begin{bmatrix} \Delta P_T \\ -\Delta P_{CH} \\ -\Delta P_{CL} \\ -\Delta Q_{CH} \\ -\Delta Q_{CL} \end{bmatrix} = \begin{bmatrix} A_1 & B_{1H} & 0 & D_{1H} & 0 \\ A_{2H} & B_{2HH} & B_{2HL} & D_{2HH} & D_{2HL} \\ 0 & B_{2LH} & B_{2LL} & D_{2LH} & D_{2LL} \\ A_{4H} & B_{4HH} & B_{4HL} & D_{4HH} & D_{4HL} \\ 0 & B_{4LH} & B_{4LL} & D_{4LH} & D_{4LL} \end{bmatrix} \begin{bmatrix} \Delta\theta_T \\ \Delta\theta_H \\ \Delta\theta_L \\ \Delta V_H \\ \Delta V_L \end{bmatrix} + \begin{bmatrix} C_1 \\ C_{2H} \\ 0 \\ C_{4H} \\ 0 \end{bmatrix} \Delta V_T \tag{3-2a}$$

$$\Delta Q_T = [\, A_3 \;\; B_{3H} \;\; 0 \;\; D_{3H} \;\; 0 \,] \begin{bmatrix} \Delta\theta_T \\ \Delta\theta_H \\ \Delta\theta_L \\ \Delta V_H \\ \Delta V_L \end{bmatrix} + C_3\,\Delta V_T \rightarrow \textit{Output Equation}$$

$$\Delta P_Q = -\Delta\mu_1 = [\, \Delta P_T{}^t \;\; -\Delta P_{CH}{}^t \;\; -\Delta P_{CL}{}^t \;\; -\Delta Q_{CH}{}^t \;\; -\Delta Q_{CL}{}^t \,]^t$$

$$\Delta y_1 = [\, \Delta\theta_T{}^t \;\; \Delta\theta_H{}^t \;\; \Delta\theta_L{}^t \;\; \Delta V_H{}^t \;\; \Delta V_L{}^t \,]^t \;\; ; \;\; \Delta y_2 = \Delta V_T$$

$$\Delta Q_{PV} = \Delta Q_{GT} \;\; ; \;\; -\Delta Q_{CT} = -\Delta\mu_2$$

where,

$\Delta P_T = \Delta P_{GT} - \Delta P_{CT}$: active power injections at terminal buses;

$\Delta Q_T = \Delta Q_{GT} - \Delta Q_{CT}$: reactive power injections at terminal buses;

ΔP_Q: P and Q injection vector of the left hand side of (3-2a).

subscript T: represents the generator terminal PV-buses (including switchable shunt capacitor buses), i.e., P_{Gt}, P_{Ct}, θ_t, Q_{Gt}, Q_{Ct}, V_t, $t = 2, ..., m$.

subscript H: represents the generator-transformer high-side PQ-buses. If the connection between each generator and its transformer high-side bus is equivalently one-to-one, then P_{Ch}, θ_h, Q_{Ch}, V_h, $h = m + 1, ..., m + m$.

subscript L: represents the rest of the PQ-buses. If the above one-to-one connection is assumed, then P_{Cl}, θ_l, Q_{Cl}, V_l, $l = 2m + 1, ..., n$.

subscript G: active or reactive power generations;

subscript C: not-voltage-dependent (or constant) active or reactive power load demand or injection;

The above matrices can be partitioned and defined as follows:

$$J_{LF} = J_{11} = \frac{\partial g_1}{\partial y_1} = \begin{bmatrix} J_{P\theta} & J_{PV} \\ J_{Q\theta} & J_{QV} \end{bmatrix} \; ; \; J_{12} = \frac{\partial g_1}{\partial y_2} = \begin{bmatrix} C_1 \\ C_{2H} \\ 0 \\ C_{4H} \\ 0 \end{bmatrix}$$

$$J_{21} = \frac{\partial g_2}{\partial y_1} = [\, A_3 \;\; B_{3H} \;\; 0 \;\; D_{3H} \;\; 0 \,] \; ; \; J_{22} = \frac{\partial g_2}{\partial y_2} = C_3$$

$$J_{P\theta} = \begin{bmatrix} A_1 & B_1 \\ A_2 & B_2 \end{bmatrix} = \begin{bmatrix} A_1 & B_{1H} & 0 \\ A_{2H} & B_{2HH} & B_{2HL} \\ 0 & B_{2LH} & B_{2LL} \end{bmatrix} \; ; \; J_{PV} = \begin{bmatrix} D_1 \\ D_2 \end{bmatrix} = \begin{bmatrix} D_{1H} & 0 \\ D_{2HH} & D_{2HL} \\ D_{2LH} & D_{2LL} \end{bmatrix}$$

$$J_{Q\theta} = [\,A_4 \;\; B_4\,] = \begin{bmatrix} A_{4H} & B_{4HH} & B_{4HL} \\ 0 & B_{4LH} & B_{4LL} \end{bmatrix} \;;\; J_{QV} = D_4 = \begin{bmatrix} D_{4HH} & D_{4HL} \\ D_{4LH} & D_{4LL} \end{bmatrix}$$

where, J_{LF} is referred as to the load flow Jacobian matrix. The output equation then becomes

$$\Delta Q_T = S_{QV}\,\Delta V_T + S_{QP}\,\Delta P_Q \tag{3-2b}$$

$$S_{QV} = J_{22} - J_{21}\,J_{LF}^{-1}\,J_{12} \;;\; S_{QP} = J_{21}\,J_{LF}^{-1}$$

where, S_{QV} is the equivalent $Q-V$ sensitivity matrix of PV-buses when the load flow Jacobian matrix J_{LF} of (3-2) is nonsingular.

Based on the assumed one-to-one connection between each generator bus and its transformer high-side bus (simply called the high-side bus), the following properties are observed.

(1) A_1, A_3, C_1, and C_3 are all $(m-1)\,x\,(m-1)$ diagonal matrices;

(2) A_{2H}, A_{4H}, C_{2H}, and C_{4H} are all $m\,x\,(m-1)$ matrices. Each has the first row being zero and the rest being an diagonal $(m-1)\,x\,(m-1)$ submatrix.

(3) B_{1H}, B_{3H}, D_{1H}, and D_{3H} are all $(m-1)\,x\,m$ matrices. Each has the first column being zero and the rest being an diagonal $(m-1)\,x\,(m-1)$ submatrix.

(4) Since the power balance equation of each bus is function of the angle differences between this bus and other buses that connect to it, each diagonal element of the power-angle Jacobian matrices ($J_{P\theta}$ and $J_{Q\theta}$) of the above load flow Jacobian matrix J_{LF}, shown in the matrices of A and B, is the negative sum of its corresponding off-diagonal elements; except the first diagonal elements of the matrices B_{2HH} and B_{4HH}, which are associated with the swing bus. Thus, if the angle of the swing bus is not set to be

zero as the reference of the system, the load flow Jacobian matrix J_{LF} will be singular [45].

(5) With the angle reference of the swing bus, the diagonal matrix A_1 is equal to the diagonal submatrix of $-B_{1H}$; and the diagonal matrix A_3 is equal to the diagonal submatrix of $-B_{3H}$, where the submatrix means the matrix without the row and/or the column corresponding to the swing bus.

(6) ΔP_C and ΔQ_C are respectively the coefficients of active and reactive power load demand, P_D and Q_D, which are not function of bus voltage. Hence, the effect of the voltage dependence of load demand model, mentioned in Chapter 2, is included in each diagonal element of the power-voltage Jacobian matrices (J_{PV} and J_{QV}) of the load flow Jacobian matrix J_{LF}, shown in the matrices of C and D.

(7) Recalling (2-1) and (2-2)

$$P_{ij} = V_i^2\, G_{ij} - V_i\, V_j\, [\, G_{ij} \cos(\theta_i - \theta_j) + B_{ij} \sin(\theta_i - \theta_j)\,]$$

$$= V_i^2\, G_{ij} - V_i\, V_j\, T_{ij} \tag{3-3a}$$

$$Q_{ij} = -\, V_i^2\, B_{ij} - V_i\, V_j\, [\, G_{ij} \sin(\theta_i - \theta_j) - B_{ij} \cos(\theta_i - \theta_j)\,]$$

$$= -\, V_i^2\, B_{ij} - V_i\, V_j\, U_{ij} \tag{3-3b}$$

we have the following properties shown in (2-48):

$$\frac{\partial T_{ij}}{\partial \theta_i} = -\frac{\partial T_{ij}}{\partial \theta_j} = -\, U_{ij} \quad ; \; i \neq j \tag{3-4a}$$

$$\frac{\partial U_{ij}}{\partial \theta_i} = -\frac{\partial U_{ij}}{\partial \theta_j} = T_{ij} \quad ; \; i \neq j \tag{3-4b}$$

$$\frac{\partial P_{ij}}{\partial \theta_i} = -\frac{\partial P_{ij}}{\partial \theta_j} = V_i\, V_j\, U_{ij} \tag{3-5a}$$

$$\frac{\partial Q_{ij}}{\partial \theta_i} = -\frac{\partial Q_{ij}}{\partial \theta_j} = -\, V_i\, V_j\, T_{ij} \tag{3-5b}$$

$$\frac{\partial P_{ij}}{\partial V_i} = 2\, V_i\, G_{ij} - V_j\, T_{ij} \;\; ; \;\; \frac{\partial P_{ij}}{\partial V_j} = -\, V_i\, T_{ij} \tag{3-5c}$$

$$\frac{\partial Q_{ij}}{\partial V_i} = -\, 2\, V_i\, B_{ij} - V_j\, U_{ij} \;\; ; \;\; \frac{\partial Q_{ij}}{\partial V_j} = -\, V_i\, U_{ij} \tag{3-5d}$$

Note that in general, $T_{ij} \neq \pm T_{ji}$ and $U_{ij} \neq \pm U_{ji}$. However, if the network does not have phase shifter branch so that $G_{ij} = G_{ji}$ and $B_{ij} = B_{ji}$, and if the series resistance of each network branch is small enough and is neglected ($G_{ij} = 0$), then $T_{ij} = -\, T_{ji}$ and $U_{ij} = U_{ji}$. Thus,

$$\frac{\partial P_{ij}}{\partial \theta_j} = \frac{\partial P_{ji}}{\partial \theta_i} = -\, V_i\, V_j\, U_{ij} = -\, V_j\, V_i\, U_{ji} \tag{3-6a}$$

$$\frac{\partial Q_{ij}}{\partial \theta_j} = -\, \frac{\partial Q_{ji}}{\partial \theta_i} = V_i\, V_j\, T_{ij} = -\, V_j\, V_i\, T_{ji} \tag{3-6b}$$

so that the Jacobian matrix $J_{P\theta}$ is symmetric, B_4 is screw-symmetric, and $A_{4H} = -\, B_{3H}^t$ where superscript t means matrix transpose. This presents the sparse property of the load flow Jacobian matrix.

(8) If the voltage variable is chosen as per unit deviation, i.e., $\Delta V/V$, then, without the assumption $G_{ij} = 0$, we have

$$\frac{\partial P_{ij}}{\partial \theta_j} = \frac{\partial Q_{ij}}{\partial V_j / V_j} = -\, V_i\, V_j\, U_{ij} \tag{3-7a}$$

$$\frac{\partial Q_{ij}}{\partial \theta_j} = -\, \frac{\partial P_{ij}}{\partial V_j / V_j} = V_i\, V_j\, T_{ij} \tag{3-7b}$$

so that $A_{2H} = C_{4H}$, $B_{1H} = D_{3H}$, and both B_2 and D_4 have the same off-diagonal elements, and that $A_{4H} = -\, C_{2H}$, $B_{3H} = -\, D_{1H}$, and each off-diagonal element of B_4 is the negative sign of that of D_2. This further shows the another sparse property of the load flow Jacobian matrix.

When any generator PV-bus becomes a PQ-bus due to exhausting its reactive power reserve or hitting its reactive power generation high or low limit, the defining equations for the load flow model change by adding a reactive power balance equation at the generator terminal bus, because the voltage magnitude at the generator terminal bus is no longer specified. At this generator PQ-bus, its reactive power generation is set to be fixed at the limit. Hence, in the case that any generator PV-bus becomes a PQ-bus, using the following matrix partitions associated with terminal buses:

$$\Delta P_T = \begin{bmatrix} \Delta P_T^{PV} \\ \Delta P_T^{PQ} \end{bmatrix} \; ; \; \Delta\theta_T = \begin{bmatrix} \Delta\theta_t^{PV} \\ \Delta\theta_T^{PQ} \end{bmatrix}$$

$$\Delta Q_T = \begin{bmatrix} \Delta Q_T^{PV} \\ \Delta Q_T^{PQ} \end{bmatrix} \; ; \; \Delta V_T = \begin{bmatrix} \Delta V_T^{PV} \\ \Delta V_T^{PQ} \end{bmatrix}$$

$$A_1 = \begin{bmatrix} A_1^{PV} \\ A_1^{PQ} \end{bmatrix} = \begin{bmatrix} A_{1PV}^{PV} & 0 \\ 0 & A_{1PQ}^{PQ} \end{bmatrix} \; ; \; B_{1H} = \begin{bmatrix} B_{1H}^{PV} \\ B_{1H}^{PQ} \end{bmatrix}$$

$$C_1 = [\, C_1^{PV} \;\; C_1^{PQ} \,] = \begin{bmatrix} C_{1PV}^{PV} & 0 \\ 0 & C_{1PQ}^{PQ} \end{bmatrix} \; ; \; D_{1H} = \begin{bmatrix} D_{1H}^{PV} \\ D_{1H}^{PQ} \end{bmatrix}$$

$$A_{2H} = [\, A_{2H}^{PV} \;\; A_{2H}^{PQ} \,] \; ; \; C_{2H} = [\, C_{2H}^{PV} \;\; C_{2H}^{PQ} \,]$$

$$A_3 = \begin{bmatrix} A_3^{PV} \\ A_3^{PQ} \end{bmatrix} = \begin{bmatrix} A_{3PV}^{PV} & 0 \\ 0 & A_{3PQ}^{PQ} \end{bmatrix} \; ; \; B_{3H} = \begin{bmatrix} B_{3H}^{PV} \\ B_{3H}^{PQ} \end{bmatrix}$$

$$C_3 = [\, C_3^{PV} \;\; C_3^{PQ} \,] = \begin{bmatrix} C_{3PV}^{PV} & 0 \\ 0 & C_{3PQ}^{PQ} \end{bmatrix} \; ; \; D_{3H} = \begin{bmatrix} D_{3H}^{PV} \\ D_{3H}^{PQ} \end{bmatrix}$$

$$A_{4H} = [\, A_{4H}^{PV} \;\; A_{4H}^{PQ} \,] \; ; \; C_{4H} = [\, C_{4H}^{PV} \;\; C_{4H}^{PQ} \,]$$

then the linearized load flow model and its corresponding Jacobian matrix J_{LF} would become as follows.

$$\begin{bmatrix} \Delta P_T \\ -\Delta P_{CH} \\ -\Delta P_{CL} \\ \Delta Q_T^{PQ} \\ -\Delta Q_{CH} \\ -\Delta Q_{CL} \end{bmatrix} = \begin{bmatrix} A_1 & B_{1H} & 0 & C_1^{PQ} & D_{1H} & 0 \\ A_{2H} & B_{2HH} & B_{2HL} & C_{2H}^{PQ} & D_{2HH} & D_{2HL} \\ 0 & B_{2LH} & B_{2LL} & 0 & D_{2LH} & D_{2LL} \\ A_3^{PQ} & B_{3H}^{PQ} & 0 & C_{3PQ}^{PQ} & D_{3H}^{PQ} & 0 \\ A_{4H} & B_{4HH} & B_{4HL} & C_{4H}^{PQ} & D_{4HH} & D_{4HL} \\ 0 & B_{4LH} & B_{4LL} & 0 & D_{4LH} & D_{4LL} \end{bmatrix} \begin{bmatrix} \Delta\theta_T \\ \Delta\theta_H \\ \Delta\theta_L \\ \Delta V_T^{PQ} \\ \Delta V_H \\ \Delta V_L \end{bmatrix} + \begin{bmatrix} C_1^{PV} \\ C_{2H}^{PV} \\ 0 \\ 0 \\ C_{4H}^{PV} \\ 0 \end{bmatrix} \Delta V_T^{PV}$$

$$\Delta Q_T^{PV} = [\, A_3^{PV} \;\; B_{3H}^{PV} \;\; 0 \;\; 0 \;\; D_{3H}^{PV} \;\; 0 \,] \begin{bmatrix} \Delta\theta_T \\ \Delta\theta_H \\ \Delta\theta_L \\ V_T^{PQ} \\ \Delta V_H \\ \Delta V_L \end{bmatrix} + C_{3PV}^{PV} \, \Delta V_T^{PV}$$

$$= S_{QV} \, \Delta V_T^{PV} + S_{QP} \, \Delta P_Q \;\rightarrow\; \textit{Output Equation}$$

$$J_{LF} = \begin{bmatrix} J_{P\theta} & J_{PV} \\ J_{Q\theta} & J_{QV} \end{bmatrix} \tag{3-8}$$

$$J_{P\theta} = \begin{bmatrix} A_1 & B_1 \\ A_2 & B_2 \end{bmatrix} = \begin{bmatrix} A_1 & B_{1H} & 0 \\ A_{2H} & B_{2HH} & B_{2HL} \\ 0 & B_{2LH} & B_{2LL} \end{bmatrix} \; ; \; J_{PV} = \begin{bmatrix} C_1^{PQ} & D_{1H} & 0 \\ C_{2H}^{PQ} & D_{2HH} & D_{2HL} \\ 0 & D_{2LH} & D_{2LL} \end{bmatrix}$$

$$J_{Q\theta} = \begin{bmatrix} A_3^{PQ} & B_{3H}^{PQ} & 0 \\ A_{4H} & B_{4HH} & B_{4HL} \\ 0 & B_{4LH} & B_{4LL} \end{bmatrix} \; ; \; J_{QV} = \begin{bmatrix} C_{3PQ}^{PQ} & D_{3H}^{PQ} & 0 \\ C_{4H}^{PQ} & D_{4HH} & D_{4HL} \\ 0 & D_{4LH} & D_{4LL} \end{bmatrix}$$

3.2 Load Flow Bifurcation

Load flow bifurcation will occur when the load flow Jacobian matrix J_{LF} is singular. This section will comprehensively discuss the subclasses of load flow bifurcation based on the the structure and the properties of the load flow Jacobian matrix. These subclasses are due to row dependence associated with different types of buses leading to the singularity of load flow Jacobian matrix, when some of generator PV-buses become PQ-buses (see (3-8)), which is more generic than when all generators have reactive power reserves and are PV-buses (see (3-2)).

Based on the matrix partitions associated with terminal buses shown in (3-8), the load flow Jacobian matrix J_{LF} (3-8) can be rewritten as the following form:

$$J_{LF} = \begin{bmatrix} J_{PT} \\ J_{QT}^{PQ} \\ J_{PH} \\ J_{QH} \\ J_{PL} \\ J_{QL} \end{bmatrix} = \begin{bmatrix} A_1 & B_{1H} & 0 & C_1^{PQ} & D_{1H} & 0 \\ A_3^{PQ} & B_{3H}^{PQ} & 0 & C_{3PQ}^{PQ} & D_{3H}^{PQ} & 0 \\ A_{2H} & B_{2HH} & B_{2HL} & C_{2H}^{PQ} & D_{2HH} & D_{2HL} \\ A_{4H} & B_{4HH} & B_{4HL} & C_{4H}^{PQ} & D_{4HH} & D_{4HL} \\ 0 & B_{2LH} & B_{2LL} & 0 & D_{2LH} & D_{2LL} \\ 0 & B_{4LH} & B_{4LL} & 0 & D_{4LH} & D_{4LL} \end{bmatrix} \tag{3-9}$$

$$J_{PT} = \begin{bmatrix} J_{PT}^{PV} \\ J_{PT}^{PQ} \end{bmatrix} = \begin{bmatrix} A_1^{PV} & B_{1H}^{PV} & 0 & 0 & D_{1H}^{PV} & 0 \\ A_1^{PQ} & B_{1H}^{PQ} & 0 & C_{1PQ}^{PQ} & D_{1H}^{PQ} & 0 \end{bmatrix}$$

or more precisely:

$$J_{PT}^{PV} = [\, A_{1PV}^{PV} \;\; 0 \;\; B_{1H}^{PV} \;\; 0 \;\; 0 \;\; D_{1H}^{PV} \;\; 0 \,]$$

$$J_{PT}^{PQ} = [\, 0 \;\; A_{1PQ}^{PQ} \;\; B_{1H}^{PQ} \;\; 0 \;\; C_{1PQ}^{PQ} \;\; D_{1H}^{PQ} \;\; 0 \,]$$

$$J_{QT}^{PQ} = [\, 0 \;\; A_{3PQ}^{PQ} \;\; B_{3H}^{PQ} \;\; 0 \;\; C_{3PQ}^{PQ} \;\; D_{3H}^{PQ} \;\; 0 \,]$$

$$J_{PH} = [\, A_{2H}^{PV} \;\; A_{2H}^{PQ} \;\; B_{2HH} \;\; B_{2HL} \;\; C_{2H}^{PQ} \;\; D_{2HH} \;\; D_{2HL} \,]$$

$$J_{QH} = [\, A_{4H}^{PV} \;\; A_{4H}^{PQ} \;\; B_{4HH} \;\; B_{4HL} \;\; C_{4H}^{PQ} \;\; D_{4HH} \;\; D_{4HL} \,]$$

$$J_{PL} = [\, 0 \;\; 0 \;\; B_{2LH} \;\; B_{2LL} \;\; 0 \;\; D_{2LH} \;\; D_{2LL} \,]$$

$$J_{QL} = [\, 0 \;\; 0 \;\; B_{4LH} \;\; B_{4LL} \;\; 0 \;\; D_{4LH} \;\; D_{4LL} \,]$$

Note that this arrangement of J_{LF} according to the type of bus shows that J_{PT}^{PQ} and J_{QT}^{PQ}, J_{PH} and J_{QH}, and J_{PL} and J_{QL} respectively have the same structure. Hence, basically from the structure and the properties of the load flow Jacobian matrix J_{LF} (3-9), there are three possible single-bus subclasses of load flow bifurcation leading to the singularity of load flow Jacobian matrix. These single-bus bifurcations, if they exist, would establish the correspondence between the load flow bifurcation that occurs due to the singularity of J_{LF} and the bifurcation that is evident in a transfer versus voltage nose curve for a two bus model. These three subclasses are due to row dependence associated with the power balance equations at PQ-buses: terminal (T), high-side (H), and load (L).

$LF-T$: This type of bifurcation is solely due to row dependence associated with the active and reactive power balance equations at terminal PQ-buses (J_{PT}^{PQ} and J_{QT}^{PQ}).

$LF-H$: This type of bifurcation is solely due to row dependence associated with the active and reactive power balance equations at high-side buses (J_{PH} and J_{QH}).

$LF-L$: This type of bifurcation is solely due to row dependence associated with the active and reactive power balance equations at load buses (J_{PL} and J_{QL}).

Note that since the diagonal properties of A and C matrices shown in Section 3.1 (property (1) and property (2)), other types of bifurcation due to the combination from any two of above three are not possible at all. However, the following subsections will prove that none of the above subclasses of load flow bifurcation can happen, and will derive a reduced form of J_{LF} based on the generic form of J_{LF} with the structure of (3-8) or (3-9) [87].

3.2.1 $LF-T$ Bifurcation ?

Since under the assumption that the connection between each generator terminal bus and its transformer high-side bus is one to one, all the submatrices of J_{PT}^{PQ} and J_{QT}^{PQ}, i.e., A_{1PQ}^{PQ}, B_{1H}^{PQ}, C_{1PQ}^{PQ}, D_{1H}^{PQ}, A_{3PQ}^{PQ}, B_{3H}^{PQ}, C_{3PQ}^{PQ}, and D_{3H}^{PQ}, are diagonal matrices.

The only condition for row dependence leading to the $LF-T$ type of bifurcation is that the ratios of each corresponding pair of elements of these diagonal matrices must be the same:

$$k_T = \frac{a_1}{a_3} = \frac{b_{1H}}{b_{3H}} = \frac{c_1}{c_3} = \frac{d_{1H}}{d_{3H}} \tag{3-10}$$

where, each small character represents the element corresponding to the matrix with the same subscript, and the superscript PQ is omitted. Using the following facts and definitions from Chapter 2 and Section 3.1:

$$T_{ij} = G_{ij} \cos(\theta_i - \theta_j) + B_{ij} \sin(\theta_i - \theta_j)$$

$$= Y_{ij} \cos(\theta_i - \theta_j - \gamma_{ij}) \;\; ; \;\; i \neq j \tag{3-11a}$$

$$U_{ij} = G_{ij} \sin(\theta_i - \theta_j) - B_{ij} \cos(\theta_i - \theta_j)$$

$$= Y_{ij} \sin(\theta_i - \theta_j - \gamma_{ij}) \;\; ; \;\; i \neq j \tag{3-11b}$$

$$Y_{ij} = \sqrt{G_{ij}^2 + B_{ij}^2} \;\; ; \;\; \gamma_{ij} = \tan^{-1}\frac{B_{ij}}{G_{ij}} \;\; ; \;\; i \neq j \tag{3-11c}$$

$$\frac{\partial T_{ij}}{\partial \theta_i} = -\frac{\partial T_{ij}}{\partial \theta_j} = -U_{ij} \;\; ; \;\; i \neq j \tag{3-11d}$$

$$\frac{\partial U_{ij}}{\partial \theta_i} = -\frac{\partial U_{ij}}{\partial \theta_j} = T_{ij} \;\; ; \;\; i \neq j \tag{3-11e}$$

we can obtain each element as follows:

$$a_1 = V_t \, V_h \, Y_{th} \sin(\theta_t - \theta_h - \gamma_{th}) \tag{3-12a}$$

$$b_{1H} = -V_t \, V_h \, Y_{th} \sin(\theta_t - \theta_h - \gamma_{th}) \tag{3-12b}$$

$$c_1 = 2 \, V_t \, (G_{St} + G_{Cth} + G_{th}) - V_h \, Y_{th} \cos(\theta_t - \theta_h - \gamma_{th}) + I_{Pt} \tag{3-12c}$$

$$d_{1H} = -V_t \, Y_{th} \cos(\theta_t - \theta_h - \gamma_{th}) \tag{3-12d}$$

$$a_3 = -V_t \, V_h \, Y_{th} \cos(\theta_t - \theta_h - \gamma_{th}) \tag{3-13a}$$

$$b_{3H} = V_t \, V_h \, Y_{th} \cos(\theta_t - \theta_h - \gamma_{th}) \tag{3-13b}$$

$$c_3 = -\,2\, V_t \, (B_{St} + B_{Cth} + B_{th}) - V_h \, Y_{th} \sin(\theta_t - \theta_h - \gamma_{th}) + I_{Qt} \tag{3-13c}$$

$$d_{3H} = -\, V_t \, Y_{th} \sin(\theta_t - \theta_h - \gamma_{th}) \tag{3-13d}$$

Note that the load demand model adopted here is the combination of constant power, constant impedance, and constant current models. It is clear that

$$k_T^{ab} = \frac{a_1}{a_3} = \frac{b_{1H}}{b_{3H}} = \frac{Y_{th} \sin(\theta_t - \theta_h - \gamma_{th})}{-\, Y_{th} \cos(\theta_t - \theta_h - \gamma_{th})} \tag{3-14}$$

$$k_T^d = \frac{d_{1H}}{d_{3H}} = \frac{Y_{th} \cos(\theta_t - \theta_h - \gamma_{th})}{Y_{th} \sin(\theta_t - \theta_h - \gamma_{th})} \tag{3-15}$$

which makes the satisfaction of (3-10) impossible unless $Y_{th} = 0$. Computing the ratio of the element in C_1 to that in C_3 is not necessary. Thus, it is concluded that the $LF\!-\!T$ type of load flow bifurcation due to the row dependence associated with the active and reactive power balance equations at a single generator terminal PQ-bus can never happen. This proof holds for every generator terminal bus.

3.2.2 $LF\!-\!H$ Bifurcation ?

Under the same one-to-one connection assumption, among the Jacobian submatrices of J_{PH} and J_{QH}, both $A_{2H} = [\, A_{2H}^{PV} \;\; A_{2H}^{PQ} \,]$ and $A_{4H} = [\, A_{4H}^{PV} \;\; A_{4H}^{PQ} \,]$ are diagonal matrices, and both C_{2H}^{PQ} and C_{4H}^{PQ} have the same structure with diagonal submatrices. Hence, to determine whether the $LF\!-\!H$ bifurcation can occur or not, one can first check if the corresponding elements of the above four matrices have the same ratio or not. Similarly, letting the notation of small character with the same subscript represent the element of that matrix, and using the facts stated in (3-11), we have

$$a_{2H} = -\, V_h \, V_t \, Y_{ht} \sin(\theta_h - \theta_t - \gamma_{ht}) \tag{3-16a}$$

$$c_{2H} = -\, V_h \, Y_{ht} \cos(\theta_h - \theta_t - \gamma_{ht}) \tag{3-16b}$$

$$a_{4H} = V_h \, V_t \, Y_{ht} \cos(\theta_h - \theta_t - \gamma_{ht}) \tag{3-17a}$$

$$c_{4H} = - V_h \, Y_{ht} \sin(\theta_h - \theta_t - \gamma_{ht}) \tag{3-17b}$$

$$k_H^a = \frac{a_{2H}}{a_{4H}} = \frac{- Y_{ht} \sin(\theta_h - \theta_t - \gamma_{ht})}{Y_{ht} \cos(\theta_h - \theta_t - \gamma_{ht})} \tag{3-18}$$

$$k_H^c = \frac{c_{2H}}{c_{4H}} = \frac{Y_{ht} \cos(\theta_h - \theta_t - \gamma_{ht})}{Y_{ht} \sin(\theta_h - \theta_t - \gamma_{ht})} \tag{3-19}$$

Since $k_H^a \neq k_H^c$, the $LF-H$ type of load flow bifurcation due to the row dependence associated with the active and reactive power balance equations at a single high-side bus can never occur either. This proof holds for every generator-transformer high-side bus.

3.2.3 $LF-L$ Bifurcation ?

To check whether the $LF-L$ bifurcation is possible to occur or not, one can first compare the corresponding elements of off-diagonal Jacobian submatrices of J_{PL} and J_{QL}, i.e., B_{2LH}, D_{2LH}, B_{4LH}, and D_{4LH}. Similarly, using the facts of (3-11), we have

$$b_{2LH} = - V_l \, V_h \, Y_{lh} \sin(\theta_l - \theta_h - \gamma_{lh}) \tag{3-20a}$$

$$d_{2LH} = - V_l \, V_h \, Y_{lh} \cos(\theta_l - \theta_h - \gamma_{lh}) \tag{3-20b}$$

$$b_{4LH} = V_l \, V_h \, Y_{lh} \cos(\theta_l - \theta_h - \gamma_{lh}) \tag{3-21a}$$

$$d_{4LH} = - V_l \, V_h \, Y_{lh} \sin(\theta_l - \theta_h - \gamma_{lh}) \tag{3-21b}$$

$$k_L^b = \frac{b_{2LH}}{b_{4LH}} = \frac{- Y_{lh} \sin(\theta_l - \theta_h - \gamma_{lh})}{Y_{lh} \cos(\theta_l - \theta_h - \gamma_{lh})} \tag{3-22}$$

$$k_L^d = \frac{d_{2LH}}{d_{4LH}} = \frac{Y_{lh} \cos(\theta_l - \theta_h - \gamma_{lh})}{Y_{lh} \sin(\theta_l - \theta_h - \gamma_{lh})} \tag{3-23}$$

Since $k_L^b \neq k_L^d$, the $LF-L$ type of load flow bifurcation due to the row dependence associated with the active and reactive power balance equations at a single load bus can never occur. This proof holds for every load bus.

3.3 Generic Load Flow Bifurcation

From the above, it can be concluded that there are no load flow bifurcation subclasses due to the row dependence of some particular rows of the load flow Jacobian matrix associated with single buses. Thus, analogies between bifurcation in a two-bus model have limited usefulness in understanding how voltage instability develops in the large power system load flow model. The only necessary and sufficient test condition for the load flow bifurcation is the test for the singularity of the load flow Jacobian matrix J_{LF} (3-9) due to joint row dependence at all buses. This generic load flow bifurcation is called the voltage/angle bifurcation because it occurs due to not only the active power-angle coupling ($J_{P\theta}$) and the reactive power-voltage coupling (J_{QV}), but also due to the active power-voltage coupling (J_{PV}) and the reactive power-angle coupling ($J_{Q\theta}$) at all the buses [53,87].

If the active power-voltage coupling and the reactive power-angle coupling can be ignored, or a decoupled load flow model is assumed, then the voltage bifurcation and/or the angle bifurcation can approximately occur. The voltage bifurcation [53], due to the row dependence of the reactive power balance equations of J_{LF} or the singularity of J_{QV}, is a bifurcation that solely leads to voltage instability. The angle bifurcation, due to the row dependence of the active power balance equations of J_{LF} or the singularity of $J_{P\theta}$, is a bifurcation that solely leads to steady state angle instability. The voltage bifurcation [53] when a bus or a group of buses can not be loaded with an additional increment of reactive power load, because the reactive power supply from the generator PV-buses with reactive power reserves that would attempt to supply this reactive power load is totally consumed in the network reactive power losses. The angle instability would occur when a transmission interface or boundary has reached its active power transfer limit. Note that since there always is some active power-voltage coupling and reactive power-angle coupling, the load flow Jacobian matrix J_{LF} can be singular, even though the matrix $J_{P\theta}$ is nonsingular or the matrix J_{QV} is nonsingular. Thus, the generic voltage/angle load flow bifurcation can be understood to be caused by the active and reactive power transfer limitation, and can occur before the active power transfer limitation due to the angle bifurcation or the reactive power transfer limitation due to the voltage bifurcation is reached in a decoupled load flow model.

It should be pointed out that the above proof not only indicates that the singularity of the load flow Jacobian matrix J_{LF} leading to the load flow bifurcation can not occur due to the row dependence associated with the active power and reactive power balance equations at a single bus, but also implies that the load flow bifurcation can not occur due to the row dependence associated with any subset of rows of J_{LF}. The singularity of J_{LF} requires that $v^t\ J_{LF} = 0$, where v is the left eigenvector of J_{LF} associated with the zero eigenvalue of J_{LF}. The requirement that only a subset of the rows of J_{LF} be row dependent amounts to finding a point of singularity where $v^t\ J_{LF} = 0$ such that elements of v are specified to be zero and not free. Thus, load flow bifurcations due to the row dependence associated with any subset of rows of J_{LF} can be considered as very rare types of the load flow bifurcation since the constrains associated with forcing elements of v to be zero for the operating conditions where $v^t\ J_{LF} = 0$ make it so.

It has been proven [53] that a $Q-V$ curve test is a test for voltage/angle bifurcation that occurs at the $Q-V$ curve minimum. The $Q-V$ curve has a minimum when the load flow Jacobian matrix J_{LF} is singular due to the row dependence of both active and reactive power balance equations at all the buses [53,87]. The minimal of $Q-V$ curve test for voltage collapse is the test for the singularity of the equivalent $Q-V$ sensitivity matrix S_{QV} (3-8), where the test bus (pattern) is treated as a (set of) PV-bus. It has also been shown that the $V-P$ (or $V-Q$) curve test is a test for voltage/angle bifurcation which occurs when the nose of the $V-P$ (or $V-Q$) curve is reached, where the load flow Jacobian matrix J_{LF} is singular also due to the row dependence of both active and reactive power balance equations at all the buses. The nose of $V-P$ (or $V-Q$) curve test for voltage collapse is the test for the singularity of the load flow Jacobian matrix J_{LF} ((3-8) or (3-9)) solely due to the row dependence between the rows associated with the active (or reactive) power balance equation at the test bus pattern and the rest rows of load flow Jacobian matrix.

It should be noted that the singularity of the load flow Jacobian matrix J_{LF} is approached continuously with added active or reactive power transfer across an interface or boundary as long as generator PV-buses do not experience exhausting reactive power reserves. When a generator PV-bus exhausts its reactive power reserve and becomes a PQ-bus, the addition of another reactive power balance equation and another voltage variable causes a discontinuity in the measure of the singularity of J_{LF}. This discontinuity often occurs at the point of voltage collapse because the load flow Jacobian matrix for the case where this bus is still a PV-bus are row independent but yet no voltage instability would occur because the load flow Jacobian matrix is nonsingular. If this PV-bus became a PQ-bus so that the Jacobian of the reactive power balance equation at this bus was added to the load flow Jacobian that existed prior to this bus becoming a PQ-bus, the expanded Jacobian matrix would be singular and the loss of voltage stability would begin immediately. This phenomenon will be observed in the simulation results of a 9-bus 3-machine power system shown in the following section.

3.4 Simulation Results

The 9-bus 3-machine power system of Fig. 3-1 [26] is adopted to confirm the load flow bifurcation test. Figure 3-1 shows the transmission network configuration, and gives the base case data, where the resistance, reactance, and line charging

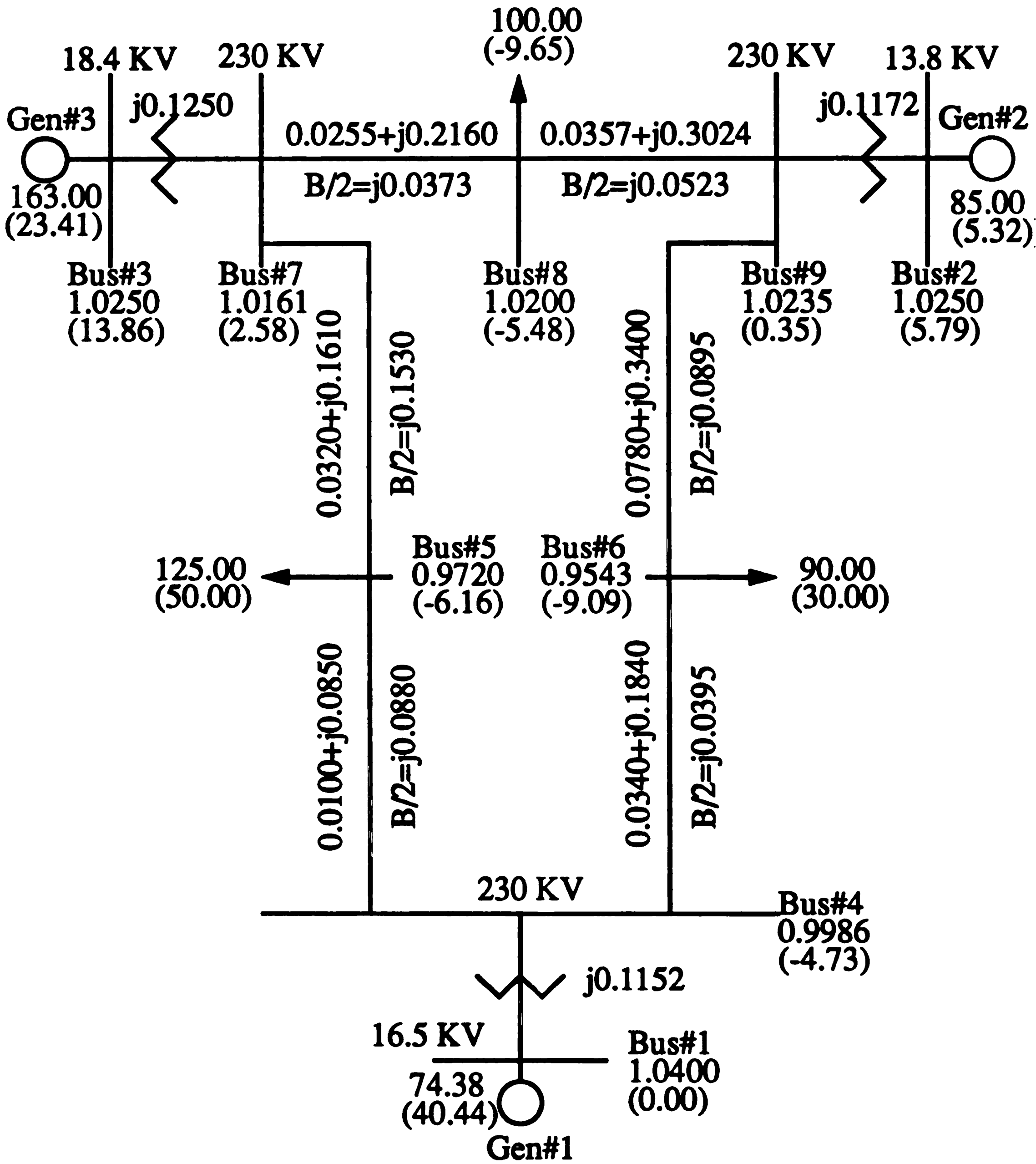

Fig. 3-1 9-bus 3-machine Power System Diagram susceptance of the transmission network is in *pu* based on 100.00 *MVA* and the rated bus voltage as shown in Fig. 3-1; the bus voltage is shown in the format: $V\ (\theta)$ with V in *pu* and θ in degree; and the active and reactive power injection at each bus is given in the format: $P\ (Q)$ with P in *MW* and Q in *MVAR*. These three generators are operated as follows: the generator terminal bus#1 is the swing (infinity) bus; the generator terminal bus#2 is a PV-bus with reactive power generation limit $\pm$ 40.00 *MVAR*; and the generator terminal bus#3 is a PV-bus with reactive power generation limit $\pm$ 50.00 *MVAR*. Note that the resistance, reactance, and line charging susceptance of this power system are adjusted and are different from the original data in [26].

The $Q-V$ curve test of the point of voltage collapse method [53] is used to show the load flow bifurcation as shown in Fig. 3-2(b). The bus#8 is treated as a fictitious PV-bus — a dummy generator test bus — whose voltage is assigned and changed from the base case voltage 1.02 *pu* with reactive power "generation" (its negative sign is the actual reactive power load) 0.0965 *pu*. Figure 3-2(a) shows two matrix determinants: one with the notation $Det\ (LF0)$ is for the load flow Jacobian matrix J_{LF} ((3-2) or (3-8)) excluding the fictitious PV-bus; the other $Det\ (LF1)$ is for the load flow Jacobian matrix including the fictitious PV-bus. Figure 3-2(b) shows the $Q-V$ curve at the fictitious PV-bus, and its slope $Det\ (QV)$ (a scalar) which is the corresponding diagonal element of the sensitivity matrix S_{QV} ((3-2) or (3-8)) of this $Q-V$ curve. Figure 3-2(c) gives the $Q-V$ curve profile of the generator buses with reactive power generation high limits, and Figure 3-2(d) represents the voltage profile of each bus. The voltage angle (in degree) of each bus, and the active power generation of each generator bus are respectively shown in Fig. 3-2(e) and Fig. 3-2(f), which should help understand the phenomena of the power system when the voltage and the reactive power injection at the test bus (fictitious PV-bus) are changed.

Fig. 3-2(a) --- Det(LF0):o ; Det(LF1):x

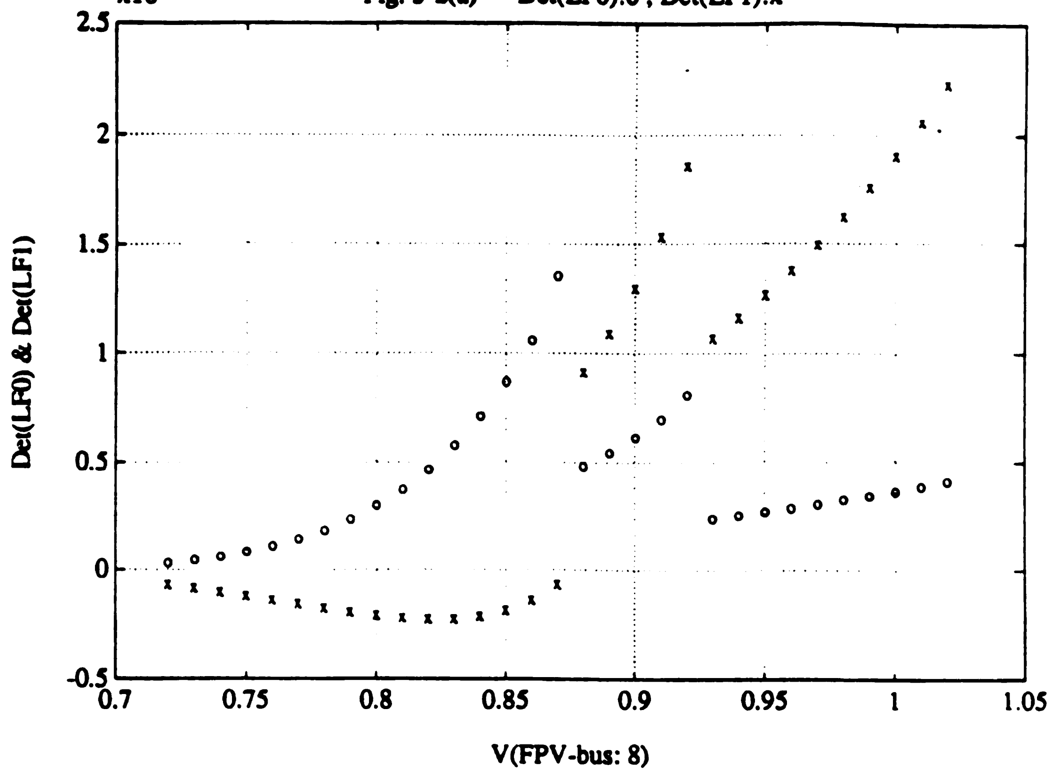

Fig. 3-2(b) --- Qgt8:x ; Det(QV):*

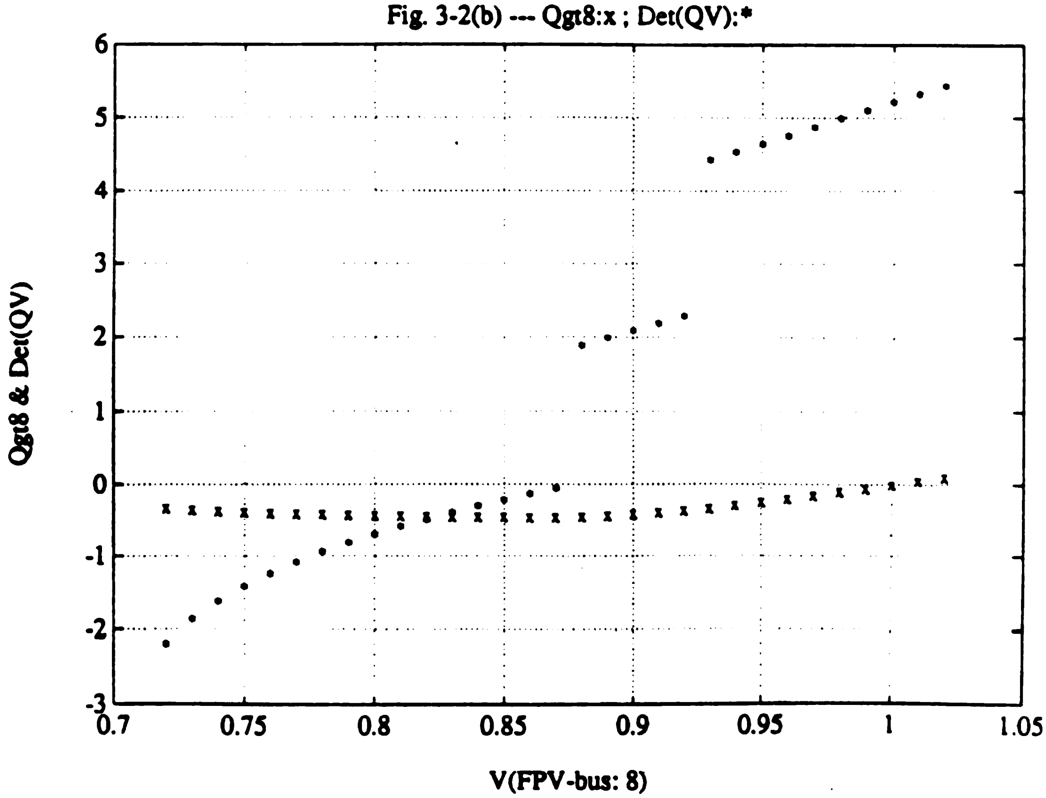

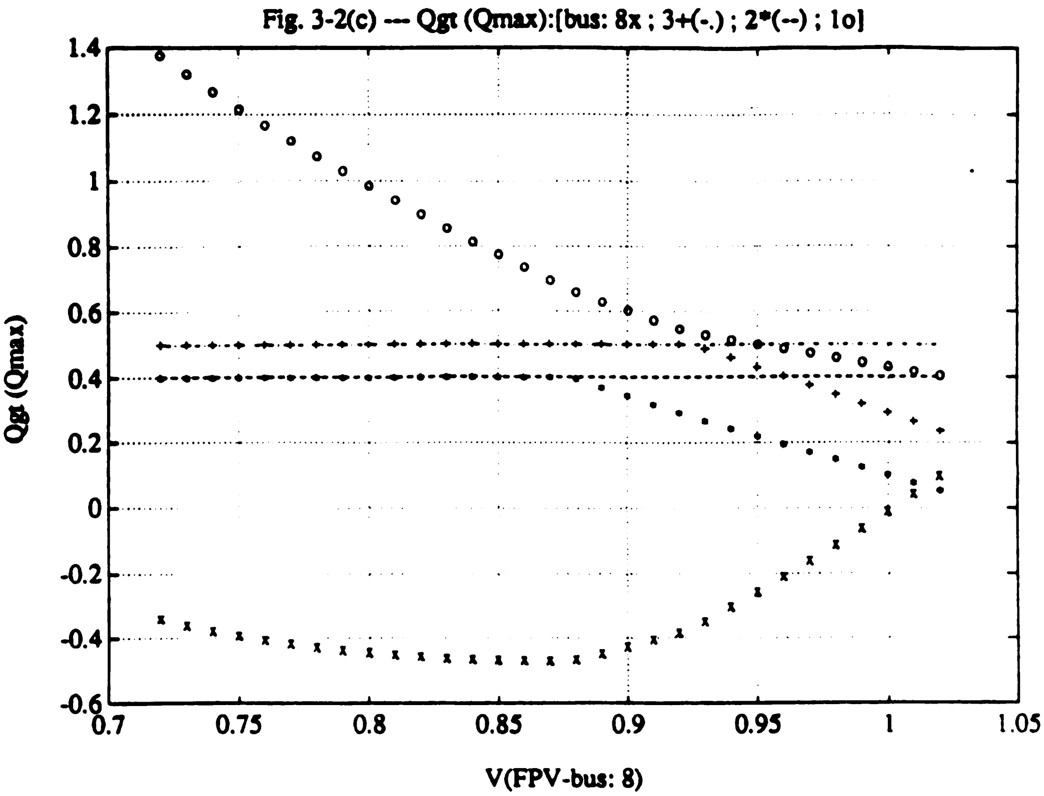
Fig. 3-2(c) --- Qgt (Qmax):[bus: 8x ; 3+(-.) ; 2*(--) ; 1o]
Qgt (Qmax)
1.4
1.2
1
0.8
0.6
0.4
0.2
0
-0.2
-0.4
-0.6
0.7
0.75
0.8
0.85
0.9
0.95
1
1.05
V(FPV-bus: 8)

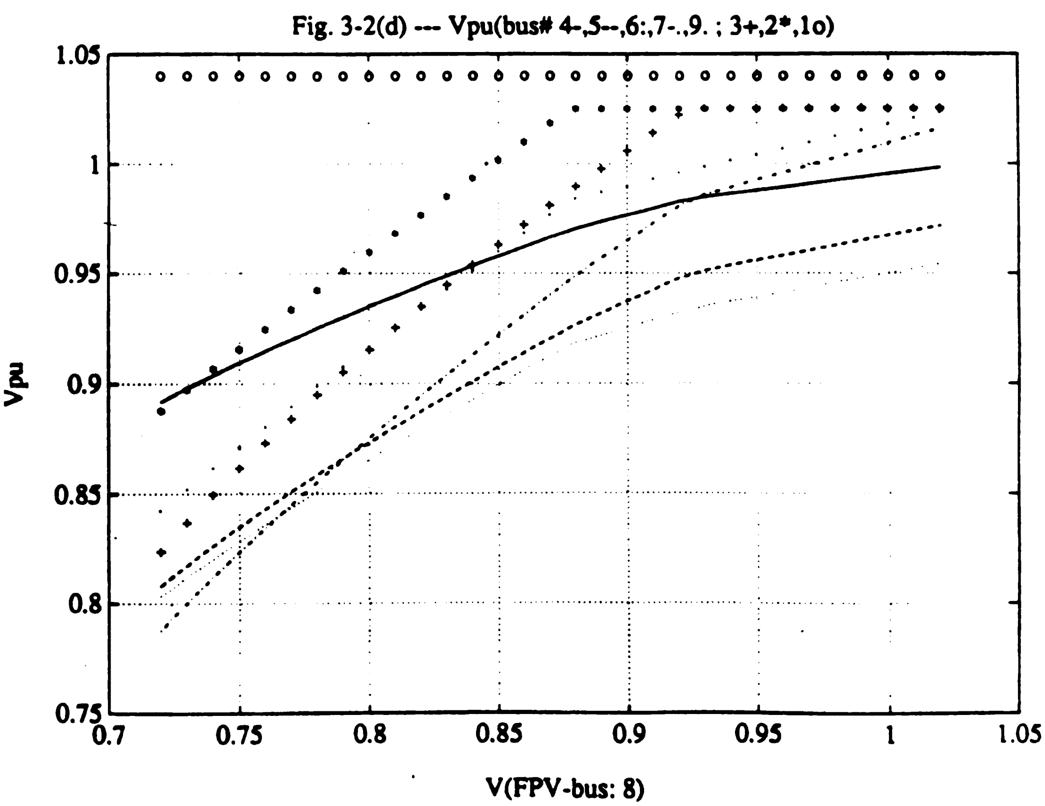
Fig. 3-2(d) --- Vpu(bus# 4-,5--,6:,7-.,9. ; 3+,2*,1o)
Vpu
1.05
1
0.95
0.9
0.85
0.8
0.75
0.7
0.75
0.8
0.85
0.9
0.95
1
1.05
V(FPV-bus: 8)

Fig. 3-2(e) --- Angle(bus# 4-,5--,6:,7-.,8x,9. ; 3+,2*,1o)

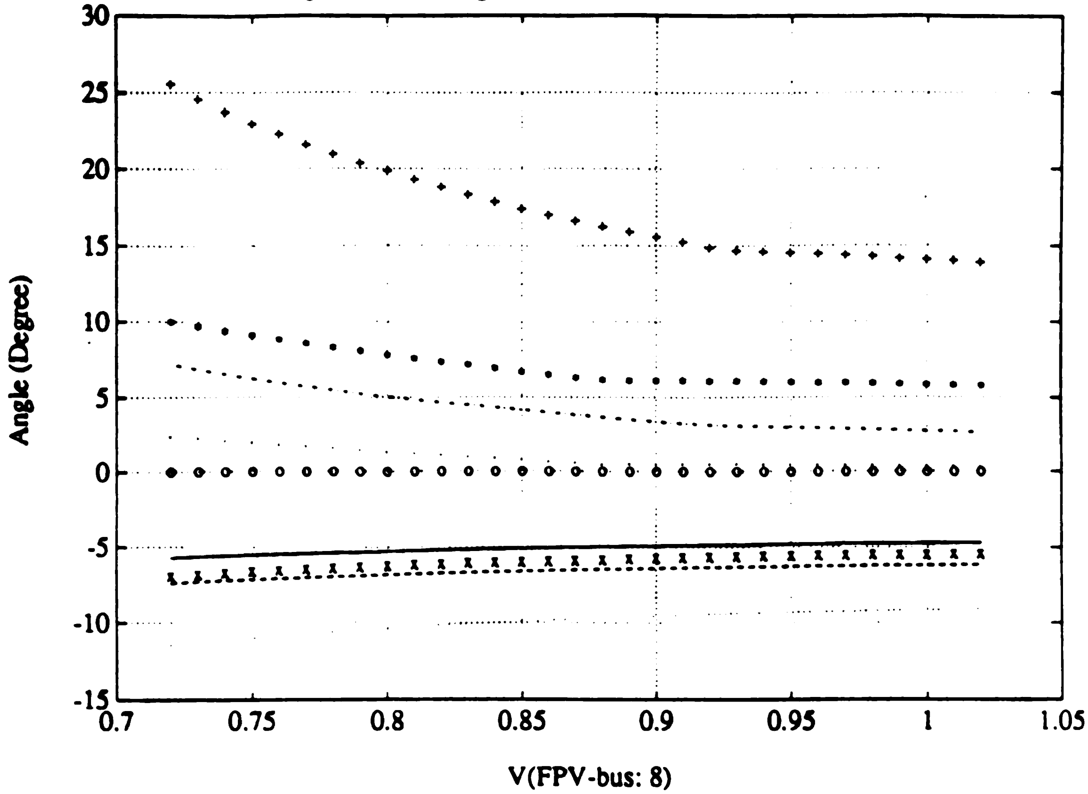

Fig. 3-2(f) --- Pgt(bus# 3+, 2*, 1o)

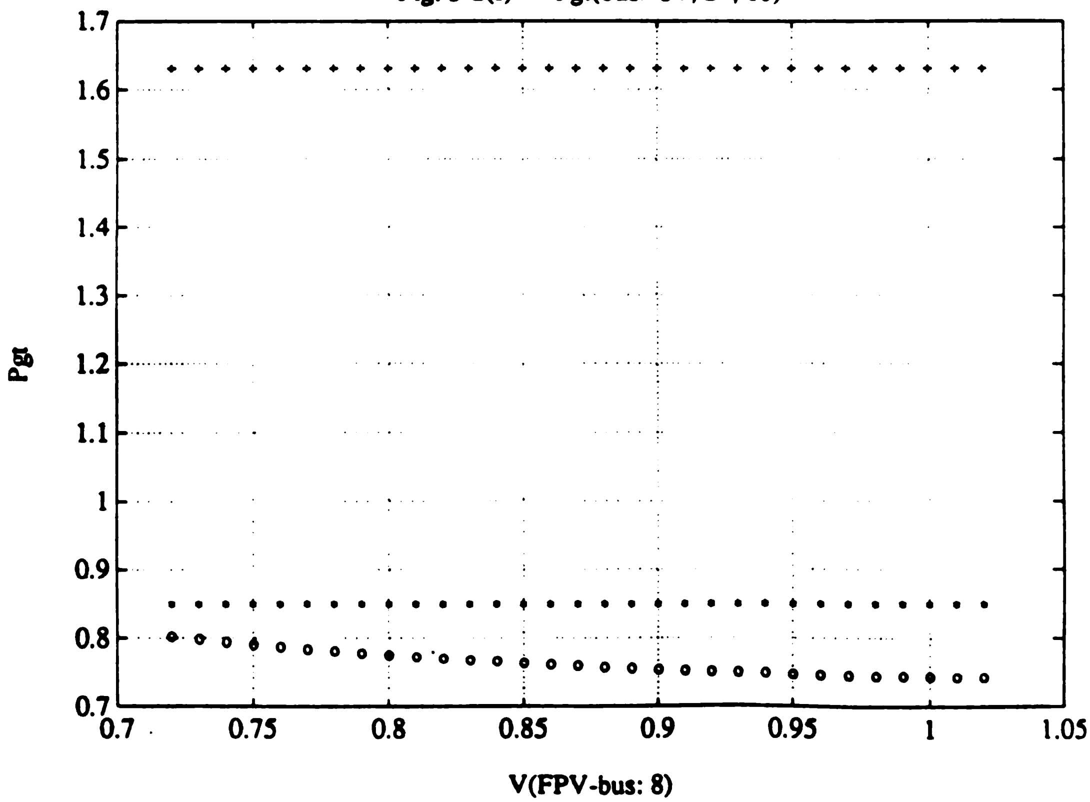

It is observed from Fig. 3-2 that the load flow bifurcation occurs at the minimum of the test bus#8 $Q-V$ curve when the reactive power load about 0.467 pu is added at the bus#8 whose voltage is assigned at 0.87 pu. Note from Fig. 3-2 (a) - Fig. 3-2 (c) that the generator bus#3 hits its reactive power generation high limit 0.50 pu before the generator bus#2 does, and that whenever one generator hits its reactive power generation (high) limit and becomes a PQ-bus, the dimension of the load flow Jacobian matrix J_{LF} changes by increasing one; whereas the dimension of the $Q-V$ sensitivity matrix S_{QV} reduces by one. This causes the jump phenomena of the determinant of the load flow Jacobian matrix and that of the slope of the test bus $Q-V$ curve. Note also that, from Fig. 3-2(c), the load flow bifurcation occurs at about the point where the generator bus#3 becomes a PQ-bus (the generator bus#2 has already become a PQ-bus), even though the swing bus#1 has infinite active and reactive power reserves. This result shows that the voltage collapse is a problem of (reactive) power demand and supply. Each time a PV-bus changes to a PQ-bus, the supply rate from the PV-bus is lost and the rate of increase in reactive power losses increase with further voltage decline. The effective reactive power supply rate to the bus with voltage drop decreases until the reactive power load demand at the bus#8 is 0.467 pu, where the transmission network does not have the ability to transfer enough reactive power to meet the requirement at bus#8 and the losses in the transmission network, even though this system still has reactive power reserve at bus#1.

It should be pointed out that from Fig. 3-2(e), the angle differences between any two contiguous buses are never more than about 40.00^o. In addition, after bus#3 changes from a PV-bus to PQ-bus, its voltage angle starts dramatically increasing when the system is more stressed. The voltage angle at bus#2 also begins to increase rapidly after it becomes a PQ-bus. Whenever a generator PV-bus becomes a PQ-bus, its voltage is no longer constant and begins to decrease when the system gets more stressed, but it still keeps constant active power output (see Fig. 3-2(f)). The generator

PQ-bus then needs to increase its angle to compensate the voltage drop in order to keep its active power output to be constant. When both voltage and angle change as stress is added, a voltage/angle bifurcation is being approached.

Chapter 4
Stability Problems in a Differential-Algebraic Model

The theory of bifurcation [36-38] has been applied to investigate dynamic stability and voltage collapse problems, under the assumption that the causality condition [39,40] holds in the differential-algebraic power system dynamic model. The equivalent system Jacobian matrix can then be obtained after inverting the causality matrix and aggregating the transmission network back to the generator internal buses. One of the necessary conditions for static/saddle-node or dynamic/Hopf bifurcations is that the equivalent system Jacobian matrix has eigenvalues with zero real parts (others are transversality and nondegeneracy conditions) [36-38]. The above bifurcations have been shown to lead to loss of dynamic stability and/or voltage collapse, and been shown to be mainly associated with both mechanical and electrical system dynamics of generators [39-45,52,53,64-73,78,79,87,88]. However, most of the studies have used eigenvalue analysis on the equivalent system Jacobian matrix to establish if these bifurcations can occur. Eigenvalue analysis is not only computationally memory intensive, but also computationally time intensive for a large power system dynamic model. Furthermore, eigenvalue analysis has not generally been applied to the very large data bases to study voltage stability problems. Moreover, the main assumption that the causality condition holds may not be true, such that the equivalent dynamic system Jacobian matrix can not be simply defined. The stability problems due to loss of causality are not described and are not associated with the eigenvalues of the equivalent system Jacobian matrix.

This chapter will classify the types of bifurcation and stability problems in the differential-algebraic model. Necessary conditions are determined for each of these types of bifurcation and stability problems. Several of these bifurcations are shown to be non-generic. The static and dynamic bifurcations associated with eigenvalues of the equivalent system Jacobian matrix having zero real parts are shown to be generic bifurcations. The stability problems due to loss of causality and due to loss of stability of the generator dynamics are also identified as possible, if not improbable, stability problems. The static/algebraic bifurcation will be shown to be equivalent to the static bifurcation. The static/algebraic Jacobian matrix has similar structure to the load flow Jacobian matrix. This static/algebraic Jacobian matrix is associated with a set of linearized algebraic equations that produces the equilibrium point of the differential-algebraic model, which is very similar to the load flow model. In addition, this static/algebraic bifurcation test matrix avoids the inverse of causality matrix. Finally, the static bifurcation test due to the singularity of the static/algebraic Jacobian matrix will be shown to occur based on the simulation results of a 9-bus 3-machine power system.

4.1 Linearized Power System Dynamic Model

From Chapter 2, the dynamics of a power system is characterized by two types of equations: (1) the differential equations of rotor and flux decay dynamics of machines, and those of their control systems (that include (a) Excitation System with Load (Line-Drop) Compensator [85], (b) Power System Stabilizer (PSS) [85], and (c) Speed-Governing-Turbine System [86]), and (2) the active and reactive power balance (algebraic) equations at the internal and terminal buses of machines, at the transformer high-side buses of machines (simply called high-side buses), and at the load buses. Hence, the specific power system dynamic model can be represented as follows:

$$\dot{x} = f\ (x\ , y\ ; \mu\ ) \tag{4-1a}$$

$$0 = g\ (x\ , y\ ; \mu\ ) \tag{4-1b}$$

where,

x : the M-vector of dynamic states of generators and control systems;

y : the N-vector of network dependent variables, i.e., the voltage and angle at each terminal bus (V_T, θ_T), high-side bus (V_H, θ_H), and load bus (V_L, θ_L);

μ : the vector of independent parameters, such as reference voltage of excitation system (V_{ref}), mechanical power setting of speed-governing-turbine system (P_0), and load demand parameters (P_D, Q_D);

f : the function describing the relationship among the dynamic states, network dependent variables, and control parameters, through the coupling branch between internal bus and terminal bus of each generator;

g : the function describing the power balance equation at generator terminal buses, at high-side buses, and at load buses.

All the solutions of (4-1) must belong to the M-dimensional surface S_g which is defined as all points x and y where (4-1b) is satisfied. The Jacobian matrix of (4-1) at any equilibrium point (x_e^*, y_e^*; μ_e^*) can be obtained from the linearized power system dynamic model, that has the following matrix form, by combining the linearized equation of each component in the power system shown in Section 2.6. The relationship between the Jacobian submatrices is shown in Fig. 4-1.

$$J = \begin{bmatrix} J_f \\ J_g \end{bmatrix} = \begin{bmatrix} f_x & f_y \\ g_x & g_y \end{bmatrix} = \begin{bmatrix} \frac{\partial f}{\partial x} & \frac{\partial f}{\partial y} \\ \frac{\partial g}{\partial x} & \frac{\partial g}{\partial y} \end{bmatrix}_{(x_e^*,\, y_e^*;\, \mu_e^*)} \tag{4-2a}$$

$$\begin{bmatrix} T_{XX}\,\Delta\dot{X}_X \\ T_{EE}\,\Delta\dot{X}_E \\ T_{GG}\,\Delta\dot{X}_G \\ T_{SS}\,\Delta\dot{X}_S \\ -\Delta P_C \\ -\Delta Q_C \end{bmatrix} = \begin{bmatrix} A_{XX} & A_{XE} & A_{XG} & 0 & A_{X\theta} & A_{XV} \\ A_{EX} & A_{EE} & 0 & A_{ES} & A_{E\theta} & A_{EV} \\ A_{GX} & 0 & A_{GG} & 0 & 0 & 0 \\ A_{SX} & 0 & 0 & A_{SS} & 0 & 0 \\ A_{PX} & 0 & 0 & 0 & A_{P\theta} & A_{PV} \\ A_{QX} & 0 & 0 & 0 & A_{Q\theta} & A_{QV} \end{bmatrix} \begin{bmatrix} \Delta X_X \\ \Delta X_E \\ \Delta X_G \\ \Delta X_S \\ \Delta\theta \\ \Delta V \end{bmatrix} + \begin{bmatrix} 0 \\ B_{E0} \\ B_{G0} \\ 0 \\ 0 \\ 0 \end{bmatrix} \Delta U_0 \tag{4-2b}$$

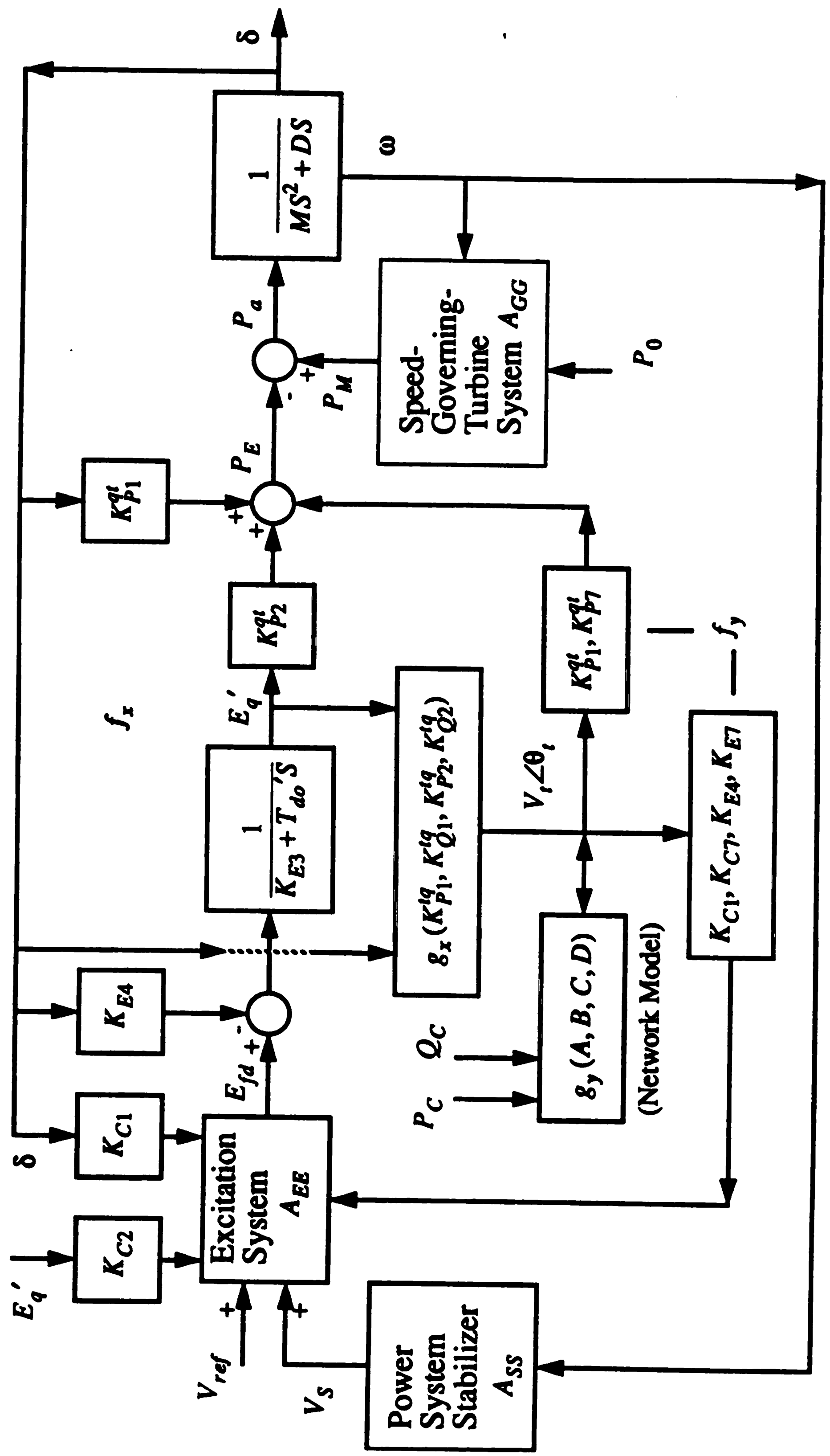

Fig. 4-1 Block Diagram of Power System Jacobian Matrices

where,

$$f_x = (diag\,[\,T_{XX}\;\; T_{EE}\;\; T_{GG}\;\; T_{SS}\,])^{-1} \begin{bmatrix} A_{XX} & A_{XE} & A_{XG} & 0 \\ A_{EX} & A_{EE} & 0 & A_{ES} \\ A_{GX} & 0 & A_{GG} & 0 \\ A_{SX} & 0 & 0 & A_{SS} \end{bmatrix}$$

$$f_y = (diag\,[\,T_{XX}\;\; T_{EE}\;\; T_{GG}\;\; T_{SS}\,])^{-1} \begin{bmatrix} A_{X\theta} & A_{XV} \\ A_{E\theta} & A_{EV} \\ 0 & 0 \\ 0 & 0 \end{bmatrix}$$

$$g_x = \begin{bmatrix} A_{PX} & 0 & 0 & 0 \\ A_{QX} & 0 & 0 & 0 \end{bmatrix}$$

$$g_y = \begin{bmatrix} A_{P\theta} & A_{PV} \\ A_{Q\theta} & A_{QV} \end{bmatrix}$$

$\Delta X_X \;= [\,\Delta\omega^t\;\; \Delta\delta^t\;\; \Delta E_q'^{\,t}\,]^t$

: states of mechanical and flux decay dynamics;

$\Delta X_E \;= [\,\Delta V_D{}^t\;\; \Delta V_F{}^t\;\; \Delta V_A{}^t\;\; \Delta V_B{}^t\;\; \Delta E_{fd}{}^t\,]^t$

: states of excitation systems (see Fig. 2-5);

$\Delta X_G \;= [\,\Delta P_1{}^t\;\; \Delta P_{GV}{}^t\;\; \Delta P_{VHP}{}^t\;\; \Delta P_{HP}{}^t\;\; \Delta P_{IP}{}^t\;\; \Delta P_{LP}{}^t\,]^t$

: states of speed-governing-turbine systems (see Fig. 2-8);

$\Delta X_S \;= [\,\Delta V_{S0}{}^t\;\; \Delta V_{S2}{}^t\;\; \Delta V_{S4}{}^t\,]^t$

: states of power system stabilizers (see Fig. 2-7);

$\Delta\theta \;= [\,\Delta\theta_T{}^t\;\; \Delta\theta_H{}^t\;\; \Delta\theta_L{}^t\,]^t$

: angle variables at network buses (terminal: T, high-side: H, load: L);

$\Delta V \;= [\,\Delta V_T{}^t\;\; \Delta V_H{}^t\;\; \Delta V_L{}^t\,]^t$

: voltage variables at network buses;

$\Delta P_C \;= [\; \Delta P_{CT}{}^t \;\; \Delta P_{CH}{}^t \;\; \Delta P_{CL}{}^t \;]^t$

: coefficients of non-voltage-dependent active power load demand model;

$\Delta Q_C \;= [\; \Delta Q_{CT}{}^t \;\; \Delta Q_{CH}{}^t \;\; \Delta Q_{CL}{}^t \;]^t$

: coefficients of non-voltage-dependent reactive power load demand model;

$$T_{XX} = diag\ [\, M \;\; I \;\; T'_{do} \,] = \begin{bmatrix} M & 0 & 0 \\ 0 & I & 0 \\ 0 & 0 & T'_{do} \end{bmatrix}$$

$M \quad = diag\ [\, M_1 , M_2 , \ldots , M_m \,]$

: inertia constants of m synchronous machines;

$I \quad$: $m \ x \ m$ identity matrix;

T'_{do} : $m \ x \ m$ diagonal time constant matrix of flux decay dynamics;

$T_{EE} \;= diag\ [\, T_D \;\; T_F \;\; T_A \;\; T_B \;\; T_E \,]$

: time constants of excitation systems (see Fig. 2-5);

$T_{GG} \;= diag\ [\, T_1 \;\; T_3 \;\; T_{CH} \;\; T_{RH1} \;\; T_{RH2} \;\; T_{CO} \,]$

: time constants of speed-governing-turbine systems (see Fig. 2-8);

$T_{SS} \;= diag\ [\, T_S \;\; T_{S2} \;\; T_{S4} \,]$

: time constants of power system stabilizers (see Fig. 2-7);

Note that T_{EE}, T_{GG}, and T_{SS} submatrices above are defined using a similar notation to that used in defining T_{XX}, and the submatrices $T'_{do}, \cdots, T_{S4}$ are m dimensional diagonal matrices composed of the appropriate time constants of the generator and control systems models. The A-matrices of each Jacobian submatrix are defined as follows.

$$A_{XX} = \begin{bmatrix} -D & -K^{gt}_{P1} & -K^{gt}_{P2} \\ I & 0 & 0 \\ 0 & -K_{E4} & -K_{E3} \end{bmatrix}$$

$$A_{XE} = \begin{bmatrix} 0 \\ 0 \\ A_{FE} \end{bmatrix} = \begin{bmatrix} 0 & 0 & 0 & 0 & 0 \\ 0 & 0 & 0 & 0 & 0 \\ 0 & 0 & 0 & 0 & I \end{bmatrix}$$

$$A_{XG} = \begin{bmatrix} A_{\omega G} \\ 0 \\ 0 \end{bmatrix} = \begin{bmatrix} 0 & 0 & F_{VHP} & F_{HP} & F_{IP} & F_{LP} \\ 0 & 0 & 0 & 0 & 0 & 0 \\ 0 & 0 & 0 & 0 & 0 & 0 \end{bmatrix}$$

$$A_{EX} = [\, A_{E\omega} \;\; A_{EC1} \;\; A_{EC2} \,] = \begin{bmatrix} 0 & K_D K_{C1} & K_D K_{C2} \\ 0 & 0 & 0 \\ A_{A\omega} & 0 & 0 \\ A_{B\omega} & 0 & 0 \\ 0 & 0 & 0 \end{bmatrix}$$

$$A_{A\omega} = K_A T_{BC} T_{43} T_{21} K_S \;\; ; \;\; A_{B\omega} = I_{BC} T_{43} T_{21} K_S$$

$$T_{BC} = T_B^{-1} T_C \;\; ; \;\; I_{BC} = I - T_{BC}$$

$$T_{43} = T_{S4}^{-1} T_{S3} \;\; ; \;\; T_{21} = T_{S2}^{-1} T_{S1}$$

$$A_{EE} = \begin{bmatrix} -I & 0 & 0 & 0 & 0 \\ 0 & -I & 0 & 0 & -T_F^{-1} K_F \\ -K_A T_{BC} & -K_A T_{BC} & -I & K_A & -K_A T_{BC} T_F^{-1} K_F \\ -I_{BC} & -I_{BC} & 0 & -I & -I_{BC} T_F^{-1} K_F \\ 0 & 0 & I & 0 & -K_{SE} \end{bmatrix}$$

$$A_{ES} = \begin{bmatrix} 0 & 0 & 0 \\ 0 & 0 & 0 \\ K_A T_{BC} T_{43} T_{21} & K_A T_{BC} T_{43} & K_A T_{BC} \\ I_{BC} T_{43} T_{21} & I_{BC} T_{43} & I_{BC} \\ 0 & 0 & 0 \end{bmatrix}$$

$$A_{GX} = [\, A_{G\omega} \;\; 0 \;\; 0 \,] = \begin{bmatrix} (I - T_1^{-1} T_2) K_G & 0 & 0 \\ -T_1^{-1} T_2 K_G & 0 & 0 \\ 0 & 0 & 0 \\ 0 & 0 & 0 \\ 0 & 0 & 0 \\ 0 & 0 & 0 \end{bmatrix}$$

$$A_{GG} = \begin{bmatrix} -I & 0 & 0 & 0 & 0 & 0 \\ -I & -I & 0 & 0 & 0 & 0 \\ 0 & I & -I & 0 & 0 & 0 \\ 0 & 0 & I & -I & 0 & 0 \\ 0 & 0 & 0 & I & -I & 0 \\ 0 & 0 & 0 & 0 & I & -I \end{bmatrix}$$

$$A_{SX} = [\, A_{S\omega} \;\; 0 \;\; 0 \,] = \begin{bmatrix} -K_S & 0 & 0 \\ I_{21}K_S & 0 & 0 \\ I_{43}T_{21}K_S & 0 & 0 \end{bmatrix}$$

$$I_{43} = I - T_{43} \;\; ; \;\; I_{21} = I - T_{21}$$

$$A_{SS} = \begin{bmatrix} -I & 0 & 0 \\ I_{21} & -I & 0 \\ I_{43}T_{21} & I_{43} & -I \end{bmatrix}$$

$$\Delta U_0 = [\, \Delta V_{ref}{}^t \;\; \Delta P_0{}^t \,]^t$$

$$B_{E0} = [\, B_{EE} \;\; 0 \,] = \begin{bmatrix} 0 & 0 \\ 0 & 0 \\ K_A T_B^{-1} T_C & 0 \\ I - T_B^{-1} T_C & 0 \\ 0 & 0 \end{bmatrix} \;\; ; \;\; B_{G0} = [\, 0 \;\; B_{GG} \,] = \begin{bmatrix} 0 & 0 \\ 0 & I \\ 0 & 0 \\ 0 & 0 \\ 0 & 0 \\ 0 & 0 \end{bmatrix}$$

$$A_{X\theta} = \begin{bmatrix} K_{P1}^{gt} & 0 & 0 \\ 0 & 0 & 0 \\ K_{E4} & 0 & 0 \end{bmatrix} \;\; ; \;\; A_{XV} = \begin{bmatrix} -K_{P7}^{gt} & 0 & 0 \\ 0 & 0 & 0 \\ K_{E7} & 0 & 0 \end{bmatrix}$$

$$A_{E\theta} = \begin{bmatrix} -K_D K_{C1} & 0 & 0 \\ 0 & 0 & 0 \\ 0 & 0 & 0 \\ 0 & 0 & 0 \\ 0 & 0 & 0 \end{bmatrix} \;\; ; \;\; A_{EV} = \begin{bmatrix} K_D K_{C7} & 0 & 0 \\ 0 & 0 & 0 \\ 0 & 0 & 0 \\ 0 & 0 & 0 \\ 0 & 0 & 0 \end{bmatrix}$$

$$A_{PX} = \begin{bmatrix} 0 & -K_{P1}^{tq} & K_{P2}^{tq} \\ 0 & 0 & 0 \\ 0 & 0 & 0 \end{bmatrix} \;\; ; \;\; A_{QX} = \begin{bmatrix} 0 & -K_{Q1}^{tq} & K_{Q2}^{tq} \\ 0 & 0 & 0 \\ 0 & 0 & 0 \end{bmatrix}$$

$$A_{P\theta} = \begin{bmatrix} A_{1K} & B_{1H} & 0 \\ A_{2H} & B_{2HH} & B_{2HL} \\ 0 & B_{2LH} & B_{2LL} \end{bmatrix} \; ; \; A_{PV} = \begin{bmatrix} C_{1K} & D_{1H} & 0 \\ C_{2H} & D_{2HH} & D_{2HL} \\ 0 & D_{2LH} & D_{2LL} \end{bmatrix}$$

$$A_{1K} = K_{P1}^{tq} + A_1 \; ; \; C_{1K} = K_{P7}^{tq} + C_1$$

$$A_{Q\theta} = \begin{bmatrix} A_{3K} & B_{3H} & 0 \\ A_{4H} & B_{4HH} & B_{4HL} \\ 0 & B_{4LH} & B_{4LL} \end{bmatrix} \; ; \; A_{QV} = \begin{bmatrix} C_{3K} & D_{3H} & 0 \\ C_{4H} & D_{4HH} & D_{4HL} \\ 0 & D_{4LH} & D_{4LL} \end{bmatrix}$$

$$A_{3K} = K_{Q1}^{tq} + A_3 \; ; \; C_{3K} = K_{Q7}^{tq} + C_3$$

The following properties of the submatrices of the linearized power system model help provide understanding of the model.

(1) All the K matrices are m x m diagonal matrices. Among them, the matrices, K_{P2}^{qt}, K_{E3}, K_{E4}, K_{E7}, K_{P2}^{tq}, K_{Q2}^{tq}, and K_{C2}, are associated with the flux decay dynamic states E_q' of the single-axis modeled synchronous machines.

(2) The matrices K^{qt} and K^{tq} of the power balance equations at internal buses and terminal buses of synchronous machines represent the coupling between both buses. In general, $K^{tq} \neq K^{qt}$, because of the armature and salient-pole effects of synchronous machines, that cause X_d, X_q, and X_d' are different. If the armature resistances (R_a) and salient-pole effects are neglected, then $P_E = P_{Gt} = -P_{tq}$ such that $K_{P1}^{qt} = K_{P1}^{tq}$, $K_{P2}^{qt} = -K_{P2}^{tq}$, and $K_{P7}^{qt} = -K_{P7}^{tq}$.

(3) The load compensator is characterized by the diagonal matrices: K_{C1}, K_{C2}, and K_{C7}. If a load compensator is not employed, then $V_C = V_T$, i.e., $K_{C1} = 0$, $K_{C2} = 0$, and $K_{C7} = I$.

(4) Due to the effects of transformers, phase-shifters, and network conductances, each of these network submatrices, $A_{P\theta}$, A_{PV}, $A_{Q\theta}$, and A_{QV},

composing of the network Jacobian matrix is not symmetric.

(5) The coefficients of voltage dependent load demand model are embedded in the diagonal elements of C and D submatrices.

(6) Under the assumption that the connection between each generator terminal bus and its transformer high-side bus is one-to-one, the submatrices A_i, C_i, $i = 1, 2, 3, 4$, and B_{jH}, D_{jH}, $j = 1, 3$ are diagonal.

(7) Other properties of the network Jacobian matrix can be found in Section 3.1, that are associated with the submatrices of the load flow Jacobian matrix in the load flow model.

4.2 Bifurcations in Power System Dynamic Model

At any parameter pattern $\mu = \mu_e$ of the power system dynamic model (4-1), an equilibrium point $(x_e, y_e; \mu_e)$ on the surface S_g defined by (4-1b) is a solution to

$$0 = f\ (x\ , y\ ; \mu\ ) \tag{4-3a}$$

$$0 = g\ (x\ , y\ ; \mu\ ) \tag{4-3b}$$

Note that the precise formula of (4-3) for solving for the equilibrium point(s) of the power system dynamic model has been discussed in Section 2.5. The bifurcation problem is to characterize the solution set of (4-3) in a neighborhood of an equilibrium point $(x_e, y_e; \mu_e)$. The equilibrium point $(x_e^*, y_e^*; \mu_e^*)$ is a bifurcation point and μ_e^* is a bifurcation value of the parameter if the system satisfies one of the following conditions.

(a) The complete system Jacobian matrix

$$J = \begin{bmatrix} J_f \\ J_g \end{bmatrix} = \begin{bmatrix} f_x & f_y \\ g_x & g_y \end{bmatrix} = \begin{bmatrix} \dfrac{\partial f}{\partial x} & \dfrac{\partial f}{\partial y} \\ \dfrac{\partial g}{\partial x} & \dfrac{\partial g}{\partial y} \end{bmatrix}_{(x_e^*,\, y_e^*\, ;\, \mu_e^*)} \tag{4-4}$$

is singular.

(b) The equivalent static/algebraic Jacobian matrix

$$J_y = g_y - g_x f_x^{-1} f_y \tag{4-5}$$

is singular, provided that f_x is nonsingular.

(c) The equivalent system Jacobian matrix

$$J_x = f_x - f_y g_y^{-1} g_x \tag{4-6}$$

has eigenvalues with zero real parts, provided that g_y is nonsingular.

Note that Jacobian submatrices, f_x, f_y, g_x, and g_y, can be found from the linearized power system dynamic model (4-2).

From the above, six subclasses of bifurcation in power system dynamic model are identified.

(1) A static/algebraic bifurcation occurs when the equivalent static/algebraic Jacobian matrix J_y is singular, but J_g is row independent and g_y and f_x are nonsingular [52,53,87,88].

(2) A static bifurcation occurs when the equivalent system Jacobian matrix J_x is singular and does not have pure imaginary eigenvalues, but J_f is row independent and g_y and f_x are nonsingular. The static bifurcation could be the saddle node bifurcation if the matrix J_x has a simple zero eigenvalue, and the transversality and nondegeneracy condition of J_x at the bifurcation point holds [36-38].

(3) A dynamic bifurcation occurs when the equivalent system Jacobian matrix J_x is nonsingular and has pure imaginary eigenvalues, but g_y and f_x are nonsingular. The dynamic bifurcation could be Hopf bifurcation if the matrix J_x has a pair of pure imaginary eigenvalues, and the nondegeneracy condition of J_x at the bifurcation point holds [36-38].

(4) A differential bifurcation occurs when the equivalent system Jacobian matrix J_x is singular due to the row dependence of J_f (but g_y is nonsingular) [53].

(5) An algebraic bifurcation occurs when the equivalent static/algebraic Jacobian matrix J_y is singular due to the row dependence of J_g (but f_x is nonsingular) [53].

(6) A differential-algebraic bifurcation occurs when the complete system Jacobian matrix J is singular due to both the row dependence of J_f and the row dependence of J_g.

Note that two specially stability problems occur along with the above bifurcations:

(a) A single-machine instability occurs when the machine Jacobian matrix f_x is singular, or when f_x has complex eigenvalues with zero real parts, but J_f is row independent.

(b) Loss of causality occurs when the transmission network Jacobian matrix g_y is singular, but J_g is row independent.

The above stated conditions are necessary conditions for these specific types of bifurcation. Transversality condition for saddle-node bifurcation and nondegeneracy condition for Hopf bifurcation [36-38] which control the nondegeneracy of the behavior with respect to the μ parameter change and the dominant effects of the nonlinear terms of power system dynamic model will not be discussed in this dissertation.

Note that type 1, type 2, and type 3 bifurcations require that both f_x and g_y be nonsingular and both J_f and J_g be row independent, and that type 4, type 5, and type 6 bifurcations are due to the characteristics of row dependence either in J_f, or J_g, or both. The first three types of bifurcation require both f_x and g_y be nonsingular making both J_x and J_y well defined. The type 4 differential bifurcation requires J_g be row independent and g_y be nonsingular so that J_x is well defined. This differential bifurcation also requires f_x be singular and J_f be row dependent leading to the singularity of both J and J_x. The type 5 algebraic bifurcation requires that f_x be nonsingular so that J_y is well defined, and that g_y be singular and J_g be row dependent resulting in the singularity of both J and J_y. The type 6 differential-algebraic bifurcation is restricted to the case where both f_x and g_y are singular and both J_f and J_g are row dependent causing J to be singular and both J_x and J_y to be undefined. The above restrictions on the above bifurcation tests make sure that the classifications are distinct. The relationship and difference between the six classes of bifurcation are now discussed.

It can be shown, using Schur's formula (Appendix A), that the static/algebraic bifurcation due to the singularity of J_y (4-5) can be proven to be equivalent to the static bifurcation due to the singularity of J_x (4-6), provided that both f_x and g_y are nonsingular which is assumed in the definition of the static and static/algebraic bifurcations. Thus, one could consider making the static and static/algebraic bifurcations as a single bifurcation class. The two reasons this wasn't done was (a) a proof is required to establish they are completely equivalent, and (b) at an initial review one would consider singularity of J_y and singularity of J_x as different stability problems, which indeed they would be if all of the possible stability problems due to singularity of J_x or J_y were considered as one class of stability problem. The classification of the bifurcations and the stability problems indicates that there are different stability problems associated with singularity of J_x (static; differential) and different stability problems associated with singularity of J_y (static/algebraic; algebraic); but when f_x and g_y are nonsingular, then there is one stability problem associated with J_x and J_y being singular. If one chose to make the static and static/algebraic one class of bifurcation problem based on the fact that f_x and g_y are assumed nonsingular in the definition of these stability problems, it would be called a static bifurcation, static/algebraic bifurcation, or singularity induced static bifurcation, since both J_x and J_y are singular for this bifurcation to occur. A singularity induced static bifurcation will be shown to be caused by the transmission network stress (see Section 4.6), in a manner almost identical to that causing the load flow bifurcation as shown by the simulation results in Section 3.4.

Note that the type 4 differential bifurcation is not equivalent to the type 2 static bifurcation even though both occur when J_x is singular. The difference between them is that the differential bifurcation is solely due to the instability of the single machine dynamics (J_f is row dependent and f_x is singular), whereas the static bifurcation is due to the instability of the transmission network coupled with the dynamic states represented by J_x. Likewise, the type 5 algebraic bifurcation is not equivalent to the type 1 static/algebraic bifurcation even though both occur when J_y is singular. The difference between them is that the algebraic bifurcation is solely due to the lack of solutions or multiple solutions of the transmission network (J_g is row dependent and g_y is singular), whereas the static/algebraic bifurcation is due to the instability of the transmission network coupled with the dynamic states represented by J_y. The similarity of J_y and the load flow Jacobian matrix J_{LF} is discussed in Section 4.4. It should also be pointed out that the row dependence of J_g and loss of causality (g_y singular) indicate that the set of algebraic equations (4-3b) may have either no solutions or multiple solutions; but the static/algebraic bifurcation is a bifurcation in both machine dynamics and transmission network. The two special stability problems due to the singularity of f_x and that of g_y will be discussed in Section 4.3, even though they are not bifurcations because they indicate loss of stability and because the tests for the static/algebraic, static, and dynamic bifurcations require that they be nonsingular.

4.3 Prerequisites of Bifurcation Study

Having classified the simplest types of bifurcation for a differential-algebraic power system model, it will now be shown that the type 4 differential bifurcation due to J_f being row dependent, the type 5 algebraic bifurcation due to J_g being row dependent, and the type 6 differential-algebraic bifurcation due to both J_f and J_g being row dependent are not generic types of bifurcation. The singularity of J requires that $v^t J = 0$, where v is the left eigenvector of J associated with the zero eigenvalue of J. The requirement that an only subset of the rows of J be row dependent amounts to finding a point of singularity where $v^t J = 0$ such that the elements of v are specified to be zero and not free. Thus, the differential bifurcation, the algebraic bifurcation, and the differential-algebraic bifurcation can be considered as very rare types of bifurcation since the constraints associated with forcing elements of v to be zero for the operating conditions where $v^t J_{LF} = 0$ make it so.

Therefore, although we started with the possibility of six different types of bifurcation in the power system dynamic model of (4-1) and (4-2), only three types, type 1, type 2, and type 3, of bifurcation appear to remain as likely, and will be discussed in the rest of this dissertation. Both type 1 and type 2 are singularity induced static bifurcations and equivalent to each other when f_x and g_y are always nonsingular, which are required to be based on their definitions. The type 3 of bifurcation is the dynamic bifurcation. It should be pointed out that both f_x and g_y might still be singular [87] and produce non-bifurcation stability problems. The behavior of the system due to loss of causality will now be discussed further in Section 4.3.1. The singularity of f_x will be further addressed in Section 4.3.2, and be argued to be improbable, but the proof is not strong enough to prove that the singularity of f_x is non-generic. Thus, singularity induced bifurcation, dynamic bifurcation, and loss of causality will remain as generic stability problems. Although loss of causality must be considered as a generic stability problem, discussion concerning the structure of g_y compared to the static/algebraic Jacobian matrix J_y addressed in Section 4.4 and the simulation results of the static/algebraic bifurcation test for a power system with the reactive power generation reserve constraints addressed in Section 4.6 suggest that loss of causality may not be a generic stability problem.

Chapter 5 will concentrate on systematically developing test conditions for the static and dynamic bifurcations (type 2 and type 3), based on the equivalent dynamic Jacobian matrix J_x, under the assumptions that causality condition holds (g_y is nonsingular) and that transversality/nondegeneracy condition holds. Test conditions for the static and dynamic bifurcations pertaining to mechanical and flux decay dynamics will also be established [88], based on the property that each of control systems itself does not have eigenvalues with zero real parts which will also be proven to be true in Section 4.3.2.

4.3.1 Causality Condition — g_y

In Section 4.1, the M-dimensional surface S_g is defined, which requires that all the solutions of the power system dynamic model (4-1) x and y must satisfy (4-1b) $0 = g(x, y; \mu)$ at any μ parameter. The causality condition of the power system, $g_y = \partial g / \partial y$ being nonsingular, means that every solution x and y must belong to the regular part of S_g,

$S_{gr} = \{0 = g(x, y; \mu) \; ; \; J_g \text{ is row independent.}\}$

which is an M-dimensional submanifold in S_g [89].

When J_g is row dependent, the solutions x and y on the surface S_g are no longer regular and do not belong to S_{gr}. Thus, there can not only be more than one y solution for each x but several x solutions with more than one y solution for each x. These x and y, when J_g is row dependent, lie on the geometric boundary separating the regular part of S_g from the remainder of S_g. Note that the row dependence of J_g implies the singularity of g_y leading to loss of causality. Since loss of causality can still happen even when J_g is row independent, this boundary is characterized by the particularly complicated type of stability problems observed as being associated with loss of causality.

Loss of causality (g_y is singular) occurs on the so-called frontier

$$F_g = \{0 = g(x, y; \mu) \; ; \; g_y \text{ is singular.}\}$$

which is an $M-1$-dimensional surface [89]. On the frontier, y in (4-1b) can no longer be solved as a unique function of x. Loss of causality results in uncertain dynamic behavior of two different types: singular points and impasse points can occur on the F_g surface. At an impasse point, a solution may not be continued for all time after an impasse point is encountered on the frontier. This is not the case for a singular point. If the initial condition is a singular point, then solutions exist but are not unique. A solution can switch from component to component of the regular part of the solution set via singular points. Jump phenomena and complicated periodic solutions can occur at these impasse and singular points.

From the linearized power system dynamic model (4-2), the causality matrix g_y can be structurally represented as follows:

$$g_y = \begin{bmatrix} A_{P\theta} & A_{PV} \\ A_{Q\theta} & A_{QV} \end{bmatrix}$$

$$= \begin{bmatrix} A_{1K} & B_{1H} & 0 & C_{1K} & D_{1H} & 0 \\ A_{2H} & B_{2HH} & B_{2HL} & C_{2H} & D_{2HH} & D_{2HL} \\ 0 & B_{2LH} & B_{2LL} & 0 & D_{2LH} & D_{2LL} \\ A_{3K} & B_{3H} & 0 & C_{3K} & D_{3H} & 0 \\ A_{4H} & B_{4HH} & B_{4HL} & C_{4H} & D_{4HH} & D_{4HL} \\ 0 & B_{4LH} & B_{4LL} & 0 & D_{4LH} & D_{4LL} \end{bmatrix} \tag{4-7}$$

Note that the structure and properties of the causality matrix g_y and the Jacobian matrix $J_g = [\, g_x \;\; g_y \,]$ are very similar to those of the generic load flow Jacobian matrix J_{LF} shown in (3-8). The only differences are that there are reactive power balance equations at all terminal buses and that the inequality of the diagonal matrices $A_{1K} \neq B_{1H}$, $C_{1K} \neq D_{1H}$, $A_{3K} \neq B_{3H}$, and $C_{3K} \neq D_{3H}$ holds in g_y but not in J_{LF}, because A_{1K}, C_{1K}, A_{3K}, and C_{3K} have the effects of the coupling between the internal buses and terminal buses in g_y. This results in a significant diagonal dominance in g_y that is not present in J_{LF} if all the generator terminal buses were PQ-buses. Note that since the reactive power balance equations at all the generator terminal buses are included in g_y, the eigenvalues of g_y will not change discontinuously when reactive power generation limits are reached and PV-bus to PQ-bus changes occur. The test for the static/algebraic bifurcation on J_y will be shown to be similar to J_{LF}, and will experience discontinuous change when any generator exhausts it reactive power generation reserve and changes to a PQ-bus. The simulation results will also show that the singularity of g_y is not likely to happen when the reactive power generation limits are included in the model for the simple power system considered.

Loss of causality (g_y singular) will occur due to the row dependence of J_g. The discussion of the various possible subclasses of the load flow bifurcation due to the singularity of J_{LF} can be viewed as possible subclasses of loss of causality. The discussion in Section 3.2, that illustrated that (a) the bifurcation at a single bus due to the row dependence of the rows of J_{LF} associated with the active and reactive power balance equations at this bus, (b) the voltage bifurcation due to the row dependence of rows of J_{LF} associated with the reactive power balance equations, (c) the angle bifurcation due to the row dependence of rows of J_{LF} associated with the active power balance equations can not happen, can be carried over to J_g and loss of causality.

4.3.2 Single Machine Condition — f_x

From the linearized power system dynamic model and the Jacobian submatrices of (4-2), the matrix f_x is defined as

$$f_x = (\, diag[\, T_{XX} \quad T_{EE} \quad T_{GG} \quad T_{SS} \,]\,)^{-1} F_X \tag{4-8a}$$

$$F_X = \begin{bmatrix} A_{XX} & A_{XE} & A_{XG} & 0 \\ A_{EX} & A_{EE} & 0 & A_{ES} \\ A_{GX} & 0 & A_{GG} & 0 \\ A_{SX} & 0 & 0 & A_{SS} \end{bmatrix} = \begin{bmatrix} A_{XX} & A_{XC} \\ A_{CX} & A_{CC} \end{bmatrix} \tag{4-8b}$$

where,

$$A_{XC} = [\, A_{XE} \;\; A_{XG} \;\; 0 \,] \;\; ; \;\; A_{CX} = \begin{bmatrix} A_{EX} \\ A_{GX} \\ A_{SX} \end{bmatrix} \;\; ; \;\; A_{CC} = \begin{bmatrix} A_{EE} & 0 & A_{ES} \\ 0 & A_{GG} & 0 \\ 0 & 0 & A_{SS} \end{bmatrix} \tag{4-8c}$$

It is observed that the matrix f_x represents the operation condition where each synchronous machine is assumed to have a swing (infinite) bus at its terminal bus, since f_x is formed by diagonal block submatrices composed of the K-coefficients of each machine, as shown in the steady state block diagram Fig. 4-2. The nonsingularity and lack of complex eigenvalues with zero real parts of f_x or the singularity of $\{f_x - j\Omega\}$ for some frequency $\Omega \geq 0$ characterizes the "proper" or "nonproper" basic design of each machine when its terminal bus is treated as the swing bus of the power system. The matrix f_x can now be argued to be nonsingular and has no complex eigenvalues with zero real parts because the system is designed so that loss of stability will not occur on the machine dynamics only (f_x), but rather on the complete system dynamics (J_x). It should be noted that the excitation systems and power system stabilizers are designed to prevent stability problems and thus the stability problems in f_x are not likely to occur. However, the stability problems may occur in J_x, especially when the system is heavily stressed or when some machines are operated in underexcited condition (leading power factor at the terminal bus) [27]. A simple test matrix for testing the (non)singularity of f_x will also be derived for the case where the machine is not sure to meet the basic operating and design practice for a single machine operated independent of the transmission network.

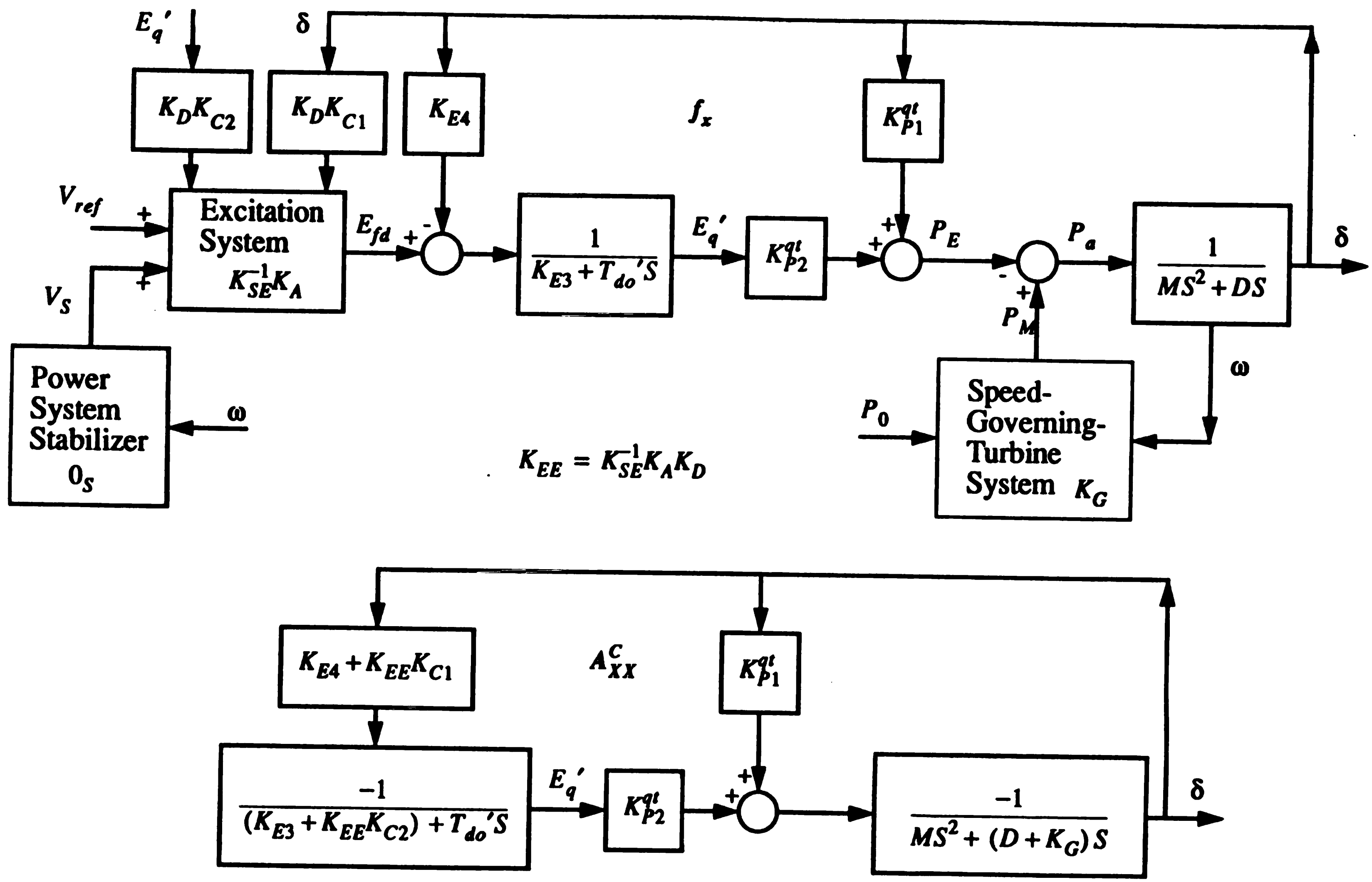

Fig. 4-2 Steady State $(S=0)$ Block Diagram of f_x and A_{XX}^C

Note that each block submatrix of f_x is diagonal and can be viewed as an element, since the dynamics of each machine is uncoupled in f_x. From (4-8), it is obvious that the control systems form an upper triangular block matrix A_{CC}, hence the eigenvalues of A_{CC} are those of each control system, A_{EE}, A_{GG}, and A_{SS}. Moreover, based on the IEEE general model of speed-governing-turbine systems (Fig. 2-8) [86], for both steam and hydro turbines, and the model of power system stabilizer (Fig. 2-7) [85], both A_{GG} and A_{SS} are lower triangular matrices with real and negative eigenvalues. Regarding the excitation system matrix A_{EE}, if the excitation system is "properly tuned" and is able to be manually operated, A_{EE} should not have any eigenvalue with zero real part. Hence, the control system matrix A_{CC} is virtually certain to be nonsingular. Therefore, the control systems matrix A_{CC} can be aggregated into the mechanical and flux decay matrix A_{XX}, such that the singularity of f_x is equivalent to the singularity of the following matrix (Appendix B: A_{CC}^{-1}):

$$A_{XX}^{C} = A_{XX} - A_{XC}\, A_{CC}^{-1}\, A_{CX}$$

$$= \begin{bmatrix} -(D + K_G) & -K_{\beta 1}^{gt} & -K_{\beta 2}^{gt} \\ I & 0 & 0 \\ 0_S & -(K_{E4} + K_{E1}) & -(K_{E3} + K_{E2}) \end{bmatrix} \qquad (4\text{-}9)$$

where, the following matrices are defined

$K_G \quad = A_{\omega G}\, A_{GG}^{-1}\, A_{G\omega}$

: effects of speed-governing-turbine system;

$0_S \quad = A_{FE}\, A_{EE}^{-1}\, [\, A_{E\omega} - A_{ES}\, A_{SS}^{-1}\, A_{S\omega}\,] = 0$

: effects of power system stabilizer;

$K_{E1} \quad = A_{FE}\, A_{EE}^{-1}\, A_{EC1} = K_{EE}\, K_{C1}$

: effects of excitation system on $\Delta\delta$;

$K_{E2} \quad = A_{FE}\, A_{EE}^{-1}\, A_{EC2} = K_{EE}\, K_{C2}$

: effects of excitation system on $\Delta E_q'$;

$K_{EE} \ = K_{SE}^{-1} \ K_A \ K_D$.

The block diagram of A_{CC}^{X} is also shown in Fig. 4-2.

Note that K_G is the D.C. gain of speed-governing-turbine system (Fig. 2-8), and K_{EE} is the D.C. gain of excitation system (Fig. 2-5). The power system stabilizer does not show any effects on A_{XX}^{C} due to its D.C. washout transfer function (Fig. 2-7). Hence, the singularity of f_x is fully dependent upon the D.C. gains of excitation systems K_{EE} and speed-governing-turbine systems K_G, and upon network effects through the six diagonal coefficient matrices: K_{P1}^{gt}, K_{P2}^{gt}, K_{E3}, K_{E4}, K_{C1}, and K_{C2}. The notation of these diagonal K-matrices are adopted so that they are consistent with those K-matrices [23,26] of the single-machine-to-infinite-bus power system where synchronous machine is represented as the single-axis model and does not have control systems ($K_{EE} = 0$): $K_{P1} = K_1$, $K_{P2} = K_2$, $K_{E3} = K_3$, $K_{E4} = K_4$, and $K_5 = 0$, $K_6 = 0$ since in this case the generator terminal bus is the infinite bus.

Note also that based on the theory of synchronous machine, when all the derivatives of dynamic states are set to be zero (at steady state), all the induced currents at damper windings are also zero. Hence, the synchronous machine can be represented by single-axis model, such that only the dynamic state $E_q^{'}$ of flux decay dynamics needs to be preserved. Therefore, A_{XX}^{C} represents the Jacobian matrix of (single-axis modeled) synchronous machines at steady state condition with the D.C. gains of control systems [87]. It will now be shown that f_x and A_{XX}^{C} would not be singular and would have asymptotically stable eigenvalues, provided that each generator is operated at the usually overexcited condition (lagging power factor) and at the power levels where steady state angle stability limit, and its excitation D.C. gain is not "badly" tuned [23,26].

Each synchronous machine is assumed to be operated below its steady state stability limit so that each element of the diagonal matrix K_{P1}^{gt} which is the power-angle coefficient at internal bus is not zero (Appendix C). The matrix

$$A_M = \begin{bmatrix} -(D + K_G) & -K^{gt}_{\beta 1} \\ I & 0 \end{bmatrix} \tag{4-10}$$

is thus nonsingular, assuming that $K^{gt}_{\beta 1}$ is nonsingular. This is also true even though the damper constant D and the D.C. gain of speed-governing-turbine system K_G are neglected, because from (4-8) setting $D + K_G$ to be zero does not affect the singularity or the determinant of A^C_{XX}. Hence, the singularity of f_x can be shown to be equivalent to that of the following matrix:

$$\begin{aligned} K_{FD} &= (K_{E3} + K_{E2}) + [\,0 \quad (K_{E4} + K_{E1})\,]\, A_M^{-1} \begin{bmatrix} K^{gt}_{\beta 2} \\ 0 \end{bmatrix} \\ &= (K_{E3} + K_{E2}) - (K_{E4} + K_{E1})\, {K^{gt}_{\beta 1}}^{-1} K^{gt}_{\beta 2} \end{aligned} \tag{4-11}$$

assuming that $K^{gt}_{\beta 1}$ is nonsingular. Thus, the singularity of f_x is solely a function of the D.C. gain matrix of excitation systems K_{EE}, and the six diagonal coefficient matrices: $K^{gt}_{\beta 1}$, $K^{gt}_{\beta 2}$, K_{E3}, K_{E4}, K_{C1}, and K_{C2}. In other words, the singularity of K_{FD} is a necessary and sufficient condition for the singularity of f_x, provided that $K^{gt}_{\beta 1}$ is nonsingular. Checking the singularity of f_x can thus be performed neglecting the effects of damping constant D, speed-governing-turbine systems, and power system stabilizers, which tremendously reduces the computational burden.

Note that the characteristics of f_x and A^C_{XX} describes the steady state operation condition of each synchronous machine when its terminal bus is assumed to be the infinite (swing) bus. The matrix K_{FD} provides an equivalent singularity test of f_x and A^C_{XX} associated with the flux decay dynamics when $K^{gt}_{\beta 1}$ is nonsingular. At the steady state condition, f_x, A^C_{XX}, and K_{FD} (Appendix C) should be nonsingular and have (asymptotical) stable eigenvalues, except when the synchronous machine is operated at the steady state angle stability limit and/or the D.C. gain of the excitation system is "badly tuned". Thus, it is likely that f_x is nonsingular.

It should be pointed out that the test matrix K_{FD} will be shown to be the same as the test matrix $T_{FDr}(\Omega = 0)$, derived in Chapter 5, for the static bifurcation associated with the flux decay dynamics except K_{FD} neglects the network effects. The test conditions of singularity of $\{f_x - j\Omega\}$ for all $\Omega \geq 0$ were not established in a manner that test conditions of singularity of $\{J_x - j\Omega\}$ are obtained in Chapter 5. It is important to make certain that $\{f_x - j\Omega\}$ has neither singularity for $\Omega = 0$, nor for all $\Omega > 0$ since stability problems could well result in the full model that includes the effects of the transmission network.

4.4 Structure of Static/Algebraic Jacobian Matrix — J_y

In this section, the structure of the static/algebraic Jacobian matrix J_y will be derived based on the assumption that f_x is nonsingular as indicated in previous section. The structure of the matrix J_y will also be shown to be similar to that of the causality matrix g_y (4-7).

The relationship between the power system Jacobian submatrices, f_x, f_y, g_x, and g_y, has been represented by the block diagram as shown in Fig. 4-1. The static/algebraic Jacobian matrix is defined as

$$J_y = g_y - g_x\, f_x^{-1}\, f_y \tag{4-12}$$

provided that both g_y and f_x are nonsingular. Based on the properties of f_x shown in previous section, the matrix f_x only directly affects the internal bus and terminal bus variables of each generator, and can be represented by its reduced form A_{XX}^{C} as shown in Fig. 4-2. Likewise, the Jacobian matrices f_y and g_x composed of diagonal K-submatrices show the coupling between the internal bus and terminal bus of each generator. Thus, the second part of the matrix J_y, $\{g_x\, f_x^{-1}\, f_y\}$, should only show the effects on the terminal bus variables, and the static/algebraic Jacobian matrix J_y would in turn keep the same structure as that of the causality matrix g_y, where only the diagonal block submatrices associated with the active and reactive power balance equations at the terminal buses are expected to be modified.

From Fig. 4-1 and Fig. 4-2, the relationship between f_x and f_y can be illustrated by the steady state block diagram of each machine shown in Fig. 4-3, where the incremental symbol Δ in front of each variable is omitted. At steady state condition, $\Delta\omega = 0$ and only the D.C. gain of the excitation system shows the effects of the complete control systems. Based on Fig. 4-3, the mechanical and flux decay states $\Delta\delta$ and $\Delta E_q'$ can be represented in terms of the terminal bus variables $\Delta\theta_T$ and ΔV_T as follows:

$$\begin{bmatrix} \Delta P_0 \\ K_{SE}^{-1}\ K_A\ \Delta V_{ref} \end{bmatrix} = \begin{bmatrix} K_{\beta 1}^{gt} & K_{\beta 2}^{gt} \\ [\ K_{E4} + K_{EE}\ K_{C1}\ ] & [\ K_{E3} + K_{EE}\ K_{C2}\ ] \end{bmatrix} \begin{bmatrix} \Delta\delta \\ \Delta E_q' \end{bmatrix}$$
$$+ \begin{bmatrix} -K_{\beta 1}^{gt} & K_{\beta 7}^{gt} \\ -[\ K_{E4} + K_{EE}\ K_{C1}\ ] & -[\ K_{E7} - K_{EE}\ K_{C7}\ ] \end{bmatrix} \begin{bmatrix} \Delta\theta_T \\ \Delta V_T \end{bmatrix} \quad \text{(4-13a)}$$

$$\begin{bmatrix} \Delta\delta \\ \Delta E_q' \end{bmatrix} = \begin{bmatrix} K_{\beta 1}^{gt} & K_{\beta 2}^{gt} \\ [\ K_{E4} + K_{EE}\ K_{C1}\ ] & [\ K_{E3} + K_{EE}\ K_{C2}\ ] \end{bmatrix}^{-1} \cdot \left(\begin{bmatrix} \Delta P_0 \\ K_{SE}^{-1}\ K_A\ \Delta V_{ref} \end{bmatrix} \right.$$
$$\left. - \begin{bmatrix} -K_{\beta 1}^{gt} & K_{\beta 7}^{gt} \\ -[\ K_{E4} + K_{EE}\ K_{C1}\ ] & -[\ K_{E7} - K_{EE}\ K_{C7}\ ] \end{bmatrix} \begin{bmatrix} \Delta\theta_T \\ \Delta V_T \end{bmatrix} \right) \quad \text{(4-13b)}$$

Note that $f_x^{-1}\ f_y$ is embedded in the above formulation:

$$(f_x^{-1}\ f_y)_I = \begin{bmatrix} K_{\beta 1}^{gt} & K_{\beta 2}^{gt} \\ [\ K_{E4} + K_{EE}\ K_{C1}\ ] & [\ K_{E3} + K_{EE}\ K_{C2}\ ] \end{bmatrix}^{-1}$$
$$\cdot \begin{bmatrix} -K_{\beta 1}^{gt} & K_{\beta 7}^{gt} \\ -[\ K_{E4} + K_{EE}\ K_{C1}\ ] & -[\ K_{E7} - K_{EE}\ K_{C7}\ ] \end{bmatrix} \quad \text{(4-14)}$$

where, $(f_x^{-1}\ f_y)_I$ represents that $f_x^{-1}\ f_y$ has only effects on the internal bus variables

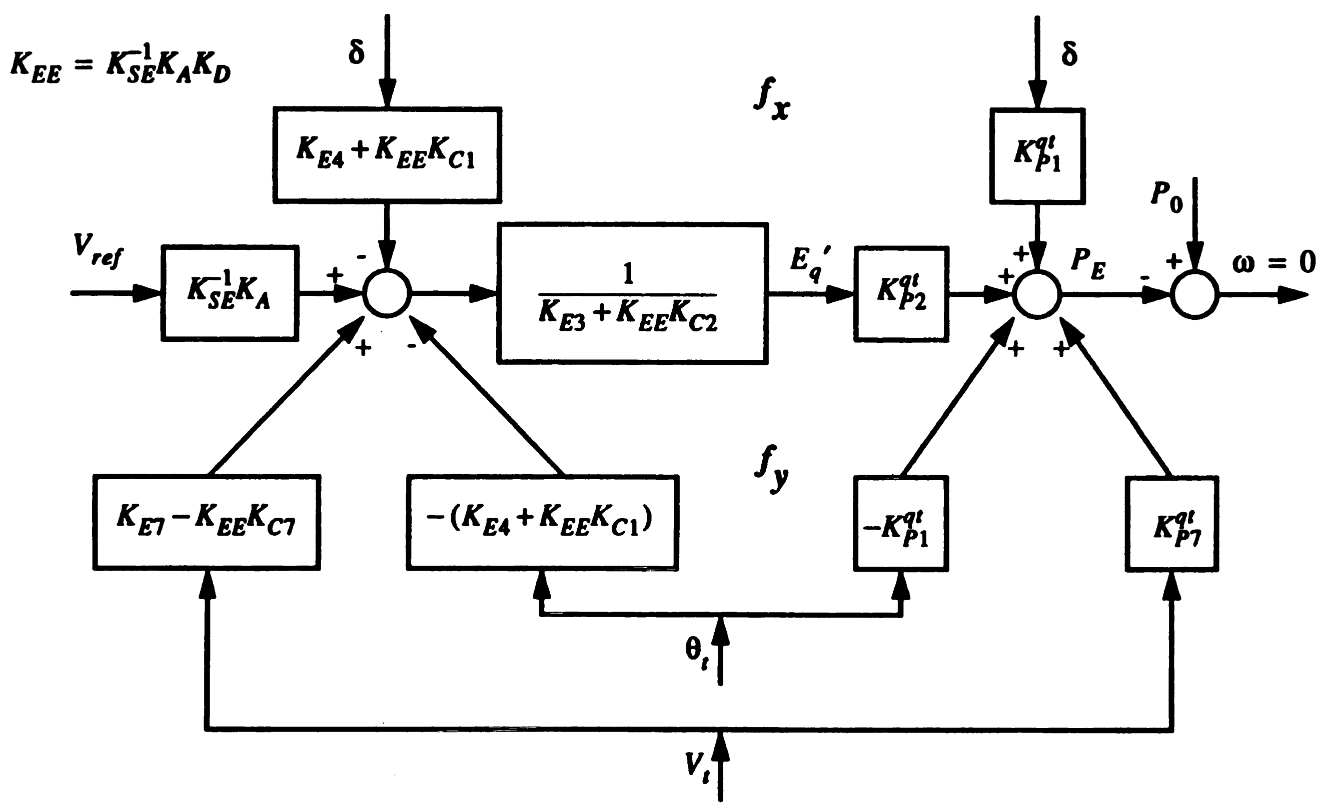

Fig. 4-3 Steady State $(S = 0)$ Block Diagram of $f_x^{-1}f_y$

$\Delta\delta$ and $\Delta E_q'$, since the rest of block matrices of $f_x^{-1} f_y$ are zero. Note that each of the matrices in each of the sub-blocks is diagonal. Based on the assumption that f_x and $K\beta_1^{gt}$ are nonsingular, and on the two equalities $K_{E1} = K_{EE}\ K_{C1}$ and $K_{E2} = K_{EE}\ K_{C2}$ defined in A_{XX}^{C} (4-9) and in K_{FD} (4-11), and applying the inverse matrix formula provided in Appendix A, we have the further formulation for $(f_x^{-1} f_y)_I$ as follows. Let

$$\begin{bmatrix} K\beta_1^{gt} & K\beta_2^{gt} \\ [\,K_{E4} + K_{E1}\,] & [\,K_{E3} + K_{E2}\,] \end{bmatrix}^{-1} = \begin{bmatrix} G_{11} & G_{12} \\ G_{21} & G_{22} \end{bmatrix}$$

then

$$\begin{aligned} G_{22} &= (\,[\,K_{E3} + K_{E2}\,] - [\,K_{E4} + K_{E1}\,]\,K\beta_1^{gt\,-1}\,K\beta_2^{gt}\,)^{-1} \\ &= K_{FD}^{-1} \\ G_{21} &= -\,K_{FD}^{-1}\,[\,K_{E4} + K_{E1}\,]\,K\beta_1^{gt\,-1} \\ G_{12} &= -\,K\beta_1^{gt\,-1}\,K\beta_2^{gt}\,K_{FD}^{-1} \\ G_{11} &= K\beta_1^{gt\,-1}\,[\,I - K\beta_2^{gt}\,G_{21}\,] \\ &= K\beta_1^{gt\,-1} + K\beta_1^{gt\,-1}\,K\beta_2^{gt}\,K_{FD}^{-1}\,[\,K_{E4} + K_{E1}\,]\,K\beta_1^{gt\,-1} \end{aligned}$$

Hence, $(f_x^{-1} f_y)_I$ can be written as

$$\begin{aligned} (f_x^{-1} f_y)_I &= \begin{bmatrix} G_{11} & G_{12} \\ G_{21} & G_{22} \end{bmatrix} \begin{bmatrix} -\,K\beta_1^{gt} & K\beta_7^{gt} \\ -\,[\,K_{E4} + K_{E1}\,] & -\,[\,K_{E7} - K_{EE}\,K_{C7}\,] \end{bmatrix} \\ &= \begin{bmatrix} -\,I & H_{12} \\ 0 & H_{22} \end{bmatrix} \end{aligned} \qquad (4\text{-}14a)$$

where,

$$\begin{aligned} H_{21} &= K\beta_1^{gt\,-1}\,K\beta_7^{gt} + K\beta_1^{gt\,-1}\,K\beta_2^{gt}\,K_{FD}^{-1}\,[\,K_{E4} + K_{E1}\,]\,K\beta_1^{gt\,-1}\,K\beta_7^{gt} \\ &\quad + K\beta_1^{gt\,-1}\,K\beta_2^{gt}\,K_{FD}^{-1}\,[\,K_{E7} - K_{EE}\,K_{C7}\,] \\ &= K\beta_1^{gt\,-1}\,K\beta_7^{gt} + K\beta_1^{gt\,-1}\,K\beta_2^{gt}\,K_{FD}^{-1}\,K_{EC} \end{aligned} \qquad (4\text{-}14b)$$

$$H_{22} = -K_{FD}^{-1}\,[\,K_{E4} + K_{E1}\,]\,K_{P1}^{gt\;-1}\,K_{P7}^{gt} - K_{FD}^{-1}\,[\,K_{E7} - K_{EE}\,K_{C7}\,]$$

$$= -K_{FD}^{-1}\,K_{EC} \tag{4-14c}$$

$$K_{EC} = (K_{E4} + K_{EE}\,K_{C1})\,K_{P1}^{gt\;-1}\,K_{P7}^{gt} + (K_{E7} - K_{EE}\,K_{C7})$$

Note that $K_{E1} = K_{EE}\,K_{C1}$.

Likewise, the active and reactive power balance equations show the coupling between the internal bus and terminal bus of each machine as follows (from (4-2)):

$$\begin{bmatrix} -\Delta P_{CT} \\ -\Delta Q_{CT} \end{bmatrix} = \begin{bmatrix} -K_{P1}^{tq} & K_{P2}^{tq} \\ -K_{Q1}^{tq} & K_{Q2}^{tq} \end{bmatrix} \begin{bmatrix} \Delta\delta \\ \Delta E_q' \end{bmatrix} + \begin{bmatrix} A_{1K} & C_{1K} \\ A_{3K} & C_{3K} \end{bmatrix} \begin{bmatrix} \Delta\theta_T \\ \Delta V_T \end{bmatrix}$$

$$+ \begin{bmatrix} B_{1H} & D_{1H} \\ B_{3H} & D_{3H} \end{bmatrix} \begin{bmatrix} \Delta\theta_H \\ \Delta V_H \end{bmatrix} \tag{4-15}$$

where, the main submatrices of g_x associated with the internal bus variables $\Delta\delta$ and $\Delta E_q'$, K_{P1}^{tq}, K_{P2}^{tq}, K_{Q1}^{tq}, and K_{Q2}^{tq}, are included. Note that each submatrix in the above representation is diagonal. Then substituting (4-13b) into (4-15), we have

$$\begin{bmatrix} -\Delta P_{CT} \\ -\Delta Q_{CT} \end{bmatrix} = \left(\begin{bmatrix} A_{1K} & C_{1K} \\ A_{3K} & C_{3K} \end{bmatrix} - \begin{bmatrix} K_{P1}^{tq} & C_{1X} \\ K_{Q1}^{tq} & C_{3X} \end{bmatrix} \right) \begin{bmatrix} \Delta\theta_T \\ \Delta V_T \end{bmatrix}$$

$$+ \begin{bmatrix} B_{1H} & D_{1H} \\ B_{3H} & D_{3H} \end{bmatrix} \begin{bmatrix} \Delta\theta_H \\ \Delta V_H \end{bmatrix} + G_T \begin{bmatrix} \Delta P_0 \\ K_{SE}^{-1}\,K_A\,\Delta V_{ref} \end{bmatrix} \tag{4-16}$$

since the computation of $g_x\,f_x^{-1}\,f_y$ shows the first part of (4-16) and its sub-block matrix associated with the terminal bus variables $\Delta\theta_T$ and ΔV_T, $(g_x\,f_x^{-1}\,f_y)_T$ has the form:

$$(g_x\,f_x^{-1}\,f_y)_T = \begin{bmatrix} -K_{P1}^{tq} & K_{P2}^{tq} \\ -K_{Q1}^{tq} & K_{Q2}^{tq} \end{bmatrix} \cdot (f_x^{-1}\,f_y)_I$$

$$= \begin{bmatrix} K_{P1}^{tq} & C_{1X} \\ K_{Q1}^{tq} & C_{3X} \end{bmatrix} \tag{4-17}$$

where,

$$C_{1X} = -K_{P1}^{tg} \, K_{P1}^{gt\,-1} \, K_{P7}^{gt} - (K_{P1}^{tg} \, K_{P1}^{gt\,-1} \, K_{P2}^{gt} + K_{P2}^{tg}) \, K_{FD}^{-1} \, K_{EC}$$

$$C_{3X} = -K_{Q1}^{tg} \, K_{P1}^{gt\,-1} \, K_{P7}^{gt} - (K_{Q1}^{tg} \, K_{P1}^{gt\,-1} \, K_{P2}^{gt} + K_{Q2}^{tg}) \, K_{FD}^{-1} \, K_{EC}$$

Note that the rest of block matrices of $g_x \, f_x^{-1} \, f_y$ are zero. The expression for G_T is omitted without loss of continuity.

It is observed from (4-16) and (4-17) that $g_x \, f_x^{-1} \, f_y$ only affects the diagonal submatrices of g_y associated with the terminal bus variables. Thus, substituting (from (4-2))

$$A_{1K} = K_{P1}^{tg} + A_1 \;\; ; \;\; C_{1K} = K_{P7}^{tg} + C_1$$

$$A_{3K} = K_{Q1}^{tg} + A_3 \;\; ; \;\; C_{3K} = K_{Q7}^{tg} + C_3$$

and (4-17) into (4-12) by combining the Jacobian submatrices of g_y associated with the power balance equations at high-side buses and load buses, we have the final form of the static/algebraic Jacobian matrix J_y as follows:

$$J_y = \begin{bmatrix} A_1 & B_{1H} & 0 & C_{1K}^X & D_{1H} & 0 \\ A_{2H} & B_{2HH} & B_{2HL} & C_{2H} & D_{2HH} & D_{2HL} \\ 0 & B_{2LH} & B_{2LL} & 0 & D_{2LH} & D_{2LL} \\ A_3 & B_{3H} & 0 & C_{3K}^X & D_{3H} & 0 \\ A_{4H} & B_{4HH} & B_{4HL} & C_{4H} & D_{4HH} & D_{4HL} \\ 0 & B_{4LH} & B_{4LL} & 0 & D_{4LH} & D_{4LL} \end{bmatrix} = \begin{bmatrix} J_y^{PT} \\ J_y^{PH} \\ J_y^{PL} \\ J_y^{QT} \\ J_y^{QH} \\ J_y^{QL} \end{bmatrix} \qquad (4\text{-}18)$$

where,

$$C_{1K}^X = K_{P7}^{tg} + C_1 - C_{1X}$$

$$C_{3K}^X = K_{Q7}^{tg} + C_3 - C_{3X}$$

Note that both C_{1K}^X and C_{3K}^X are still diagonal matrices, and that A_1, C_1, A_3, and C_3 are the appropriate diagonal sub-blocks of the load flow Jacobian matrix J_{LF} defined in

(3-9).

The above shows that J_y can be obtained from the causality matrix g_y by slightly modifying the submatrices associated with the (active and reactive) power-angle and power-voltage diagonal Jacobian matrices at terminal buses. Note that the active and reactive power-angle Jacobian matrix of g_y are $A_{1K} = K_{P1}^{tq} + A_1$ and $A_{3K} = K_{Q1}^{tq} + A_3$; but those of J_y become A_1 and A_3 that are the same as those in the load flow model of the specific case where all the generator terminal buses are represented as PQ-buses. This is because in each generator, except the swing bus, the power-angle Jacobian matrices associated with the internal bus angle δ and the terminal bus angle θ_t are opposite in sign. This also implies that the control systems at steady state do not have direct effects on the terminal bus angle through the coupling coefficient matrices K_{P1} and K_{Q1}. Moreover, in the active power-voltage Jacobian matrices C_{1K}^X and C_{1K} of J_y and g_y respectively, the difference between them is due to the fact that $K^{qt} \neq K^{tq}$ which represents the active power losses in the armature resistance R_a and the reactive power losses in the reactances of synchronous machines. Note that if R_a is neglected, then $P_E = P_{Gt} = -P_{tq}$ such that $K_{P1}^{qt} = K_{P1}^{tq}$, $K_{P2}^{qt} = -K_{P2}^{tq}$, and $K_{P7}^{qt} = -K_{P7}^{tq}$. Hence, $C_{1X} = -K_{P7}^{qt} = K_{P7}^{tq}$, and $C_{1K}^X = C_1$ whether the generator has reached reactive power generation limits and disabled the excitation control or not. This result implies that if R_a is neglected, the control systems at steady state do not have any direct effects on the active power-voltage coefficient matrix $C_{1K}^X = C_1$. However, C_{3K}^X of J_y is not equal to C_3 of J_{LF}, which indicates the excitation control has effect on the reactive power generation of the synchronous machine by controlling the generator terminal voltage.

Thus, the structure of the static/algebraic Jacobian matrix J_y is like the load flow Jacobian matrix J_{LF} except for C_{3K}^X, since $C_{3K}^X = K_{Q7}^{tq} + C_3 - C_{3X}$. Note that since $-C_{3X}$ is a diagonal matrix with positive elements (see Appendix D) that increase almost linearly with K_{EE} when it is assumed that the load compensators are not used in the model, the matrix C^X_{3K} is then also a diagonal matrix with positive elements that increase almost linearly with K_{EE} because the D.C. gain of the excitation system K_{EE} is in general very large compared to the rest of terms in C^X_{3K}. Hence, the load flow bifurcation is an excellent predictor of the singularity induced static bifurcation because

(a) there are rows associated with the reactive power balance equations at all generator terminal buses in J_y, but only in J_{LF} when the reactive power generation reserves are exhausted;

(b) the reactive power-voltage Jacobian matrix in J_y is extremely diagonally dominant when the reactive power generation limits are not reached and exciters are not disabled (C^X_{3K} is a diagonal matrix with very large positive elements), which is much like adding equations $V_T = V_{T0}$ or $\Delta V_T = 0$ for the generator terminal buses in the load flow model;

(c) the rows of J_y and J_{LF} associated with the reactive power balance equations at the generator PQ-buses, when the reactive power generation reserves are exhausted, are identical.

This similarity between the static/algebraic bifurcation test and the load flow bifurcation test will be shown in Section 4.6.

The difference between the static/algebraic Jacobian matrix J_y (4-18) and the causality matrix g_y (4-7) is that the four diagonal submatrices associated with the power balance equations at the terminal buses: A_1, C_1, A_3, and $C^X_{3K} = K^{tg}_{Q7} + C_3 - C_{3X}$ of J_y; and $A_{1K} = A_1 + K^{tg}_{P1}$, $C_{1K} = C_1 + K^{tg}_{P7}$, $A_{3K} = A_3 + K^{tg}_{Q1}$, and $C_{3K} = C_3 + K^{tg}_{Q7}$ of g_y. When generators do not reach their reactive power generation limits, J_y is more diagonally dominant than g_y in the reactive power-voltage Jacobian matrix at terminal buses ($\partial Q_T / \partial V_T$) since C^X_{3K} in J_y is a diagonal matrix with very large positive elements proportional to K_{EE}. When generators exhaust their reactive power generation reserves and become PQ-buses, C_{3K}^{X} in J_y then becomes C_3 which is less dominant than C_{3K} in g_y. Furthermore, the active power-angle $(\partial P_T / \partial \theta_T)$ matrix in J_y is A_1, but the matrix in g_y is A_{1K} which is more diagonally dominant. Hence, J_y is less diagonally dominant than g_y in both $\partial P_T / \partial \theta_T$ and $\partial Q_T / \partial V_T$ matrices when the reactive power generation limits are reached. Thus, when the reactive power generation limits of all the generators in a region are reached, J_y should generally become singular before g_y. If the reactive power generation limits are ignored, loss of causality (g_y singular) may occur before the static/algebraic bifurcation (J_y singular), since $\partial Q_T / \partial V_T$ is more diagonally dominant in J_y than in g_y, but $\partial P_T / \partial \theta_T$ is more diagonally dominant in g_y than in J_y. Moreover, the discontinuous changes will occur in J_y causing the static bifurcation, but do not occur in g_y which becomes singular as a continuous function of the imposed stress on the system. This will be shown in the simulation results of the static/algebraic bifurcation test in Section 4.6.

Testing the singularity of the static/algebraic Jacobian matrix J_y for identifying the singularity induced static bifurcation rather than testing the singularity of the equivalent system Jacobian matrix J_x is recommended since both tests are valid and should theoretically always become singular at the same point as long as f_x and g_y are nonsingular. This proposed static/algebraic bifurcation test matrix is proven to have similar structure to the causality matrix g_y, and is virtually identical to the load flow Jacobian matrix J_{LF}. A set of nonlinear equations is thus proposed with J_y that computes the equilibrium point of the power system differential-algebraic model. The equivalent load flow model would represent generators which have not reached reactive power generation limits by the steady state model of generators and excitation systems, and by the reactive power balance equations when reactive power generation limits are reached. This equivalent load flow model for the static/algebraic Jacobian matrix J_y would precisely determine when a static bifurcation occurs in the differential-algebraic power system model. Testing for a static bifurcation using J_y does not require inverting g_y which is required when J_x is used.

The load flow model for the load flow bifurcation test on J_{LF} and the equivalent load flow model for the static/algebraic bifurcation test on J_y are shown to be virtually identical for all rows of J_{LF} and J_y if the D.C. gains of the excitation systems are very high so that the generator terminal voltage can be kept constant, and if the flux decay equations are replaced by the reactive power balance equations at terminal buses for those generators exhausting reactive power generation reserves and being modeled as PQ-buses like in the load flow model. However, they would not be identical if the equivalent load flow model includes the effects of the generator flux decay dynamics, excitation system dynamics, and field current limit controller dynamics at steady state condition when the reactive power generation limits or field current limits are reached. The reason is that a static bifurcation in flux decay dynamics or in both flux decay dynamics and mechanical dynamics would be captured by the equivalent load flow model if steady state representation of flux decay dynamics, excitation system dynamics, and field current limit controller dynamics is used when field current limits are reached; but would not be captured in the load flow model or in the equivalent load flow model if the generator and excitation system dynamics is replaced by a reactive power balance equation (simply called the conventionally equivalent load flow model).

This result is quite important because it indicates that the conventionally equivalent load flow model can only capture one of the three generic static bifurcations (in mechanical dynamics, in flux decay dynamics, and in both) that occurs in mechanical dynamics [39,40,57,62]. The static bifurcations that occur in flux decay dynamics [52,53], and mechanical and flux decay dynamics are most likely to occur when field current limits are reached and the field current limit controller works through the excitation system to fix field current to the continuous rating value. A modified load flow model that properly reflects the steady state behavior of the generator flux decay dynamics, excitation system dynamics, and field current limit controller dynamics would accurately determine the equilibrium point(s) of the differential-algebraic model, and experience all of the static bifurcations of the differential-algebraic model.

The comparison of the static/algebraic Jacobian matrix J_y, the causality matrix g_y, and the load flow Jacobian matrix J_{LF}, carried out in this dissertation, is for the case where the flux decay dynamics and excitation system dynamics are replaced by the reactive power balance equations when the reactive power generation limits are reached. The use of the reactive power balance equations is justified based on the approximation of operation action to maintain the units close to their capability curves when the reactive power generation limits or field current limits are reached.

4.5 Generic Static/Algebraic Bifurcation Test

This section will discuss the subclasses of static/algebraic bifurcation due to the singularity of equivalent static/algebraic Jacobian matrix J_y, which is structurally similar to that of the load flow Jacobian matrix J_{LF}. Based on the structure of J_y shown in (4-15), basically it seems that there will be three possibilities leading to the singularity of J_y that can causes static bifurcation [87].

$SA-T$: This type of bifurcation is solely due to row dependence associated with the active and reactive power balance equations at terminal buses (J_y^{PT} and J_y^{QT}).

$SA-H$: This type of bifurcation is solely due to row dependence associated with the active and reactive power balance equations at high-side buses (J_y^{PH} and J_y^{QH}).

$SA-L$: This type of bifurcation is solely due to row dependence associated with the active and reactive power balance equations at load buses (J_y^{PL} and

J_y^{QL}).

Note that since A and C submatrices of J_y (4-15) are diagonal, other types of bifurcation due to the combination from any two of above three are not possible at all.

The $SA-H$ and $SA-L$ types of static/algebraic bifurcation are identical to the $LF-H$ and $LF-L$ types of load flow bifurcation, respectively. The $LF-H$ and $LF-L$ bifurcations have been shown to never happen in Section 3.2.2 and Section 3.2.3, and the $SA-H$ and $SA-L$ bifurcations will never occur based on the same argument. The $SA-T$ type of bifurcation is similar to $LF-T$ type of bifurcation, and will also never occur due to the fact that $k_T^{ab} \neq k_T^d$ shown in Section 3.2.1, even though the C matrices associated with $SA-T$ and $LF-T$ types of bifurcation are different. Hence, none of the above subclasses of static/algebraic bifurcation will happen. The analogies between the bifurcations in a two-bus model and those of the model considered in this dissertation are shown to have limited validity. It was shown that voltage bifurcation due to the row dependence of the Jacobian rows associated with the reactive power balance equations will not occur, and that angle bifurcation due to the row dependence of the Jacobian rows associated with the active power balance equations can never happen. Thus, the generic type of static/algebraic bifurcation is shown to be the one that has row dependence in all the rows of the static/algebraic Jacobian matrix J_y [87].

4.6 Simulation Results

The 9-bus 3-machine power system with the base case data as the one shown in Fig. 3-1 [26] is adopted to confirm that the following three tests for the static bifurcation in the power system dynamic model are equivalent to each other:

(1) testing the singularity of the static/algebraic Jacobian matrix J_y for the singularity induced static bifurcation;

(2) testing the singularity of the complete system Jacobian matrix J, that allows the detection of all the types of bifurcation except the dynamic bifurcation (differential algebraic, differential-algebraic, static/algebraic, and static bifurcation);

(3) testing the singularity of the equivalent dynamic system Jacobian matrix J_x for the static bifurcation due to the static/algebraic or differential bifurcation;

(4) testing the singularity of f_x for single machine instability;

(5) testing the singularity of g_y for loss of causality.

The purpose of these results is to show that the static/algebraic bifurcation due to the singularity of J_y will be the generic singularity induced static bifurcation that is equivalent to the static bifurcation due the singularity of J_x, and that the differential, algebraic, differential-algebraic bifurcations and loss of causality do not occur in a practical sense. Note that if the static/algebraic bifurcation is the generic static bifurcation, testing for the singularity of J_y is far easier to implement than other tests, since it is easy to compute from the load flow Jacobian matrix and because it does not require the inversion of g_y as does J_x.

It should be noted that these simulation results are only searching for the static bifurcation even though the theory suggests that both static bifurcation and dynamic bifurcation be generic. The static and dynamic bifurcations are studied and classified in the Chapter 5 of this dissertation. Simulation results in Chapter 5 compute both the various types of static bifurcation and dynamic bifurcation.

Along with the base case shown in Fig. 3-1, the dynamic system data required for the static/algebraic bifurcation test is the single-axis parameter data of each synchronous machine as listed in Table 4-1 [4].

Table 4-1 Static Data of Synchronous Machines

	R_a	X_d	X_d'	X_q	K_{EE}
Gen#1:	0.0000	1.7900	0.3000	1.7000	19.000
Gen#2:	0.0000	1.9400	0.2900	1.9100	44.000
Gen#3:	0.0000	1.7200	0.2400	1.6600	270.00

* Data is on machine base.

* Gen#1: 150.0 MVA ; Gen#2: 150.0 MVA ; Gen#3: 250.0 MVA .

Note that the D.C. gain $K_{EE} = K_{SE}^{-1} K_A K_D$ of the excitation system of each machine can be obtained from the complete data machine parameter data set (see Table 5-1, where the dynamic data of the power system is adopted from [4]).

Similar to the load flow bifurcation test used in Section 3.4, the static/algebraic point of voltage collapse method [53] is used to find the static/algebraic bifurcation by making bus#8 a fictitious PV-bus. Figure 4-4(a) shows the determinant of f_x with the notation $Det\ (\ F_x\ )$, that of g_y with the notation $Det\ (\ G_y\ )$, and that of J_y with the notation $Det\ (\ J_y\ )$. Figure 4-4(b) shows the $Q-V$ curve at the fictitious PV-bus, and its slope $Det\ (\ QV\ )$ (a scalar) which is the corresponding diagonal element of the sensitivity matrix similar to S_{QV} of (3-8) of this $Q-V$ curve. Figure 4-4(c) gives the $Q-V$ curve profile of the generator buses with reactive power generation high limits, and Figure 4-4(d) represents the voltage profile of each bus. The voltage angle (in degree) of each bus, and the active power generation of each generator bus are respectively shown in Fig. 4-4(e) and Fig. 4-4(f), which should help understand the phenomena of the transmission network when the voltage and the reactive power injection at the test bus (fictitious PV-bus) are changed. Figure 4-4(g) shows the profile of

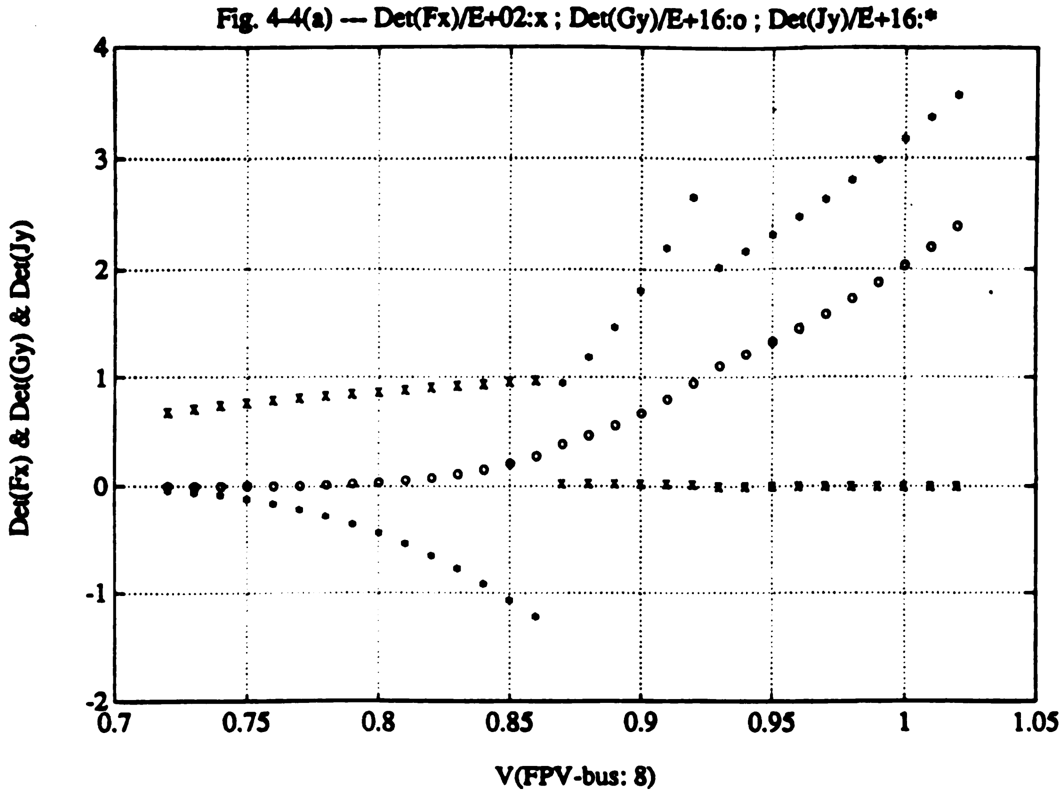
Fig. 4-4(a) --- Det(Fx)/E+02:x ; Det(Gy)/E+16:o ; Det(Jy)/E+16:*
Det(Fx) & Det(Gy) & Det(Jy)
4
3
2
1
0
-1
-2
0.7
0.75
0.8
0.85
0.9
0.95
1
1.05
V(FPV-bus: 8)

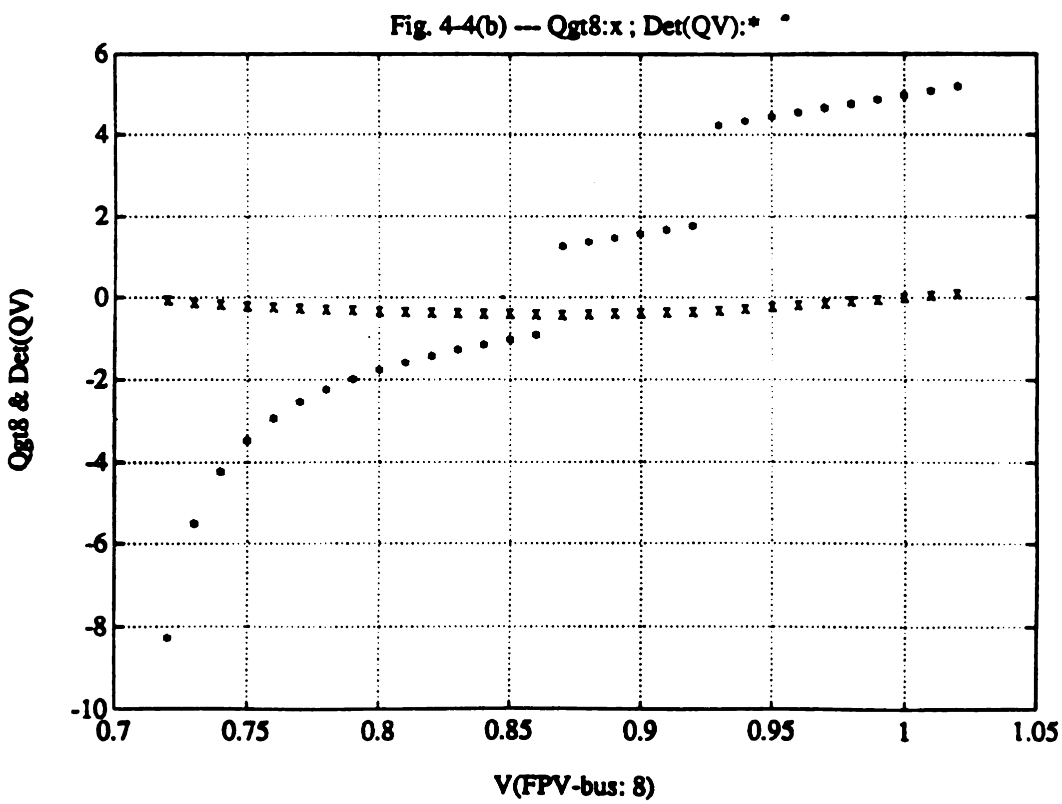
Fig. 4-4(b) --- Qgt8:x ; Det(QV):*
Qgt8 & Det(QV)
6
4
2
0
-2
-4
-6
-8
-10
0.7
0.75
0.8
0.85
0.9
0.95
1
1.05
V(FPV-bus: 8)

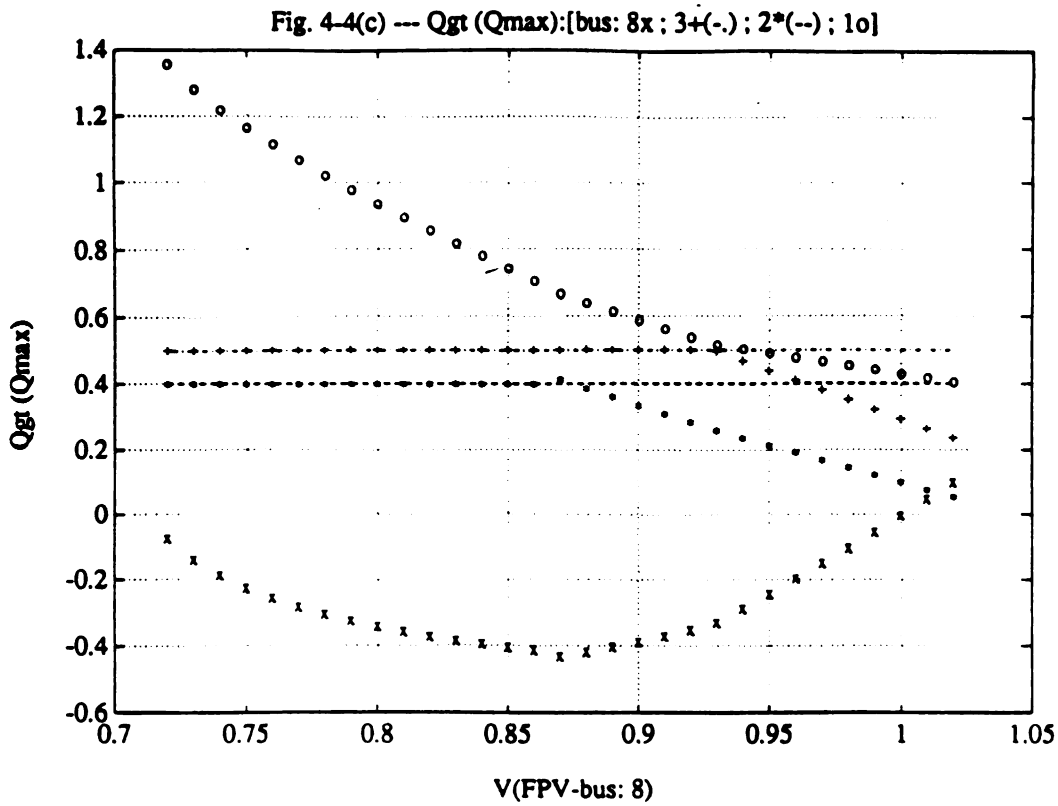
Fig. 4-4(c) --- Qgt (Qmax):[bus: 8x ; 3+(-.) ; 2*(--) ; 1o]
Qgt (Qmax)
V(FPV-bus: 8)
1.4
1.2
1
0.8
0.6
0.4
0.2
0
-0.2
-0.4
-0.6
0.7
0.75
0.8
0.85
0.9
0.95
1
1.05

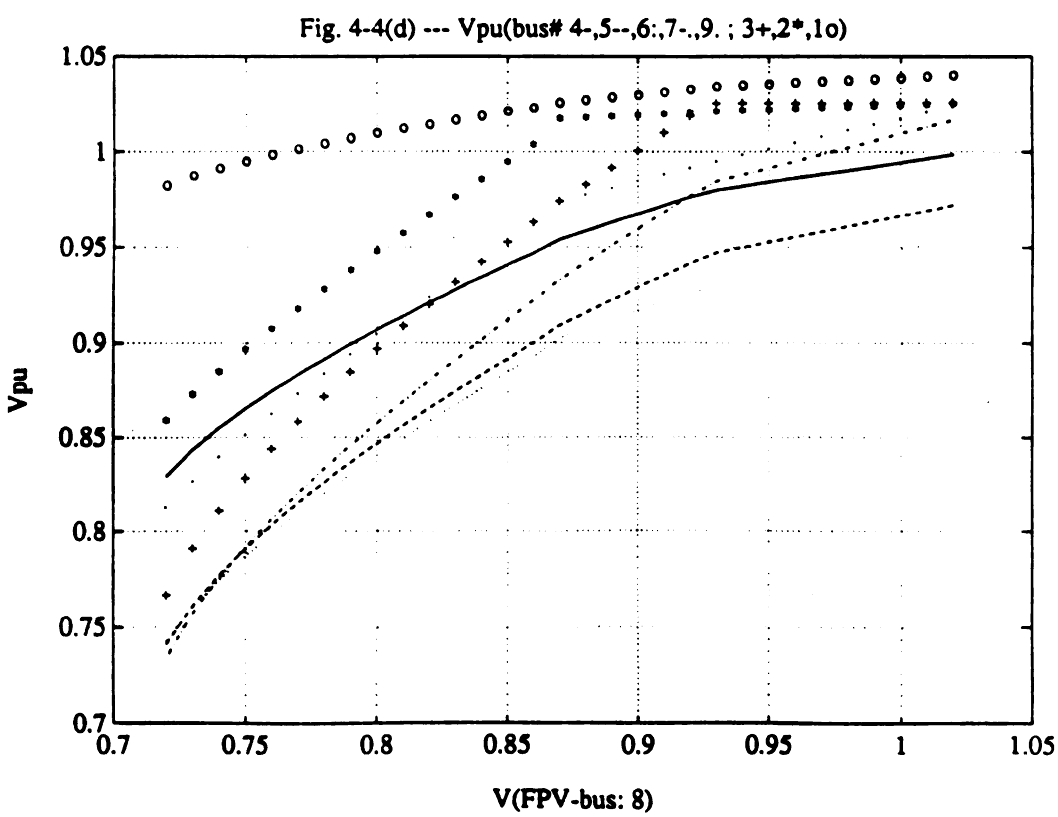
Fig. 4-4(d) --- Vpu(bus# 4-,5--,6:,7-.,9. ; 3+,2*,1o)
Vpu
V(FPV-bus: 8)
1.05
1
0.95
0.9
0.85
0.8
0.75
0.7
0.7
0.75
0.8
0.85
0.9
0.95
1
1.05

Fig. 4-4(e) --- Angle(bus# 4-,5--,6:,7-.,8x,9. ; 3+,2*,1o)

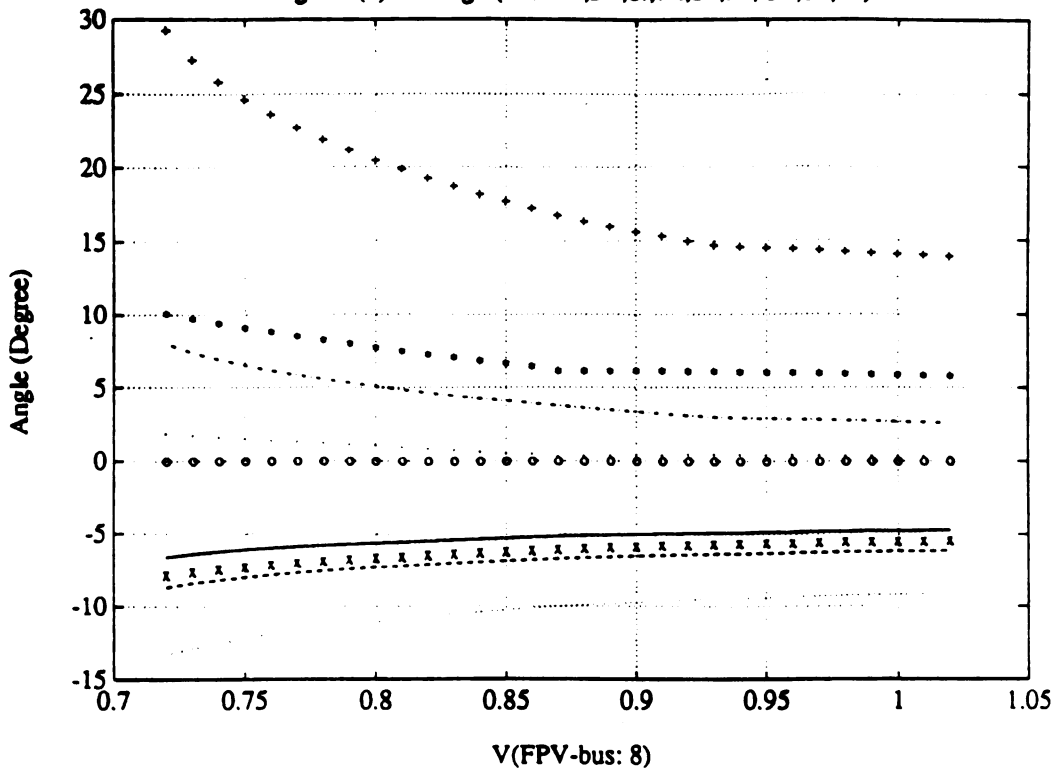

Fig. 4-4(f) --- Pgt(bus# 3+, 2*, 1o)

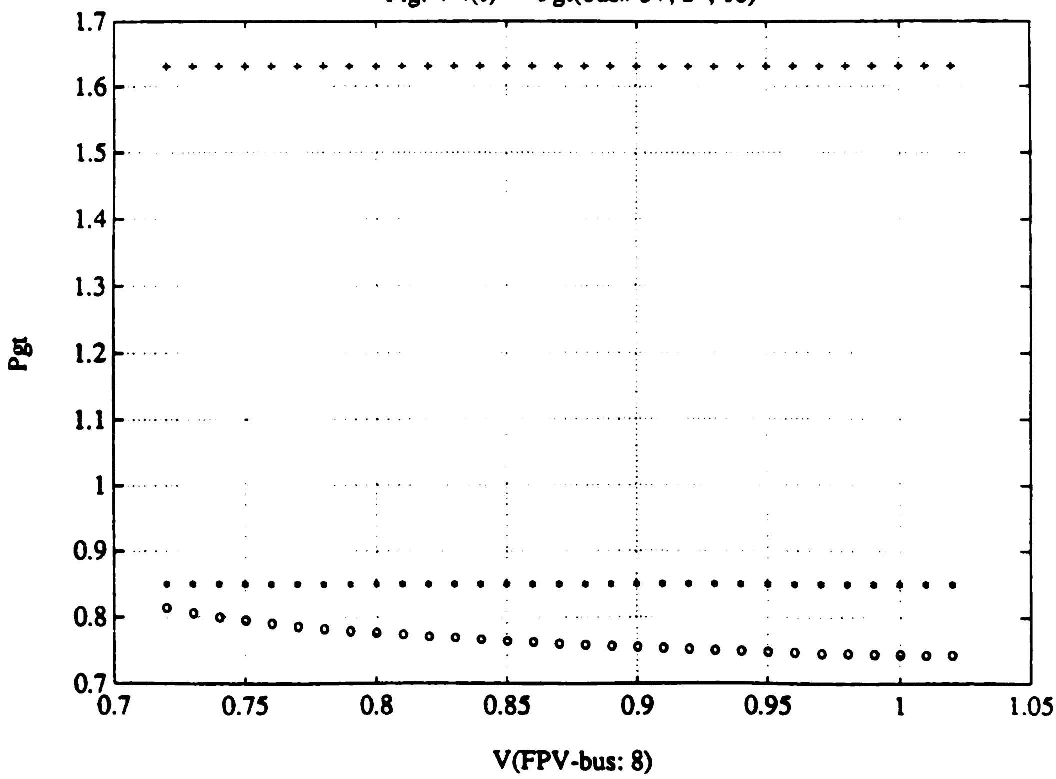

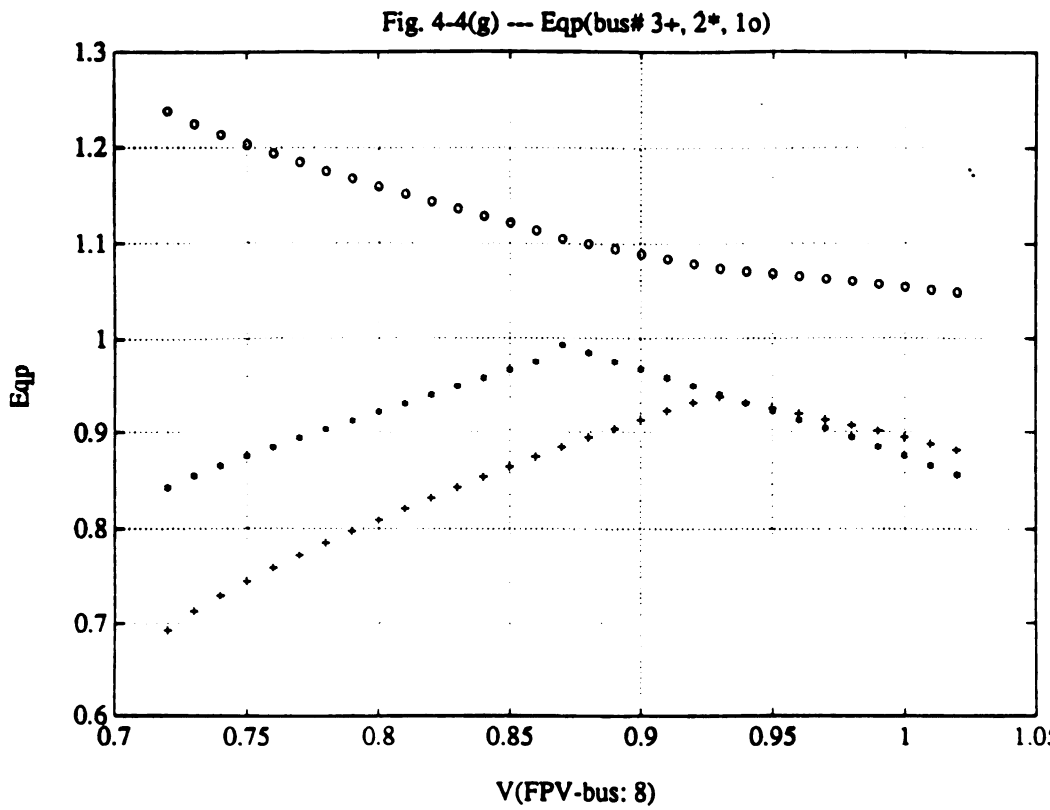
Fig. 4-4(g) --- Eqp(bus# 3+, 2*, 1o)
Eqp
1.3
1.2
1.1
1
0.9
0.8
0.7
0.6
0.7
0.75
0.8
0.85
0.9
0.95
1
1.05
V(FPV-bus: 8)

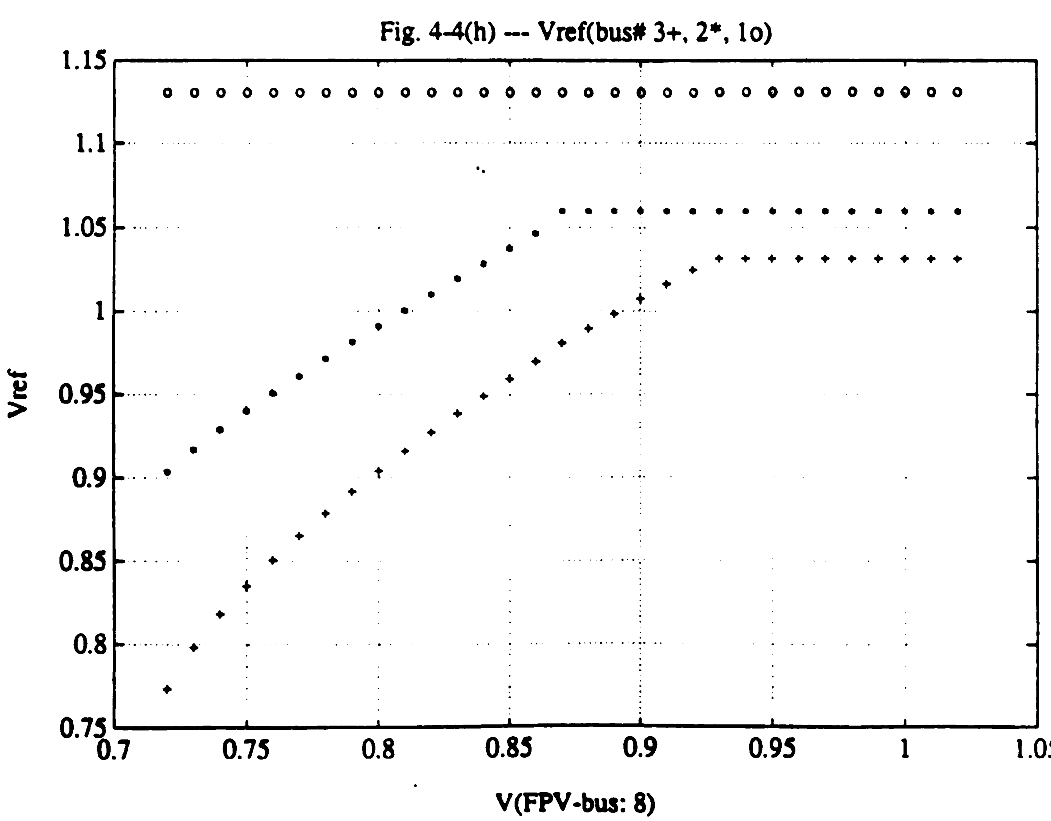
Fig. 4-4(h) --- Vref(bus# 3+, 2*, 1o)
Vref
1.15
1.1
1.05
1
0.95
0.9
0.85
0.8
0.75
0.7
0.75
0.8
0.85
0.9
0.95
1
1.05
V(FPV-bus: 8)

the internal bus voltage $E_q^{'}$, and Figure 4-4(h) gives the voltage set points V_{ref} of the excitation systems which control the voltage at terminal buses, that are not provided in the load flow bifurcation test. Note that the reactive power generation limits (Gen#2: $\pm$ 40.00 $MVAR$; Gen#3: $\pm$50.00 $MVAR$) are still used as the constraints whose violation causes the excitation systems on these generators to be disabled. If the generator exhausts its reactive power reserves, it is operated as a constant active and reactive power generation unit.

It is observed from Fig. 4-4(a) that this power system experiences a static/algebraic bifurcation when 43.11 $MVAR$ reactive power load is added at bus#8 which occurs when the voltage at this bus is about 0.86 pu. At the bifurcation point, the static/algebraic Jacobian matrix J_y becomes singular; while both the matrix f_x and the causality matrix g_y are nonsingular. Note that the matrix f_x is always nonsingular, whose determinant starts with 0.0057 at the base case, and graduately increases as the system is more stressed and before any generator operates in PQ-bus mode. When Gen#3 becomes a PQ-bus when bus#8 is at 0.92 pu voltage and 35.26 $MVAR$ load, the determinant of f_x jumps to 2.1407, and then increases slowly until Gen#2 becomes a PQ-bus. When Gen#2 exhausts its reactive power reserve, the determinant of f_x jumps more dramatically to 97.0080 where bus#8 is at 0.86 pu voltage and 43.11 $MVAR$ load. The static/algebraic bifurcation Jacobian matrix J_y becomes singular at this point. The causality matrix g_y is nonsingular until the voltage at bus#8 is down to about 0.73 pu with 14.14 $MVAR$ load far after the static/algebraic bifurcation point. This confirms that in general the matrix f_x is not singular and that g_y is more diagonally dominant than J_y if reactive power generation limits are reached. Moreover, this proposed approach for assessing the test for the static bifurcation by testing the singularity of the static/algebraic Jacobian matrix J_y rather than the dynamic Jacobian matrix J_x provides the advantages that no test for causality condition is necessary. In addition, this test can be performed by slightly modifying the load flow program, since the structure of J_y is similar to that of the load flow Jacobian matrix J_{LF}.

It should be pointed out that comparing Fig. 4-4(a) - Fig. 4-4(f) with Fig. 3-2(a) - Fig. 3-2(f), the results of the load flow bifurcation test and the static/algebraic bifurcation test are very similar. This is because of the high D.C. gain of the excitation system of each machine kept the generator terminal voltage almost constant until the generator exhausts its reactive power reserve and becomes a PQ-bus. Note that when a generator operates in a manner of a PQ-bus and the system is getting more stressed, its internal voltage $E_q^{'}$ should be controlled by the voltage set point V_{ref} of the excitation system to produce constant power output at its terminal bus, as shown in Fig. 4-4(g) and Fig. 4-4(h). This type of control reflects the operator action that attempts to keep the generator near its capability curve.

Chapter 5
Static/Dynamic Bifurcation in Dynamic Model

In Chapter 4, the basic necessary conditions for a power system dynamic model to experience static and/or dynamic bifurcation were categorized:

(a) The system Jacobian matrix $J = \begin{bmatrix} f_x & f_y \\ g_x & g_y \end{bmatrix}$ is singular.

(b) The equivalent static/algebraic Jacobian matrix $J_y = g_y - g_x\, f_x^{-1} f_y$ is singular, provided that f_x is nonsingular and J_g is row independent. The singularity of J_y is the generic test for the static/algebraic bifurcation or what has been called the singularity induced static bifurcation.

(c) The equivalent system Jacobian matrix $J_x = f_x - f_y\, g_y^{-1}\, g_x$ has eigenvalues with zero real parts, provided that g_y is nonsingular and J_f is row independent. When J_x has zero eigenvalues, a static bifurcation is said to occur. This is the generic type of static bifurcation due to the singularity of J_x, since J_f has been shown to be row independent and f_x has been shown to be nonsingular. This type of static bifurcation is equivalent to the static/algebraic bifurcation, and is also referred to as a singularity induced static bifurcation. A dynamic bifurcation occurs when J_x has complex eigenvalues with zero real parts.

The differential, algebraic, and differential-algebraic bifurcations have been identified that are respectively associated with the row dependence of J_f, of J_g, and of both J_f and J_g. These three bifurcations have been shown to be nongeneric and thus extremely rare. Moreover, it has been argued that both f_x and g_y should be nonsingular in practical power systems, and that f_x should have no complex eigenvalues with zero real parts if the control systems of each generator are designed properly and each generator is operated within design limits. Thus, the singularity induced bifurcation and dynamic bifurcation are the most probably generic bifurcations of the power system dynamics.

This chapter will thus assume that the system is causal, and will be devoted to the discussion of static/dynamic bifurcation [88] that occurs when J_x is singular or has pure imaginary eigenvalues. The static bifurcation could be saddle node bifurcation if J_x has a simple zero eigenvalue, and if the transversality condition of J_x at the bifurcation point holds. The dynamic bifurcation could be Hopf bifurcation if J_x has a pair of pure imaginary eigenvalues, and if the nondegeneracy condition of J_x at the bifurcation point holds. Note that the auxiliary necessary conditions — transversality condition for saddle-node bifurcation and nondegeneracy condition for Hopf bifurcation — will not be discussed in this dissertation.

In general, the dynamic angle and voltage stability problems are associated with the mechanical and flux decay dynamics of the power system equivalent dynamic model, and are particularly in the modes of low frequency oscillation. This chapter will study low frequency oscillation and voltage collapse bifurcations by identifying static and dynamic bifurcations associated with mechanical and flux decay dynamics, and by developing tests for these bifurcations, based on the fact that the control systems themselves have stable eigenvalues as proven in Chapter 4. A reduced Laplace transformed ($S = j\Omega$) model is produced that is composed of solely mechanical and flux decay dynamics, after the elimination of the control system dynamics since they are not singular for any $\Omega \geq 0$. A test matrix for bifurcations of mechanical and flux decay dynamics is then developed. Damping and synchronizing power coefficient matrices associated with the mechanical dynamics will be further derived, and test conditions on these matrices for identification and prevention of bifurcations of the mechanical dynamics will be established. Test matrices for identification and prevention of flux decay bifurcation will be similarly generated from the reduced model. These tests not only avoid the intensive computation of eigenvalue analysis, but also structurally show the effects of transmission network and control systems. Finally, the simulation on a 9-bus 3-machine power system model confirms the results [88].

5.1 Static/Dynamic Bifurcation

The equivalent system Jacobian matrix is defined as

$$J_x = f_x - f_y \, g_y^{-1} \, g_x$$

provided that the causality matrix g_y is nonsingular. If the equivalent system Jacobian matrix J_x is obtained by directly substituting the corresponding Jacobian submatrices, f_x, f_y, g_x, and g_y, from the linearized power system dynamic model (4-2), significant matrix manipulations would be required. In this section, an equivalent system Jacobian matrix J_x will be derived in more physically understandable manner based on the relationship between these Jacobian submatrices shown in Fig. 4.1.

Under the assumption that the causality condition holds (g_y is nonsingular), from the linearized power system dynamic model (4-2) and Fig. 4-1, one can represent the variables at terminal buses, $\Delta\theta_T$ and ΔV_T, in terms of mechanical and flux decay states, $\Delta\delta$ and $\Delta E_q'$, as follows:

$$\begin{bmatrix} \Delta\theta \\ \Delta V \end{bmatrix} = g_y^{-1} \cdot \left(\begin{bmatrix} \Delta P_C \\ \Delta Q_C \end{bmatrix} - g_x \begin{bmatrix} \Delta X_X \\ \Delta X_E \\ \Delta X_G \\ \Delta X_S \end{bmatrix} \right)$$

$$g_y = \begin{bmatrix} A_{P\theta} & A_{PV} \\ A_{Q\theta} & A_{QV} \end{bmatrix} \; ; \; g_x = \begin{bmatrix} A_{PX} & 0 & 0 & 0 \\ A_{QX} & 0 & 0 & 0 \end{bmatrix}$$

$$\begin{bmatrix} \Delta\theta \\ \Delta V \end{bmatrix} = \begin{bmatrix} A_{P\theta} & A_{PV} \\ A_{Q\theta} & A_{QV} \end{bmatrix}^{-1} \cdot \left(\begin{bmatrix} \Delta P_C \\ \Delta Q_C \end{bmatrix} - \begin{bmatrix} A_{PX} \\ A_{QX} \end{bmatrix} \Delta X_X \right) \tag{5-1a}$$

$$\begin{bmatrix} \Delta\theta_T \\ \Delta V_T \end{bmatrix} = \begin{bmatrix} I_T & 0 \\ 0 & I_T \end{bmatrix} \begin{bmatrix} \Delta\theta \\ \Delta V \end{bmatrix} = \begin{bmatrix} I & 0 & 0 & 0 & 0 & 0 \\ 0 & 0 & 0 & I & 0 & 0 \end{bmatrix} \begin{bmatrix} \Delta\theta_T \\ \Delta\theta_H \\ \Delta\theta_L \\ \Delta V_T \\ \Delta V_H \\ \Delta V_L \end{bmatrix}$$

$$= \begin{bmatrix} S_7 & S_8 \\ S_5 & S_6 \end{bmatrix} \begin{bmatrix} \Delta\delta \\ \Delta E_q' \end{bmatrix} + \begin{bmatrix} S_{\theta P} & S_{\theta Q} \\ S_{VP} & S_{VQ} \end{bmatrix} \begin{bmatrix} \Delta P_C \\ \Delta Q_C \end{bmatrix} \qquad (5\text{-}1b)$$

Substituting (5-1b) into the active power output equations at internal bus (for the swing equations), flux decay equations of machines, and load compensators of excitation systems, we have:

$$P_E = K_{P1}^{gt} \left(\Delta\delta - \Delta\theta_T \right) + K_{P2}^{gt} \Delta E_q' + K_{P7}^{gt} \Delta V_T$$

$$= S_{P1} \Delta\delta + S_{P2} \Delta E_q' + S_{PP} \Delta P_C + S_{QQ} \Delta Q_C \qquad (5\text{-}2)$$

$$T_{do}' \Delta \dot{E}_q' = \Delta E_{FD} - K_{E4} \left(\Delta\delta - \Delta\theta_T \right) - K_{E3} \Delta E_q' + K_{E7} \Delta V_T$$

$$= \Delta E_{FD} - S_4 \Delta\delta - S_3 \Delta E_q' + S_{EP} \Delta P_C + S_{EQ} \Delta Q_C \qquad (5\text{-}3)$$

$$T_D \Delta \dot{V}_D = K_D \Delta V_C \qquad (5\text{-}4a)$$

$$\Delta V_C = K_{C1} \left(\Delta\delta - \Delta\theta_T \right) K_{C2} \Delta E_q' + K_{C7} \Delta V_T$$

$$= S_{C1} \Delta\delta + S_{C2} \Delta E_q' + S_{CP} \Delta P_C + S_{CQ} \Delta Q_C \qquad (5\text{-}4b)$$

where,

$$S_{P1} = K_{P1}^{gt} - K_{P1}^{gt} S_7 + K_{P7} S_5$$

$$S_{P2} = K_{P2}^{gt} - K_{P1}^{gt} S_8 + K_{P7} S_6$$

$$S_4 = K_{E4} - K_{E4} S_7 - K_{E7} S_5$$

$$S_3 = K_{E3} - K_{E4} S_8 - K_{E7} S_6$$

$$S_{C1} = K_{C1} - K_{C1} S_7 + K_{C7} S_5$$

$$S_{C2} = K_{C2} - K_{C1} S_8 + K_{C7} S_6$$

Note that these S-matrices might not be symmetric if the network is not symmetric (see Section 2.6). The notation of these S-matrices are adopted so that they are consistent with those K-matrices [23,26] of single-machine-to-infinite-bus power system where the synchronous machine is also represented by single-axis model: $S_{P1} = K_1$, $S_{P2} = K_2$, $S_3 = K_3$, $S_4 = K_4$, $S_5 = K_5$, and $S_6 = K_6$. Recalling that if the load compensator is not employed, then $K_{C1} = 0$, $K_{C2} = 0$, and $K_{C7} = I$, such that $S_{C1} = S_5 = K_5$, and $S_{C2} = S_6 = K_6$.

It should be noted that the above derivation for the active power equations at the internal buses, the flux decay equations, and the voltage detector and load compensator equations by aggregating the terminal bus variables ($\Delta\theta_T$ and ΔV_T) through the transmission network is equivalent to performing the computation of $f_y\ g_y^{-1}\ g_x$, the second part of the equivalent dynamic Jacobian matrix J_x. Thus, after the elimination of the network variables, the equivalent dynamic model and the equivalent system Jacobian matrix J_x can be structurally written as follows:

$$\begin{bmatrix} T_{XX}\ \Delta\dot{X}_X \\ T_{EE}\ \Delta\dot{X}_E \\ T_{GG}\ \Delta\dot{X}_G \\ T_{SS}\ \Delta\dot{X}_S \end{bmatrix} = \begin{bmatrix} A_{XX}^S & A_{XE} & A_{XG} & 0 \\ A_{EX}^S & A_{EE} & 0 & A_{ES} \\ A_{GX} & 0 & A_{GG} & 0 \\ A_{SX} & 0 & 0 & A_{SS} \end{bmatrix} \begin{bmatrix} \Delta X_X \\ \Delta X_E \\ \Delta X_G \\ \Delta X_S \end{bmatrix} + B\ \Delta U \tag{5-5}$$

$$\begin{aligned} J_x &= f_x - f_y\ g_y^{-1}\ g_x \\ &= T_X^{-1}\ F_X^S \end{aligned} \tag{5-5a}$$

$$T_X = diag\,[\ T_{XX}\ \ T_{EE}\ \ T_{GG}\ \ T_{SS}\ ] \tag{5-5b}$$

$$F_X^S = \begin{bmatrix} A_{XX}^S & A_{XE} & A_{XG} & 0 \\ A_{EX}^S & A_{EE} & 0 & A_{ES} \\ A_{GX} & 0 & A_{GG} & 0 \\ A_{SX} & 0 & 0 & A_{SS} \end{bmatrix} \tag{5-5c}$$

where,

$$A_{XX}^{S} = \begin{bmatrix} -D & -S_{P1} & -S_{P2} \\ I & 0 & 0 \\ 0 & -S_4 & -S_3 \end{bmatrix} ; \; A_{EX}^{S} = \begin{bmatrix} 0 & K_D\, S_{C1} & K_D\, S_{C2} \\ 0 & 0 & 0 \\ A_{A\omega} & 0 & 0 \\ A_{B\omega} & 0 & 0 \\ 0 & 0 & 0 \end{bmatrix}$$

$$B = \begin{bmatrix} 0 & 0 & B_{XP} & B_{XQ} \\ B_{EE} & 0 & B_{EP} & B_{EQ} \\ 0 & B_{GG} & 0 & 0 \\ 0 & 0 & 0 & 0 \end{bmatrix} ; \; \Delta U = \begin{bmatrix} \Delta V_{ref} \\ \Delta P_0 \\ \Delta P_C \\ \Delta Q_C \end{bmatrix}$$

The complete expressions of the A submatrices can be found from (4-2). The detailed form of the B matrix is omitted without loss of continuity. The equivalent power system dynamic model can also be shown in Fig. 5-1, which help provide understanding of the model.

It is observed that the structure of the equivalent dynamic Jacobian matrix J_x is the same as that of the matrix f_x and that of the matrix F_X defined in (4-8). The difference between them is shown by the superscript S and by the sensitivity S-matrices replacing the coefficient K-matrices. This indicates the physical meaning that the effects from the transmission network through the terminal buses on the internal buses are responded by the corresponding dynamics that governs or feeds back the terminal bus variables.

The static and/or dynamic bifurcation may occur when the equivalent system Jacobian matrix J_x of (5-5) has eigenvalues with zero real parts. Taking the Laplace transform, $S = j\Omega$ where $j = \sqrt{-1}$ and $\Omega = 2\,\pi\, f_O$, on (5-5) and on (4-2), it can be shown that for all $\Omega \geq 0$, the singularity of the matrix

$$J_x(j\Omega) = J_x - j\Omega\, I \tag{5-6}$$

is a test condition for static and dynamic bifurcations, since, by Schur's formula (Appendix A), the singularity of $J_x(j\Omega)$ and that of

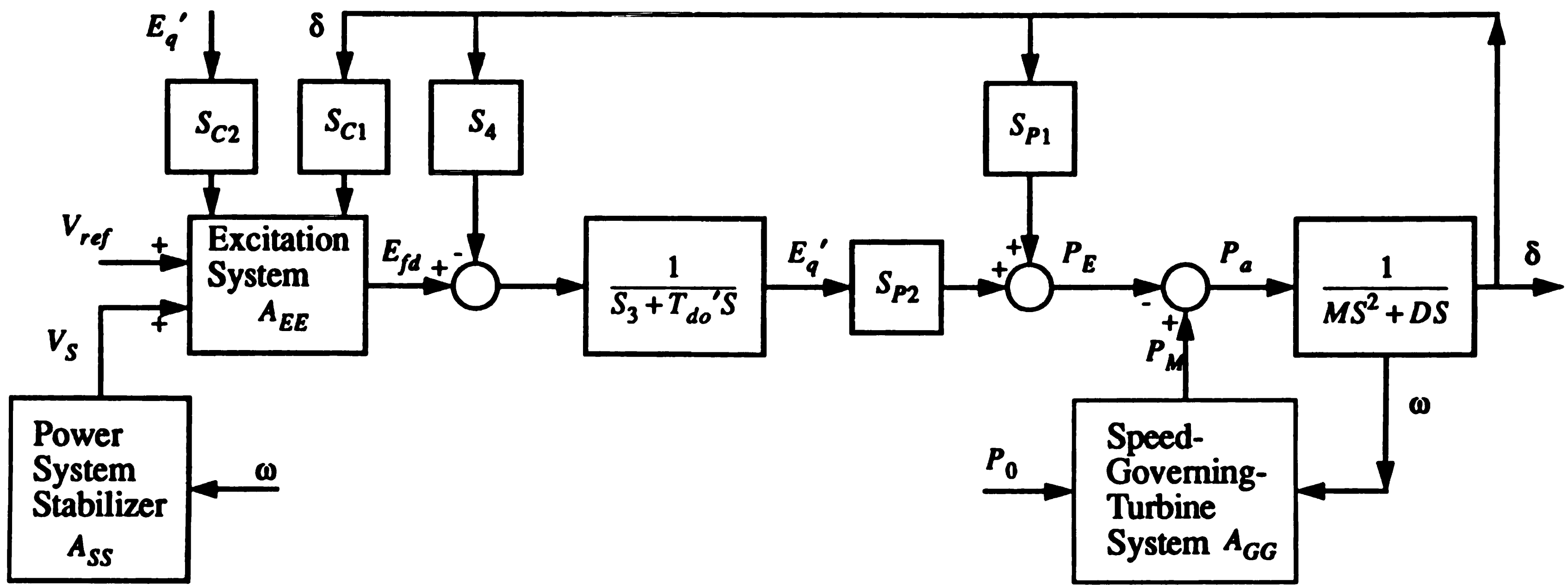

Fig. 5-1 Equivalent Power System Dynamic Model

$$J_I(j\Omega) = J - \begin{bmatrix} j\Omega I & 0 \\ 0 & 0 \end{bmatrix} \tag{5-7}$$

are equivalent if causality holds. In other words, assuming that causality condition and transversality/nondegeneracy condition hold, the singularity of $J_x(j\Omega)$ is a necessary condition for either static/saddle node bifurcation if $\Omega = 0$, or dynamic/Hopf bifurcation if $\Omega > 0$. The static and dynamic bifurcations due to the singularity of the matrix $J_x(j\Omega)$ (5-6) is associated with the mechanical dynamics, the flux decay dynamics, the control systems dynamics, and their couplings.

5.2 Mechanical and Flux Decay Dynamics

In general, from the experimental results of SSSP [4,21], low frequency oscillations often link with mechanical and flux decay dynamics, but are rarely associated with control systems dynamics. This characteristics of the mechanical and flux decay dynamics can be self-explained by the properties of f_x shown in Section 4.3, and by the structure of the static/dynamic Jacobian matrix J_x (5-5). It is observed that J_x has the same structure as f_x (4-8), and that the transmission network effects only show on the mechanical and flux decay dynamics — A_{XX}^S, and on the dynamics of voltage detectors of the excitation systems through the load compensators — A_{EX}^S. Moreover, the excitation systems govern the field voltage E_{FD} and in turn affect the internal bus voltage $E_q^{'}$. However, the main diagonal matrix A_{CC} (4-8c) of both f_x and J_x does not change, which indicates that the bifurcations or low frequency oscillations would not be associated with the dynamics of control systems, if the bifurcations or low frequency oscillations are caused by the transmission network effects.

In other words, the static and dynamic bifurcations due to the singularity of $J_x(j\Omega)$ (5-6) associated with all the dynamic states of synchronous machines could be further reduced to a Jacobian matrix solely pertaining to the mechanical and flux decay dynamics. In order to obtain the equivalent Jacobian matrix associated with mechanical and flux decay dynamics, the effects of exciter, governor, and stabilizer control systems are going to be aggregated. As discussed in Section 4.3, the control systems themselves are usually asymptotically stable, i.e., no eigenvalues with zero real parts. Thus, the Laplace transformed diagonal block matrix of the control systems (from (4-8c))

$$A_{CC}(j\Omega) = \begin{bmatrix} A_{EE} - j\Omega\, T_{EE} & 0 & A_{ES} \\ 0 & A_{GG} - j\Omega\, T_{GG} & 0 \\ 0 & 0 & A_{SS} - j\Omega\, T_{SS} \end{bmatrix} \tag{5-8}$$

should be nonsingular for all $\Omega \geq 0$, and its inverse is as follows.

$$A_{CC}^{-1}(j\Omega) = \begin{bmatrix} [A_{EE} - j\Omega\, T_{EE}]^{-1} & 0 & A_{ES}(j\Omega) \\ 0 & [A_{GG} - j\Omega\, T_{GG}]^{-1} & 0 \\ 0 & 0 & [A_{SS} - j\Omega\, T_{SS}]^{-1} \end{bmatrix}$$

$$A_{ES}(j\Omega) = -\,[A_{EE} - j\Omega\, T_{EE}]^{-1}\, A_{ES}\, [A_{SS} - j\Omega\, T_{SS}]^{-1}$$

Therefore, aggregating control systems from (5-5), one can produce the following equivalent model solely associated with mechanical and flux decay dynamics where the input matrix B is omitted without loss of continuity.

$$T_{XX}\, j\Omega\, \Delta X_X = \left(A_{XX}^{S} - [\, A_{XE} \;\; A_{XG} \;\; 0 \,]\, A_{CC}^{-1}(j\Omega) \begin{bmatrix} A_{EX}^{S} \\ A_{GX} \\ A_{SX} \end{bmatrix} \right) \Delta X_X \tag{5-9a}$$

$$\begin{bmatrix} M\, j\Omega\, \Delta\omega \\ j\Omega\, \Delta\delta \\ T_{do}'\, j\Omega\, \Delta E_q' \end{bmatrix} = A_{XX}^{S}(j\Omega) \begin{bmatrix} \Delta\omega \\ \Delta\delta \\ \Delta E_q' \end{bmatrix} \tag{5-9b}$$

$$\begin{aligned} A_{XX}^{S}(j\Omega) &= A_{XX}^{S} - A_{XG}\, [\, A_{GG} - j\Omega\, T_{GG} \,]^{-1}\, A_{GX} \\ &\quad - A_{XE}\, [\, A_{ES}(j\Omega)\, A_{SX} + [A_{EE} - j\Omega\, T_{EE}]^{-1}\, A_{EX}^{S} \,] \\ &= A_{XX}^{S} - A_{XX}^{GG}(j\Omega) - A_{XX}^{ES}(j\Omega) - A_{XX}^{EE}(j\Omega) \end{aligned} \tag{5-9c}$$

$$= \begin{bmatrix} -[\,D + D_G(j\Omega)\,] & -S_{P1} & -S_{P2} \\ I & 0 & 0 \\ -S_S(j\Omega) & -[\,S_4 + S_{E1}(j\Omega)\,] & -[\,S_3 + S_{E2}(j\Omega)\,] \end{bmatrix}$$

where, the following complex matrices are defined

$$A_{XX}^{GG}(j\Omega) = A_{XG}\,[\,A_{GG} - j\Omega\, T_{GG}\,]^{-1} A_{GX}$$

$$= \begin{bmatrix} D_G(j\Omega) & 0 & 0 \\ 0 & 0 & 0 \\ 0 & 0 & 0 \end{bmatrix}$$

$$D_G(j\Omega) = D_{Gr}(\Omega) + j\Omega\, D_{Gi}(\Omega)$$

$$= A_{\omega G}\,[\,A_{GG} - j\Omega\, T_{GG}\,]^{-1} A_{G\omega}$$

: effects of speed-governing-turbine system;

$$A_{XX}^{ES}(j\Omega) = A_{XE}\, A_{ES}(j\Omega)\, A_{SX}$$

$$= \begin{bmatrix} 0 & 0 & 0 \\ 0 & 0 & 0 \\ S_S(j\Omega) & 0 & 0 \end{bmatrix}$$

$$S_S(j\Omega) = S_{Sr}(\Omega) + j\Omega\, S_{Si}(\Omega)$$

$$= A_{FE}[\,A_{EE} - j\Omega T_{EE}\,]^{-1}\,[\,A_{E\omega} - A_{ES}\,[\,A_{SS} - j\Omega\, T_{SS}\,]^{-1} A_{S\omega}\,]$$

: effects of power system stabilizer;

$$A_{XX}^{EE}(j\Omega) = A_{XE}\,[\,A_{EE} - j\Omega\, T_{EE}\,]^{-1} A_{EX}^{S}$$

$$= \begin{bmatrix} 0 & 0 & 0 \\ 0 & 0 & 0 \\ 0 & S_{E1}(j\Omega) & S_{E2}(j\Omega) \end{bmatrix}$$

$$S_{E1}(j\Omega) = S_{E1r}(\Omega) + j\Omega\, S_{E1i}(\Omega)$$

$$= A_{FE}\,[\,A_{EE} - j\Omega\, T_{EE}\,]^{-1} A_{EC1}$$

: effects of excitation system on $\Delta\delta$;

$$S_{E2}(j\Omega) = S_{E2r}(\Omega) + j\Omega\, S_{E2i}(\Omega)$$

$$= A_{FE}\,[\,A_{EE} - j\Omega\, T_{EE}\,]^{-1} A_{EC2}$$

: effects of excitation system on $\Delta E_q'$.

Note that A_{FE} is a submatrix of A_{XE} defined in (4-2), and that $A_{E\infty}$, A_{EC1}, and A_{EC2} are submatrices of A_{EX} (4-2). Each matrix with (Ω), that is defined as a function of Ω, is a real matrix. Figure 5-2 shows the equivalent model of mechanical and flux decay dynamics.

From Schur's formula (Appendix A), it is observed that the test for the singularity of the matrix

$$J_{XX}(j\Omega) = A^{S}_{XX}(j\Omega) - j\Omega\, T_{XX} \tag{5-10}$$

$$T_{XX} = diag\ [\ M \quad I \quad T'_{do}\ ]$$

is equivalent to the test for the singularity of $J_x(j\Omega) = J_x - j\Omega\, I$ (5-6), if $A_{CC}(j\Omega)$ (5-8) is nonsingular for all $\Omega \geq 0$ of interest. Thus, adding one more condition, $A_{CC}(j\Omega)$ is nonsingular for all $\Omega \geq 0$ (which has been proven to be true in Section 4.3), to these two preliminary conditions: causality and transversality/nondegeneracy, allows one to focus the necessary test condition on $J_{XX}(j\Omega)$ (5-10) for the static and dynamic bifurcation associated with the mechanical and flux decay dynamics, rather than on $J_x(j\Omega)$ (5-6) or on $J_l(j\Omega)$ (5-7).

In addition, $A^{S}_{XX}(j\Omega)$ (5-9) structurally shows the effects of different control systems and those of transmission network sensitivity matrices. It should also be pointed out that $A_{CC}(j\Omega)$ represents the frequency response of the control systems (in general, the frequency range of interest is from 0.00 H_Z to 2.00 H_Z for the studies of low frequency oscillations), is only function of the parameters of the control systems that are usually constant, and is an upper-triangular matrix preserving the structure of each component of control systems. The inverse of $A_{CC}(j\Omega)$ (5-8) keeps the structural sparse property, and needs to be performed only once. This indicates the savings on the computation and memory if the bifurcation test is performed based on $J_{XX}(j\Omega)$ (5-10). Furthermore, the structure of $J_{XX}(j\Omega)$ can be analyzed either analytically or computationally to establish the causes of various static bifurcations, dynamic

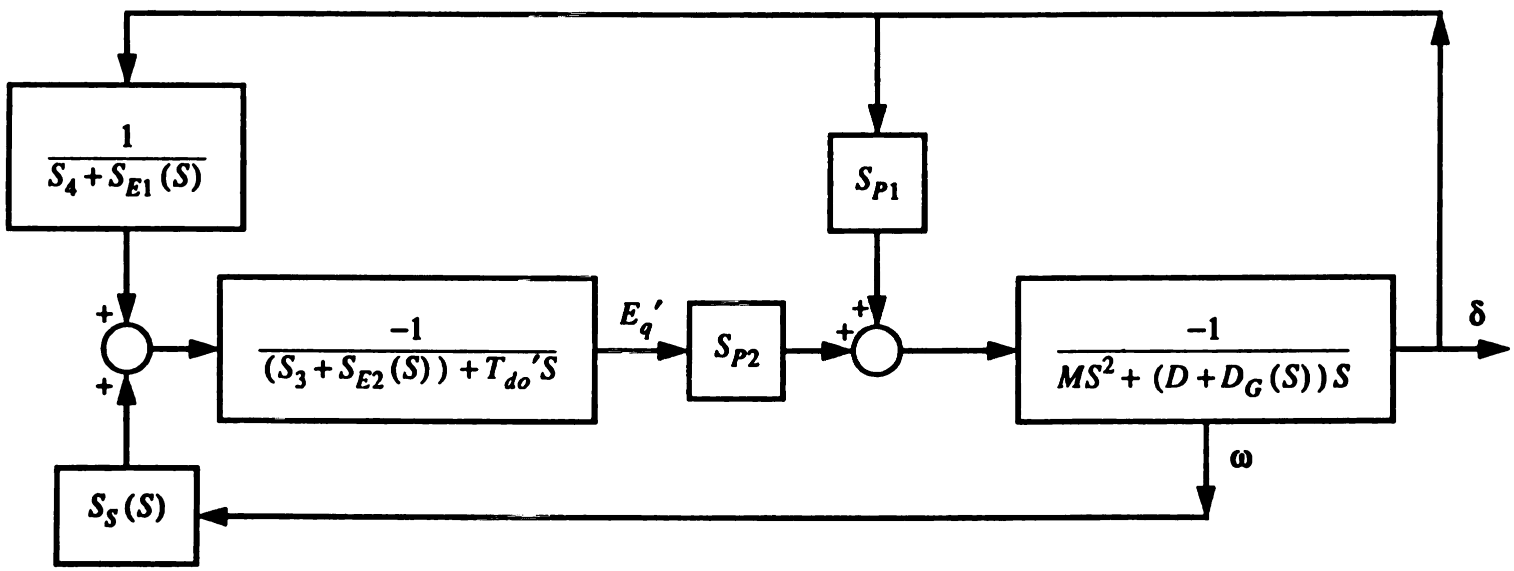

Fig. 5-2 Equivalent Model of Mechanical and Flux Decay Dynamics

$(S=j\Omega)$

bifurcations or even complex dynamical phenomena.

5.3 Mechanical Dynamics

In this section and next section, test conditions solely associated with the mechanical dynamics and solely associated with the flux decay dynamics will be established, respectively. The objective is to more precisely determine to "main" dynamics that could be vulnerable to experience the static and/or dynamic bifurcations, if the coupling between the mechanical dynamics and flux decay dynamics is "weak".

In this section, damping and synchronizing power coefficient matrices will be derived, and test condition for the static and dynamic bifurcations strongly associated with the mechanical dynamics will be developed from these two matrices. This provides a measure of proximity to static/dynamic bifurcation pertaining to the mechanical dynamics. To accomplish the above purpose, it is assumed that the main block matrix of the flux decay dynamics of (5-9)

$$S_3(j\Omega) = S_3 + S_{E2}(j\Omega) + j\Omega\, T_{do}'$$

$$= S_{3_r}(\Omega) + j\Omega\, S_{3_i}(\Omega) \tag{5-11}$$

is nonsingular, or that both real and imaginary components

$$S_{3_r}(\Omega) = S_3 + S_{E2_r}(\Omega) \tag{5-11a}$$

$$S_{3_i}(\Omega) = T_{do}' + S_{E2_i}(\Omega) \tag{5-11b}$$

are nonsingular for all $\Omega \geq 0$ of interest. These conditions along with the conditions that $A_{CC}(j\Omega)$ (5-8) is nonsingular and that causality and transversality/nondegeneracy hold assure that if the power system (4-2) experiences a bifurcation, it will mainly occur in the mechanical dynamics.

Thus, from (5-9), aggregating the flux decay states back into mechanical states we have

$$\begin{bmatrix} M\ j\Omega\ \Delta\omega \\ j\Omega\ \Delta\delta \end{bmatrix} = (\begin{bmatrix} -[\ D + D_G(j\Omega)\ ] & -S_{P1} \\ I & 0 \end{bmatrix}$$

$$- \begin{bmatrix} -S_{P2} \\ 0 \end{bmatrix} S_3^{-1}(j\Omega)\ [\ -S_S(j\Omega)\ -(\ S_4 + S_{E1}(j\Omega)\ )\ ]\ ) \begin{bmatrix} \Delta\omega \\ \Delta\delta \end{bmatrix}$$

$$= \begin{bmatrix} -K_d(j\Omega) & -K_s(j\Omega) \\ I & 0 \end{bmatrix} \begin{bmatrix} \Delta\omega \\ \Delta\delta \end{bmatrix} \tag{5-12}$$

$$K_d(j\Omega) = D + D_G(j\Omega) + D_{ES}(j\Omega) \tag{5-12a}$$

$$K_s(j\Omega) = S_{P1} + D_{EE}(j\Omega) \tag{5-12b}$$

where,

$$D_{ES}(j\Omega) = -\ S_{P2}\ [\ S_3 + S_{E2}(j\Omega) + j\Omega\ T'_{do}\ ]^{-1}\ S_S(j\Omega)$$

$$= D_{ESr}(\Omega) + j\Omega\ D_{ESi}(\Omega)$$

$$D_{EE}(j\Omega) = -\ S_{P2}\ [\ S_3 + S_{E2}(j\Omega) + j\Omega\ T'_{do}\ ]^{-1}\ [\ S_4 + S_{E1}(j\Omega)\ ]$$

$$= D_{EEr}(\Omega) + j\Omega\ D_{EEi}(\Omega)$$

Using the following properties of the rotor angle and rotor speed

$$\Delta\omega(j\Omega) = j\Omega\ \Delta\delta(j\Omega) \tag{5-13a}$$

$$-\ \Omega^2\ \Delta\delta(j\Omega) = j\Omega\ \Delta\omega(j\Omega) \tag{5-13b}$$

we define the following damping and synchronizing power coefficient matrices in a manner similar to that of Concordia and deMello [23] for a single-machine-to-infinite-bus system.

$$\begin{bmatrix} M\ j\Omega\ \Delta\omega \\ j\Omega\ \Delta\delta \end{bmatrix} = \begin{bmatrix} -K_{damp}(\Omega) & -K_{sync}(\Omega) \\ I & 0 \end{bmatrix} \begin{bmatrix} \Delta\omega \\ \Delta\delta \end{bmatrix} \tag{5-14}$$

$$K_{damp}(\Omega) = D + D_{Gr}(\Omega) + D_{ESr}(\Omega) + D_{EEi}(\Omega) \tag{5-14a}$$

$$K_{sync}(\Omega) = S_{P1} + D_{EEr}(\Omega) - \Omega^2\ [\ D_{Gi}(\Omega) + D_{ESi}(\Omega)\ ] \tag{5-14b}$$

It is observed that excitation system, power system stabilizer, and speed-governing-turbine system have effects on both damping and synchronizing power coefficient matrices $K_{damp}(\Omega)$ and $K_{sync}(\Omega)$, which are functions of the six sensitivity matrices: S_{P1}, S_{P2}, S_3, S_4, S_{C1}, and S_{C2}. If load compensators are not employed, S_{C1} and S_{C2} will respectively become S_5 and S_6 in (5-1), since $K_{C1} = 0$, $K_{C2} = 0$, and $K_{C7} = I$.

Note that for all $\Omega \geq 0$, the singularity of (5-14) is equivalent to that of

$$0 = - j\Omega\, K_{damp}(\Omega) - K_{sync}(\Omega) + \Omega^2 M$$

$$= - j\Omega\, K_{damp}(\Omega) - K_{sm}(\Omega) \qquad (5\text{-}14c)$$

$$K_{sm}(\Omega) = K_{sync}(\Omega) - \Omega^2 M \qquad (5\text{-}14d)$$

It can be concluded that the necessary condition for static and dynamic bifurcations associated with mechanical dynamics is that

(1) for static bifurcation: $\Omega = 0$,
$K_{sync}(\Omega = 0)$ is singular;

(2) for dynamic bifurcation: $\Omega > 0$,
both $K_{damp}(\Omega)$ and $K_{sm}(\Omega) = K_{sync}(\Omega) - \Omega^2 M$ are singular;

when

(a) causality is assumed,

(b) transversality/nondegeneracy is assumed,

(c) $A_{CC}(j\Omega)$ is assumed nonsingular, and

(d) $S_3(j\Omega) = S_3 + S_{E2r}(\Omega) + j\Omega\,[\, T'_{do} + S_{E2i}(\Omega)\,]$ is assumed nonsingular.

It should be noted, for $\Omega = 0$, that the imaginary component of each matrix with subscript i is equal to zero, such that

$$D_{Gr}(\Omega = 0) = A_{\omega G}\, A_{GG}^{-1}\, A_{G\omega} = K_G \qquad (5\text{-}15a)$$

$$S_{Sr}(\Omega = 0) = A_{FE}\, A_{EE}^{-1}\,[\, A_{E\omega} - A_{ES}\, A_{SS}^{-1}\, A_{S\omega}\,] = 0 \qquad (5\text{-}15b)$$

$$S_{E1r}(\Omega = 0) = A_{FE}\ A_{EE}^{-1}\ A_{EC1} = K_{EE}\ S_{C1} \tag{5-15c}$$

$$S_{E2r}(\Omega = 0) = A_{FE}\ A_{EE}^{-1}\ A_{EC2} = K_{EE}\ S_{C2} \tag{5-15d}$$

$$D_{ESr}(\Omega = 0) = -\ S_{P2}\ [\ S_3 + S_{E2r}(\Omega = 0)\ ]^{-1}\ S_{Sr}(\Omega = 0) = 0 \tag{5-15e}$$

$$D_{EEr}(\Omega = 0) = -\ S_{P2}\ [\ S_3 + S_{E2r}(\Omega = 0)\ ]^{-1}\ [\ S_4 + S_{E1r}(\Omega = 0)\ ]$$

$$= -\ S_{P2}\ [\ S_3 + K_{EE} S_{C2}\ ]^{-1}\ [\ S_4 + K_{EE}\ S_{C1}\ ] \tag{5-15f}$$

$$K_{EE} = K_{SE}^{-1}\ K_A\ K_D \tag{5-15g}$$

and that

$$K_{damp}(\Omega = 0) = D\ + K_G \tag{5-16a}$$

$$K_{sync}(\Omega = 0) = S_{P1} + D_{EEr}(\Omega = 0) \tag{5-16b}$$

where, K_G is a diagonal matrix composed of the D.C. gains of the speed-governing-turbine systems (see Fig. 2-8) [86]; and K_{EE} is the D.C. gain diagonal matrix of the excitation systems (see Fig. 2-5) [85]. The power system stabilizers do not show any effects on damping and synchronizing power coefficient matrices when $\Omega = 0$ ($S_{Sr}(\Omega = 0) = 0$ is the same as the 0_S shown in A_{XX}^{C} (4-9)), due to their D.C. washout transfer functions (see Fig. 2-7) [85]. Since $D > 0$ and $K_G > 0$ (positive definite) such that $K_{damp}(\Omega = 0) > 0$, the stability of the mechanical dynamics at $\Omega = 0$ will fully depend on $K_{sync}(\Omega = 0)$ which in turn depends on the D.C. gains of excitation systems K_{EE} and the transmission network effects through the six sensitivity matrices: S_{P1}, S_{P2}, S_3, S_4, S_{C1}, and S_{C2}. It is obvious that from the Lyapunov stability theory, the sufficient condition for this system being locally stable is that both $K_{damp}(\Omega = 0)$ and $K_{sync}(\Omega = 0)$ are positive definite [22-35].

Moreover, testing the singularity of $K_{sync}(\Omega = 0)$ leading to static bifurcation associated with mechanical dynamics is equivalent to testing the singularity of the static/algebraic Jacobian matrix J_y discussed in Chapter 4. However, for $K_{sync}(\Omega = 0)$, inverse of causality matrix g_y is needed; for J_y, there is no further information about participation dynamics or states provided. Note also that the dependence of $K_{sync}(\Omega = 0)$ on the the D.C. gains of excitation systems and on network sensitivity matrices is similar to the dependence of J_y on them shown in Section 4.4.

These tests for static and dynamic bifurcations associated with the mechanical dynamics are the first time such tests have been derived for a multimachine power system model, although such tests for static bifurcations have existed for single-machine-to-infinite-bus models [23]. These tests clearly show the roles of various control systems and the effects of transmission network on the development of static and dynamic mechanical stability problems. These results open up the possibility of analytically and computationally investigating the generic causes of such stability problems in a manner heretofore impossible. In addition, these test matrices allow sensitivities to be analytically derived or to be computationally calculated to help understand the specific cause of the stability problem of the mechanical dynamics and the most appropriate remedial actions. These results may be extremely useful and further research is necessary to investigate their usefulness.

5.4 Flux Decay Dynamics

In this section, a necessary condition is developed for the static and dynamic bifurcations associated with flux decay dynamics. This test condition provides an identification and an prevention measure of proximity to static/dynamic bifurcation strongly pertaining to the mechanical dynamics, likewise the one for the mechanical dynamics.

From (5-9), if for all $\Omega \geq 0$ of interest, the main block matrix of the mechanical dynamics

$$A_M(j\Omega) = \begin{bmatrix} -[\,D + D_G(j\Omega)\,] & -S_{P1} \\ I & 0 \end{bmatrix} - \begin{bmatrix} j\Omega M & 0 \\ 0 & j\Omega I \end{bmatrix}$$

$$= \begin{bmatrix} -[\,D + D_G(j\Omega)\,] - j\Omega\, M & -S_{P1} \\ I & -j\Omega\, I \end{bmatrix} \tag{5-17a}$$

is nonsingular, which is equivalent to require the matrix

$$S_M(j\Omega) = S_{P1} + j\Omega\,[\,D + D_G(j\Omega) + j\Omega\, M\,]$$

$$= S_{Mr}(\Omega) + j\Omega\, S_{Mi}(\Omega) \tag{5-17b}$$

be nonsingular, or both real and imaginary components

$$S_{Mr}(\Omega) = S_{P1} - \Omega^2\,[\,M + D_{Gi}(\Omega)\,] \tag{5-17c}$$

$$S_{Mi}(\Omega) = D + D_{Gr}(\Omega) \tag{5-17d}$$

be nonsingular, we can aggregate the mechanical states back into the flux decay states in order to investigate the equivalent flux decay dynamics:

$$T_{do}'\, j\Omega\, \Delta E_q' = -\,T_{FD}(j\Omega)\, \Delta E_q' \tag{5-18}$$

$$T_{FD}(j\Omega) = S_3 + S_{E2}(j\Omega) - [\,S_S(j\Omega)\;\; S_4 + S_{E1}(j\Omega)\,]\, A_M(j\Omega)^{-1} \begin{bmatrix} -S_{P2} \\ 0 \end{bmatrix}$$

$$= S_3 + S_{E2}(j\Omega) - [\,j\Omega\, S_S(j\Omega) + S_4 + S_{E1}(j\Omega)\,]\, S_M^{-1}(j\Omega)\, S_{P2}$$

$$= T_{FDr}(\Omega) + j\Omega\, T_{FDi}(\Omega)$$

For all $\Omega \geq 0$, the singularity of (5-18) is equivalent to that of

$$0 = j\Omega\, T_{do}' + T_{FD}(j\Omega)$$

$$= T_{FDr}(\Omega) + j\Omega\, T_{FDx}(\Omega) \tag{5-18a}$$

$$T_{FDx}(\Omega) = T_{do}' + T_{FDi}(\Omega) \tag{5-18b}$$

Thus, the necessary condition for static and dynamic bifurcations associated with flux decay dynamics is that

(1) for static bifurcation: $\Omega = 0$,

$T_{FDr}(\Omega = 0)$ is singular;

(2) for dynamic bifurcation: $\Omega > 0$,

both $T_{FDr}(\Omega)$ and $T_{FDx}(\Omega) = T'_{do} + T_{FDi}(\Omega)$ are singular;

when

(a) causality is assumed,

(b) transversality/nondegeneracy is assumed,

(c) $A_{CC}(j\Omega)$ is assumed nonsingular, and

(e) $S_M(j\Omega) = S_{P1} - \Omega^2 [\, M + D_{Gi}(\Omega)\,] + j\Omega\, [\, D + D_{Gr}(\Omega)\,]$ is nonsingular.

Note that for $\Omega = 0$, using the facts shown in (5-15) and $S_{Mr}(\Omega = 0) = S_{P1}$, we have

$$T_{FDr}(\Omega = 0) = [\, S_3 + S_{E2r}(\Omega = 0)\,] - [\, S_4 + S_{E1r}(\Omega = 0)\,]\, S_{Mr}^{-1}(\Omega = 0)\, S_{P2}$$
$$= [\, S_3 + K_{EE}\; S_{C2}\,] - [\, S_4 + K_{EE}\; S_{C1}\,]\, S_{P1}^{-1}\; S_{P2} \qquad (5\text{-}19)$$

This test matrix $T_{FDr}(\Omega = 0)$ for static bifurcation in flux decay dynamics shows the dependence on the the D.C. gains of excitation systems K_{EE} and on the transmission network sensitivity matrices: S_{P1}, S_{P2}, S_3, S_4, S_{C1}, and S_{C2}; similarly to the synchronizing coefficient matrix $K_{sync}(\Omega = 0)$ (5-16), and to the equivalent static/algebraic Jacobian matrix J_y (Chapter 4). In addition, $T_{FDr}(\Omega = 0)$ has another similar characteristic to $K_{sync}(\Omega = 0)$ about the inverse of the causality matrix g_y. Testing the singularity of $T_{FDr}(\Omega = 0)$ leading to the static bifurcation associated with flux decay dynamics is also equivalent to testing the singularity of the static/algebraic Jacobian matrix J_y. However, for $T_{FDr}(\Omega = 0)$, inverse of causality matrix g_y is needed; for J_y, there is no further information about participation dynamics or states provided.

It should be pointed out that the test matrix $T_{FDr}(\Omega = 0)$ is consistent with the one previously derived in [52,53] for the flux decay dynamics of a power system without both power system stabilizers and speed-governing-turbine systems, but using a very different procedure. The static bifurcation in flux decay dynamics due to the singularity of $T_{FDr}(\Omega = 0)$ has also been experimentally shown to cause voltage collapse, especially when field current limits are reached and then the normal excitation controls are disabled [52,53].

The Hopf bifurcation of flux decay dynamics has been shown to occur when mechanical dynamics, speed-governing-turbine dynamics, and power system stabilizer dynamics are ignored [42,68]. Whereas, the test condition on $T_{FDr}(\Omega)$ and $T_{FDi}(\Omega)$ for $\Omega > 0$ can test for this Hopf bifurcation, including all the effects of mechanical and control systems dynamics.

The tests for the static and dynamic bifurcations of the generator flux decay dynamics are the first tests of their kind ever developed for multimachine power systems, although such problems have been studied in small power system models with simple excitation controls [39-42,45,52,53,64-73,78,79]. These tests clearly show the effects of various control systems and transmission network on the development of static and dynamic stability problems associated with flux decay dynamics. These results probably make the analytically and computationally investigating the generic causes of such stability problems possible. Moreover, these test matrices provide the significance of the sensitivity matrices of the control systems and transmission network, which allows further analytical development or computationally calculation on these sensitivity matrices to help understand the cause of flux decay dynamic stability problem and the most appropriate remedial measures.

5.5 Simulation Results

The 9-bus 3-machine power system shown in Fig. 5-3 [4] is adopted to confirm the above bifurcation tests associated with mechanical and flux decay dynamics. Figure 5-3 also shows the operating condition of this power system. This power system is very similar to the ones used in the previous two chapters. The difference between these two systems is that the system of Fig. 5-3 has less transmission line impedance

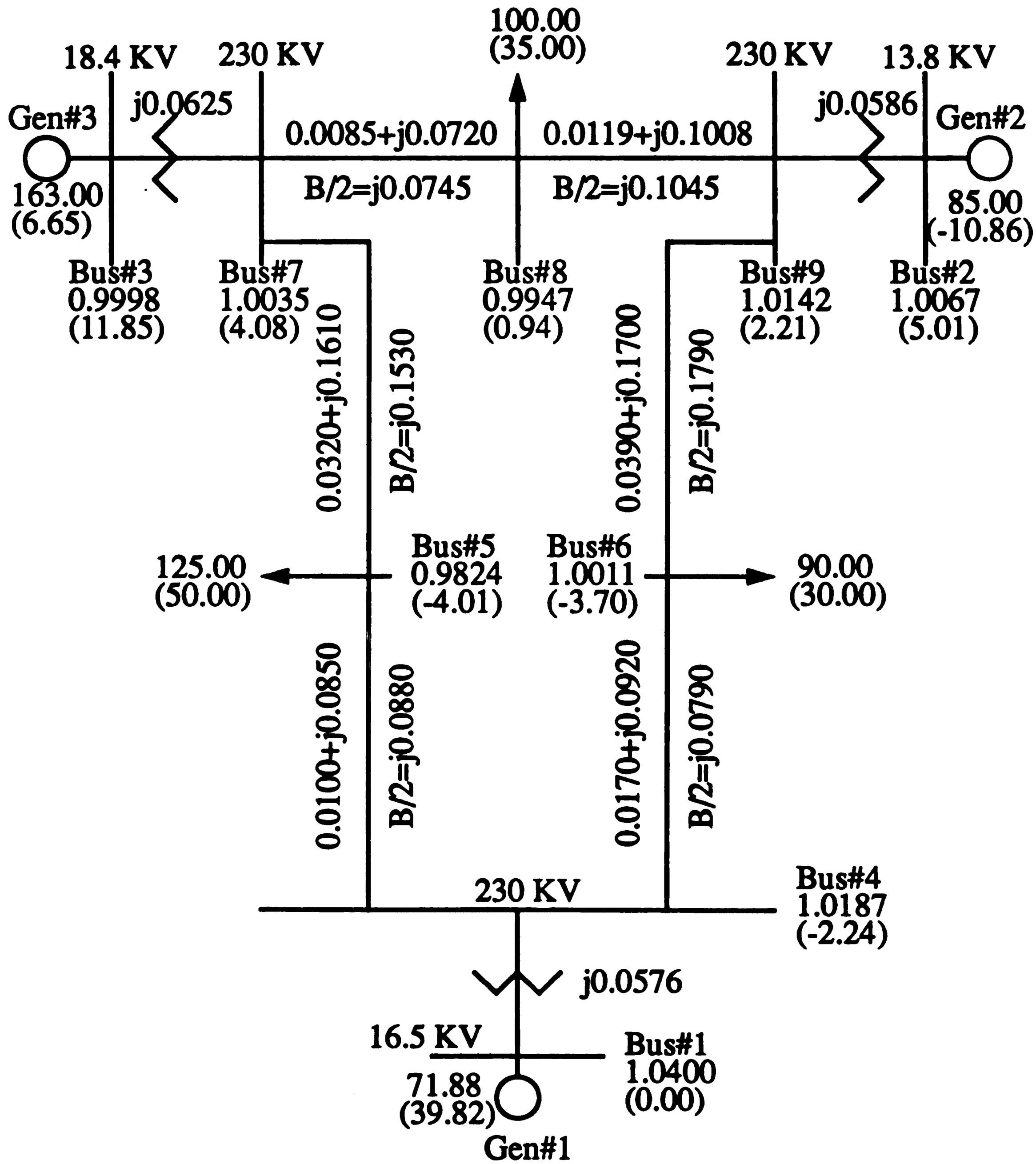

Fig. 5-3 9-bus 3-machine Power System Diagram and has more line charging susceptance, so that the generators Gen#2 and Gen#3 operate at lower terminal voltage and provide less reactive power generation. The dynamic data of the synchronous machines is listed in Table 5-1. Table 5-2 shows the eigenvalue analysis [4] for this system data which is provided for reference. These results will be compared with the bifurcation test results from the proposed approach. It should be noted that the causality condition of this system operation condition holds. It is observed, from Table 5-2, that the system has two pairs of complex eigenvalues with very small real parts — one pair associated with mechanical dynamics (Mode#1), and the other associated with both mechanical dynamics and flux decay dynamics (Mode#3). Note that the mechanical and flux decay dynamics associated with these two pairs of complex eigenvalue are also coupled with other states (control systems dynamics).

Figure 5-4(a) and Figure 5-4(b) respectively show the determinant of $K_{damp}(\Omega)$ and that of $K_{sm}(\Omega) = K_{sync}(\Omega) - \Omega^2 M$ where $\Omega = 2\pi f_O$ for f_O from 0.0 H_Z to 2.0 H_Z, which is in general the range of low frequency oscillation. It is observed that these two determinants are simultaneously approaching zero in these two frequency ranges: 0.0 $\rightarrow$ 0.03 H_Z and 1.1 $\rightarrow$ 1.5 H_Z, which are consistent with the oscillation frequencies associated with mechanical dynamics as obtained from the eigenvalue analysis shown in Table 5-2. Figure 5-4(c) and Figure 5-4(d) more precisely show both determinants in the above two ranges, respectively. It is observed from Fig. 5-4(c) that both the determinants of $K_{damp}(\Omega)$ and $K_{sm}(\Omega)$ are zero at about 0.01 H_Z. These results indicate that the system is close to experiencing low frequency (interarea) oscillation in the mode of 0.01 H_Z associated with mechanical dynamics. Compared with the eigenvalue analysis, this proposed approach clearly points out that there is only one low frequency oscillation mode at about 0.01 H_Z in the mechanical dynamics. Some other (asymptotically) stable modes in the same frequency range are also associated with the mechanical dynamics, Mode#9 (0.05 H_Z) and Mode#12 (0.007 H_Z)

Table 5-1 Dynamic Data of Synchronous Machines

Gen:	H	D	X_d	X_q	X_d'	T_{do}'
#1	4.00	1.00	1.79	1.70	0.30	5.70
#2	3.80	1.00	1.94	1.91	0.29	7.30
#3	3.00	0.00	1.72	1.66	0.24	7.10
Exciter:	K_A	T_A	K_{SE}	T_E	K_F	T_F
#1	19.0	0.12	1.00	0.65	0.05	2.00
#2	44.0	0.10	1.00	0.30	0.075	2.00
#3	270.0	1.20	0.00	0.00	0.00	0.00
Exciter:	T_B	T_C	K_D	T_D	R_C	X_C
#1	0.00	0.00	1.00	0.06	0.00	0.00
#2	0.00	0.00	1.00	0.00	0.00	0.00
#3	2.00	1.00	1.00	0.05	0.00	0.00
PSS:	K_S	T_S	T_{S1}	T_{S2}	T_{S3}	T_{S4}
#3	10.00	1.50	0.15	0.02	0.15	0.02

* Data is on machine base, and $R_a = 0$.
* Gen#1: 150.0 MVA; Gen#2: 150 MVA; Gen#3: 250 MVA.

Table 5-2 Eigenvalue Analysis for 9-bus System

Mode	Eigenvalue	Frequency	Major States*
1	$-0.0219 \pm j\ 0.0483$	0.0077	δ_1 , δ_2 , δ_3
3	$-0.0038 \pm j\ 3.9144$	0.6230	ω_1 , ω_2 , ω_3 , E'_{q3} , V_{A3} , PSS_3
5	$-0.1714 \pm j\ 7.6557$	1.2184	ω_1 , ω_2 , ω_3 , PSS_3
7	$-0.2631 \pm j\ 9.1871$	1.4622	ω_2 , δ_2 , ω_3 , δ_3 , PSS_3
9	$-0.3946 \pm j\ 0.3210$	0.0511	δ_1 , δ_2 , δ_3 , E'_{q2} , V_{F2}
11	-0.5206		E'_{q1} , V_{F1}
12	$-0.9983 \pm j\ 0.0448$	0.0071	E'_{q1} , V_{F1} , ω_3 , δ_3 , V_{B3} , PSS_3
14	$-1.2839 \pm j\ 1.2844$	0.2044	E'_{q1} , E_{FD1} , ω_3 , PSS_3
16	$-6.3489 \pm j\ 6.1678$	0.9816	V_{A2} , E_{FD2}
18	-8.4695		E'_{q1} , V_{D1} , V_{A1}
19	-16.429		V_{D1}
20	-20.539		V_{D3}
21	-44.405		PSS_3
22	-55.192		PSS_3

* due to high participating factor and high magnitude of eigenvector

Fig. 5-4(a) : Kdamp

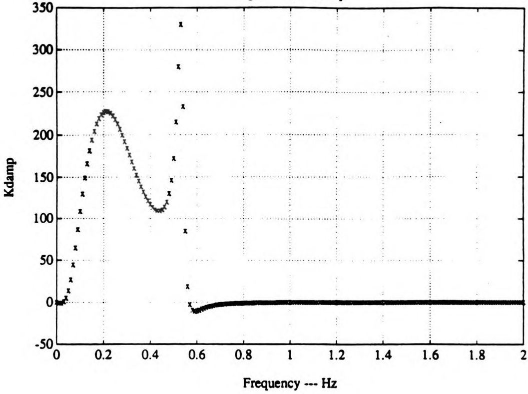

Fig. 5-4(b) : Ksm

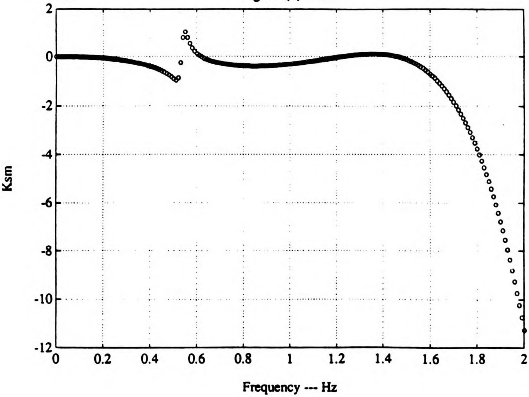

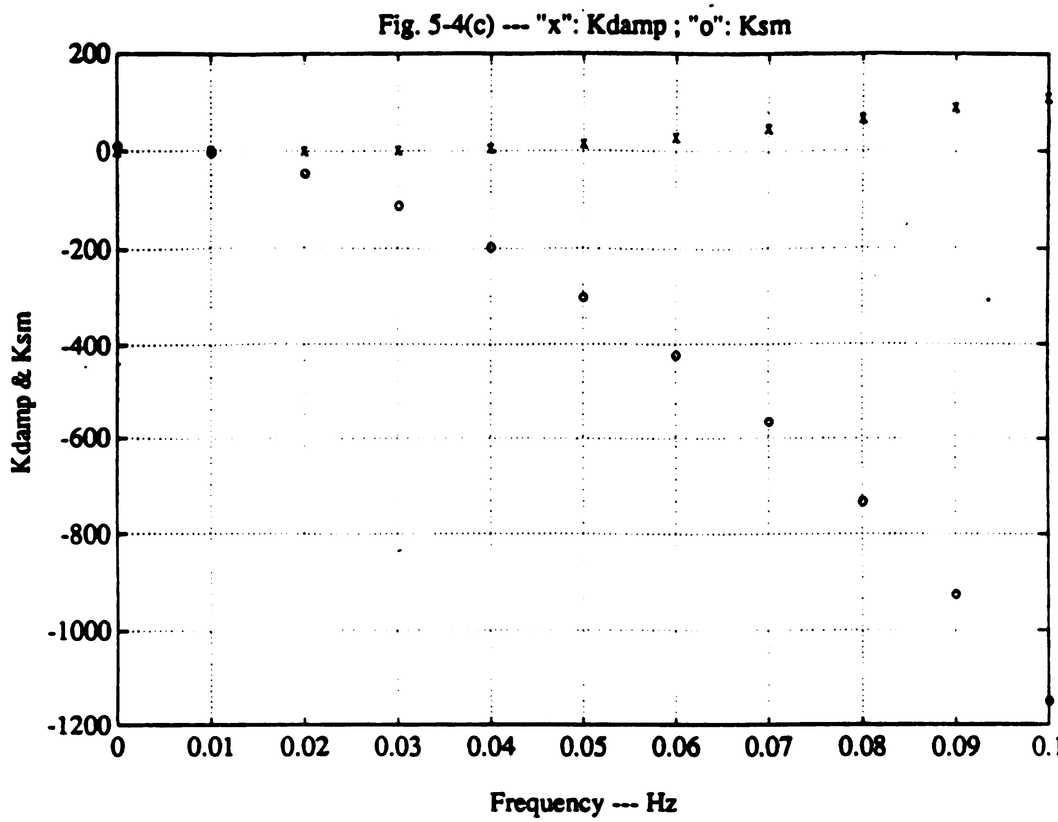

Fig. 5-4(c) --- "x": Kdamp ; "o": Ksm
200
0
-200
-400
-600
-800
-1000
-1200
0
0.01
0.02
0.03
0.04
0.05
0.06
0.07
0.08
0.09
0.1
Kdamp & Ksm
Frequency --- Hz

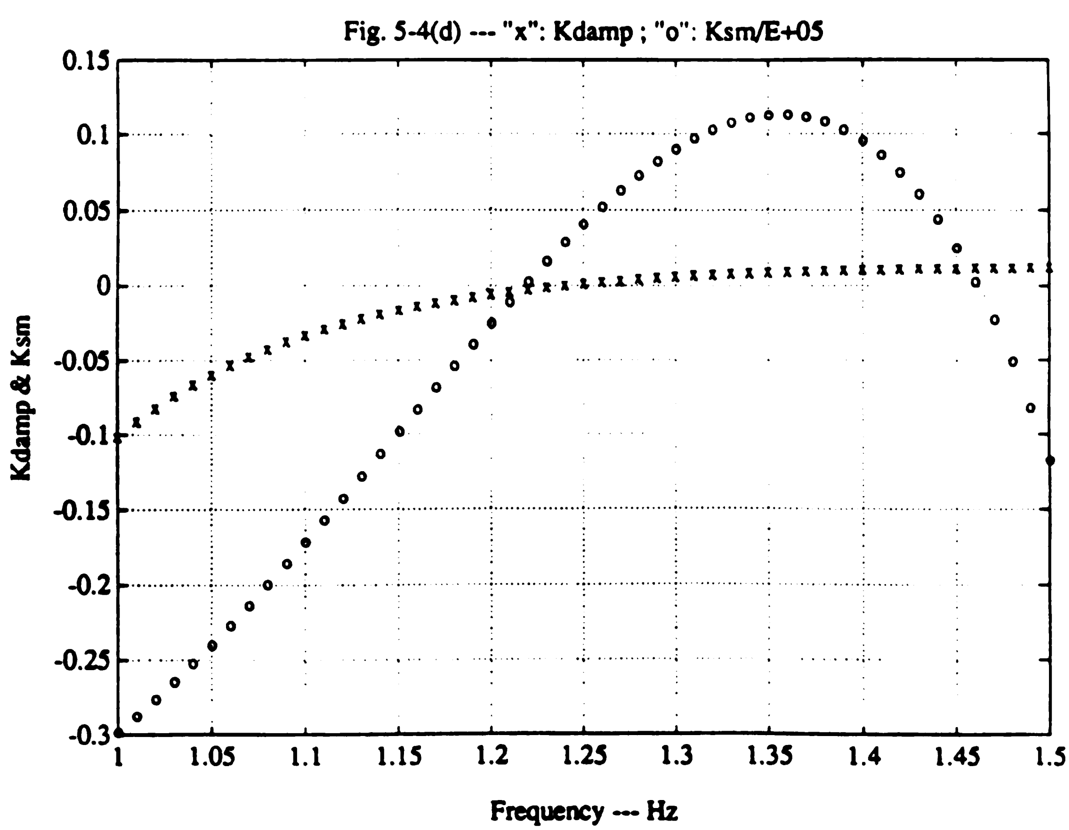

Fig. 5-4(d) --- "x": Kdamp ; "o": Ksm/E+05
0.15
0.1
0.05
0
-0.05
-0.1
-0.15
-0.2
-0.25
-0.3
1
1.05
1.1
1.15
1.2
1.25
1.3
1.35
1.4
1.45
1.5
Kdamp & Ksm
Frequency --- Hz

from the eigenvalue analysis results in Table 5.2. However, the determinants of $K_{damp}(\Omega)$ and $K_{sm}(\Omega)$ do not approach zero at these frequencies, since these modes are not close to or on the $j\Omega$ axis and thus not close to causing bifurcations. The eigenvalue analysis shows two other modes (Mode#5 and Mode#7) are associated with mechanical dynamics. From Fig. 5-4(d) ($K_{sm}(\Omega)$ is rescaled by 10^{-5}), these two modes at 1.22 H_Z and 1.46 H_Z have effects on the determinants of $K_{damp}(\Omega)$ and $K_{sm}(\Omega)$. Since these two modes are asymptotically stable modes, the determinants of $K_{damp}(\Omega)$ and $K_{sm}(\Omega)$ do not approach zero simultaneously. When one of the determinants is zero, the other is above or below zero, and the determinant of $K_{sm}(\Omega)$ is on the order of 10^5. Note that from the eigenvalue analysis, Mode#14 (0.20 H_Z) and Mode#16 (0.98 H_Z) are also asymptotically stable modes associated with flux decay dynamics. Note also that at these two frequencies, the determinants of $K_{damp}(\Omega)$ and $K_{sm}(\Omega)$ do not approach zero or even change significantly since they are not coupled to the mechanical dynamics.

It should be pointed out that from Fig. 5-4(a) and Fig. 5-4(b) both the determinants of $K_{damp}(\Omega)$ and $K_{sm}(\Omega)$ have sudden changes and have sign changes in the frequency range of $0.55 \rightarrow 0.62$ H_Z. This indicates that there exists one eigenvalue with small real part and with imaginary part whose frequency is in the the frequency range or close to these two boundary frequencies associated with mechanical dynamics and other dynamics or solely associated with other dynamics. From the eigenvalue analysis, Mode#3 (0.62 H_Z) is associated with mechanical, flux decay, and other (control systems) dynamics. This mode will be shown to be a mode close to dynamic/Hopf bifurcation (low frequency oscillation) mostly pertaining to flux decay dynamics in Fig. 5-5.

Figure 5-5(a) and Figure 5-5(b) respectively show the determinant of $T_{FDr}(\Omega)$ and that of $T_{FDx}(\Omega) = T_{FF} + T_{FDi}(\Omega)$. Both determinants are close to zero in the

Fig. 5-5(a) : Tfdx

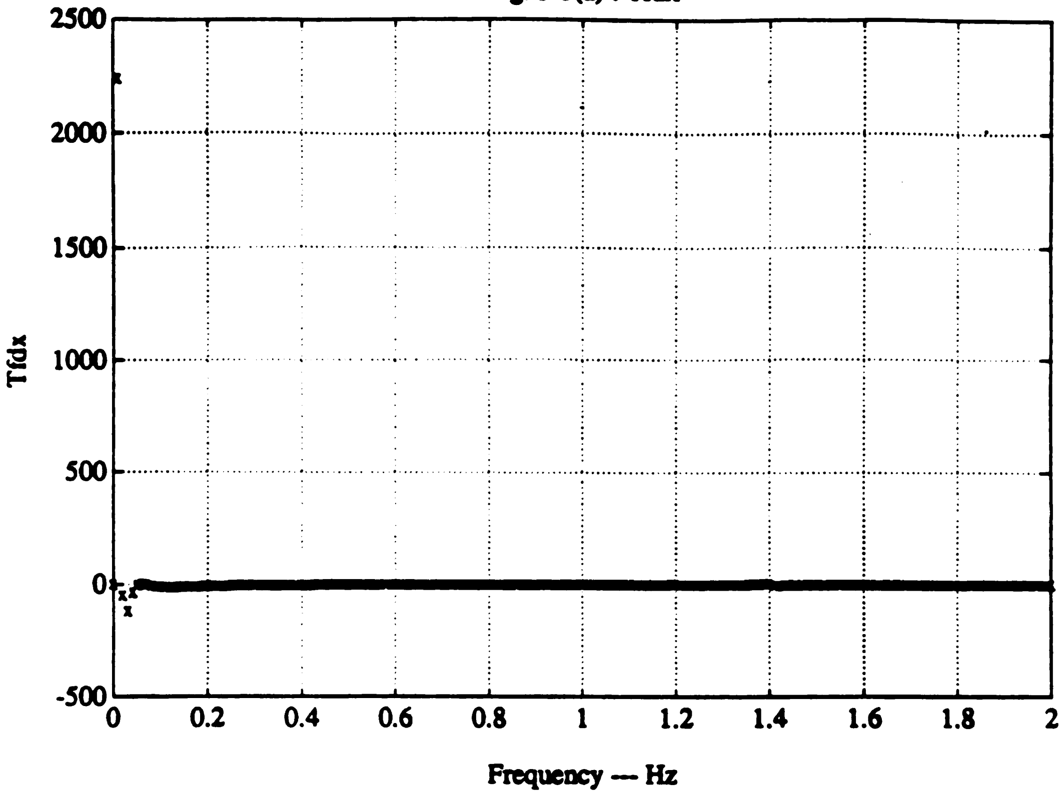

Fig. 5-5(b) : Tfdr

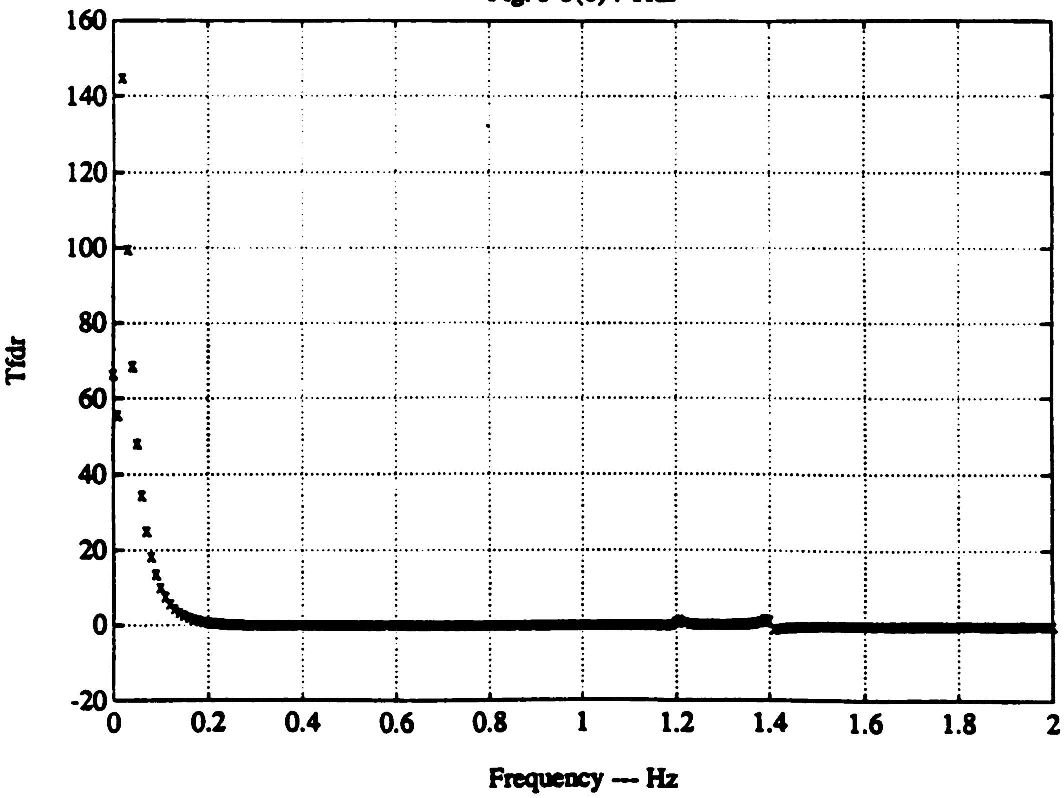

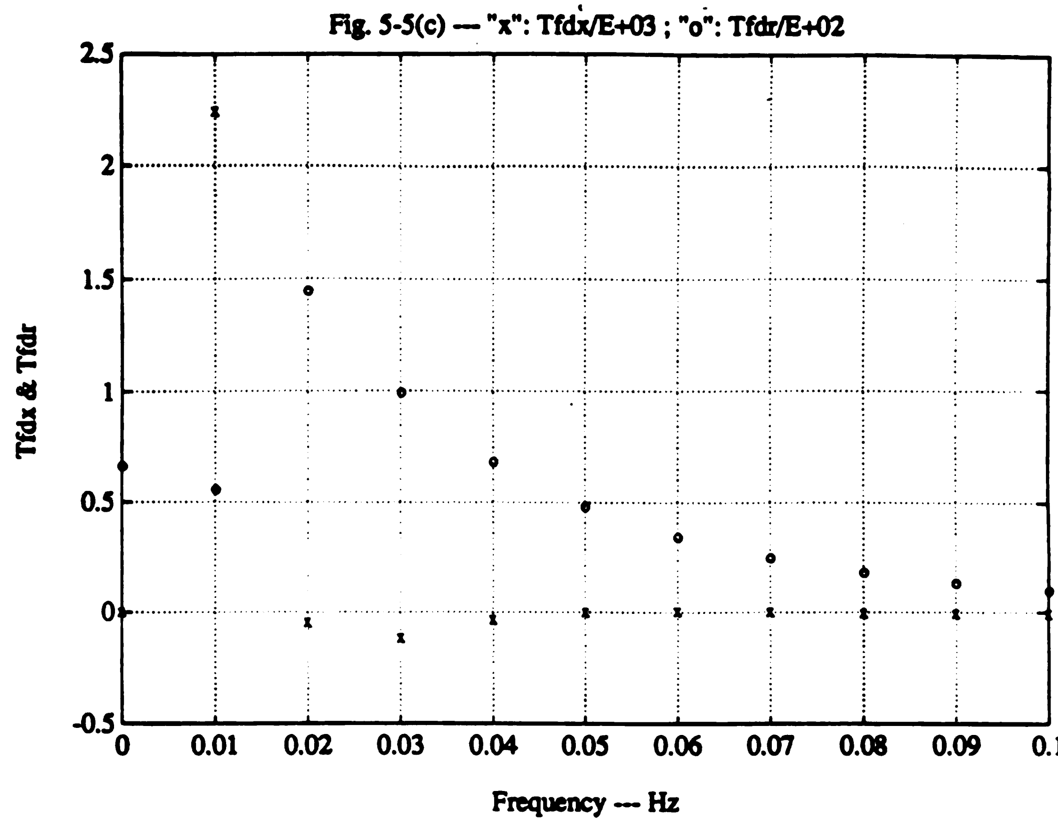
Fig. 5-5(c) --- "x": Tfdx/E+03 ; "o": Tfdr/E+02
Tfdx & Tfdr
Frequency --- Hz
2.5
2
1.5
1
0.5
0
-0.5
0
0.01
0.02
0.03
0.04
0.05
0.06
0.07
0.08
0.09
0.1

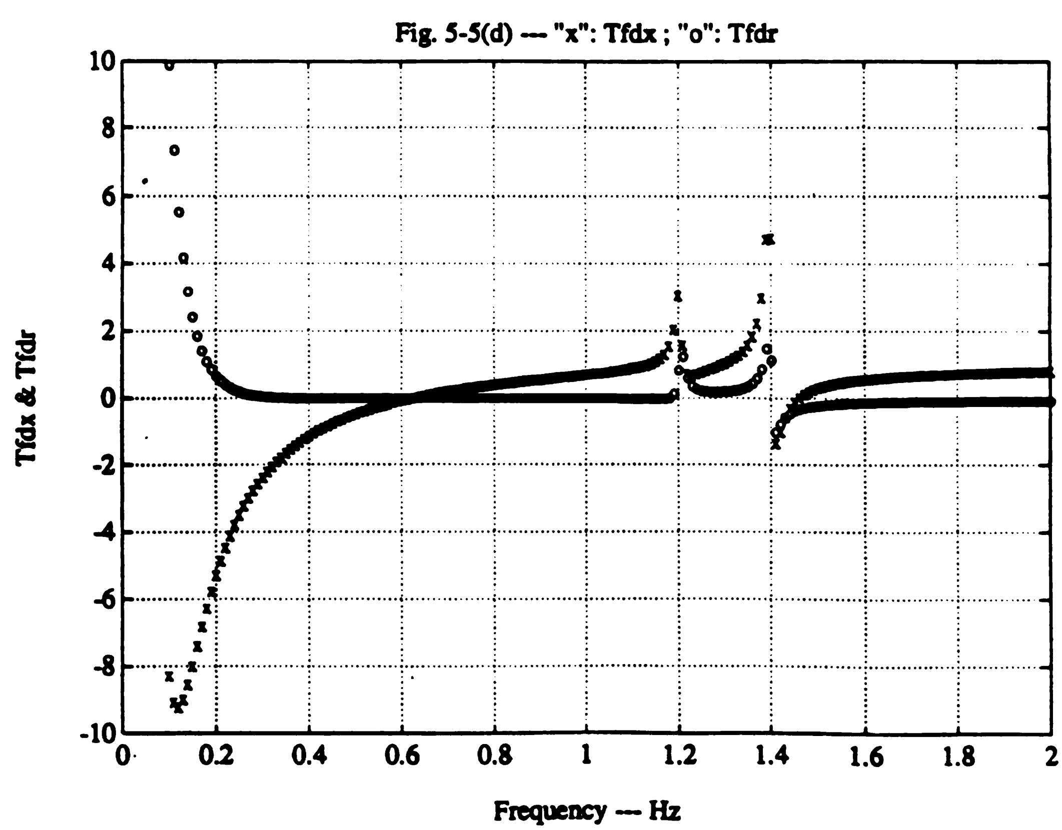
Fig. 5-5(d) --- "x": Tfdx ; "o": Tfdr
Tfdx & Tfdr
Frequency --- Hz
10
8
6
4
2
0
-2
-4
-6
-8
-10
0
0.2
0.4
0.6
0.8
1
1.2
1.4
1.6
1.8
2

frequency range 0.05 $\rightarrow$ 2.00 H_Z. Figure 5-5(c) and Figure 5-5(d) more precisely show how both determinants are approaching zero simultaneously. It is observed that there is a mode about 0.62 H_Z of a pair of complex eigenvalue with very small real part associated with the flux decay dynamics. This proposed approach precisely points out that the system experiences the 0.62 H_Z mode of low frequency oscillation, or is close to experiencing dynamic/Hopf bifurcation of flux decay dynamics at this frequency. The eigenvalue analysis indicates that this mode affects both mechanical and electrical states of the generator. But these proposed tests for the dynamic bifurcation of flux decay dynamics in Fig. 5-5(c) and Fig. 5-5(d), and the dynamic bifurcation of mechanical dynamics in Fig. 5-4(a) and Fig. 5-4(b) clearly identify this mode as being associated with the dynamic bifurcation of flux decay dynamics. These tests are thus more precise in establishing the cause of bifurcation mode than eigenvalue analysis.

It can be observed from the eigenvalue analysis that Mode#9 (0.05 H_Z) and Mode#12 (0.007 H_Z) are asymptotically stable modes associated with mechanical and flux decay dynamics. The tests for the flux decay dynamic bifurcation in Fig. 5-5(c) and the mechanical dynamic bifurcation in Fig. 5-4(c) show that these two modes are unrelated to the dynamic bifurcation in either mechanical dynamics or flux decay dynamics. Note also that two sudden changes shown in Fig. 5-5(d) at 1.20 H_Z and 1.40 H_Z reciprocally illustrate that there are two modes around these two frequency associated with other dynamics, which has been shown from Fig. 5-4 to be the asymptotically stable modes in terms of mechanical dynamics.

Chapter 6
Conclusion and Discussion

The principal contribution of this dissertation is the systematic categorization of the stability problems and the establishment of necessary test conditions for different types bifurcations leading to voltage collapse and low frequency oscillation in multimachine power systems, based on a differential-algebraic power system model. Bifurcations in a load flow model are also classified, since the load flow model is an approximation to the steady state behavior in the differential-algebraic model. Both the linearized load flow model and the linearized differential-algebraic power system model, and their Jacobian matrices are systematically and structurally formulated in this dissertation. This dissertation concludes that the generic types of bifurcation in the power system model can be

VAB: Voltage/Angle Bifurcation in a Load Flow Model,

SAB: Static/Algebraic Bifurcation in a Differential-Algebraic Model,

SDB: Static/Dynamic Bifurcation in a Differential-Algebraic Model.

This dissertation establishes a test condition for each kind of bifurcation identified above. Singularity of the full load flow Jacobian matrix J_{LF} is the generic form for the voltage/angle (load flow) bifurcation test. Singularity of the equivalent static/algebraic Jacobian matrix J_y is the generic form for the static/algebraic bifurcation test. The load flow Jacobian matrix J_{LF} is shown to be similar to the static/algebraic Jacobian matrix J_y, and to have similar bifurcation properties if the generator and excitation system model is replaced by the reactive power balance equation when the reactive power generation limit or the field current limit is reached.

The replacement of the generator and excitation system dynamics by the reactive power balance equation is an approximation to the insertion of the field current limit controller. If the field current limit controller is inserted into the model, then the static/algebraic Jacobian matrix J_y can experience static bifurcation in flux decay dynamics, in mechanical dynamics, and in flux decay and mechanical dynamics as can be observed from the results of Chapter 5. However, if the generator and excitation system dynamics is replaced by the reactive power balance equation to reflect the operator actions to hold the generator near its capability curve, then the static/algebraic bifurcation can only occur in mechanical dynamics. It is possible to conclude that bifurcations in the equivalent load flow model only approximate the static bifurcations in mechanical dynamics but not in flux decay dynamics or not in mechanical and flux decay dynamics. This equivalent load flow model certainly can not indicate the occurrence of the dynamic bifurcations.

Singularity of the reduced equivalent dynamic system Jacobian matrix $A_{XX}^{C}(j\Omega)$ solely associated with mechanical and flux decay dynamics at any $\Omega \geq 0$ is the generic form for the static/dynamic bifurcation test at that Ω. The static/algebraic bifurcation and the static bifurcation are equivalent to each other, and are generic types of singularity induced static bifurcation. Although loss of causality (singularity of g_y) and loss of stability of single machine dynamics (singularity of f_x) have not been proven to be non-generic stability problems, arguments have been made that suggest they be highly improbable.

A second contribution of this dissertation is the identification of three different static bifurcations and three different dynamic bifurcations. A static bifurcation can occur in mechanical dynamics, can occur in flux decay dynamics, and can occur in both mechanical and flux decay dynamics if they are "strongly" coupled. Specific test matrices for identification when these specific bifurcations have occurred are derived which may indicate why, where, and how each of these three static bifurcations occurs.

An equivalent test, singularity of the static/algebraic Jacobian matrix, for the static bifurcation is also established, that has similar structure to the load flow Jacobian matrix so that this test can be performed by slightly modifying the load flow program. A dynamic bifurcation can occur in mechanical dynamics, can occur in flux decay dynamics, and can occur in both mechanical and flux decay dynamics if they are "strongly" coupled. Specific test matrices for identification when these specific bifurcations have occurred are developed which may indicate why, where, and how each of these three dynamic bifurcations occurs. A static and a dynamic bifurcation can occur in both mechanical and flux decay dynamics. An algorithm for testing the static/dynamic bifurcation in mechanical and flux decay dynamics is proposed that allows one to classify bifurcations into dynamic or static and whether they affect mechanical, flux decay, or both mechanical and flux decay dynamics.

6.1 Main Contributions of This Dissertation

(A) Power System Model

Both the load flow model and the power system dynamic model are used and are systematically formulated in this dissertation. The load flow model describes the power system steady state operation condition of the transmission network. The load flow model is a set of algebraic equations composed of the active and reactive power balance equations of the transmission network excluding the reactive power balance equations at generator terminal PV-buses. The power system dynamic model is characterized by a set of differential-algebraic equations (or differential-algebraic model). The set of algebraic equations describes the active and reactive power balance equations of the transmission network including all generator terminal buses. The set of differential equations can include

(1) synchronous machine mechanical and flux decay dynamics, and

(2) control systems dynamics of machines:

  (a) excitation systems with load compensators,

  (b) power system stabilizers, and

  (c) speed-governing-turbine systems.

Power system stabilizers and speed-governing-turbine systems have not been used in any of the previous studies of bifurcations in a power system model. Furthermore, the excitation system model is often quite simple and the load compensator is omitted in most of the previous studies of bifurcations in a power system model.

Note that the load demand model adopted in this dissertation can be voltage dependent, including any combination of

(1) constant power load,

(2) constant impedance load,

(3) constant current load, and

(4) any other voltage dependent load.

This detailed modeling of load demand is necessary to study voltage collapse and low frequency oscillation.

In addition, the model of a general branch between two buses is also derived, which can be any combination of

(1) regular transmission line,

(2) transformer, and

(3) phase shifter.

The general branch model is used since tap changing transformers, phase shifters, and switchable shunt capacitors affect voltage collapse and low frequency oscillation. These devices have often been ignored in the studies of voltage collapse, low frequency oscillation, and bifurcations in power systems.

Both the linearized load flow model and the linearized power system model, and their Jacobian matrices are systematically and structurally formulated in this dissertation. The matrix form of the linearized power system model shows the structure of the Jacobian matrix and the Jacobian submatrices show the coupling between components of the power system. The properties of these Jacobian matrices are also clearly discussed and organized. This structural representation of power system Jacobian matrix provides valuable evidence for classifying the various bifurcation and stability problems, and establishing those generic bifurcations in the power system model:

(1) Voltage/Angle Bifurcation in a Load Flow Model,

(2) Static/Algebraic Bifurcation in a Differential-Algebraic Model,

(3) Static/Dynamic Bifurcation in a Differential-Algebraic Model.

It has also been shown that

(1) single-machine stability generally holds,

(2) control systems stability holds, and

(3) causality condition is generally maintained.

Having provided a brief summary of contributions above, a more complete set of contributions follows.

(B) Load Flow Bifurcation

The Load Flow Bifurcation occurs when the load flow Jacobian matrix J_{LF} is singular. The voltage, angle, and voltage/angle bifurcations have been shown to be the three types of bifurcations that could occur in a power system model. The voltage bifurcation and angle bifurcation are shown to be non-generic bifurcations which can only occur when a decoupled load flow model is used. The voltage bifurcation occurs when only the load flow Jacobian rows associated with the reactive power balance equations are row dependent and the load flow model is decoupled. The angle bifurcation occurs when only the load flow Jacobian rows associated with the active power balance equations are row dependent and the load flow model is decoupled. The angle bifurcation occurs due to the active power transfer limits across some boundary or interface. The voltage bifurcation occurs due to the reactive power transfer limits across some boundary or interface. Thus, the voltage/angle bifurcation, which occurs when the load flow Jacobian rows associated with the active and reactive power balance equations become row dependent, is due to both the active and reactive power transfer limits across some boundary or interface. This theoretical result corresponds with observation and with design and operating practice that constrains power transfer and loading, and constrains the lower reactive margin from a $Q-V$ curve that assures reactive power transfer capability. It is also shown that bifurcations can not occur due to the row dependence of the load flow Jacobian rows associated with the active and reactive power balance equations at a single bus. Hence, the analogies between the bifurcations in a two bus model to the bifurcations in a large power system load flow model have limited validity. Finally, it is shown that the bifurcations due to the row dependence of subsets of the load flow Jacobian rows are nongeneric bifurcations. This result indicates that bifurcations generally affect a very large region, if not the entire system, when under voltage relaying, load shedding, and control actions do not prevent the bifurcations from occurring or from spreading.

The simulation for the load flow bifurcation test is performed on a 9-bus 3-machine power system by applying the $Q-V$ curve point of voltage collapse method. The simulation results for the load flow bifurcation illustrate the important role of maintaining the reactive power generation reserves at PV-buses in preventing voltage collapse. Whenever a generator PV-bus exhausts its reactive power generation reserve and becomes a PQ-bus, the determinant of load flow Jacobian matrix decreases discontinuously toward zero and then load flow bifurcation occurs resulting in voltage collapse or loss of steady state stability. The more generators at which reactive power generation reserves are exhausted, the closer the system comes to experiencing the load flow bifurcation.

(C) Classification of Stability Problems in a Differential-Algebraic Model

Eight distinct types of stability problems are identified and necessary conditions for each of these stability problems are given based on the Jacobian matrix of the differential-algebraic power system model:

$$J = \begin{bmatrix} J_f \\ J_g \end{bmatrix} = \begin{bmatrix} f_x & f_y \\ g_x & g_y \end{bmatrix} \tag{6-1}$$

The differential, algebraic, and differential-algebraic bifurcations, that could occur due to the row dependence of J_f, of J_g, and of both J_f and J_g respectively, are shown to be non-generic bifurcations just as the bifurcations which occur due to the row dependence of subset rows of the load flow Jacobian matrix are non-generic. Loss of causality due to g_y being singular and loss of stability in the single machine dynamics due to f_x having eigenvalues with zero real parts are two special stability problems. Although these two stability problems and are not proven to be nongeneric, they are proven to be improbable when the generator controls are properly designed, the generators are properly operated within design limits, and the generator reactive power generation limits are included in the model. The remaining three generic bifurcations assuming that f_x and g_y are nonsingular are

(a) the static bifurcation which may occur when the equivalent system Jacobian matrix

$$J_x = f_x - f_y \, g_y^{-1} \, g_x \tag{6-1a}$$

is singular;

(b) the dynamic bifurcation which may occur when J_x has complex eigenvalues with zero real parts;

(c) the static/algebraic bifurcation which occurs when the equivalent static/algebraic Jacobian matrix

$$J_y = g_y - g_x f_x^{-1} f_y \qquad (6\text{-}1b)$$

is singular.

It is proven that a static bifurcation is identical to a static/algebraic bifurcation which indicates that J_x, J_y, and J are singular for this bifurcation where J_f and J_g are row independent, and f_x and g_y are nonsingular. This static or static/algebraic bifurcation is also called a singularity induced bifurcation, and results in voltage collapse and/or loss of steady state stability.

The prerequisite for the static/algebraic bifurcation is that the single-machine stability Jacobian matrix f_x is nonsingular in order to obtain the equivalent static/algebraic Jacobian matrix. The matrix f_x is shown to equivalently (1) model each synchronous machine as the single-axis model, (2) represent excitation systems as D.C. gains K_{EE}, and (3) neglect all the effects of machine damping constant D, speed-governing-turbine systems, and power system stabilizers. This prerequisite for f_x being nonsingular is argued to be true, since each synchronous machine should be designed to be operated in a stable manner below its steady state stability limit when its terminal bus is operated as the swing bus. The prerequisite for the static and dynamic bifurcations is that the transmission network Jacobian matrix g_y is nonsingular in order to obtain the equivalent system Jacobian matrix J_x. This prerequisite is also referred to as the causality condition of the differential-algebraic model, and is discussed in this dissertation. The transversality and nondegeneracy conditions for static/saddle-node and dynamic/Hopf bifurcations, controlling the nondegeneracy of the behavior with respect to the parameter change and the dominant effects of the nonlinear terms of power system dynamic model are not discussed in this dissertation. The system behavior when the system loses the causality condition is briefly discussed in this dissertation.

Testing the singularity of the static/algebraic Jacobian matrix J_y for identifying the singularity induced static bifurcation rather than testing the singularity of the equivalent system Jacobian matrix J_x is recommended since both tests are valid and should theoretically always become singular at the same point as long as f_x and g_y are nonsingular. This proposed static/algebraic bifurcation test matrix is proven to have similar structure to the causality matrix g_y, and is virtually identical to the load flow Jacobian matrix J_{LF}. A set of nonlinear equations is thus proposed with J_y that computes the equilibrium point of the power system differential-algebraic model. The equivalent load flow model would represent generators which have not reached reactive power generation limits by the steady state model of generators and excitation systems, and by the reactive power balance equations when reactive power generation limits are reached. This equivalent load flow model for the static/algebraic Jacobian matrix J_y would precisely determine when a static bifurcation occurs in the differential-algebraic power system model. Testing for a static bifurcation using J_y does not require inverting g_y which is required when J_x is used.

The load flow model for the load flow bifurcation test on J_{LF} and the equivalent load flow model for the static/algebraic bifurcation test on J_y are shown to be virtually identical for all rows of J_{LF} and J_y if the D.C. gains of the excitation systems are very high so that the generator terminal voltage can be kept constant, and if the flux decay equations are replaced by the reactive power balance equations at terminal buses for those generators exhausting reactive power generation reserves and being modeled as PQ-buses like in the load flow model. However, they would not be identical if the equivalent load flow model includes the effects of the generator flux decay dynamics, excitation system dynamics, and field current limit controller dynamics at steady state condition when the reactive power generation limits or field current limits are reached. The reason is that a static bifurcation in flux decay dynamics or in both flux decay dynamics and mechanical dynamics would be captured by the equivalent load flow model if steady state representation of flux decay dynamics, excitation system dynamics, and field current limit controller dynamics is used when field current limits are reached; but would not be captured in the load flow model or in the equivalent load flow model if the generator and excitation system dynamics is replaced by a reactive power balance equation (simply called the conventionally equivalent load flow model).

This result is quite important because it indicates that the conventionally equivalent load flow model can only capture one of the three generic static bifurcations (in mechanical dynamics, in flux decay dynamics, and in both) that occurs in mechanical dynamics [39,40,57,62]. The static bifurcations that occur in flux decay dynamics [52,53], and mechanical and flux decay dynamics are most likely to occur when field current limits are reached and the field current limit controller works through the excitation system to fix field current to the continuous rating value. A modified load flow model that properly reflects the steady state behavior of the generator flux decay dynamics, excitation system dynamics, and field current limit controller dynamics would accurately determine the equilibrium point(s) of the differential-algebraic model, and experience all of the static bifurcations of the differential-algebraic model.

The comparison of the static/algebraic Jacobian matrix J_y, the causality matrix g_y, and the load flow Jacobian matrix J_{LF}, carried out in this dissertation, is for the case where the flux decay dynamics and excitation system dynamics are replaced by the reactive power balance equations when the reactive power generation limits are reached. The use of the reactive power balance equations is justified based on the approximation of operation action to maintain the units close to their capability curves when the reactive power generation limits or field current limits are reached. The comparison carried of J_y, g_y, and J_{LF} is now reviewed.

It should be noted that all elements that are not associated with the generator terminal bus variables of the static/algebraic Jacobian matrix J_y and those of the causality matrix g_y are identical. The only difference between J_y and g_y are those diagonal matrices of $\partial P_T/\partial\theta_T$, $\partial P_T/\partial V_T$, $\partial Q_T/\partial\theta_T$, and $\partial Q_T/\partial V_T$. In g_y, the elements of these four diagonal matrices are composed of the elements in load flow model and the elements of the coupling between generator terminal buses and internal buses. In J_y, the elements of $\partial P_T/\partial\theta_T$, $\partial P_T/\partial V_T$, $\partial Q_T/\partial\theta_T$, are identical to those in load flow model. However, if the generators do not reach their reactive power generation limits, the elements of $\partial Q_T/\partial V_T$ include not only the elements of g_y, but also the elements proportional to the D.C. gains of the excitation systems; if the generators reach the limits, these elements become the same as those in load flow model. Hence, the diagonal elements of $\partial Q_T/V_T$ of J_y where generators have not reached their reactive power generation limits are much larger than the same elements of g_y which do not change whether generators reach the limits or not. When generators reach the limits, the diagonal elements of J_y, which are much larger than the same elements of g_y before the limits are reached, then become the same elements as those in load flow model which are smaller than those of g_y. Thus, in the region where reactive power generation limits are reached and the reactive power transfer limits are violated, the static/algebraic Jacobian matrix J_y is closer to singularity than the causality matrix g_y. This result indicates that loss of causality is not a likely cause of loss of stability compared to a static bifurcation which is tested by the singularity of J_y.

The values of these diagonal elements of $\partial Q_T/V_T$ of the static/algebraic Jacobian matrix J_y are very large when reactive power generation limits are not reached, that are the only different elements compared to the load flow Jacobian matrix J_{LF}. These diagonal elements (a) are very diagonally dominant compared to the rest elements of the rows associated with reactive power balance equations at generator terminal buses, causing the generator terminal voltage to remain constant when reactive power generation limits are not reached, and (b) are identical to the elements of J_{LF} when reactive power generation limits are reached. Thus, J_{LF} and J_y are virtually identical whether reactive power generation limits are reached or not reached at any bus.

The results of the classification of stability problems in the differential-algebraic power system model are important contributions because

(1) A static bifurcation was not known to be identical to a static/algebraic bifurcation.

(2) The occurrence of a static bifurcation can be determined using an equivalent load flow model rather than a transient mid-term stability model (differential-algebraic model).

(3) The bifurcation properties of the load flow model approximate the static bifurcation properties of the differential-algebraic model if generator terminal buses are modeled as PQ-buses when their reactive power generation limits are reached. The static bifurcation properties of solely mechanical dynamics would be captured using such a differential-algebraic model (or equivalent load flow model). The static bifurcation of flux decay dynamics could also be detected if the equivalent load flow model includes the effects of flux decay dynamics after the generator reactive power generation limits are reached.

(4) Loss of causality has been considered as an important type of loss of stability based on the results in [70]. The results derived in this dissertation also shows that loss of causality can occur before the static/algebraic bifurcation occurs if the generator reactive power generation limits are ignored in the model. Questions arose whether the network algebraic model is valid when loss of causality occurs and whether the algebraic model should be replaced by a partial differential equation model. The validity of the differential-algebraic model on the frontier where loss of causality occurs is uncertain, because the reality of the lumped model that includes the concept of reactive power may be invalid on the frontier. Significant

research effort is expected on replacing the differential-algebraic model by a differential-partial differential model either to confirm the validity of the differential-algebraic model on the frontier or to show that a differential-partial differential model is required if loss of causality is closely approached or occurs. However, the result that loss of causality is not probable if the reactive power generation limits are included, suggests that this effort at focusing on a differential-partial differential model may be of minimal value practically. If loss of causality can be shown to be non-generic, the investigation of bifurcations in a differential-partial differential model may be of limited value theoretically and practically.

(5) The differential bifurcation has been shown to be a non-generic class of power system stability problems, despite the fact that much of the study has been on a single machine to infinite bus model where the network equations are nonexistent. Such simple models can only have differential bifurcations which are the same as the single machine stability problems due to the singularity of f_x, being proven improbable in this dissertation.

(6) The algebraic bifurcation has been previously identified as a separate type of stability problem [9,10]. This dissertation has shown it to be nongeneric.

(7) The dynamic bifurcation is shown to be a second generic class of bifurcation problems, and be principally associated with the mechanical and flux decay dynamics, since the bifurcations in control systems are argued to be nongeneric.

The simulation for the static/algebraic bifurcation test on the same power system used to test for the load flow bifurcation shows similar results. This is expected since the D.C. gains of the excitation systems are enough high to keep the generator voltage almost constant as they are PV-buses in the load flow model until they exhausted reactive power generation reserves. In addition, these simulation results also point out that both loss of causality (g_y singular) and loss of single machine stability (f_x singular) are not likely to occur in a practical power system where the reactive power generation limits are taken into account.

(D) Classification of Static and Dynamic Bifurcations

The static/dynamic bifurcation is identified when the equivalent system Jacobian matrix J_x has eigenvalues with zero real parts. It could be the static/saddle-node bifurcation if J_x has a simple zero eigenvalue, and could be the dynamic/Hopf bifurcation if J_x has a pair of pure imaginary eigenvalues, provided that

(a) causality condition holds, and

(b) transversality/nondegeneracy condition holds.

The research has identified that there can be static or dynamic bifurcation associated with

(1) solely mechanical dynamics;

(2) solely flux decay dynamics;

(3) both mechanical and flux decay dynamics.

Test matrices are developed for identifying and preventing each of these bifurcations. The structure of these test matrices can indicate the causes of the bifurcations and the sensitivity of a particular type of bifurcation to various operating changes or control system design changes. These test matrices are derived using the procedure described below.

The Jacobian matrix of the control systems themselves A_{CC} is shown to have stable eigenvalues, meaning that the assumption:

(c) $A_{CC}(j\Omega)$ is nonsingular,

holds. Then the reduced Laplace transformed ($S = j\Omega$) model of J_x, $A_{XX}^S(j\Omega)$,

$$\begin{bmatrix} M\ j\Omega\ \Delta\omega \\ j\Omega\ \Delta\delta \\ T_{FF}\ j\Omega\ \Delta E_F \end{bmatrix} = A^S_{XX}(j\Omega) \begin{bmatrix} \Delta\omega \\ \Delta\delta \\ \Delta E_F \end{bmatrix} \tag{6-2}$$

$$A^S_{XX}(j\Omega) = \begin{bmatrix} -[\,D + D_G(j\Omega)\,] & -S_{P1} & -S_{P2} \\ I & 0 & 0 \\ -S_S(j\Omega) & -[\,S_4 + S_{E1}(j\Omega)\,] & -[\,S_3 + S_{E2}(j\Omega)\,] \end{bmatrix}$$

is produced that is composed of solely mechanical and flux decay dynamics, after the elimination of the control system dynamics since they are not singular for any $\Omega \geq 0$. The matrix $A^S_{XX}(j\Omega)$ provides the test of static/dynamic bifurcation if it is singular at some $\Omega \geq 0$: static if $\Omega = 0$, and dynamic if $\Omega > 0$. Note that this test matrix structurally shows the effects of network and control systems:

network: S_{P1}, S_{P2}, S_3, and S_4;

control: D_G, S_S, S_{E1}, and S_{E2};

D_G: effects of speed-governing system

S_S: effects of power system stabilizer

S_{E1}: effects of excitation system on $\Delta\delta$

S_{E2}: effects of excitation system on ΔE_F

where, S_{E1} and S_{E2} include the effects of load compensator, S_{C1} and S_{C2} respectively. These six sensitivity matrices: S_{P1}, S_{P2}, S_3, S_4, S_{C1} and S_{C2}, are consistent with those K constants of the single-machine power system without load compensator: $S_{P1} = K_1$, $S_{P2} = K_2$, $S_3 = K_3$, $S_4 = K_4$, $S_{C1} = K_5$, $S_{C2} = K_6$.

Damping and synchronizing power coefficient matrices, $K_{damp}(\Omega)$ and $K_{sync}(\Omega)$, associated with the mechanical dynamics are further derived, under the assumption:

(d) $S_3(j\Omega) = S_3 + S_{E2r}(\Omega) + j\Omega\,[\,T_{FF} + S_{E2i}(\Omega)\,]$ is nonsingular.

Then test condition on these matrices for identification and prevention of bifurcations of the mechanical dynamics are established. Similarly, flux decay matrices, $T_{FDr}(\Omega)$

and $T_{FDi}(\Omega)$, are derived, and test matrices for identification and prevention of flux decay bifurcation are also generated from the reduced model, under the assumption:

(e) $S_M(j\Omega) = S_{P1} - \Omega^2 [M + D_{Gi}(\Omega)] + j\Omega [D + D_{Gr}(\Omega)]$ is nonsingular.

Figure 6-1 shows the flow chart of static and dynamics bifurcation tests on mechanical and flux decay dynamics. When the above assumptions (a)-(c) hold, the reduced model pertaining to mechanical and flux decay states, $A_{XX}^S(j\Omega)$, is obtained by eliminating the network variables and control systems states. Then damping $K_{damp}(\Omega)$ and synchronizing $K_{sync}(\Omega)$ power coefficient matrices of mechanical dynamics, and flux decay matrices $T_{FDr}(\Omega)$ and $T_{FDi}(\Omega)$ are derived when further assumption (d) and (e) hold respectively. Based on these matrices, necessary test conditions for static/dynamic bifurcations associated with mechanical dynamics and flux decay dynamics are initiated as shown in Fig. 6-1.

Option 0: mechanical and flux decay dynamics

(a) for static bifurcation: $\Omega = 0$,

$A_{XX}^S(\Omega = 0)$ is singular;

(b) for dynamic bifurcation: $\Omega > 0$,

$A_{XX}^S(j\Omega)$ is singular.

Option 1: mechanical dynamics

(a) for static bifurcation: $\Omega = 0$,

$K_{sync}(\Omega = 0)$ is singular;

(b) for dynamic bifurcation: $\Omega > 0$,

both $K_{damp}(\Omega)$ and $K_{sm}(\Omega) = K_{sync}(\Omega) - \Omega^2 M$ are singular.

Option 2: flux decay dynamics

(a) for static bifurcation: $\Omega = 0$,

$T_{FDr}(\Omega = 0)$ is singular;

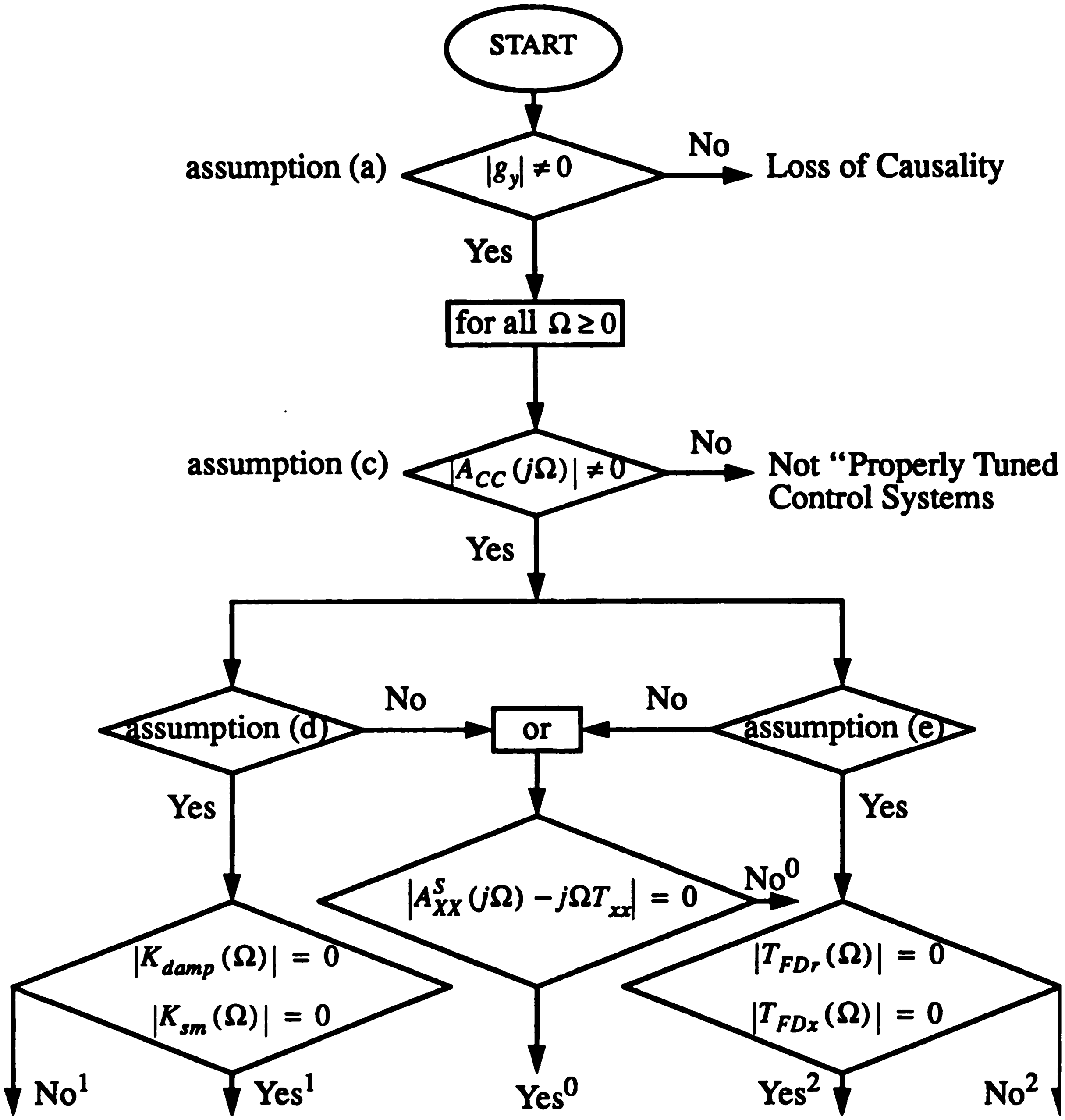

0 : Bifurcation of Mechanical and Flux Decay Dynamics
1 : Bifurcation of Mechanical Dynamics
2 : Bifurcation of Flux Decay Dynamics
Yes : assumption (b) for Transversality/Nondegeneracy Condition

Fig. 6-1 Flow Chart of Bifurcation Tests for Mechanical and Flux Decay Dynamics

(b) for dynamic bifurcation: $\Omega > 0$,

both $T_{FDr}(\Omega)$ and $T_{FDx}(\Omega) = T'_{do} + T_{FDi}(\Omega)$ are singular.

It should be noted that the flow chart shown in Fig. 6-1 provides a static/dynamic point of collapse/oscillation method [53] that would test for the closest bifurcation as the system operation condition is continually changed in a manner that could cause one or more of the bifurcation or stability problems to occur. The point of collapse/oscillation method would be similar to computing a $Q-V$ curve by adding reactive load at buses until bifurcation occurs, or a $P-V$ curve where active power transfer or active power load level is increased at some pattern buses until bifurcation occurs. This approach indicates the stress level in reactive power load, active power transfer, or active power load at some pattern buses that brings about the closest bifurcation in that subregion of the network. This method also indicates that the bifurcation is static and/or dynamic, and points out that the bifurcation is associated with mechanical dynamics and/or flux decay dynamics. The test condition matrices structurally show the effects of operation conditions and control systems as well. Analysis of the components of these test matrices should help understand the factors causing bifurcations and help design controls and change operating limits to prevent bifurcations. This approach avoids the computational burden of all eigenvalues of the equivalent system Jacobian matrix J_x, provided that causality holds.

The simulation for the static/dynamic bifurcation tests associated with mechanical and flux decay dynamics is performed on the same power system where load flow bifurcation was tested but with dynamic data of the synchronous machines and control systems provided from [4]. At some operation condition, the system is in the proximity to experiencing dynamic bifurcation leading to low frequency oscillation in both mechanical dynamics and flux decay dynamics. The proposed approach clearly identifies the mode mainly associated with mechanical dynamics, and the mode principally pertaining to flux decay dynamics without having to perform any eigenvalue analysis. The eigenvalue analysis is shown to have difficulty identifying whether a bifurcation is possibly occurring in mechanical or in flux decay dynamics.

6.2 Relationship to Literature

Regarding the studies of voltage collapse, the point of voltage collapse method is a very popular approach to establishing a bifurcation point based on the load flow model by increasing active or reactive load or transfer at a pattern of bus or branch in order to understand the margin in terms of the additional load or transfer that can be added at the bus or branch pattern before loss of voltage stability will occur [53]. The point of voltage collapse method is usually referred to the $V-P$, $V-Q$, or $Q-V$ curve approach, or to the sensitivity matrix approach [48-59], or to the optimization approach [60,61]. This dissertation derived the generic load flow bifurcation that has not been pointed out in the literature.

In the power system differential-algebraic model, the voltage collapse problem has been investigated by applying the theory of bifurcation on the complete system Jacobian matrix [39-45,52,53,64-79]. The research was generally confined to a simple power system where excitation systems were simplified or neglected, and speed-governing-turbine systems and power system stabilizers were omitted. Under the assumption that the causality condition holds, the static bifurcation leading to loss of steady-state stability and/or voltage collapse has been studied based on testing the singularity of the equivalent system Jacobian matrix [39-41,45,52,53,64-67,69,70,73,78,79], where transversality/nondegeneracy condition for the static/saddle-node bifurcation was not discussed. A test matrix for the static bifurcation solely associated with flux decay dynamics has been derived and defined as flux decay bifurcation [52,53] for a power system without both power system stabilizers and speed-governing-turbine systems, provided that the causality condition holds. If this flux decay bifurcation test matrix is approaching singularity, experimental results show that the system is at the proximity to voltage collapse, especially when field current limits are reached and then the normal excitation controls are disabled [52,53].

In this dissertation, static voltage stability is investigated based on the two different representations of the power system: (a) algebraic load flow model, and (b) differential-algebraic power system dynamic model. The load flow bifurcation due to the singularity of the load flow Jacobian matrix is studied from the viewpoint of the point of voltage collapse method for the load flow model. The load flow Jacobian matrix is also proven to be the generic test matrix for load flow bifurcation. In the power system dynamic model, the equivalent static/algebraic Jacobian matrix is developed, and is also shown to be the generic test matrix for the singularity induced static bifurcation due to the singularity of this test matrix. The static/algebraic bifurcation test is equivalent to the static bifurcation test due to the singularity of the equivalent system Jacobian matrix. However, testing the singularity of the static/algebraic Jacobian matrix for the singularity induced static bifurcation, rather than testing the equivalent system Jacobian matrix, avoids the inverse of the causality matrix. Moreover, this test matrix preserves the form of the linearized load flow model so that this static/algebraic bifurcation test can be performed by slightly modifying the load flow program.

This dissertation further develops test matrix for the static bifurcation associated with mechanical dynamics and flux decay dynamics, after proving that the control systems themselves have asymptotically stable eigenvalues. The static flux decay bifurcation test matrix is consistent with the one proposed in [52,53].

In the studies of dynamic stability, especially for low frequency oscillation, both bifurcation theory and eigenvalue analysis have been applied. A dynamic/Hopf bifurcation can occur when the power system is at the operating condition such that the equivalent system Jacobian matrix has a pair of pure imaginary eigenvalues, provided that causality and transversality/nondegeneracy conditions hold. Hopf bifurcation of flux decay dynamics has been shown to occur when mechanical dynamics are ignored [42,68]. Low frequency oscillation has experimentally been shown to be associated with mechanical and flux decay dynamics [3,4,21], mainly due to lack of damping and synchronizing power [22-30].

This dissertation establishes more precise test conditions for the static/dynamic bifurcation pertaining to mechanical and flux decay dynamics by proving that the control systems themselves have stable eigenvalues. Moreover, damping and synchronizing power coefficient matrices are derived, and test conditions based on these two matrices are established for the static and dynamic bifurcation in mechanical dynamics. Flux decay test matrices are also defined for the static and dynamic bifurcation in flux decay dynamics. This approach not only precisely identifies the modes principally associated with mechanical dynamics and flux decay dynamics, but also does not involved in the computationally intensive eigenvalue analysis.

6.3 Future Work

Although a classification of the types of stability problems has been developed and generic stability problems have been identified, much additional work is necessary. The generic static and dynamic bifurcations have been studied solely for identifying and preventing generic static/saddle-node and dynamic/Hopf bifurcations in power system models. Research is needed to more thoroughly describe the center manifold and the behavior of the system dynamics and the network response near the bifurcation point. Loss of stability in single machine dynamics and loss of causality have been argued to be improbable. Research on these two special stability problems is also needed to show whether they are generic or not. If loss of causality is a generic stability problem, more effort must be put on the study of the validity of the differential-algebraic power system model. The validity of the differential algebraic model on the frontier, where loss of causality occurs, can be assessed by using a differential-partial differential model. If the differential-algebraic model is invalid on the frontier, it may also be invalid as one approaches the frontier. A differential-partial differential model would be used rather than a differential-algebraic model wherever the differential-algebraic model proves invalid.

Although some understanding of these stability problems exists for the single machine to infinite bus model, little understanding exists for the multimachine power system stability model. Moreover, no methods exists for establishing where, why, and when certain stability problems occur. The test matrices proposed in this dissertation for the generic stability problems structurally show the effects of the transmission network and control systems, that may be useful in understanding the causes of the stability problems. Methods for preventing and correcting the various stability problems should be undertaken once the above understanding is comprehensive. The computer program for the point of collapse/oscillation method also needs to be developed.

Regarding the parameters of the control systems, it should be noted that only the D.C. gain of excitation system affects the necessary condition of the static bifurcation; but each control system has the effect on the necessary condition of the dynamic bifurcation. It can be concluded that the proper tuning of each parameter of each control system, especially the excitation system, is also another main concern of power system planning. Moreover, the particular parameters of control systems that have major effects on the damping margin before the power system experiences static/dynamic bifurcation should be identified, and their relationship should also be established. Some particular parameters of major control systems are expected to be the D.C. gain of the excitation system, the gain and time constant of the stabilizing feedback of the excitation system, and the lead-lag time constants of the power system stabilizer.

Based on the simulation results shown in this dissertation and the experimental results from previous research [48-53], the reactive power generation reserve of the power system plays a very important role in the studies of voltage collapse and low frequency oscillation. Sufficient and properly placed reactive power supply in the system should be carefully studied to prevent the generic bifurcations identified in this dissertation.

APPENDICES

Appendix A
Schur's Formula and Inverse Matrix

Consider an $(m+n)$-dimensional square matrix A which can be partitioned as follows:

$$A = \begin{bmatrix} A_{11} & A_{12} \\ A_{21} & A_{22} \end{bmatrix} \tag{A-1a}$$

where, A_{11} is an $m \ x \ m$-dimensional square matrix; A_{12} is an $m \ x \ n$-dimensional matrix; A_{21} is an $n \ x \ m$-dimensional matrix; and A_{22} is an $n \ x \ n$-dimensional square matrix.

If the matrix A is nonsingular, its inverse, A^{-1}, has the following form:

$$A^{-1} = \begin{bmatrix} B_{11} & B_{12} \\ B_{21} & B_{22} \end{bmatrix} = B \tag{A-1b}$$

satisfying

$$A \ B = B \ A = \begin{bmatrix} I_m & 0 \\ 0 & I_n \end{bmatrix} \tag{A-1c}$$

where, each B-submatrix has the same dimension as A-submatrix with the same subscript; I_m and I_n are the m- and n-dimensional identity matrices, respectively; and 0 is the zero matrix with appropriate dimension.

(1) If A_{11} is nonsingular, the determinant of the matrix A, ($Det[\ A\ ]$), can be written as

$$Det[\ A\ ] = Det[\ A_{11}\ ] \cdot Det[\ A_{22} - A_{21}\, A_{11}^{-1}\, A_{12}\ ] \tag{A-2}$$

Then the submatrices of B, the inverse of A, can be represented as

$$B_{22} = [\, A_{22} - A_{21} A_{11}^{-1} A_{12} \,]^{-1} \tag{A-2a}$$

$$B_{21} = -\, B_{22} A_{21} A_{11}^{-1} \tag{A-2b}$$

$$B_{12} = -\, A_{11}^{-1} A_{12} B_{22} \tag{A-2c}$$

$$B_{11} = A_{11}^{-1} [\, I_m - A_{12} B_{21} \,] \tag{A-2d}$$

(2) If A_{22} is nonsingular, then

$$Det[\, A \,] = Det[\, A_{22} \,] \cdot Det[\, A_{11} - A_{12} A_{22}^{-1} A_{21} \,] \tag{A-3}$$

and

$$B_{11} = [\, A_{11} - A_{12} A_{22}^{-1} A_{21} \,]^{-1} \tag{A-3a}$$

$$B_{12} = -\, B_{11} A_{12} A_{22}^{-1} \tag{A-3b}$$

$$B_{21} = -\, A_{22}^{-1} A_{21} B_{11} \tag{A-3c}$$

$$B_{22} = A_{22}^{-1} [\, I_n - A_{21} B_{12} \,] \tag{A-3d}$$

(3) If both A_{11} and A_{22} are nonsingular, then both case (1) and case (2) are valid, and the B-submatrices with the same subscripts are equal to each other.

Appendix B

A_{CC}^{-1}

Rewrite the matrix A_{CC} (4-8c), which is formed by the control systems of the synchronous machines, as follows:

$$A_{CC} = \begin{bmatrix} A_{EE} & 0 & A_{ES} \\ 0 & A_{GG} & 0 \\ 0 & 0 & A_{SS} \end{bmatrix} \tag{B-1}$$

where, A_{EE} represents the block matrix of the excitation systems; A_{GG} represents the block matrix of the speed-governing-turbine systems; A_{SS} represents the block matrix of the power system stabilizers; and A_{ES} represents the block matrix of the PSS controls through the excitation systems. The complete forms of these control systems matrices are rewritten from (4-2) with some short notations for the excitation systems and power system stabilizers:

$$T_{BC} = T_B^{-1} T_C \;\; ; \;\; I_{BC} = I - T_{BC}$$

$$T_{21} = T_{S2}^{-1} T_{S1} \;\; ; \;\; I_{21} = I - T_{21}$$

$$T_{43} = T_{S4}^{-1} T_{S3} \;\; ; \;\; I_{43} = I - T_{43}$$

$$A_{EE} = \begin{bmatrix} -I & 0 & 0 & 0 & 0 \\ 0 & -I & 0 & 0 & -T_F^{-1} K_F \\ -K_A T_{BC} & -K_A T_{BC} & -I & K_A & -K_A T_{BC} T_F^{-1} K_F \\ -I_{BC} & -I_{BC} & 0 & -I & -I_{BC} T_F^{-1} K_F \\ 0 & 0 & I & 0 & -K_{SE} \end{bmatrix} \tag{B-1a}$$

$$A_{GG} = \begin{bmatrix} -I & 0 & 0 & 0 & 0 & 0 \\ -I & -I & 0 & 0 & 0 & 0 \\ 0 & I & -I & 0 & 0 & 0 \\ 0 & 0 & I & -I & 0 & 0 \\ 0 & 0 & 0 & I & -I & 0 \\ 0 & 0 & 0 & 0 & I & -I \end{bmatrix} \tag{B-1b}$$

$$A_{SS} = \begin{bmatrix} -I & 0 & 0 \\ I_{21} & -I & 0 \\ I_{43}T_{21} & I_{43} & -I \end{bmatrix} \tag{B-1c}$$

$$A_{ES} = \begin{bmatrix} 0 & 0 & 0 \\ 0 & 0 & 0 \\ K_A T_{BC} T_{43} T_{21} & K_A T_{BC} T_{43} & K_A T_{BC} \\ I_{BC} T_{43} T_{21} & I_{BC} T_{43} & I_{BC} \\ 0 & 0 & 0 \end{bmatrix} \tag{B-1d}$$

Note that the submatrices of each control system block matrix are all diagonal.

The matrix A_{CC} (B-1) is an upper-triangular matrix, and has been proven to be nonsingular based on the nonsingularity of individual control system. Thus, its inverse, A_{CC}^{-1}, can be represented as follows:

$$A_{CC}^{-1} = \begin{bmatrix} A_{EE}^{-1} & 0 & -A_{EE}^{-1} A_{ES} A_{SS}^{-1} \\ 0 & A_{GG}^{-1} & 0 \\ 0 & 0 & A_{SS}^{-1} \end{bmatrix} \tag{B-2}$$

Since A_{GG} and A_{SS} are lower-triangular matrices, we have

$$A_{GG}^{-1} = \begin{bmatrix} -I & 0 & 0 & 0 & 0 & 0 \\ I & -I & 0 & 0 & 0 & 0 \\ I & -I & -I & 0 & 0 & 0 \\ I & -I & -I & -I & 0 & 0 \\ I & -I & -I & -I & -I & 0 \\ I & -I & -I & -I & -I & -I \end{bmatrix} \tag{B-3}$$

$$A_{SS}^{-1} = \begin{bmatrix} -I & 0 & 0 \\ -I_{21} & -I & 0 \\ -I_{43} & -I_{43} & -I \end{bmatrix} \tag{B-4}$$

Regarding A_{EE}^{-1}, one can apply the Schur's formula shown in Appendix A. Based on the structure of A_{EE} (B-1a), A_{EE} can be partitioned and has its inverse as follows:

$$A_{EE} = \begin{bmatrix} E_{11} & E_{12} \\ E_{21} & E_{22} \end{bmatrix} \tag{B-5a}$$

$$A_{EE}^{-1} = \begin{bmatrix} F_{11} & F_{12} \\ F_{21} & F_{22} \end{bmatrix} \tag{B-5b}$$

where,

$$E_{11} = \begin{bmatrix} -I & 0 & 0 \\ 0 & -I & 0 \\ -K_A\,T_{BC} & -K_A\,T_{BC} & -I \end{bmatrix} \; ; \; E_{12} = \begin{bmatrix} 0 & 0 \\ 0 & -T_F^{-1}\,K_F \\ K_A & -K_A\,T_{BC}\,T_F^{-1}\,K_F \end{bmatrix}$$

$$E_{21} = \begin{bmatrix} -I_{BC} & -I_{BC} & 0 \\ 0 & 0 & I \end{bmatrix} \; ; \; E_{22} = \begin{bmatrix} -I & -I_{BC}\,T_F^{-1}\,K_F \\ 0 & -K_{SE} \end{bmatrix}$$

$$F_{11} = [\,E_{11} - E_{12}\,E_{22}^{-1}\,E_{21}\,]^{-1}$$

$$F_{12} = -F_{11}\,E_{12}\,E_{22}^{-1}$$

$$F_{22} = [\,E_{22} - E_{21}\,E_{11}^{-1}\,E_{12}\,]^{-1}$$

$$F_{21} = -F_{22}\,E_{21}\,E_{11}^{-1}$$

Note that the main diagonal block submatrices, E_{11} and E_{22}, in the above partition are all nonsingular, since E_{11} is lower-triangular; E_{22} is upper-triangular; and both have nonzero diagonal elements. Moreover, the matrix manipulations, $\{E_{12}\,E_{22}^{-1}\,E_{21}\}$ of F_{11} and $\{E_{21}\,E_{11}^{-1}\,E_{12}\}$ of F_{22}, respectively keep the same structure as E_{11} and E_{22}. Thus, after applying the Schur's formula and performing the matrix manipulations, one can obtained the final form of A_{EE}^{-1}:

$$A_{EE}^{-1} = \begin{bmatrix} -I & 0 & 0 & 0 & 0 \\ -T_{FE}\,K_A & -I + T_{FE}\,K_A & T_{FE} & T_{FE}\,K_A & T_{FE} \\ K_A & K_A & -I & -K_A & 0 \\ I_{BC} & I_{BC} & 0 & -I & 0 \\ K_{SE}^{-1}\,K_A & -K_{SE}^{-1}\,K_A & -K_{SE}^{-1} & -K_{SE}^{-1}\,K_A & -K_{SE}^{-1} \end{bmatrix} \qquad \text{(B-5c)}$$

where

$$T_{FE} = T_F^{-1}\,K_F\,K_{SE}^{-1}$$

Having the main diagonal block matrices of A_{CC}^{-1} (B-2), one can obtain the only one off-diagonal matrix of A_{CC}^{-1} by substituting (B-1d), (B-4), and (B-5c) as follows:

$$A_{ES}\,A_{SS}^{-1} = \begin{bmatrix} 0 & 0 & 0 \\ 0 & 0 & 0 \\ -K_A\,T_{BC} & -K_A\,T_{BC} & -K_A\,T_{BC} \\ -I_{BC} & -I_{BC} & -I_{BC} \\ 0 & 0 & 0 \end{bmatrix} \qquad \text{(B-6a)}$$

$$A_{EE}^{-1}\,A_{ES}\,A_{SS}^{-1} = \begin{bmatrix} 0 & 0 & 0 \\ -T_{FE}\,K_A & -T_{FE}\,K_A & -T_{FE}\,K_A \\ K_A & K_A & K_A \\ I_{BC} & I_{BC} & I_{BC} \\ K_{SE}^{-1}\,K_A & K_{SE}^{-1}\,K_A & K_{SE}^{-1}\,K_A \end{bmatrix} \qquad \text{(B-6b)}$$

Appendix C

$K\mathcal{P}_1^t$ and K_{FD}

This Appendix will show that the diagonal matrix $K\mathcal{P}_1^t$, representing the coefficient of the active power generation at the internal bus with respect to the rotor angle, is in general positive definite if each synchronous machine is operated in the condition of lagging power factor. Then the diagonal matrix K_{FD}, representing the steady state operation condition of each synchronous machine, should also be positive definite, when it is assumed that the load compensators are not used in the power system model.

Rewrite the matrix $K\mathcal{P}_1^t$ from (2-41):

$$K\mathcal{P}_1^t = E_q^{'} \, V_t \, U_{PE} + V_t^2 \, (X_q - X_d^{'}) \, (T_{dt} \, T_{qt} - U_{dt} \, U_{qt}) \tag{C-1}$$

where,

$$U_{PE} = k_1 \, U_{dt} - G_a \, (X_q - X_d^{'}) \, T_{qt} \quad ; \quad k_1 = 1 - (X_q - X_d^{'}) \, B_q$$

$$T_{dt} = G_a \, \cos(\delta - \theta_t) + B_d^{'} \, \sin(\delta - \theta_t)$$

$$U_{dt} = G_a \, \sin(\delta - \theta_t) - B_d^{'} \, \cos(\delta - \theta_t)$$

$$T_{qt} = G_a \, \cos(\delta - \theta_t) + B_q \, \sin(\delta - \theta_t)$$

$$U_{qt} = G_a \, \sin(\delta - \theta_t) - B_q \, \cos(\delta - \theta_t)$$

$$G_a = \frac{R_a}{R_a^2 + X_d^{'} X_q} \quad ; \quad B_d^{'} = \frac{-X_d^{'}}{R_a^2 + X_d^{'} X_q} \quad ; \quad B_q = \frac{-X_q}{R_a^2 + X_d^{'} X_q}$$

Assuming that the armature resistance R_a of synchronous machines are small and neglected, then

$$G_a = 0 \;\; ; \;\; B_d' = -\,1/X_q < 0 \;\; ; \;\; B_q = -\,1/X_d' < 0$$

$$k_1 = 1 - (X_q - X_d')\,B_q = B_q/B_d' > 1$$

$$U_{PE} = -\,B_q \cos(\delta - \theta_t) > 0$$

$$T_{dt} = B_d' \sin(\delta - \theta_t) < 0$$

$$U_{dt} = -\,B_d' \cos(\delta - \theta_t) > 0$$

$$T_{qt} = B_q \sin(\delta - \theta_t) < 0$$

$$U_{qt} = -\,B_q \cos(\delta - \theta_t) > 0$$

$$T_{dt}\,T_{qt} - U_{dt}\,U_{qt} = -\,B_d'\,B_q \cos[2\,(\delta - \theta_t)]$$

Hence,

$$K_{\beta 1}^{gt} = -\,E_q'\,V_t\,B_q \cos(\delta - \theta_t) + V_t^2\,(X_q - X_d')\,(\,-\,B_d'\,B_q \cos[2\,(\delta - \theta_t)]\,)$$

$$= -\,B_q\,V_t\,[\,E_q' \cos(\delta - \theta_t)$$

$$+\,V_t\,(X_q - X_d')\,\frac{-1}{X_q}\,(\,\cos^2(\delta - \theta_t) - \sin^2(\delta - \theta_t)\,)\,]$$

$$= -\,B_q\,V_t\,[\,(\,E_q' - V_t\,(1 - \frac{X_d'}{X_q})\cos(\delta - \theta_t)\,)\cos(\delta - \theta_t)$$

$$+\,V_t\,(1 - \frac{X_d'}{X_q})\sin^2(\delta - \theta_t)\,] > 0 \qquad \text{(C-2)}$$

Note that the following factors causing $K_{\beta 1}^{gt} > 0$:

(a) $X_q \geq X_d'$, such that $0 < \{1 - \frac{X_d'}{X_q}\} < 1$.

(b) If the synchronous machine is operated in lagging power factor, then $\delta - \theta_t < 90^o$ implies $\cos(\delta - \theta_t) > 0$, and from the phasor diagram shown in Fig. 4-4(b), $\{E_q' - V_t \cos(\delta - \theta_t)\} > 0$, hence,

$$\{E_q' - V_t\,(1 - \frac{X_d'}{X_q})\cos(\delta - \theta_t)\} > 0.$$

Rewrite the matrix K_{FD} from (4-11):

$$K_{FD} = (K_{E3} + K_{E2}) - (K_{E4} + K_{E1})\, K\mathscr{g}^{t}_{\beta 1}{}^{-1}\, K\mathscr{g}^{t}_{\beta 2} \tag{C-3}$$

where,

$$K_{E1} = K_{EE}\, K_{C1} \;\; ; \;\; K_{E2} = K_{EE}\, K_{C2}$$

Note that the diagonal matrix K_{EE} represents the D.C. gains of excitation systems. Under the assumption that the load compensators are not employed, which implies that $K_{C1} = 0$, and $K_{C2} = 0$, we have

$$K_{FD} = K_{E3} - K_{E4}\, K\mathscr{g}^{t}_{\beta 1}{}^{-1}\, K\mathscr{g}^{t}_{\beta 2} \tag{C-4}$$

Each K-matrix ($K\mathscr{g}^{t}_{\beta 1}$ is discussed above) can be found from Section 2.6 as follows:

$$K\mathscr{g}^{t}_{\beta 2} = 2\, E_q^{'}\, G_{EE} - V_t\, T_{PE} \tag{C-5a}$$

$$K_{E4} = -\, (X_d - X_d^{'})\, T_{qt}\, V_t \tag{C-5b}$$

$$K_{E3} = 1 - (X_d - X_d^{'})\, B_q \tag{C-5c}$$

where,

$$G_{EE} = k_1\, G_a \;\; ; \;\; k_1 = 1 - (X_q - X_d^{'})\, B_q$$

$$T_{PE} = k_1\, T_{dt} + G_a\, (X_q - X_d^{'})\, U_{qt}$$

With the assumption $R_a = 0$, and the properties of the coefficients shown in the discussion of $K\mathscr{g}^{t}_{\beta 1}$ above, we have

$$G_{EE} = 0 \;\; ; \;\; T_{PE} = B_q\, \sin(\delta - \theta_t) < 0$$

$$K\mathscr{g}^{t}_{\beta 2} = -\, V_t\, B_q\, \sin(\delta - \theta_t) > 0 \tag{C-6a}$$

$$K_{E4} = -\, V_t\, (X_d - X_d^{'})\, B_q\, \sin(\delta - \theta_t) \tag{C-6b}$$

$$= V_t\, (\frac{X_d}{X_d^{'}} - 1)\, \sin(\delta - \theta_t) > 0$$

$$K_{E3} = 1 + (X_d - X_d')\,\frac{1}{X_d'} = \frac{X_d}{X_d'} > 0 \tag{C-6c}$$

Note that $X_d > X_d'$. If $K_{\beta 1}^{gt} > 0$ (from (C-2)), and since each K-submatrix is diagonal, then the (positive) definiteness of K_{FD} is equivalent to that of $K_{\beta 1}^{gt}\, K_{FD}$. Thus,

$$\begin{aligned}
K_{\beta 1}^{gt}\, K_{FD} &= K_{\beta 1}^{gt}\, K_{E3} - K_{E4}\, K_{\beta 2}^{gt} \\
&= -\,B_q\, V_t\, [\, E_q' \cos(\delta - \theta_t) \\
&\quad - V_t\, (1 - \frac{X_d'}{X_q})\, (\, \cos^2(\delta - \theta_t) - \sin^2(\delta - \theta_t)\,)\,]\, \frac{X_d}{X_d'} \\
&\quad - V_t\, (\frac{X_d}{X_d'} - 1)\, \sin(\delta - \theta_t)\, [\, -V_t\, B_q\, \sin(\delta - \theta_t)\,] \\
&= -\,B_q\, V_t\, [\, E_q'\, \frac{X_d}{X_d'} \cos(\delta - \theta_t) \\
&\quad - V_t\, \frac{X_d}{X_d'} \cos^2(\delta - \theta_t) + V_t\, \frac{X_d}{X_d'} \sin^2(\delta - \theta_t) \\
&\quad + V_t\, \frac{X_d}{X_q} \cos^2(\delta - \theta_t) - V_t\, \frac{X_d}{X_q} \sin^2(\delta - \theta_t) \\
&\quad - V_t\, \frac{X_d}{X_d'} \sin^2(\delta - \theta_t) + V_t\, \sin^2(\delta - \theta_t)\,] \\
&= -\,B_q\, V_t\, [\, (\, E_q' - V_t \cos(\delta - \theta_t)\,)\, \frac{X_d}{X_d'} \cos(\delta - \theta_t) \\
&\quad + V_t\, \frac{X_d}{X_q} \cos[2(\delta - \theta_t)] + V_t\, \sin^2(\delta - \theta_t)\,]
\end{aligned} \tag{C-7}$$

Conservatively, if $\delta - \theta_t \leq 45^o$ and from Fig. 4-4(b) which assure $K_{\beta 1}^{gt} > 0$, then the first two terms of $K_{\beta 1}^{gt}\, K_{FD}$ are nonnegative, and hence $K_{FD} > 0$.

Appendix D

C_{3X} and C_{3K}^{X}

This Appendix will show that $-C_{3X}$ is a diagonal matrix with positive elements that increase almost linearly with the D.C. gains of the excitation system K_{EE} that are in general very large compared to the rest of terms in C_{3X}, when it is assumed that the load compensators are not used in the power system model. Then the matrix C_{3K}^{X} is also a diagonal matrix with positive elements that increase almost linearly with K_{EE}.

Rewrite the matrix C_{3K}^{X} from (4-18):

$$C_{3K}^{X} = K_{Q7}^{tg} + C_3 - C_{3X} \tag{D-1}$$

$$C_{3X} = -K_{Q1}^{tg}\, K_{\beta 1}^{gt\,-1}\, K_{\beta 7}^{gt} - (K_{Q1}^{tg}\, K_{\beta 1}^{gt\,-1}\, K_{\beta 2}^{gt} + K_{Q2}^{tg})\, K_{FD}^{-1}\, K_{EC} \tag{D-1a}$$

$$K_{EC} = (K_{E4} + K_{EE}\, K_{C1})\, K_{\beta 1}^{gt\,-1}\, K_{\beta 7}^{gt} + (K_{E7} - K_{EE}\, K_{C7}) \tag{D-1b}$$

$$K_{FD} = (K_{E3} + K_{E2}) - (K_{E4} + K_{E1})\, K_{\beta 1}^{gt\,-1}\, K_{\beta 2}^{gt} \tag{D-1c}$$

where,

$$K_{E1} = K_{EE}\, K_{C1} \;\; ; \;\; K_{E2} = K_{EE}\, K_{C2}$$

Under the assumption that the load compensators are not employed, which implies that $K_{C1} = 0$, $K_{C2} = 0$, and $K_{C7} = I$, and if the D.C. gains of the excitation systems K_{EE} are very large, we have

$$K_{FD} = K_{E3} - K_{E4}\, K_{\beta 1}^{gt\,-1}\, K_{\beta 2}^{gt} \tag{D-2c}$$

$$K_{EC} = K_{E4}\, K_{\beta 1}^{gt\,-1}\, K_{\beta 7}^{gt} + K_{E7} - K_{EE}$$

$$\approx -K_{EE} \tag{D-2b}$$

$$C_{3X} \approx (K_{Q1}^{tg}\, K_{\beta 1}^{gt\,-1}\, K_{\beta 2}^{gt} + K_{Q2}^{tg})\, K_{FD}^{-1}\, K_{EE} \tag{D-2a}$$

As discussed in Appendix C, $K_{\beta 1}^{gt}$ and K_{FD} should be positive definite, and since K_{EE} is positive definite with very large elements, then the definiteness of C_{3X} is equivalent to that of $K_{PQ} = \{K_{Q1}^{tq}\ K_{\beta 2}^{gt} + K_{Q2}^{tq}\ K_{\beta 1}^{gt}\}$, where $K_{\beta 1}^{gt}$ and $K_{\beta 2}^{gt}$ are shown in Appendix C, and

$$K_{Q1}^{tq} = -V_t\, E_q'\, T_{tq} - V_t^2\, (B_d' - B_q)\, \sin[2(\theta_t - \delta)] \tag{D-3a}$$

$$K_{Q2}^{tq} = -V_t\, U_{tq} \tag{D-3b}$$

$$T_{tq} = G_a\, \cos(\theta_t - \delta) + B_q\, \sin(\theta_t - \delta)$$

$$U_{tq} = G_a\, \sin(\theta_t - \delta) - B_q\, \cos(\theta_t - \delta)$$

Assuming $R_a = 0$, then

$$T_{tq} = -B_q\, \sin(\delta - \theta_t) > 0$$

$$U_{tq} = -B_q\, \cos(\delta - \theta_t) > 0$$

$$K_{Q1}^{tq} = V_t\, E_q'\, B_q\, \sin(\delta - \theta_t) + V_t^2\, (B_d' - B_q)\, \sin[2\,(\delta - \theta_t)] \tag{D-4a}$$

$$K_{Q2}^{tq} = V_t\, B_q\, \cos(\delta - \theta_t) < 0 \tag{D-4b}$$

Hence, substituting (from Appendix C)

$$K_{\beta 1}^{gt} = -E_q'\, V_t\, B_q\, \cos(\delta - \theta_t) - V_t^2\, (B_d' - B_q)\, \cos[2\,(\delta - \theta_t)] \tag{D-5a}$$

$$K_{\beta 2}^{gt} = -V_t\, B_q\, \sin(\delta - \theta_t) > 0 \tag{D-5b}$$

we have

$$\begin{aligned} K_{PQ} &= K_{Q1}^{tq}\ K_{\beta 2}^{gt} + K_{Q2}^{tq}\ K_{\beta 1}^{gt} \qquad \text{(D-6)} \\ &= -B_q\, V_t^2\, [\, E_q'\, B_q\, \sin^2(\delta - \theta_t) + V_t\, (B_d' - B_q)\, \sin[2(\delta - \theta_t)]\, \sin(\delta - \theta_t) \\ &\quad + E_q'\, B_q\, \cos^2(\delta - \theta_t) + V_t\, (B_d' - B_q)\, \cos[2(\delta - \theta_t)]\, \cos(\delta - \theta_t)\,] \\ &= -B_q\, V_t^2\, [\, E_q'\, B_q + V_t\, (B_d' - B_q)\, (\, 2\, \sin^2(\delta - \theta_t)\, \cos(\delta - \theta_t) \\ &\quad + \cos^2(\delta - \theta_t)\, \cos(\delta - \theta_t) - \sin^2(\delta - \theta_t)\, \cos(\delta - \theta_t)\,)\,] \end{aligned}$$

$$= - B_q \; V_t^2 \, [\, E_q' \, B_q + V_t \, (B_d' - B_q) \cos(\delta - \theta_t) \,]$$

$$= - B_q \; V_t^2 \, [\, B_q \; [\, E_q' - V_t \, \cos(\delta - \theta_t) \,] + V_t \, B_d' \cos(\delta - \theta_t) \,] < 0$$

Note that $K_{PQ} < 0$ implies $\{ K_{Q1}^{tg} \; {K_{P1}^{gt}}^{-1} \, K^{P2\theta} + K_{Q2}^{tg} \} < 0$. Hence, $- C_{3X}$ is a diagonal and positive definite matrix with positive elements that increase almost linearly with K_{EE}. Note also that $C_{3K}^{X} = K_{Q7}^{tg} + C_3 - C_{3X}$, and that both K_{Q7}^{tg} and C_3 are the coefficients of reactive power-voltage Jacobian matrix at the terminal bus that are finite and are neglectable compared with $- C_{3X}$ when K_{EE} is very large. Thus, the matrix C_{3K}^{X} is approximately to $- C_{3X}$ and is also a diagonal matrix with the positive elements that increase almost linearly with K_{EE}.

LIST OF REFERENCES

LIST OF REFERENCES

[1] J.M. Undrill, "Power System Simulator Package Program Application Guide, PSS/E", Power Technologies Inc., Oct. 1981.

[2] "Extended Transient-Midterm Stability Package", EPRI Report, EL-2003-CCM, RP-1208, Jan. 1987.

[3] R.T. Byerly, D.E. Sherman, R.J. Bennon, "Frequency Domain Analysis of Low-Frequency Oscillations in Large Electric Power Systems", EPRI Report, EL-2348, RP-744-1, April 1982.

[4] P. Kundur, G.J. Rogers, D.Y. Wong, "Small Signal Stability Analysis Program Package", EPRI Report, EL-6678, RP-2447-1, Jan. 1990.

[5] P.W. Sauer, G. Rajagopalan, M.A. Pai, "An Explanation and Generalization of the AESOPS and PEALS Algorithms", Paper 90WM239-04PWRS, IEEE/PES Winter Meeting, Atlanta, Georgia, Feb. 4-8, 1990.

[6] P. Kundur, G.J. Rogers, D.Y. Wong, L. Wang, "A Comprehensive Computer Program Package for Small Signal Stability Analysis of Power Systems" IEEE Trans. on Power Systems, Vol. 5, No. 4, Nov. 1990, pp. 1076-1083.

[7] L. Wang, A. Semlyen, "Application of Sparse Eigenvalue Techniques to the Small Signal Stability Analysis of Large Power Systems", IEEE Trans. on Power Systems, Vol. 5, No. 2, May 1990, pp. 635-642.

[8] D.Y. Wong, G.J. Rogers, B. Porretta, P. Kundur, "Eigenvalue Analysis of Very Large Power Systems", IEEE Trans. on Power Systems, Vol. 3, No. 2, May 1988, pp. 472-480.

[9] Y.Y. Hsu, P.H. Huang, C.J. Lin, C.T. Huang, "Oscillatory Stability Considerations in Transmission Expansion Planning", Paper 89WM154-6PWRS, IEEE/PES Winter Meeting, New York, NY, Jan. 29 - Feb. 3, 1989.

[10] Y.Y. Hsu, S.W. Shyue, C.C. Su, "Low Frequency Oscillations in Longitudinal Power Systems: Experience with Dynamic Stability of Taiwan Power System", Paper 86WM070-7, IEEE/PES Winter Meeting, New York, NY, Feb. 2-7, 1986.

[11] F.L. Pagola, I.J. Perez-Arriaga, G.C. Verghese, "On Sensitivities, Residues and Participations, Applications to Oscillatory Stability Analysis and Control", Paper 88SM683-5, IEEE/PES Summer Meeting, Portland, Oregon, July 24-29, 1988.

[12] Y. Obata, S. Takeda, and H. Suzuki, "An Efficient Eigenvalue Estimation Technique for Multimachine Power System Dynamic Stability Analysis", IEEE Trans. on Power Apparatus and Systems, Vol. PAS-100, No. 1, Jan. 1981, pp. 259-263.

[13] P.J. Nolan, N.K. Sinha, R.T.H. Alden, "Eigenvalue Sensitivities of Power Systems Including Network and Shaft Dynamics", IEEE Trans. on Power Apparatus and Systems, Vol. PAS-95, No. 4, Jan./Aug. 1976, pp. 1318-1324.

[14] V. Vittal, N. Bhatia, and A.A. Fouad, "Analysis of the Inter-area Mode Phenomenon in Power Systems Following Large Disturbances", Paper 91WM228-7PWRS, IEEE/PES Winter Meeting, New York, NY, Feb. 3-7, 1991.

[15] G.C. Verghese, I.J. Perez-Arriaga, F.C. Schweppe, "Selective Modal Analysis with Applications to Electric Power Systems, Part I: Heuristic Introduction", IEEE Trans. on Power Apparatus and Systems, Vol. PAS-101, No. 9, Sep. 1982, pp. 3117-3125.

[16] G.C. Verghese, I.J. Perez-Arriaga, F.C. Schweppe, "Selective Modal Analysis with Applications to Electric Power Systems, Part II: The Dynamic Stability Problem", IEEE Trans. on Power Apparatus and Systems, Vol. PAS-101, No. 9, Sep. 1982, pp. 3126-3134.

[17] N. Martins, L.T.G. Lima, "Determination of Suitable Locations for Power System Stabilizers and Static VAR Compensators for Damping Electromechanical Oscillations in Large Scale Power Systems", IEEE Trans. on Power Systems, Vol. 5, No. 4, Nov. 1990, pp. 1455-1469.

[18] J.E. Van Ness, F.M. Brasch, G.L. Landgren, S.T. Naumann, "Analytical Investigation of Dynamic Instability Occurring at Powerton Station", IEEE Trans. on Power Apparatus and Systems, Vol. PAS-99, No. 4, July/Aug. 1980, pp. 1386-1395.

[19] V. Arcidiacono, E. Ferrari, R. Marconato, J. Dos Chali, D. Grandez, "Evaluation and Improvement of Electromechanical Oscillation Damping by means of Eigenvalue-Eigenvector Analysis. Practical Results in the Central Peru Power System", IEEE Trans. on Power Apparatus and Systems, Vol. PAS-99, No. 2, March/April 1980, pp. 769-778.

[20] S.Z. Chen, "Location and Application of Stabilizers in North-West China Network Planning and Designing", CIGRE Session Paper 38-12, Aug. 27 - Sep. 4, 1986.

[21] "Eigenanalysis and Frequency Domain Methods for System Dynamic Performance", IEEE/PES 90TH0292-3-PWR, 1990.

[22] M. Klein, G.J. Roger, P. Kundur, "A Fundamental Study of Inter-Area Oscillations in Power Systems", Paper 91WM 015-8PWRS, IEEE/PES Winter Meeting, New York, NY, Feb. 3-7, 1991.

[23] F.P. deMello, C. Concordia, "Concepts of Synchronous Machine Stability as Affected by Excitation Control", IEEE Trans. on Power Apparatus and Systems, Vol. PAS-88, No. 4, April 1969, pp. 316-329.

[24] F.P. deMello, T.F. Laskowski, "Concepts of Power System Dynamic Stability", IEEE Trans. on Power Apparatus and Systems, Vol. PAS-94, No. 3, May/June 1975, pp. 827-833.

[25] M.K. El-Sherbiny, D.M. Mehta, "Dynamic System Stability, Part I: Investigation of the Effect of Different Loading and Excitation Systems", IEEE Trans. on Power Apparatus and Systems, Vol. PAS-92, No. 5, Sep./Oct. 1973, pp. 1538-1546.

[26] P.M. Anderson, A.A. Fouad, "Power System Stability and Control", The Iowa State University Press, Ames, IOWA, 1977.

[27] M. Djuric, G. Muzdeka, "The Analysis of the Occurrence Conditions and the Possibility of Elimination of Negative Damping in the Power Systems", CIGRE Session Paper 38-06, Aug. 29 - Sep. 6, 1984.

[28] A.A. Shaltout, E.A. Abu Al-Feilat, "Damping and Synchronizing Torque Computation in Multimachine Power Systems", Paper 91SM472-1PWRS, IEEE/PES Summer Meeting, San Diego, CA, July 28 - Aug. 1, 1991.

[29] H. Saitoh, J. Toyoda, Y. Kobayashi, "A New Index Extracted From Line Flow Fluctuation to Evaluate Power System Damping", Paper 91WM208-9PWRS, IEEE/PES Winter Meeting, New York, NY, Feb. 3-7, 1991.

[30] Bo E. Eliasson, D.J. Hill, "Damping Structure and Sensitivity in the Nordel Power System", Paper 91WM205-5PWRS, IEEE/PES Winter Meeting, New York, NY, Feb. 3-7, 1991.

[31] A.R. Bergen, D.J. Hill, "A Structure Preserving Model for Power System Stability Analysis", IEEE Trans. on Power Apparatus and Systems, Vol. PAS-100, No. 1, Jan. 1981, pp. 25-35.

[32] D.J. Hill, I.M.Y. Mareels, "Stability Theory for Differential/Algebraic Systems with Application to Power Systems", IEEE Trans. on Circuit and Systems, Vol. 37, No. 11, Nov. 1990.

[33] F.M.A. Salam, "Asymptotic Stability and Estimating the Region of Attraction for the Swing Equations", Systems & Control Letters 7, 1986, pp. 309-312.

[34] A.A. Fouad, V. Vittal, "The Transient Energy Function Method", International Journal of Electrical Energy and Power Systems, Vol. 10, No. 4, Oct. 1988, pp. 233-246.

[35] N.A. Tsolas, A. Arapostathis, P.P. Varaiya, "A Structure Preserving Energy Function for Power System Transient Stability Analysis", IEEE Trans. on Circuit and Systems, Vol. 32, No. 10, Oct. 1985.

[36] S-N. Chow and J.K. Hale, "Methods of Bifurcation Theory", Springer-Verlag, 1982

[37] John Guckenheimer, Philip Holmes, "Nonlinear Oscillations, Dynamical Systems, and Bifurcations of Vector Fields", Applied Mathematical Sciences, Vol. 42, Springer-Verlag, 1986.

[38] Ferdinand Verhulst, "Nonlinear Differential Equations and Dynamical Systems", Springer-Verlag, 1989

[39] H.G. Kwatny, A.K. Pasrija, L.Y. Bahar, "Computer Analysis of Static Bifurcation in Power Networks", Proceedings of the 29th Conference on Decision and Control, Honolulu, Hawaii, Dec. 1990, pp. 3063-3064.

[40] H.G. Kwatny, A.K. Pasrija, L.Y. Bahar, "Static Bifurcation in Electric Power Networks: Loss of Steady-State Stability and Voltage Collapse", IEEE Trans. on Circuits and Systems, Vol. CAS-33, No. 10, Oct. 1986, pp. 981-991.

[41] P. Varaiya, F. Wu, H.D. Chiang, "Bifurcation and Chaos in Power Systems: A Survey", Memo. UCB/ERL M90/98, Electronics Research Laboratory, College of Engineering, University of California, Berkeley, CA, Nov. 1990.

[42] E. Abed, N. Tsolas, P. Varaiya, "Study of Nonlinear Oscillations due to Exciter Control Using Hopf Bifurcation", IEEE Trans. on Circuit and Systems, Vol. 30, No. 5, May. 1983, pp.1410-1413.

[43] Rong-Liang Chen, "Numerical Study of Hopf Bifurcation in Multimachine Power Systems", Ph.D. Dissertation, Department of Electrical Engineering and Computer Sciences, University of California, Berkeley, CA, 1988.

[44] A.M.A. Hamdan, A.H. Nayfeh, "The Effects of Nonlinearities on the Response of a Single-Machine-Quasi-Infinite-Busbar System", Paper 89WM147-0PWRS, IEEE/PES Winter Meeting, New York, NY, Jan. 29 - Feb. 3, 1989.

[45] P.W. Sauer, M.A. Pai, "Power System Steady-State Stability and the Load Flow Jacobian", IEEE Trans. on Power Systems, Vol. 5, No. 4, Nov. 1990, pp. 1374-1383.

[46] M. Langevin, P. Auriol, "Load Response to Voltage Variations and Dynamic Stability", Paper 86WM078-0, IEEE/PES Winter Meeting, New York, NY, Feb. 2-7, 1986.

[47] D.S. Brereton, D.G. Lewis, C.C. Young, "Representation of Induction-Motor Loads During Power-System Stability Studies", AIEE Trans. Vol. 76, Aug. 1957, pp. 451-461.

[48] R.A. Schlueter, et al., "Voltage Stability and Security Assessment", EPRI Report, EL-5967, RP-1999-8, May 1988.

[49] R.A. Schlueter, I. Hu, M.W. Chang, et al., "Reactive Supply On-line Criteria", Section 7, Proceeding of Workshop on Bulk Power Voltage Phenomena: Voltage Stability and Security Conference, Potosi, MO, Sep. 1988.

[50] R.A. Schlueter, T. Lie, T.Y. Guo, et al., "Reactive Supply Voltage Stability on EHV Transmission Networks", Proceedings of Workshop on High Voltage Transmission in the Mid-Atlantic region, 1990-2010, Pittsburgh, PA, Aug. 1990

[51] R.A. Schlueter, I. Hu, M.W. Chang, A. Costi, "Methods for Determining Proximity to Voltage Collapse", IEEE Trans. on Power Systems, Vol. 6, No. 2, Feb. 1991, pp. 258-292.

[52] I. Hu, "Voltage Collapse Bifurcation of a Power System Transient Stability Model", Ph.D. Dissertation, Michigan State University, July 1990.

[53] R.A. Schlueter, I. Hu, T.Y. Guo, "Dynamic/Static Voltage Stability Security Criteria", Bulk Power System Voltage Phenomena Seminar, Deep Creek, MD, Aug. 1991.

[54] M.M. Begovic, A.G. Phadke, "Control of Voltage Stability Using Sensitivity Analysis", Paper 91WM231-1PWRS, IEEE/PES Winter Meeting, New York, NY, Feb. 3-7, 1991.

[55] N. Flatabo, R. Ognedal, T. Carlsen, "Voltage Stability Condition in a Power System Transmission System Calculated by Sensitivity Methods", IEEE Trans. on Power Systems, Vol. 5, No. 4, Nov. 1990, pp. 1286-1293.

[56] C. Lemaitre, J.P. Paul, J.M. Tesseron, Y. Harmand, Y.S. Zhao, "An Indicator of the Risk of Voltage Profile Instability for Real-Time Control Applications", IEEE Trans. on Power Systems, Vol. 5, No. 1, Feb. 1990, pp. 154-161.

[57] P-A Lof, T. Smed, G. Andersson, D.J. Hill, "Fast Calculation of a Voltage Stability Index", Paper 91WM203-0PWRS, IEEE/PES Winter Meeting, New York, NY, Feb. 3-7, 1991.

[58] Y. Tamura, H. Mori, S. Iwamoto, "Relationship between Voltage Instability and Multiple Load Flow Solutions In Electric Power Systems", IEEE Trans. on Power Apparatus and Systems, Vol. PAS-102, No. 5, May 1983, pp. 1115-1125.

[59] P. Borremans, A. Calvaer, J.P. de Reuck, J. Goossens, E.V. Geert, J.V. Hecke, A.V. Ranst, "Voltage Stability — Fundamental Concepts and Comparison of Practical Criteria", CIGRE Session Paper 38-11, Aug. 29 - Sep. 6, 1984.

[60] T.V. Cutsem, "A Method to Compute Reactive Power Margins with respect to Voltage Collapse", IEEE Trans. on Power Systems, Vol. 6, No. 1, Feb. 1991, pp. 145-156.

[61] T. Gomez, J. Lumbreras, V.M. Parra, "A Security-Constrained Decomposition Approach to Optimal Reactive Power Planning", IEEE Trans. on Power Systems, Vol. 6, No. 3, Aug. 1991, pp. 1069-1076.

[62] V.A. Venikov, V.A. Stroev, V.I. Idelchick, V.I. Tarasov, "Estimation of Electrical Power System Steady-State Stability in Load Flow Calculations", IEEE Trans. on Power Apparatus and Systems, Vol. PAS-94, No. 3, May/June 1975.

[63] B. Gao, G.K. Morison, P. Kundur, "Voltage Stability Evaluation Using Modal Analysis", submitted to IEEE/PES Meeting, 1991.

[64] I. Dobson, H.D. Chiang, "Towards a Theory of Voltage Collapse in Electric Power Systems", Systems and Control Letters 13, 1989, pp. 253-262.

[65] H.D. Chiang, I. Dobson, R.J. Thomas, "On Voltage Collapse in Electric Power Systems", IEEE Trans. on Power Systems, Vol. 5, No. 2, May 1990, pp. 601-611.

[66] M.M. Begovic, A.G. Phadke, "Dynamic Simulation of Voltage Collapse", IEEE Trans. on Power Systems, Vol. 5, No. 4, Nov. 1990, pp. 1529-1534.

[67] E.H. Abed, A.M.A. Hamdan, H.C. Lee, A.G. Parlos, "On Bifurcations in Power System Models and Voltage Collapse", Proceedings of the 29th Conference on Decision and Control, Honolulu, Hawaii, Dec. 1990, pp. 3014-3015.

[68] C. Rajagopalan, P.W. Sauer, M.A. Pai, "Analysis of Voltage Control Systems Exhibiting Hopf Bifurcation", Proceedings of the 28th Conference on Decision and Control, Tempa, Florida, Dec. 1989, pp. 332-335.

[69] V. Venkatasubramanian, H. Schattler, J. Zaborszky, "Global Voltage Dynamics: Study of a Generator with Voltage Control, Transmission, and Matched MW Load", Proceedings of the 29th Conference on Decision and Control, Honolulu, Hawaii, Dec. 1990, pp. 3045-3056.

[70] V. Venkatasubramanian, H. Schattler, J. Zaborszky, "A Taxonomy of the Dynamics of the Large Power System with Emphasis on its Voltage Stability", Bulk Power System Voltage Phenomena Seminar, Deep Creek, MD, Aug. 1991.

[71] B.H. Lee, K.Y. Lee, "A Study on Voltage Collapse Mechanism in Electric Power Systems", Paper 91WM123-0PWRS, IEEE/PES Winter Meeting, New York, NY, Feb. 3-7, 1991.

[72] J.H. Chow, A. Gebreselassie, "Dynamic Voltage Stability Analysis of a Single Machine Constant Power Load System", Proceedings of the 29th Conference on Decision and Control, Honolulu, Hawaii, Dec. 1990, pp. 3057-3062.

[73] C. Rajagopalan, B. Lesieutre, P.W. Sauer, M.A. Pai, "Dynamic Aspects of Voltage/Power Characteristics", Paper 91SM419-2PWRS, IEEE/PES Summer Meeting, San Diego, CA, July 28 - Aug. 1, 1991.

[74] A.E. Hammad, M.Z. El-Sadek, "Prevention of Transient Voltage Instabilities Due to Induction Motor Loads By Static VAR Compensators", Paper 89WM149-6PWRS, IEEE/PES Winter Meeting, New York, NY, Jan. 29 - Feb. 3, 1989.

[75] S. Abe, Y. Fukunaga, A. Isono, B. Kondo, "Power System Voltage Stability", IEEE Trans. on Power Apparatus and Systems, Vol. PAS-101, No. 10, Oct. 1982, pp. 3830-3840.

[76] Y. Sekine, H. Ohtsuki, "Cascaded Voltage Collapse", IEEE Trans. on Power Systems, Vol. 5, No. 1, Feb. 1990, pp. 250-256.

[77] H. Ohtsuki, A. Yokoyama, Y. Sekine, "Reverse Action of On-Load Tap Changer in Association with Voltage Collapse", IEEE Trans. on Power Systems, Vol. 6, No. 1, Feb. 1991, pp. 300-306.

[78] N. Yorino, H. Sasaki, Y. Masuda, Y. Tamura, M. Kitagawa, A. Oshimo, "An Investigation of Voltage Instability Problems", Paper 91WM202-2PWRS, IEEE/PES Winter Meeting, New York, NY, Feb. 3-7, 1991.

[79] Y. Tamura, "A Scenario of Voltage Collapse in a Power System with Induction Motor Loads with a Cascade Transition of Bifurcations", Bulk Power System Voltage Phenomena Seminar, Deep Creek, MD, Aug. 1991.

[80] William D. Stevenson, Jr., "Elements of Power System Analysis", Fourth Edition, McGraw-Hill Book Company, 1982.

[81] Atif Debs, "Modern Power Systems Control and Operation", Kluwer Academic Publishers, 1988.

[82] IEEE Committee Report, "Common Format for Exchange of Solved Load Flow Data" IEEE Trans. on Power Apparatus and Systems, Vol. PAS-92, 1973, pp. 20-28.

[83] S.D. Umans, J.A. Mallick, G.L. Wilson, "Modeling of Solid Rotor Turbogenerators. Part II: Example of Model derivation and Use in Digital Simulation", IEEE Trans. on Power Apparatus and Systems, Vol. PAS-97, No. 1, Jan/Feb 1978, pp. 278-291.

[84] S.D. Umans, J.A. Mallick, G.L. Wilson, "Modeling of Solid Rotor Turbogenerators. Part I: Theory and Techniques", IEEE Trans. on Power Apparatus and Systems, Vol. PAS-97, No. 1, Jan/Feb 1978, pp. 269-277.

[85] IEEE Committee Report, "Excitation System Models for Power System Stability Studies", IEEE Trans. on Power Apparatus and Systems, Vol. PAS-100, No. 2, Feb. 1981, pp. 494-509.

[86] IEEE Committee Report, "Dynamic Models for Steam and Hydro Turbines in Power System Studies", IEEE Trans. on Power Apparatus and Systems, Vol. PAS-92, 1973, pp. 1904-1915.

[87] Tzong-yih Guo, Robert A. Schlueter, "Static/Algebraic Bifurcation in Multimachine Power Systems", in preparation for being sumitted to IEEE/PES Summer Meeting, 1992.

[88] Tzong-yih Guo, Robert A. Schlueter, "Static/Dynamic Bifurcation Tests for Low Frequency Oscillation and Voltage Collapse in Multimachine Power Systems", submitted to IEEE/PES Summer Meeting, 1992.

[89] Lazhar Fekih-Ahmed, Hsiao-Dong Chiang, "Stability Regions of Systems Governed by Differential-Algebraic Equations", submitted to IEEE Trans. on Automatic Control, 1991.